Author/s:
Novakovic, Sacha

Title:
Synthesis and Photophysics of Zinc Porphyrin Based Dual Absorber-Upconverters

Date:
2020

Persistent Link:
https://hdl.handle.net/11343/241936

Synthesis and Photophysics of Zinc Porphyrin Based Dual Absorber-Upconverters

Sacha Novakovic

Submitted in total fulfillment

of the requirements of the degree of

Doctor of Philosophy

February 2020

School of Chemistry

The University of Melbourne

Abstract

Several zinc porphyrin small molecules and pendant polymers were synthesized in order to assess their ability to act as dual absorber-upconverters in both solution and solid-state triplet-triplet annihilation mediated non-coherent photon upconversion (NCPU-TTA) systems. Control over the proximity, relative orientation and degree of orbital overlap between zinc porphyrin chromophores was exercised through covalent structural design in each set of studied zinc porphyrin derivatives. Structure-property relationships were determined through photophysical analyses of the zinc porphyrin compounds. Photophysical analyses were able to provide the basis for mechanistic models that detailed excitonic decay processes in the zinc porphyrin compounds.

Meso-diaryl- and *meso*-tetraaryl-substituted zinc porphyrin derivatives were synthesized with varying steric bulk at the *meso*-aryl-substituents. The absorption and S_1 emission properties of all compounds were able to be interpreted through established porphyrin orbital theory. The lower ΔOD values observed in the transient absorption spectra of the di-substituted compounds were consistent with the relative solution-state NCPU-TTA S_2 fluorescence yields obtained for the di-substituted compounds compared to the tetra-substituted compounds. The NCPU-TTA S_2 fluorescence yields generally increased with increasing steric bulk in in both the di- and tetra-substituted series in solution. NCPU-TTA S_2 fluorescence was not observable in the solid state for the di-substituted series, however the NCPU-TTA S_2 fluorescence yields increased approximately 20 fold in the solid-state for zinc(II) tetramesitylporphyrin **2.6** compared to zinc(II) tetraphenylporphyrin **2.4**. Computational analyses provided insight into the observed NCPU-TTA S_2 fluorescence trends.

A series of polymers with pendant zinc porphyrin units containing β-oligo-*para*-phenylene vinylene (β-oligo-*p*-PV) substitutents were synthesized via post-polymerization functionalization methods and Horner-Wadsworth-Emmons olefination. The β-oligo-*p*-PV substituents on the zinc porphyrin pendants were designed to act as pendant-to-backbone linking moieties in the pendant polymers. Monomeric analogues of the pendant polymers were synthesized for photophysical

comparison. The absorption spectra of the pendant polymers demonstrated reduced extinction coefficients with respect to their monomeric analogues and Soret broadening characteristic of chromophores in close proximity, however no exciton coupling was observed. The fluorescence quantum yields of the polymers remained almost unchanged with increasing β-conjugation length with the exception of a minor increase in emission intensity from the Q(0,0) vibronic band. The fluorescence quantum yields of the polymers were reduced more than 50% in comparison to the monomers. The dominant triplet absorption bands in the monomers were approximately 5 – 9% as intense in their respective polymer spectra.

Pendant zinc porphyrin polymers with rotatable stilbene and benzyl ether pendant-to-backbone linking groups were synthesized by post-polymerization functionalization. Red-shifting and broadening of absorption maxima were observed upon inclusion of porphyrins into the pendant polymer structure. Bi-exponential fits to the polymer fluorescence decay profiles were attributed to rotation-induced excimer-type quenching between pendant porphyrin units in the S_1 excited state. The polymer NCPU-TTA S_2 fluorescence quantum yields in toluene were 2 orders of magnitude lower than their respective monomer analogues, being of the order of 10^{-7}. The NCPU-TTA S_2 fluorescence intensity of the polymer **4.6** in the coordinating solvent THF was reduced less than for the analogous monomer **4.3** due to restricted access of THF molecules to the metal centre in the crowded pendant environment. Triplet absorption intensities of the polymers were approximately 10% of that observed for their respective monomeric analogues. Triplet decay profiles of the monomeric compounds were able to be fit to first-plus-second order kinetic equations that account for TTA occurring in the monomers. The polymers displayed a region of rapid decay at the beginning of their triplet decay profiles that could not be accounted for by TTA due to the very low polymer NCPU-TTA S_2 fluorescence quantum yields. The polymer triplet decay profiles were able to be adequately modeled by three competing first- and pseudo-first order decay processes which were attributed to intersystem crossing to the ground state in addition to both intra- and intermolecular quenching of pendant porphyrins by neighbouring porphyrins in the ground state. Rapid excited state decay and exciton quenching in both the singlet and triplet states of the pendant zinc porphyrin polymers studied in this thesis likely render them as poor dual absorber-upconverter compounds for NCPU-TTA systems.

Declaration

This is to certify that:

i. The thesis comprises only my original work towards the PhD except where indicated in the preface,

ii. Due acknowledgement has been made in the text to all other material used,

iii. The thesis is fewer than 100,000 words in length, exclusive of tables, maps, bibliographies and appendices.

_____

Sacha Novakovic
February 2020

Preface

The following contributions to this thesis are acknowledged:

1. All Soret excited emission, fluorescence lifetimes (τ_1), and both radiative and non-radiative rate constants for S_1 fluorescence decays (k_r and k_{nr} respectively) in Table 2.3 and solid-state absorption spectra in figure 2.20 were obtained by Dr. Ranjana Rauleta and Dr. Neeraj K. Joshi (University of Saskatchewan, Canada).

2. All NCPU-TTA experiments in sections 2.6 and 2.7.2 were performed by Dr. Ranjana Rauleta and Dr. Neeraj K. Joshi (University of Saskatchewan, Canada).

3. All computational analyses in section 2.8 were performed by Dr. Ranjana Rauleta and Dr. Neeraj K. Joshi (University of Saskatchewan, Canada).

4. The backbone polymer poly(VBC)-DoPAT **3.26** was provided by Dr. John Li (University of Melbourne).

5. ICP-OES analysis was performed by Dr. Yukie O'Bryan (University of Melbourne).

6. All X-ray crystal structures were solved by Prof. Jonathan M. White (University of Melbourne).

7. All fluorescence decay experiments in section 4.2 and NCPU-TTA data and figures in section 4.6 were performed by Dr. Amy Stevens (University of Saskatchewan).

8. Fitting of the triplet decay data for compounds **4.3** and **4.6** was performed by Prof. Trevor A. Smith (University of Melbourne).

9. The mechanistic models in figures 4.23 and 4.26 were formulated by Prof. Ronald P. Steer and Prof. Matthew F. Paige (University of Saskatchewan).

Acknowledgements

I would like to thank my supervisors Prof. Jonathan White, Prof. Ken Ghiggino and Dr. Wallace Wong for their guidance throughout my PhD candidature and for giving me the opportunity to pursue a fascinating multi-disciplinary research project. They have been amazing mentors and I am deeply grateful for everything I have learned from them.

A great thanks goes to my panel members, Prof. Trevor Smith and Prof. Paul Donnelly, who have given me useful suggestions and insight and over the years that has been helpful for the completion of this thesis.

The outcomes of the work in this thesis would not be possible without the collaboration of research members from the University of Saskatchewan. Thanks goes to Prof. Ron Steer, Prof. Matthew Paige, Dr. Neeraj Joshi, Dr. Ranjana Rauleta and Dr. Amy Stevens for their incredible knowledge in the field of porphyrin-based photon upconversion and valuable contribution to the outcomes presented in this thesis.

I would like to thank all staff members of the Bio21 Institute and the University of Melbourne who have helped or contributed in some way towards the completion of this thesis. Thanks go to Dr. John Li for providing the RAFT polymer starting material.

I thank the Australian Centre for Advanced Photovoltaics (ACAP) for providing me the opportunity to undertake this research and I thank the Australian Renewable Energy Agency (ARENA) for providing financial resources to ACAP which made this work possible.

So many thanks go out to the group members from the White, Ghiggino and Wong group, past and present, for not only their help in the lab but for all the fun and memorable times shared throughout my PhD candidature.

Lastly, I thank my friends and family for providing me unwavering support along my PhD journey. Thanks go to my parents Tanja and Simo for everything they have done for me in my life and to my sisters Katja and Mia. Thanks go to my partner Gabriela for being there for me every day and to her parents Edilson and Omaira for all of their support.

Publications

1. Rautela, R.; Joshi, N. K.; Novakovic, S.; Wong, W. W. H.; White, J. M.; Ghiggino, K. P.; Paige, M. F.; Steer, R. P. *Determinants of the efficiency of photon upconversion by triplet–triplet annihilation in the solid state: zinc porphyrin derivatives in PVA, Phys. Chem. Chem. Phys.* **2017,** 19, 23471-23482.
   DOI: 10.1039/C7CP04746K

2. Stevens, A. L.; Novakovic, S.; White, J. M.; Wong, W. W. H.; Smith, T. A.; Ghiggino, K. P.; Paige, M. F.; Steer, R. P. *Exciton Dynamics of Photoexcited Pendant Porphyrin Polymers in Solution and in Thin Films, J. Phys. Chem. A* **2018,** *122*, 9605−9614.
   DOI: 10.1021/acs.jpca.8b09321

Conference Presentations

1. Australian Centre for Advanced Photovoltaics (ACAP) Asia-Pacific Solar Research Conference (APSRC)
   December 2015 Brisbane Australia
   Poster Presentation entitled “Light Harvesting Upconversion Materials”

Table of Contents

List of Figures

absorption maxima, listed in Table 4.1. (B) S_1 fluorescence decay profiles of ZnTPP **2.4**, the ether and stilbene linked model compounds and polymers in toluene.

Figure 4.18: NCPU emission intensities in degassed toluene and the degassed coordinating solvent, THF, for the *p*-ether linked monomer *p*-EL mon **4.3** and the *p*-ether-linked polymer *p*-EL pol **4.6** at excitation wavelength of 532 nm.

Figure 4.19: (A) Power dependence of the upconverted emission intensity for the *p*-ether-linked model compound *p*-EL mon **4.3** in degassed toluene. (B) Power dependence of the upconverted emission intensity for the *p*-ether-linked polymer *p*-EL pol **4.6** in degassed toluene.

Figure 4.20: Transient absorption spectra of ZnTPP **2.4**, *p*-EL mon **4.3** and *p*-EL pol **4.6**.

Figure 4.21: (A) Transient absorption spectra of ZnTPP **2.4** and the model compounds **4.1 – 4.3** and (B) polymers **4.4 – 4.6**.

Figure 4.22: (A), (C) and (E) Kinetic traces of ΔOD for *p*-SL mon **4.1**, *m*-SL mon **4.2** and *p*-EL mon **4.3** respectively excited at pump excitation pulse energies of 1.2 mJ (green), 3.9 mJ (blue) and 8.2 mJ (red). (B), (D) and (F) Kinetic traces of ΔOD for *p*-SL mon **4.1**, *m*-SL mon **4.2** and *p*-EL mon **4.3** respectively shown with ΔOD normalized at the onset of decay to the 8.2 mJ pulse data.

Figure 4.23: Excited state decay pathways active in the monomeric zinc porphyrins upon exposure to a 532 nm wavelength excitation source in solution.

Figure 4.24: Kinetic traces of ΔOD for ZnTPP **2.4**, *p*-EL mon **4.3** and *p*-EL pol **4.6,** measured at their triplet absorption maxima of 473, 476 and 485 nm for ZnTPP **2.4**, *p*-EL mon **4.3** and *p*-EL pol **4.6** respectively. All samples were excited at pump excitation pulse energies of 8.2 mJ.

Figure 4.25: (A) Triplet kinetic traces of ΔOD for the *p*-EL pol **4.6** excited at pump excitation pulse energies of 1.2, 3.9 and 8.0 mJ. (B) Polymer triplet kinetic traces in (A) shown in the region of 20 to 25 μs after probe excitation for clarity of fast triplet decay component. (C) Polymer triplet kinetic traces for p-SL pol **4.4**, m-SL pol **4.5** and p-EL pol **4.6** at 8.2 mJ.

List of Tables

List of Abbreviations

2D	Two-dimensional
3D	Three-dimensional
AIBN	2,2-azobisisobutyronitrile
A_m	Model compound absorption intensity
A_p	Polmyer absorption intensity
AM	Air Mass
ASTM	American Society for Testing and Materials
ATRP	Atom Transfer Radical Polymerization
B	Molar mass of unfunctionalized pendant precursor unit
BM	Bohr Magneton
BODIPY	4,4-difluoro-4-bora-3a,4a-diaza-s-indacene
C	Pendant chromophore monomer unit molar mass
CdTPP	[5,10,15,20-tetraphenylporphyrinato] cadmium(II)
C_m	Concentration of chromophore units in a model compound sample
C_p	Concentration of chromophore units in a polymer sample
CTA	Chain Transfer Agent
DC	Downconversion
DF	Delayed fluorescence
DoPAT	Dodecylthiocarbonothioylthio)propanoic acid
DPA	Diphenylanthracene
E	Energy
EM	Electromagnetic

EQE	External quantum efficiency
ETU	Energy Transfer Upconversion
F	Percentage degree of polymer backbone functionalization
F_c	Fraction of chromophore monomeric unit mass contribution to total polymer mass in a sample
FF	Fill Factor
F_R	Fraction of residual mass in a polymer sample contributing to unfunctionalized backbone units and end groups combined
GPC	Gel Permeation Chromatography
Hetero-TTA	Heteromolecular triplet-triplet annihilation
HOMO	Highest Occupied Molecular Orbital
Homo-TTA	Homomolecular triplet-triplet annihilation
HWE	Horner-Wadsworth-Emmons reaction
hν	Photon
IC	Internal Conversion
ICP-OES	Inductively Coupled Plasma Optical Emission Spectroscopy
I_{in}	Incident irradiation of cell
ISC	Intersystem Crossing
J_{sc}	Short-circuit current density
k	Rate constant
kWh	Kilowatt hour
LCAO	Linear Combination of Atomic Orbitals
LUMO	Lowest Occupied Molecular Orbital
M	Monomer
MEH	Methoxy-Ethylhexyloxy
MgTPP	[5,10,15,20-tetraphenylporphyrinato] magnesium(II)

m_L	Magnetic Quantum Number
M_n	Number-Average Molecular Mass
***m*-SL mon**	*Meta*-stilbene linked monomer compound **2.2**
***m*-SL pol**	*Meta*-stilbene linked monomer compound **2.5**
MW_{FF}	Average molecular weight of a fully functionalized polymer
M_w	Weight-Average Molecular Mass
NCPU-TTA	Triplet-Triplet Annihilation mediated Non-Coherent Photon Upconversion
NMP	Nitroxide-Mediated Polymerization
$P^{\bullet}_m$	Propagating polymer radical (length m)
$P^{\bullet}_n$	Propagating polymer radical (length n)
PA	Peptide-Amphiphile
PCE	Power Conversion Efficiency
PDI	Polydispersity Index
PdOEP	[2,3,7,8,12,13,17,18-octaethylporphyrinato] palladium(II)
PdTPP	[5,10,15,20-tetraphenylporphyrinato] palladium(II)
PEG	Poly(ethylene glycol)
***p*-EL mon**	*Para*-ether linked monomer compound **2.3**
***p*-EL pol**	*Para*-ether linked polymer compound **2.6**
***p*-SL mon**	*Para*-stilbene linked monomer compound **2.1**
***p*-SL pol**	*Para*-stilbene linked polymer compound **2.4**
PPF	Post-Polymerization Functionalization
PPV	Poly(phenylene vinylene)
PtOEP	[2,3,7,8,12,13,17,18-octaethylporphyrinato] platinum(II)

PtTPP	[5,10,15,20-tetraphenylporphyrinato] platinum(II)
***p*-PV**	*Para*-phenylenevinylene
PV	Photovoltaic Device
PVA	Poly(vinyl alcohol)
QD	Quantum Dot
R	Alkyl Group
RAFT	Radical Addition-Fragmentation Chain-Transfer polymerization
ROMP	Ring Opening Metathesis Polymerization
$Ru(bpy)^{2+}$	Tris(Ruthenium(II))bipyridine complex
$Ru(dmb)^{2+}$	Tris(Ruthenium(II))dimethylbipyridine complex
S_1	First Excited Singlet State
S_2	Second Excited Singlet State
S_n	n^{th} Excited Singlet State
SQ	Shockley-Quiesser (limit)
T_1	First Excited Triplet State
T_n	n^{th} Excited Triplet State
T_s	Doubly excited triplet state
TPP	Meso-5,10,15,20-tetraphenylporphyrin
TTA	Triplet-Triplet Annihilation
TTET	Triplet-Triplet Energy Transfer
UC	Upconversion
UV	Ultraviolet
V_c	Concentration of of chromophore units in a polymer sample in units of mass per unit volume
V_{OC}	Open-Circuit Voltage
V_p	Concentration of total polymer in a polymer sample in units of mass per unit volume

x	Average number of chromophore pendant units in a polymer chain
y	Average number of unfunctionalized pendant precursor units in a polymer chain
z	Residual mass in a polymer chain due to end groups and non-pendant groups
ZnDBP	[5,15-bis-(3,5-di-*tert*-butylphenyl)porphyrinato] zinc(II) **2.2**
ZnDMP	[5,15,-dimesitylporphyrinato] zinc(II) **2.3**
ZnDPP	[5,10,15,20-tetraphenylporphyrinato] zinc(II) **2.1**
ZnTBP	[5,10,15,20-tetrakis-(3,5-di-*tert*-butylphenyl)porphyrinato] zinc(II) **2.5**
ZnTMP	[5,10,15,20-tetramesitylporphyrinato] zinc(II) **2.6**
ZnTPP	[5,10,15,20-tetraphenylporphyrinato] zinc(II) **2.4**
β-	Beta Position of Porphyrin Macrocycle
ε	Molar Extinction/Absorption Coefficient
η	Energy Conversion Efficiency
τ	Excited State Lifetime
Φ	Quantum Yield

Chapter 1

Introduction

1.1 Background

The rapid depletion of the Earth's fossil fuel resources over the last few decades has triggered a worldwide response to urgently seek renewable energy alternatives. Solar energy has become one of the most prominent renewable energy sources that has been projected to be able to meet global energy demand targets in the near future. As of 2018 only around 3% of the world's electrical energy is sourced from solar photovoltaics (PV - Figure 1.1).[1]

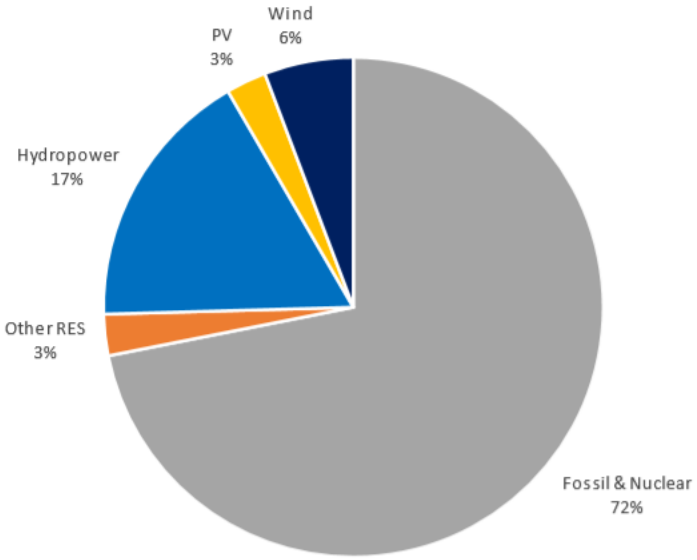

Figure 1.1: Global electrical energy generation by technology type in 2018 (IEA).[1]

The surge in research and development in the area of photovoltaic devices has seen the cost of solar PV modules drop over 90% in price per kW since 2009.[2] The prices of solar PV electrical energy generation are continuing to fall, with the global weighted-average levelised cost of electricity (LCOE) of solar PV ($0.085 US dollars per kWh) falling within the range of its fossil fuel counterpart ($0.049 - $0.174 US dollars per kWh) in 2018.[2] For the cost efficiencies of solar PV to exceed those that fossil fuel-based energy production offers, the efficiency of the chemical and physical processes that transform energy absorbed from solar radiation into electrical energy must be improved. Currently, the average energy conversion efficiency (η) of the most common commercial solar cells, those made from poly-crystalline silicon wafers, ranges between 13-16%,[3] while the highest efficiency commercial monocrystalline silicon cells exceed $\eta = 22\%$.[4]

Many photovoltaic technologies that use alternative semiconducting materials to silicon are of high research interest, such as organic solar cells and perovskite cells.[5] These cells may exceed silicon based cells in terms of cost efficiency in the future if their energy conversion efficiencies can be further increased. Significant research has been directed at fine-tuning the properties of these solar cells in order to boost efficiencies, however fundamental limitations exist that place an upper limit on the maximum achievable efficiencies of the PV systems that are currently in widespread development.[6] The discovery of practical methods that bypass or transcend the energy conversion efficiency limitations that solar cells are subject to, remains one of the most important objectives towards achieving the global transition from fossil fuel dominant energy resources to majority renewable energy resources.

1.2 Band Gap Energies and the Shockley-Queisser Limit

To understand the major losses in efficiency that occur in solar cells, it is necessary to understand the process solar cells utilize in order to convert sunlight energy into electricity. The first step in the process of producing electricity in a solar cell is to create an exciton, a bound electron-hole pair. In an inorganic cell, such as the commercially ubiquitous doped poly-crystalline silicon cell, excitons are typically formed when a photon is absorbed by the n-type (electron-donor doped) material that has energy equal to or greater than the band gap energy, which is the energy required to excite an electron from the valence band to the conductance band

of the n-type material. The exciton is then able to diffuse to the interface between the p-type and n-type materials, known as the p-n junction, and undergo charge separation of the electron and hole from the bound exciton pair for eventual diffusion of the hole and electron to the anode and cathode respectively. Most solar cells are 'single-junction' cells, meaning that they possess one type of unique p-n junction in the active layer, formed between only two unique semiconductor materials, and therefore exciton formation is controlled by the absorbance of light equal to or higher than only one band gap energy. For a solar cell with an active layer made from organic compounds, the process described for the inorganic solar cell holds, with the highest occupied molecular orbitals (HOMOs) representing the valence bands, and the lowest unoccupied molecular orbitals (LUMOs) representing the conductance bands. In organic solar cells, the bulk p-type semiconductor materials are called electron donors and the bulk n-type semiconductor materials are called electron acceptors.

Single-junction solar cells are subject to several processes that reduce the amount of incident energy from sunlight that can be converted into electricity, as outlined in Figure 1.2 below. Of the energy loss processes detailed in Figure 1.2 below, thermalization of electrons that absorb photons with greater energy than the band gap energy, and transparency of the donor material to photons with energies lower than the band gap energy result in the biggest losses of energy from incident sunlight in a single-junction solar cell.[7,8]

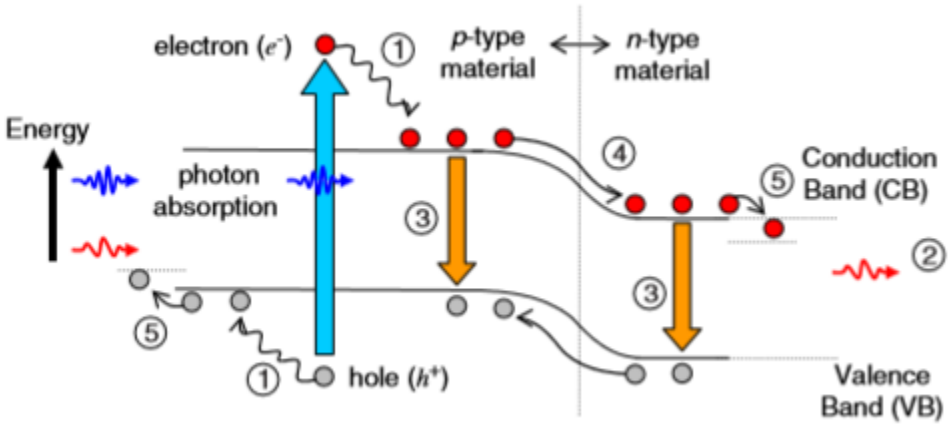

Figure 1.2: Loss processes in a single-junction solar cell: 1) Lattice thermalization loss; 2) Transparency; 3) Recombination loss; 4) Junction loss and 5) contact voltage loss. Figure reproduced from the work of Richards.[7]

These losses are a direct manifestation of the mismatch between the solar radiation distribution (Figure 1.3 below) and the band gap energy of a single junction device. It is therefore a primary objective to harvest a larger portion of the solar spectrum in order to increase overall efficiency of PV devices.

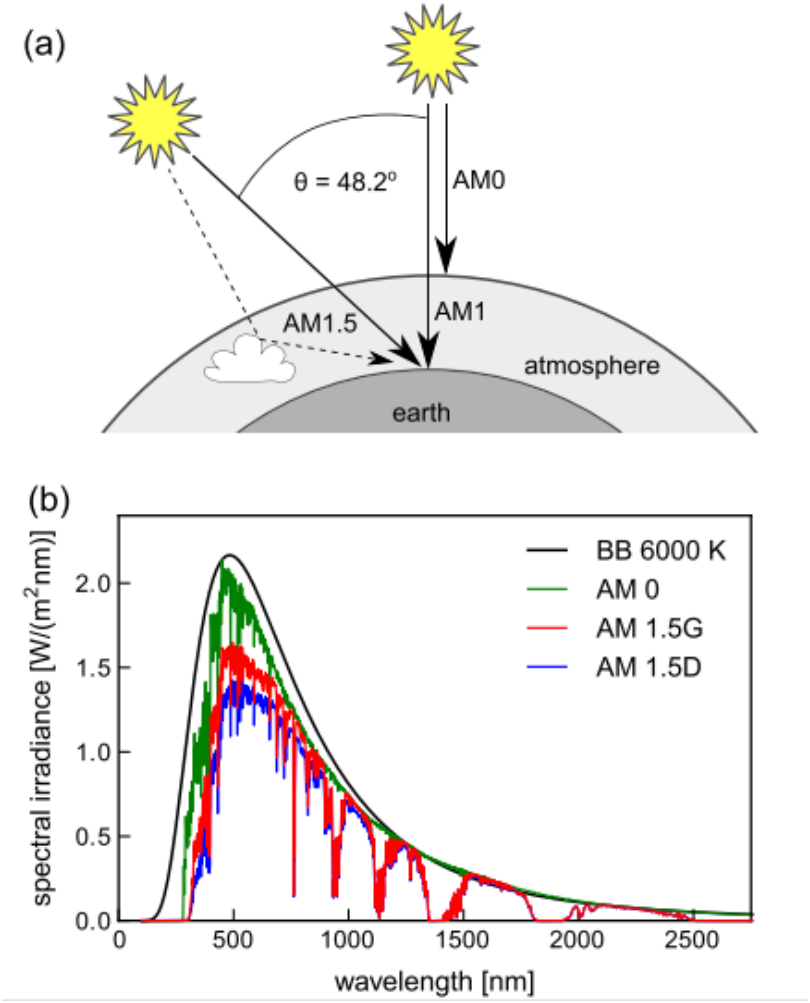

Figure 1.3: (a) Schematic representation of the spectral irradiance outside the Earth's atmosphere (AM 0) and on the Earth's surface for direct sunlight shown by a solid arrow (AM 1.5D) and the direct sunlight together with the scattered contribution from atmosphere (solid and dashed arrow) integrated over a hemisphere (AM 1.5G). (b) Spectral irradiance according to ASTM G173-03 in comparison to the spectrum used by Shockley and Queisser of a black body with a surface temperature of 6000 K (BB 6000 K). Figure reproduced from the work of Rühle.[9]

The efficiency losses described above were first quantitatively summarized in the calculations of Shockley and Queisser,[6] with their work contributing to a maximum theoretical incident light energy to power conversion efficiency of 30% for single p-n junction solar cells with band gap energy of 1.1 eV, approximating the sun to act as a black body radiator with surface temperature of 6000K (spectral irradiance distribution for a 6000K black body shown as black line curve in Figure 1.3 (b)). The true incident spectral irradiance distribution was later refined by the American Society for Testing and Materials (ASTM),[10] taking into consideration the average angle of the incident light to the surface of the Earth, and the scattering and absorption of light by the atmosphere before striking the surface of the Earth, to give a spectral irradiance distribution known as AM (air mass) 1.5 Global radiation (incident radiation path shown in Figure 1.3 (a), spectral distribution shown in red in Figure 1.3 (b)). The efficiency limit for single junction PV devices, known as the Shockley-Queisser Limit, was later revised in consideration of the AM 1.5G spectral irradiance distribution, to give an upper limit of 33.16% for PV devices with a band gap of 1.34 eV (Figure 1.4).[9]

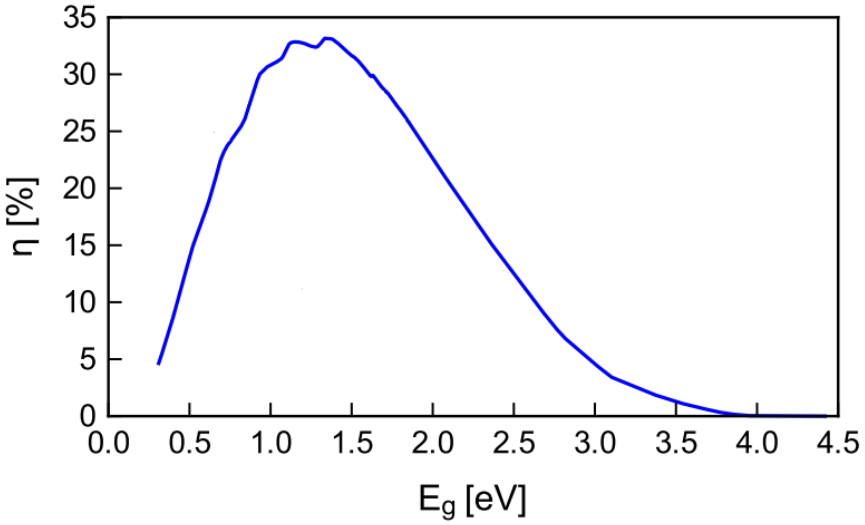

Figure 1.4: Shockley-Queisser limit for the efficiency (η) of a single-junction solar cell as a function of band gap energy operating at 298.15 K under AM 1.5 conditions. Figure adapted from the work of Rühle.[9]

1.3 Exceeding the Shockley-Queisser Limit

In order to improve the maximum theoretical limit PCEs that can be achieved by solar energy harvesting PV devices, the SQ limit must be overcome. As the SQ limit concerns single band gap devices only, there is great potential to develop PV devices that surpass the 33.16% PCE set by the SQ limit, by creating PV devices that absorb or transform sunlight energy using multiple band gaps. Previously explored methodologies that employ multiple band gaps in pursuit of exceeding the SQ limit include tandem cells[11] and multi-junction solar cells,[12-15] the latter of which has been implemented in producing the highest recorded PCE for a solar cell to date at 46%.[14] Although the efficiencies of multiple junction cells are far higher than that of single-junction cells, they are far more expensive to produce due to gallium, indium, and germanium that make up the majority of the cell layers.[12-17] Optimization of the current-mismatch between the subcells in tandem cells and multi-junction solar cells is an additional challenge that is often difficult to address.[18]

1.3.1 Photon Downconversion

Photon downconversion involves the transformation of one photon into two or more photons or excited states with lower energy. When a photon downconverting layer is integrated into a solar cell with a low band gap, multiple excitons are able to be formed from a single photon being absorbed with at least twice the energy of the band gap, effectively increasing the concentration of useful energy that can be converted to current. Photon downconversion aims to exceed the Shockley-Quiesser limit by minimizing losses of energy that would normally occur due to thermalization of electrons that have absorbed photons with energies that exceed that of the band gap of the active layer material in a solar cell. Photon downconversion is thus best applied to enhancing the efficiency of solar cells such as silicon based cells, which typically have light-absorbing layers with band gaps below the optimum band gap of 1.34 eV outlined by the SQ limit. It has been theorized that maximum efficiencies of up to 39.63% can be achieved by incorporation of a downconverter which contributes just one additional source of exciton-forming energy to a solar cell[19].

The majority of downconverting materials studied in the literature are those based on energy transfer between excited states of trivalent rare-earth ions. An example described by Wegh *et al.* for Gd^{3+} sensitizers and Eu^{3+} energy acceptor ions is shown in Figure 1.5 below.[20] For downconversion to proceed using these trivalent rare-earth ions, a photon is absorbed by a downconverting sensitizer first (purple arrow in Figure 1.5), followed by energy transfer to an acceptor ion with an excited energy level of similar energy to the energy lost by the downconverting sensitizer in the energy transfer process (1 in Figure 1.5). Upon completing the first energy transfer step, the downconverting sensitizer occupies an intermediate excited state, from which it can then participate in an additional energy transfer step (2 in Figure 1.5) to another energy acceptor ion, relaxing to its ground state upon energy transfer. The two energy acceptors could then independently transfer their energy to two donor sites in the active layer of a solar cell via fluorescence (red arrows in Figure 1.5), resulting in an efficiency increase in the cell. Other materials used for downconversion include Tb^{3+} and Yb^{3+} doped $Sr_3Gd(PO_4)_3$ phosphors[21], graphene quantum dots[22] and ZnS nanoparticles[23].

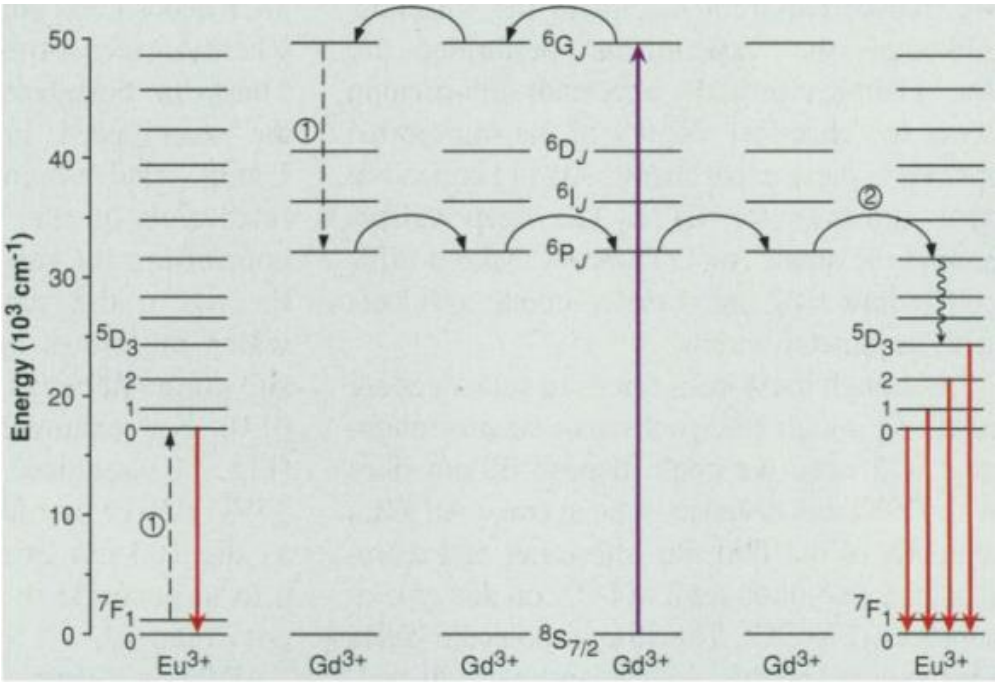

Figure 1.5: Example of photon downconversion process utilizing Gd^{3+} sensitizers and Eu^{3+} energy acceptor ions described by Wegh *et al.*[20] The circled number 1 indicates the first energy transfer step from Gd^{3+} to Eu^{3+}. The circled number 2 indicates the second energy transfer step from Gd^{3+} to Eu^{3+}.

Graphene[22] and ZnS[23] QDs have been successfully integrated as photon downconverters in solar cells with small but significant increases in PCE observed, however major optimization is required for these downconversion materials to be considered for large-scale production. Lanthanide ions are weakly absorbing ($\varepsilon = <10\ M^{-1}cm^{-1}$)[24] and therefore require a thick layer of UC material to be integrated into a solar cell in order to produce any significant increase in overall efficiency. The high cost and low abundance of rare-earth elements limit the potential of lanthanide ion-based photon DC systems to be produced on large scales required for commercial viability.

Singlet fission is an alternative form of photon DC that involves formation of two triplet states from one singlet state. Singlet fission has been observed in materials such as bisthiophene-dihydropyrrolopyrrole-dione/benzodithiophene donor-acceptor conjugated small molecules and polymers in solid films,[25] diketopyrrolopyrrrole-rylene supramolecular films[26] and ordered pentacene aggregates.[27] Although the potential of singlet fission as a method to overcome the Shockley-Queisser limit has come of interest recently, methods to extract the energy of the product triplet states for further use in photovoltaic applications have proven difficult to come by. Because triplet-to-singlet transitions are spin forbidden, radiative relaxation from the triplet states of organic molecules is limited and therefore re-absorption of triplet emission by solar cell active layers is not a plausible method of utilizing the triplet exciton energy produced from singlet fission. Only very recently have triplet excitons produced by singlet fission in tetracene crystals demonstrated charge separation across the tetracene-silicon interface in a heterojunction solar cell, leading to a small but measureable contribution of cell current generated by the singlet fission layer.[28] Of the methodologies currently being pursued in order to exceed the SQ limit, photon upconversion may be one of the most promising. Photon upconversion is outlined in detail in section 1.4.

1.4 Photon Upconversion

Increasing the band gap energy of the electron donor material in a solar cell increases the maximum open-circuit voltage (V_{OC}) that the cell can operate at. The V_{OC} of a solar cell is directly proportional to the energy conversion efficiency (η), of the solar cell, related through the following equation:

$$\eta = \frac{V_{OC} \times J_{SC} \times FF}{I_{in}} \qquad 1.1$$

Where V_{OC} is the open-circuit voltage in volts (V), J_{SC} is the short-circuit current density in mA/cm^2, FF is the fill factor, and I_{in} is the incident irradiation of the cell in W/cm^2. Solar cells with band gap energies greater than the SQ limit could therefore have the potential to produce higher power output than typical silicon solar cells, for which the band gap lies around 1.1 eV.[29] In order for an increase in η to occur in the higher band gap solar cells, the incident energy available for the electron donor material to utilize must increase. As the solar radiation distribution keeps this parameter relatively fixed at a given incident photon wavelength, energy that is not being utilized by direct band gap absorption in the cell must be transformed in such a manner that it can be fed back into the cell. Transformation of sunlight energy that is not used by direct band gap absorption can be achieved through photon upconversion (UC).

UC is a process that involves the combining of two or more photons to produce an excited electronic state, for which the energy difference between the ground state and the excited state exceeds the energy of any one of the incident photons contributing to the upconverted product excited state energy. Photon upconversion enables a significant portion of energy that would normally be lost via transparency of low energy photons in a single junction or single band gap material to be fed back into the solar cell as useful high-energy photons. Increased absorption of high-energy photons generated through UC processes, by wide band gap solar cells with large V_{OC}, would lead to increases in the overall energy conversion efficiency η of a single-junction device. The integration of a single UC layer into a solar cell has been calculated to boost the theoretical maximum efficiency of a single-junction device up to 63.2% under concentrated sunlight conditions and 47.6% under non-concentrated sunlight conditions.[30]

Several widely studied semiconducting materials with high commercial potential for solar cell production typically have band gap energies that lie above the optimal energy of 1.34 eV determined by the Shockley-Quiesser limit. These semiconducting materials include organic conjugated chromophores, GaAs, CdTe and perovskites such as $CH_3NH_3PbX_3$ where X is a halide.[5] Solar cells that employ organic-based semiconducting materials for example, are of high commercial interest currently due to their potential for low cost, easily fabricated, flexible solar cells. One of the major drawbacks of commercializing organic solar cells is that they suffer from lower energy conversion efficiencies than silicon-based solar cells in general. Significant enhancement of wide band gap cell efficiency using UC methods may contribute toward solar cells such as those made from organic semiconducting materials overtaking silicon as the dominant cost effective commercial photovoltaic technology in the near future.

1.4.1 Coherent Photon Upconversion

Two-photon absorption is a UC mechanism that involves the simultaneous absorption of two photons in a small region of space in order to populate an excited state of greater energy than any one individual incident photon. Achieving this requires that the waveform of the photons from the incident light source are highly spatially and temporally in phase in order to increase the probability of simultaneous excitation. If there exists a high degree of phase matching in the incident photon source it is said to be coherent. For two-photon absorption to occur, the light source must also produce a high number of photons per unit area that are able to strike the two-photon absorbing material. The coherent and intense radiation source required for observing two-photon absorption typically requires a laser to produce. In order to implement UC systems in solar cells, the chosen UC mechanism must be able to operate using sunlight as the photon source. Sunlight is non-coherent and of relatively low radiant intensity, thus cannot provide the conditions to allow currently known two-photon absorption materials to feed UC energy into a solar cell. Sequential excited state absorption,[31] photon avalanche[32] and cooperative energy pooling[33] are additional examples of physical mechanisms that have been shown to demonstrate photon upconversion, which require either coherent or intense light sources to produce UC states. The most successful photon upconversion mechanisms for solar cell applications currently in the literature have been those that do not require coherent photon sources, referred to in this

thesis as Non-Coherent Photon Upconversion (NCPU) mechanisms. NCPU mechanisms include energy transfer upconversion (ETU)[34-39] for inorganic UC materials, and triplet-triplet annihilation (TTA)[40-82] for organic based UC materials. ETU and TTA are discussed in sections 1.4.2 and 1.4.3 below.

1.4.2 Energy Transfer Upconversion (ETU)

To achieve energy transfer upconversion (ETU), a photon ($h\nu_1$ in Figure 1.6) is first absorbed by a sensitizer species in its ground state (G) to populate an excited state (E1 in Figure 1.6), followed by excited state energy transfer (ET 1 in Figure 1.6) to an upconverting species in order to populate an intermediate excited state (E2 in Figure 1.6) in the upconverting species. An additional energy transfer step (ET 2 in Figure 1.6) from a second excited sensitizing species proceeds to populate an excited state (E3 in Figure 1.6) in the activator, which can radiatively relax ($h\nu_2$ in Figure 1.6) with energy released higher than any of the energies initially transferred by the sensitizing species to the activator.

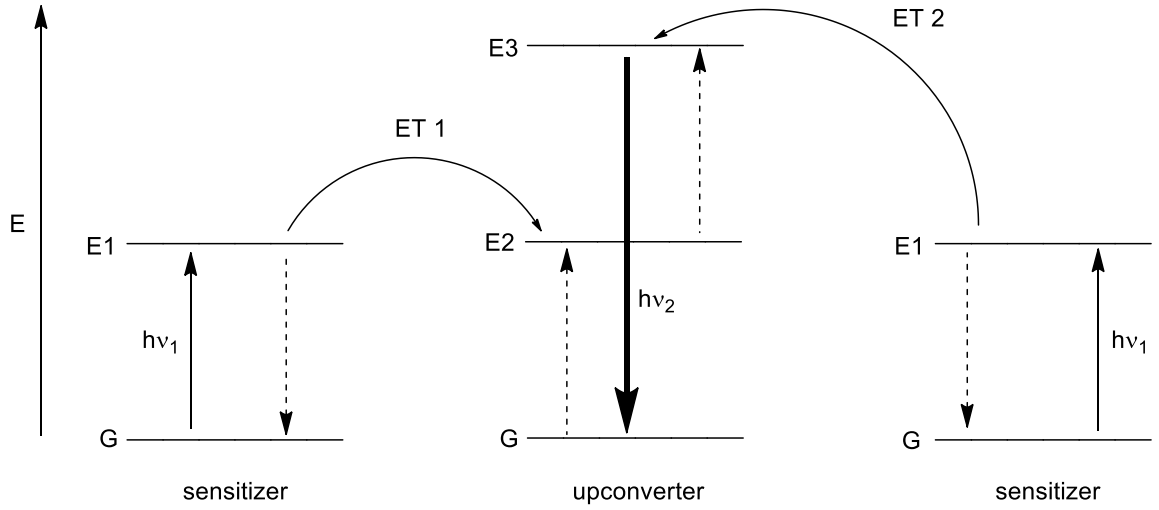

Figure 1.6: Generic mechanism for an ETU process. The dotted arrows indicate non-radiative electronic transitions whereas the solid arrows indicate radiative electronic transitions.

Typically the activator species in ETU processes are trivalent lanthanide ions such as Er^{3+} ions,[34,38] Tm^{3+} ions[37,38] or Nd^{3+} ions[37] that possess sharp 4f-4f orbital transitions due to filling of the 5s and 5p shells, hence radiatively relaxing in the visible region of the EM spectrum. As

these lanthanides contain multiple accessible orbital energy levels that are closely spaced, appropriate energy levels exist such that intermediate states can be populated for sequential energy transfer. As the f-f transitions are strongly forbidden under the Laporte rule, these intermediate excited energy levels have extended lifetimes on the order of milliseconds,[83] faciliatating non-coherent photon upconversion at low excitation densities. Yb^{3+} ions[34,38]or Er^{3+} ions [35,37] are used as energy sensitizers as they absorb wavelengths of light with energies that are appropriately matched to the energy spacings of lanthanide ion orbitals that lie between the ground and emitting energy levels.

Although ETU systems have been implemented in solar cell efficiency-enhancing applications,[34-36,39] including those studied by Song *et al.* in Figure 1.7 below,[34] only a small range of the solar spectrum can be utilized for upconversion due to limited numbers of viable energy sensitizers that can be integrated into inorganic crystalline matrixes. The materials used in ETU based photon UC systems suffer from similar issues as those mentioned for lanthanide ion based photon DC systems mentioned in **section 1.3.2**, as Yb^{3+} and Er^{3+} ions weakly absorb light, thick UC layers are required, and materials involved have high costs. Triplet-triplet annihilation mediated upconversion will be discussed in detail in the following section of the introduction.

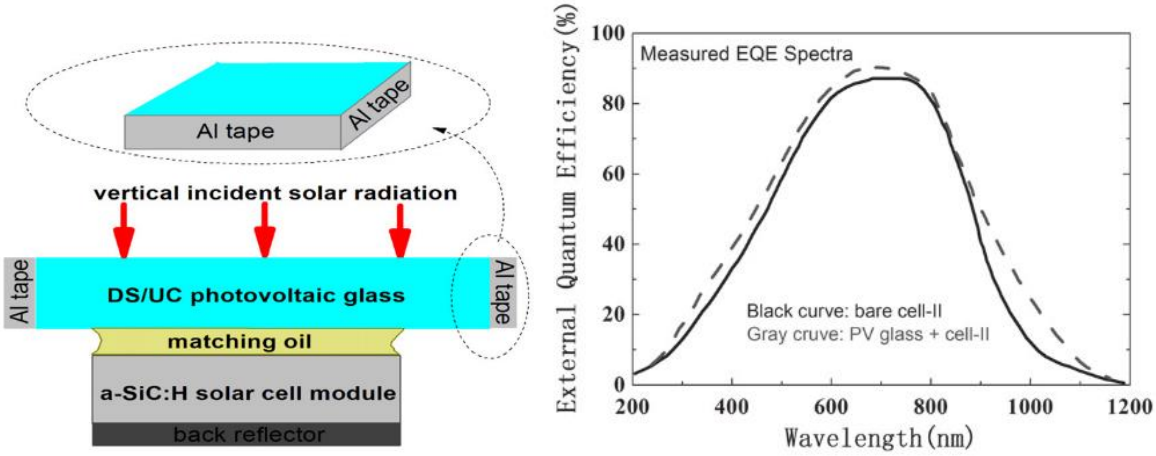

Figure 1.7: (left) An illustration of an a-SiC:H PV module integrated with an ETU layer developed by Song *et al.*[34] (labeled as a-SiC:H cell: II) covered with a PV glass sample. (right) The measured EQE spectra of the a-SiC:H cell-II with (gray dotted curve) and without (black solid curve) the PV glass.

1.4.3 Triplet-Triplet Annihilation (TTA)

1.4.3.1 Background

In 1958, Richard Williams observed an interesting phenomenon concerning the emission properties of various polycyclic aromatic hydrocarbons in the vapour phase: an identical emission spectrum to the one expected from S_1 to S_0 relaxation was obtained after a significant time delay, in addition to the aforementioned prompt fluorescence.[84] Williams reasoned that this 'delayed fluorescence' (DF) was attributed to a reversible formation of non-emissive excited state dimers AA* (eq. 1.2), formed between one excited chromophore (A*) in the singlet state and another ground state chromophore (A), which upon dissociation of the excited state dimers after some time delay (eq. 1.3), allowed for the recovery of one ground state chromophore and one single chromophore in its excited state that could fluoresce (eq. 1.4) as expected in the same manner as for prompt S_1 to S_0 relaxation.

$$A^* + A \rightarrow AA^* \tag{1.2}$$

$$AA^* \rightarrow A + A^* \tag{1.3}$$

$$A^* \rightarrow A + h\nu \tag{1.4}$$

C. A. Parker argued in 1962 that the mechanism proposed by Williams for the delayed fluorescence of polycyclic aromatic hydrocarbons could not explain the quadratic relationship between the intensity of the delayed fluorescence and the rate of light absorption in a sample of anthracene.[40] Parker conceived a new mechanism involving the quenching of the energies of two chromophores (eq. 1.5) in their triplet state (^{3}A) that would form the higher excited state X required to observe delayed fluorescence in one of the chromophores. This higher excited state X was suggested to exist within a dimer as or as a single molecule, and therefore the ground state chromophore A is regenerated either upon formation of X or dissociation of the dimer X, outlined in parentheses in eq. 1.5 and 1.6 respectively. Regardless, X could produce the excited singlet state (A*) leading to delayed fluorescence (eq. 1.4). The mechanism suggested by Parker justified the delay time due to the extended lifetimes of triplet states, and explained the quadratic relationship between DF and absorption rate as a product of a bimolecular second order excited state reaction. The process outlined by Parker is today widely referred to as TTA.

$$^3A + {}^3A \rightarrow X(+A) \quad (1.5)$$

$$X \rightarrow A^*(+A) \quad (1.6)$$

$$A^* \rightarrow A + h\nu \quad (1.4)$$

Triplet-triplet annihilation (TTA) is one of the most promising photon upconversion mechanisms currently being developed for photovoltaic applications. What makes TTA-UC systems of such high interest is that they are constructed from organic compounds, and as such they require relatively low cost raw materials, are able to be processed in solution, and can be printed roll-to-roll on flexible substrates. Unlike ETU, organic triplet sensitizers and UC fluorescence emitters have the potential to be tuned to absorb a wider range of the solar radiation spectrum, and therefore accommodate UC efficiency enhancement in a greater variety of electron donor or p-type materials than ETU sensitizers. Wu *et al.* have been able to apply various modifications to the core triplet sensitizer, 4,4-difluoro-4-bora-3a,4a-diaza-s-indacene (BODIPY), such that the absorption of a series of BODIPY sensitizers spanned from the green to the red region of the UV-visible spectrum.[41] The long lifetimes of the triplet excited states of sensitizer molecules, exceeding milliseconds in some cases for metalloporphyrin derivatives,[85] and the high extinction coefficients of triplet sensitizers such as zinc tetraphenylporphyrin, at over 5 x 10^5 $M^{-1}cm^{-1}$,[46] allow UC to proceed under non-coherent light conditions with low excitation densities making TTA appropriate for solar energy harvesting.

1.4.3.2 Mechanisms of Triplet-Triplet Annihilation

For TTA to occur, two molecules in their excited triplet state must come in close enough proximity such that they share a degree of orbital overlap, and at least one of those molecules possesses an energy level that lies at close to double the energy of the triplet states of the two molecules. Dexter energy-transfer[86] can then proceed (mechanism shown in Figure 1.8), leaving one molecule in its ground state, and the other in a higher excited state, with the energy of this product excited state being higher than that of any photon energy contributing to the initial triplet states in the electron-transfer encounter.

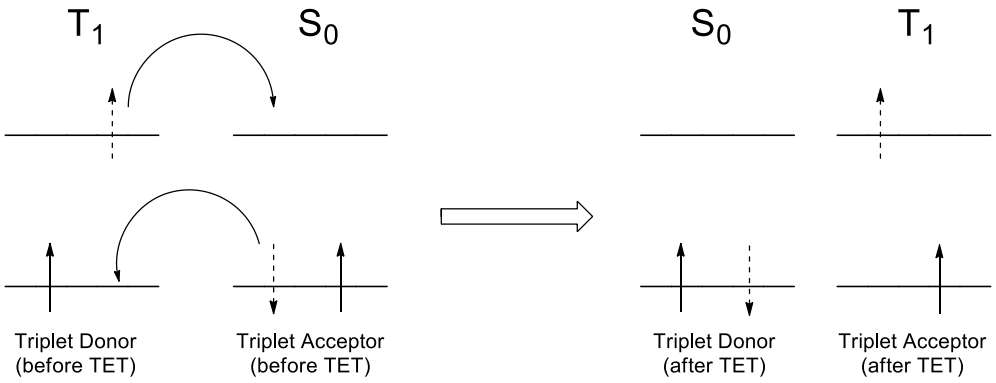

Figure 1.8: Mechanism of Dexter electron-exchange energy transfer.

In the case where the product state of TTA is a sufficiently long-lived singlet state, radiative relaxation to the ground state produces upconverted energy in the form of anti-Stokes shifted fluorescence. TTA can operate via two major pathways: if the triplet state of the annihilator cannot be populated efficiently after absorption of a photon, heteromolecular TTA (Section **1.4.3.2.1** below) must be employed; if the triplet state of the annihilator can be populated efficiently after absorption of a photon, homomolecular TTA (Section **1.4.3.2.2** below) is possible if there exists an excited state higher in energy than S_1 that can be populated upon encounter of two annihilators in their triplet states.

1.4.3.2.1 Heteromolecular TTA

In most annihilating/emitting species, the energy separation between their first singlet state (S_1) and their first triplet state (T_1) is high, which makes intersystem crossing (ISC) from S_1 to T_1 unfavourable due to insufficient vibrational energy level overlap between the S_1 and T_1 electronic energy levels. Since excitation from the ground state S_0 directly to T_1 is spin forbidden, these emitting molecules require triplet energy to be transferred to them from sensitizer molecules via Dexter electron-exchange. The overall heteromolecular TTA process is outlined in Figure 1.9. Common triplet sensitizers for heteromolecular TTA include metalloporphyrin derivatives,[49,50,56-58,60,61,63-65,72,73] functionalized BODIPY analogues,[41,53] and derivatives of Ru(II) tris (4,4'-dimethyl-2,2'-bipyridine) complexes[51,52,54,55] as shown in Figure 1.10. Triplet sensitizer molecules are able to strongly absorb light, and efficiently transform the absorbed photon energy into an excited triplet state, typically having high ISC quantum yields. The ISC quantum yields of the triplet sensitizer palladium tetraphenylporphyrin (PdTPP) is close to unity.[85]

Note: Throughout this thesis, the term 'heteromolecular TTA' (hetero-TTA) is used to describe the process in which TTA is mediated through absorption of light of a species that may be different to the species participating in the annihilation encounter (ie. a two-component system with absorber and annihilator designed to perform independent functions). Similarly, 'homomolecular TTA' (homo-TTA) refers to a TTA system where the light-absorbing molecule is also the molecule designed to participate in the TTA encounter complex (one-component system). The use of the terms 'hetero-TTA' or 'homo-TTA' in this thesis do not refer to the nature of the species in the annihilation encounter itself (although for homo-TTA this is implied by a one-component system). Although the molecular species in the TTA encounter is typically of the same nature in two-component ('heteromolecular') systems, it is still possible for TTA to proceed when the two molecules in the encounter complex are different molecular species.

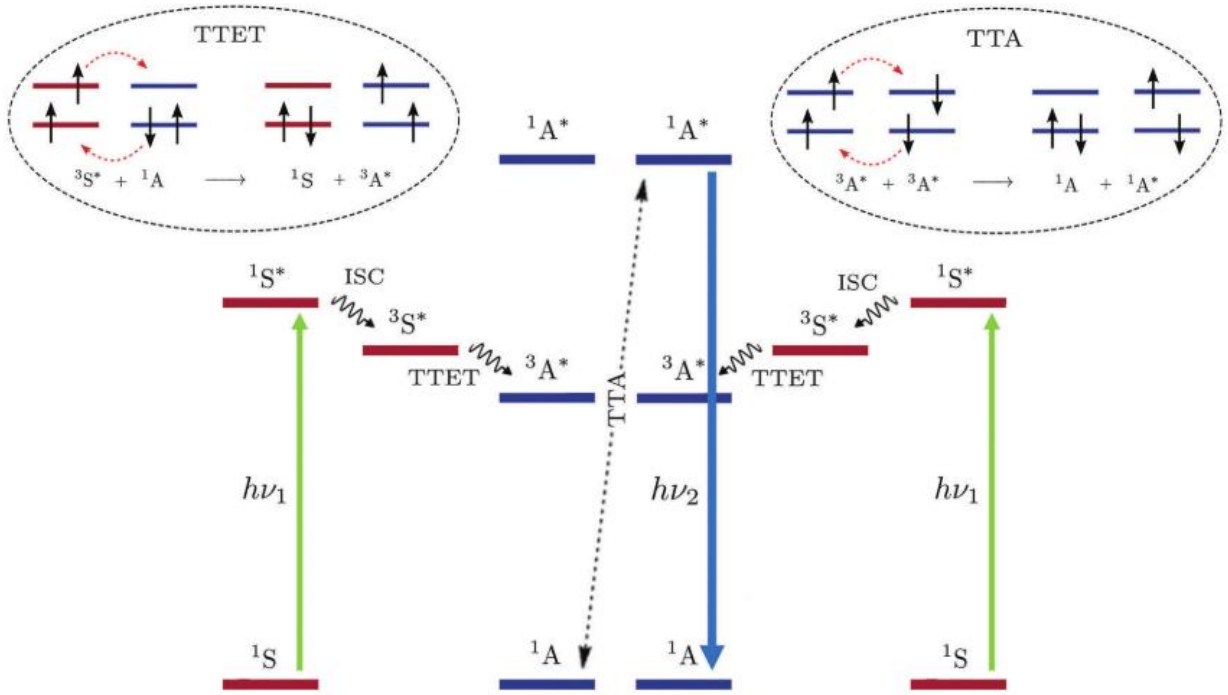

Figure 1.9: A Jablonski diagram of heteromolecular triplet–triplet annihilation photon upconversion, reproduced from Gertsen *et al.*[44] The two insets are schematics of the electron rearrangements in the highest occupied molecular orbitals (HOMOs) and lowest unoccupied molecular orbitals (LUMOs) of the sensitizers, S, and annihilators, A, during triplet–triplet energy transfer (TTET) and triplet–triplet annihilation (TTA). ISC denotes intersystem crossing.

Annihilator molecules explored in the literature include 9,10-diphenylanthracene (DPA),[40,51,55-59] rubrenes,[60,61] pyrenes[62,63] and perylenes[64,65] as seen in Figure 1.10 below. One of the benefits of annihilator molecules used in heteromolecular TTA systems is their high fluorescence quantum yields upon relaxation from S_1 to S_0, resulting in minimal energy losses from the upconverted product state. In the case of rubrene[87] and DPA,[88] conversion of S_1 directly to S_0 is quantitative in solution. DPA derivatives have exhibited fluorescence quantum yields of up to 0.87 as neat cast films and 0.95 in single crystalline form,[89] and triplet lifetimes on the order of milliseconds,[88] making them one of the most popular candidates for annihilating species in heteromolecular TTA systems designed for PV applications.

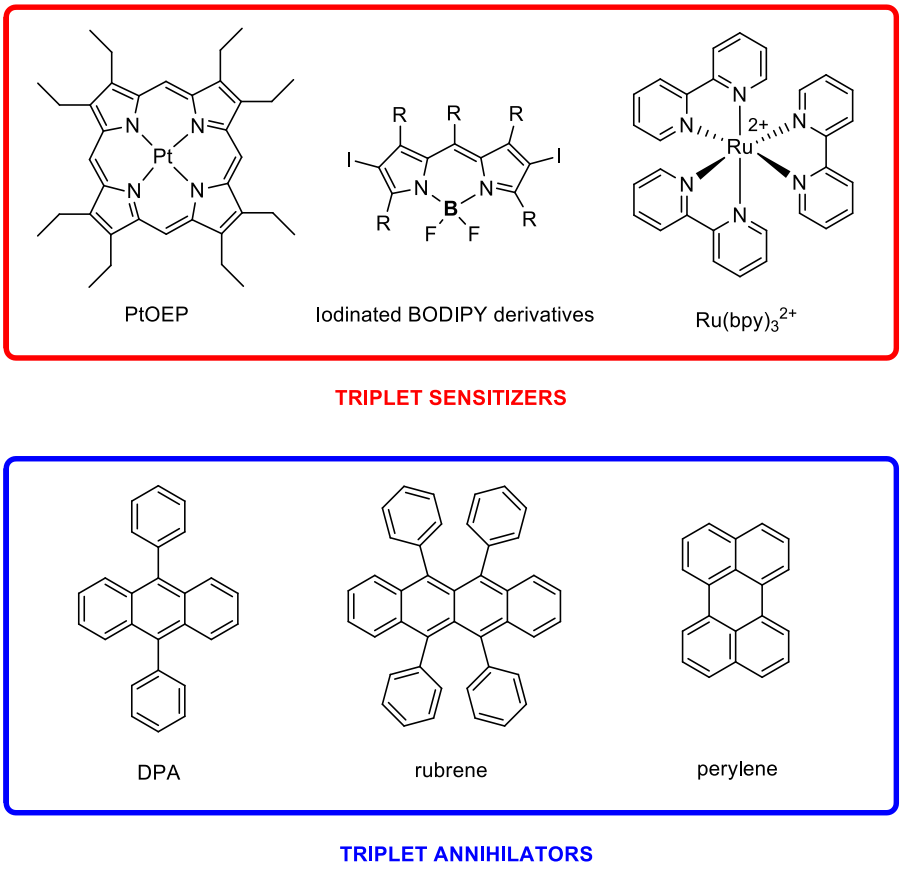

Figure 1.10: Structures of common triplet sensitizers and annihilator/emitters employed in heteromolecular TTA-UC systems.

1.4.3.2.2 Homomolecular TTA

In some cases, a triplet sensitizer in its triplet state is able to perform TTA with another triplet sensitizer of identical nature, without the need to transfer its excited state energy to a separate annihilating species, thus acting as a dual absorber-upconverter. The aforementioned process is referred to as homomolecular TTA (homo-TTA). For homo-TTA to proceed within a species acting as a dual absorber-upconverter, there must exist an energy level $E(X_n)$ within the electronic structure of the species such that the value of $2E(T_1) - E(X_n)$ is positive but small.[47] If the value of $2E(T_1) - E(X_n)$ is negative, population of the higher energy excited state upon TTA would require thermal activation from a vibration energy level below the desired product

electronic energy level, and if the value of $2E(T_1)$ - $E(X_n)$ is positive but large, the process is likely to require a significant change in vibrational energy to reach the product state and is therefore Franck-Condon forbidden.[90] For $2E(T_1) \sim E(X_n)$ to hold if X_n is S_1, T_1 must have an efficient mechanism for being populated considering ISC is improbable due to the large energy separation between S_1 and T_1. Regardless, such a TTA pathway proceeding though ISC would not yield overall UC energy since excitation to S_1 for further population of T_1 would only recover the S_1 state upon TTA, and intrinsically constitute an energy loss process. If a higher triplet state $T_{n>1}$ is populated upon homo-TTA, the energy of this state would likely decay back to T_1 via rapid IC in another energy loss process.

In most studied homo-TTA systems, the product electronic state resulting from a TTA encounter from which UC energy is extractable is a higher singlet excited state $S_{n>1}$, usually S_2. Although spin allowed, radiative transitions from states $S_{n>1}$ are forbidden by Kasha's rule[91] for most chromophores. Kasha's rule states that the radiative transition of excited molecules within a given multiplicity proceeds from the lowest excited state of that particular multiplicity due to the energy separation between S_1 and $S_{n>1}$ typically being small, increasing the likelihood of wavefunction overlap of vibronic states between S_1 and $S_{n>1}$ and therefore facilitating rapid IC. In a select few organic molecules, the energy separation between S_1 and S_2 is considerably large, increasing the lifetime of S_2 such that fluorescence is competitive with IC.

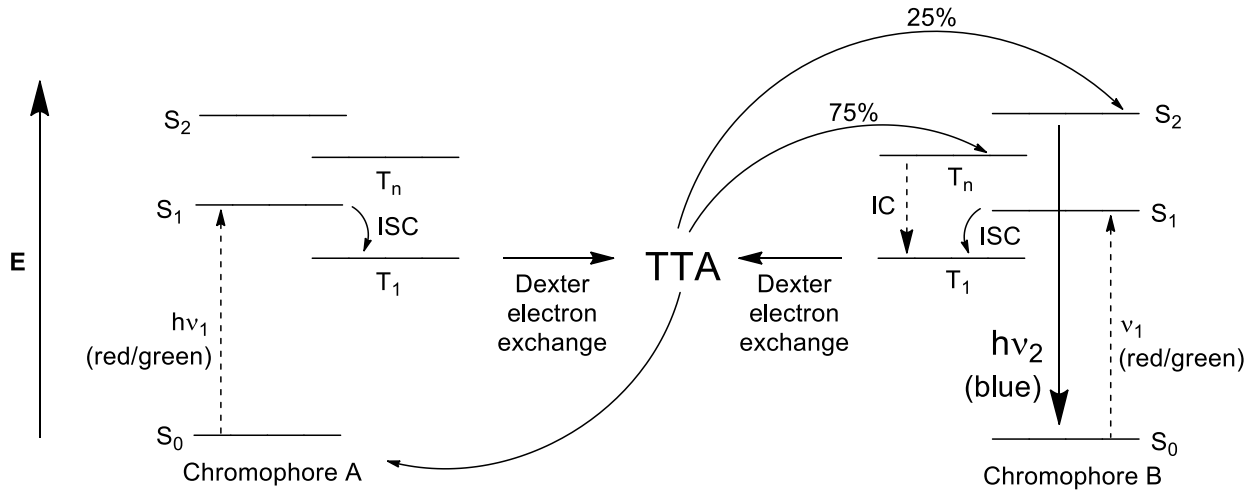

Figure 1.11: An energy level diagram illustrating the process of homomolecular triplet–triplet annihilation (TTA) in a dual absorber-upconverter system. IC is internal conversion and ISC is intersystem crossing. Chromophore A and B are two separate molecules of identical nature. TTA will yield both S_2 and T_n ($n > 1$) in a spin-statistical ratio of 1:3. Absorbed low energy photons are represented by $h\nu_1$ while delayed fluorescence from S_2 is represented by $h\nu_2$.

Delayed UC fluorescence from the S_2 state as a result of TTA has been observed for metalloporphyins,[46,48,70,78,81,82] azulenes,[67-69] and aromatic thiones[66] as seen in Figure 1.12 below. Although azulene and aromatic thione derivatives exhibit delayed UC fluorescence from the S_2 state as a result of TTA, self-mediated population of the T_1 state is inefficient, and the T_1 state is relatively short-lived at room temperature in solution (azulene for example has $\Phi_{ISC}(S_1 \rightarrow T_1) = 4 \times 10^{-6}$,$\tau(T_1) = 48$ μs),[69] making them poor candidates for homo-TTA. The most promising candidates for homo-TTA-UC are the derivatives of zinc(II) porphryins, for which an example Jablonski diagram for homo-TTA is shown in Figure 1.11. Porphyrins and metalloporphyrins are further discussed in detail in section **1.5** of the introduction chapter.

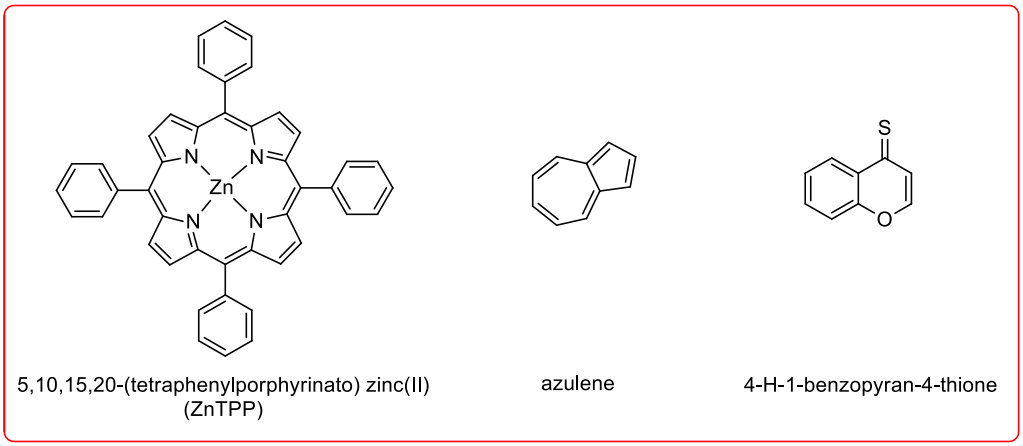

Figure 1.12: Structures of common dual absorber-upconverter molecules employed in homomolecular TTA-UC systems producing delayed fluorescence from the S_2 state.

As the S_2 state of zinc(II) metalloporphyins is relatively long-lived ($\tau(S_2)$ = 1.45 ps in benzene)[92] compared to metalloporphyin triplet sensitizers with heavier central metal ions (eg. $\tau(S_2)$ = <200 fs – for CdTPP in benzene),[92] zinc(II) metalloporphyins has shown potential for the extraction of UC energy via ultrafast electron transfer from the S_2 state, which could prove useful as an alternative method of manifesting of UC energy to S_2 fluorescence. Observation of a charge-separated state from S_2 has been confirmed by Robotham *et al.* for covalently linked zinc(II) porphyrin – naphthalene diimide electron donor-acceptor dyads,[93] and by Harada *et al.* for axially coordinated zinc(II) porphyrin – pyromellitic diimide electron donor-acceptor complexes.[94] These systems currently suffer from rapid charge recombination back to S_1 of the porphyrin, and though of interest in the development of future energy-harvesting processes, they will not be discussed in detail in the following work.

1.5 Metalloporphyrins

1.5.1 Background

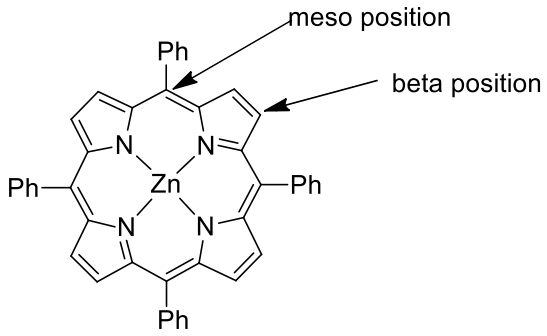

Figure 1.13: Zinc (II) meso-tetraphenylporphyrin. The meso- and β- positions on the macrocyclic periphery have been labeled.

Porphyrins are a class of conjugated macrocyclic molecules consisting of a core structure of four pyrrole units linked together at their α-carbons by methine moieties (Figure 1.13 above). The locations at the periphery of the porphyrin ring are labeled as the 'meso'-position for those substituents at the methine moieties, and 'β-'positions for those substituents at the pyrrolic moieties (meso- and β- outlined in Figure 1.13 above). The meso- and β- positions have different electronic properties and hence have different reactive character, discussed below. Porphyrins have 22 π-electrons in their overall structure, of which 18 π-electrons contribute to a 16-membered cyclic planar system obeying Hückel's rule of aromaticity. This aromatic system is able to be delocalized over the full 22 π-electrons via two resonance structures.

Due to the extended π-conjugated structure of porphyrins, they are able to absorb and emit electromagnetic radiation within the UV-visible region of the electromagnetic spectrum. As the nitrogen atoms on the pyrrolic moieties face into the centre of the porphyrin macrocycle, the molecule allows for chelation of metal ions. The metal-ion chelated porphyrins, known as metalloporphyins, have various important chemical and biological functions. Metalloporphyins are found in blood as the heme complex, as a type of porphyrin chelated to iron(III) ions used to bind to oxygen and facilitate cellular respiration.[95] The versatile nature of metalloporphyins and their variety of photophysical and electronic properties are of great interest in scientific research,

and have lead them to being used as electron donors in dye-sensitized solar cells[96] and bulk heterojunction solar cells,[97] for oxygen sensing,[98] as photosensitizers for photodynamic therapy[99] and as synthetic catalysts.[100] Of most importance to the work presented in this thesis, metalloporphyins are one of the major light absorbing species used in non-linear solar energy harvesting applications such as those based on TTA (discussed in section **1.4** of the Introduction chapter).

1.5.2 Origins of the Electronic Properties of Porphyrins

The electronic structure of porphyrins was first evaluated in detail by Simpson in 1949, in which he related electronic transitions in porphyrins to that of a 18-membered, 18 π-electron symmetric cyclic polyene.[101] The orbital structure was proposed on the basis of linear combination of atomic orbitals theory (LCAO) in a cyclic polyene with D_{4h} symmetry, yielding a doubly degenerate HOMO with magnetic quantum number (m_L) ± 4 and a doubly degenerate LUMO with magnetic quantum number (m_L) ± 5. Transitions between these orbitals correspond either to a Δm_L of ± 1 or ± 9. Under Laporte's selection rules for electronic transitions, a transition is allowed on the basis of $\Delta m_L = 0$ or ± 1.[102] The obtained value of Δm_L of ± 1 from Simpson's calculations is therefore strongly allowed and corresponds to the transition with high extinction coefficient observed in the absorption spectrum of porphyrins at ~400-450 nm known as the B-band or Soret band (S_2 excited state energy level). Conversely, the value of Δm_L of ± 9 is therefore strongly forbidden and corresponds to the transition with low extinction coefficient in the absorption spectrum of porphyrins at ~550-600 nm known as the Q-band (S_1 excited state energy level). Furthermore, Simpson performed a theoretical analysis to validate the prediction arising from Hund's rule that the weak Q-band transition of higher orbital angular momentum will be of lower energy than the strong Soret transition.

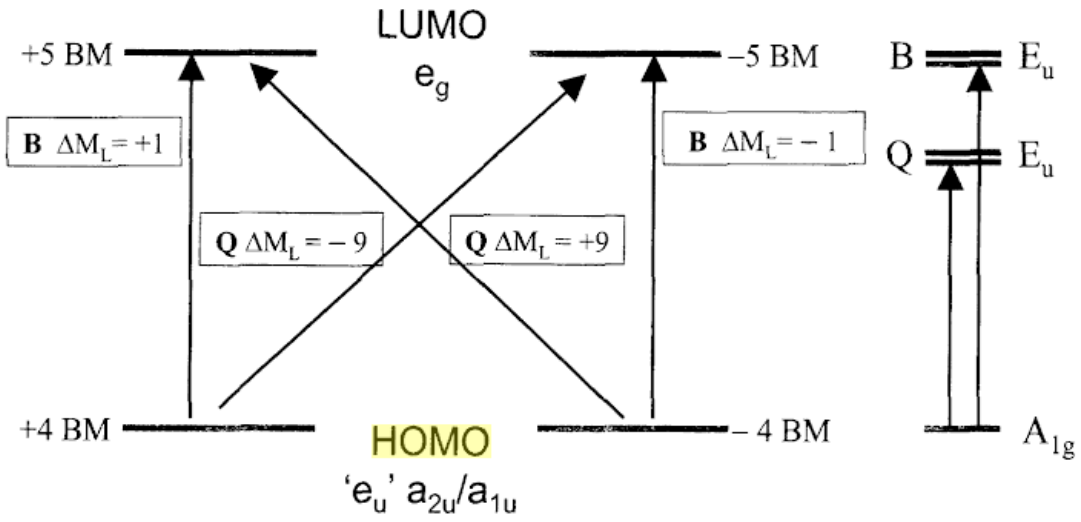

Figure 1.14: The origins of the B and Q bands in porphyrins. Figure reproduced from Kadish *et al.*[103] The configuration mixed transitions with high Δm_L values (Q band excitations) are represented by the diagonal arrows, while the vertical arrows represent the allowed B band excitations.

Martin Gouterman extended and quantitatively revised the theory of porphryin electronic structure in 1961 with his 'four orbital model' used to interpret the electronic transitions in the frontier molecular orbitals of porphyrins.[104] Unlike in the calculations of Simpson, Gouterman's model entails transitions between two distinct HOMOs (a_{1u} and a_{2u}) resulting from perturbation in the aromatic cyclic polyene due to the presence of the nitrogen atoms, and two formally degenerate LUMOs (e_g). Under LCAO calculations for true porphyrin orbitals, Gouterman proposed that HOMOs should have different energies and possess identical oscillator strengths; the latter statement running counter to widely accepted spectral evidence. Gouterman suggested that the HOMOs are 'accidentally' degenerate in the sense that their energy difference is small, and although the HOMOs are distinct on symmetry grounds, the LCAO models for cyclic polyenes may still effectively represent porphyrin orbital structures for porphyrins with true D_{2h} and D_{4h} symmetry.

1.5.3 Metalation of Porphyrins

As alluded to in **1.5.1**, chelation of metal ions by porphyrin ligands induces several important changes in the nature of the porphyrin's synthetic reactivity, electronic structure, symmetry, and intermolecular bonding properties, that allow metalloporphyrins to be useful in such a versatile range of applications. An understanding of the effect of the metal ion is essential in order to tune the character of a metalloporphyin for any particular application.

1.5.3.1 Metalloporphyrin Symmetry and Absorption Band Splitting

The cyclic polyene models used to describe electronic transitions as discussed in **1.5.2** above were initially modeled for cyclic polyenes with D_{4h} symmetry. Gouterman explains that since the most common tautomer of free-base porphyrins contain two opposing pyrrolic nitrogens bonded to protons and two that are not, the symmetry of the porphyrin is reduced to D_{2h}, and the 2 sets of 2 transitions contributing to Q- and B-bands (diagonal and vertical arrows respectively in Figure 1.14) exhibit independent polarization of their transition electric dipole moments along and against the direction of the N-H bond plane.[104] As such, the absorption spectra of free-base porphyrins contain 4 main bands labeled as Q_x, Q_y, B_x and B_y. Metalation of the porphyrin re-establishes D_{4h} symmetry, and the transition dipoles align for both the Q- and B- band sets, producing only 2 major bands in the absorption spectrum. Additional bands may be present in metalloporphyrin absorption spectra with varying intensities, though these are due to transitions from different vibrational energy levels in each band. The absorption spectrum of free-base tetraphenylporphyrin (TPP) and zinc(II) tetraphenylporphyin (ZnTPP) are shown in Figure 1.15 below. In spite of the expected increase in symmetry due to metalation of the porphyrin core, some metal ions may distort the planarity of the aromatic system. For Zn(II)TPP derivatives, there is minimal distortion of the planarity of the macrocycle, however in Fe(V) and Mn(III) metalated porphyrins, the macrocycle adopts a 'dome' shape, and in Fe(II)TPP and Co(II)TPP, the porphyrin zig-zags at the methine bridges forming a 'ruffled' shape.[105]

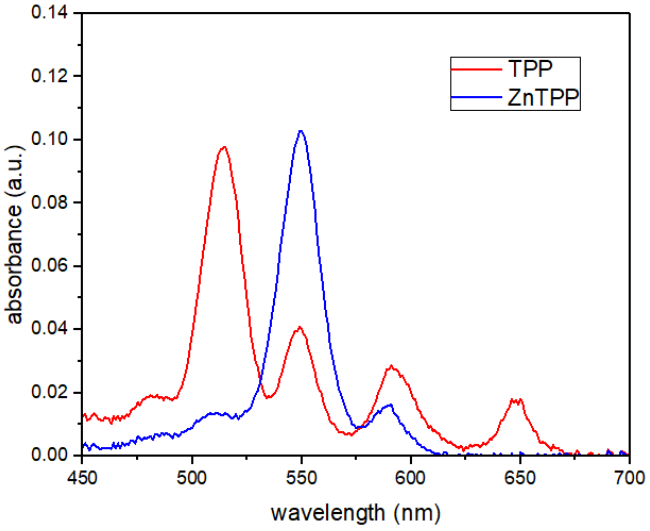

Figure 1.15: UV-visible absorption spectra of the Q-band region of free-base *meso*-tetraphenylporphyrin (TPP – red line) and its zinc metalated analogue (ZnTPP – blue line). Additional splitting of the Q- band is seen in TPP due to desymmetrization that is not seen in ZnTPP.

1.5.3.2 Metal-to-Ligand π-Backbonding Effects on Reactivity and Electronic Properties

The nature of the metal ion itself plays an additional role in shaping the electronic character and reactivity of the porphyrin it is chelated with. The electronic configuration of the metal atom dictates the degree of electron density at the periphery of the macrocycle. The d^0 and d^{10} configuration ions maximize electron density at the periphery of the macrocycle, promoting electrophilic aromatic substitution at the *meso*- and β-positions. The nucleophilicity at the periphery is due to dπ orbitals in the d^0 and d^{10} metal ions, which prevent metal-to-ligand π-backbonding interactions, effectively isolating the porphyrin ligand as a tetradentate dianion.[106] The d^1 to d^5 configuration ions strongly reduce electron density at the periphery and inhibit functionalization reactions as they allow for π-backbonding electron donation from ligand pπ to metal dπ orbitals. An important synthetic application of the variable π-backbonding strengths of metal ions in metalloporphyrins is exploited in the Vilsmeier-Haack β-formylation reaction. Zn(II) ions act as soft Lewis acids and are labile under the acidic conditions in the reaction mixture. As d^1 to d^5 configuration reduce the nucleophilicity of the periphery too strongly, d^6 to

d^9 configuration ions such as Ni(II)[107] and Cu(II)[108] have been used to facilitate Vilsmeier-Haack β-formylation, as they provide intermediate conditions in which the metal ion can be removed prior to the reaction with strong acid but remain chelated to the porphyrin under the Vilsmeier-Haack conditions without withdrawing too much electron density from the β-positions. The π-backbonding effects and electronegativity of the metal ion additionally alter the spectral properties in metalloporphyrins. π-Backbonding from the dπ orbitals of d^6 to d^9 configuration ions to π* orbitals of the porphyrin increases the energy of the porphyrin π* orbitals resulting in hypsochromic shifts in the absorption spectra.[109] Additionally, increasing the electronegativity of the metal ions in a particular metalloporphyrin will cause a hypsochromic shift in the peaks of the absorption spectra, with an accompanied rise in the oscillator strength of the Q-band transition.[110]

1.5.3.3 Triplet State Properties and Spin-Orbit Coupling

The presence of a metal atom in the metalloporphyrin structure allows for effective ISC from the singlet excited state to the triplet excited state due to the spin-orbit coupling phenomenon.[111] Spin-orbit coupling is a phenomenon arising from the interaction of an electron's spin with its motion within an orbital. Spin-orbit coupling creates splitting of discrete electronic energy levels within a molecule, therefore increasing overlap of vibrational energy levels between singlet and triplet manifolds which increases the rate of ISC. The increased rate of ISC due to metal ion chelation in metalloporphyrins is highly desirable for the design of triplet sensitizers for TTA applications.

The trend of increasing degree of spin-orbit coupling with the size of the metal ion present in the metalloporphyrin is known as the heavy atom effect. The measurements of Gurinovich and Jagarov demonstrate the heavy atom effect when observing the increase in triplet quantum yield (Φ_T) from Mg(II) mesoporphyrin (Φ_T = 0.62) to Zn(II) mesoporphyrin (Φ_T = 0.86) to Pd(II) mesoporphyrin (Φ_T = 1.00).[112] Although the triplet quantum yield increases with the size of metal ion, the triplet lifetime generally decreases with increasing size of metal ion.[112]

When designing TTA-UC systems, choice of metal ion plays an important role in the control of the triplet state properties. Typically Pt(II) or Pd(II) porphyrins are used in hetero-TTA-UC systems as the benefits of increased triplet yield outweigh having an extended triplet lifetime as TTET to an annihilating species in the system is fast with respect to the triplet lifetime. Dzebo *et al.* have calculated the rate of intermolecular TTET to be on the order of 10^9 M^{-1} s^{-1} for a PdOEP/DPA dendrimer hetero-TTA system in the solid state, which shows that TTET easily outcompetes the triplet decay rate of PdOEP on the order of 10^4 M^{-1} s^{-1}.[50] For homo-TTA-UC applications, it is necessary to use Zn(II) porphyrins derivatives, as the ultra-efficient ISC and reduced $S_2 - S_1$ energy spacing[113] that metalloporphyrins with heavier central metal ions display severely reduce the lifetimes and quantum yields of the product S_2 state formed upon homo-TTA with respect to Zn(II) porphyrins. Tripathy *et al.* have measured the S_2 lifetimes ($\tau(S_2)$) and S_2 fluorescence quantum yields ($\Phi_f(S_2)$) of the d^{10} metalloporhyrins ZnTPP and CdTPP in benzene, to obtain contrasting values of $\tau(S_2)$ = 1.45 ps, $\Phi_f(S_2) = 1.2 \times 10^{-3}$ for Zn(II)TPP, and $\tau(S_2)$ = 170 fs, $\Phi_f(S_2) = 6.5 \times 10^{-5}$ for Cd(II)TPP respectively.[92]

1.5.3.4 Axial Coordination of Ligands to Metalloporphyrins

As many metal ions in metalloporhyrins possess vacant orbitals that lie outside of the plane of the porphyrin, coordination to additional ligands other than porphyrin can occur. The class of triplet sensitizer molecules, Zn(II) porphyrins, typically form 5-coordinate complexes with square pyramidal geometry upon σ-donation by ligands that contain lone pairs on O, N, P and S atoms.[114] Complexation of σ-donors to the metalloporphyin central metal ion to form 6-coordinate complexes is also possible, however they form at a much lower proportion than 5-coordinate complexes. This is due to the larger association constant, K_1, for the 5-coordinate complexation of pyridine to zinc porphyrin compared to the association constant, K_2, for the 6-coordinate complexation shown in Figure 1.16 below.[115] Coordination of ligands perpendicular to the porphyrin plane is typically referred to as axial coordination. Axial coordination of ligands to metalloporphyrins has been shown to red-shift their absorption maxima,[115] increase their triplet absorption extinction coefficient,[116] and decrease the energies of their T_1 and T_n excited states,[117] with respect to the parent uncoordinated species.

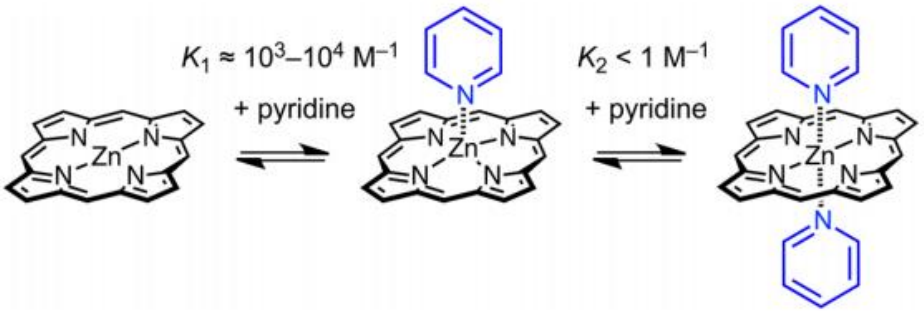

Figure 1.16: Complexation of pyridine to zinc(II) porphyrin. Figure reproduced from Favereau *et al.*[115] The association constants for the formation of the mono- and di-coordinated complexes in solution are given by K_1 and K_2 respectively.

TTA-UC systems can be significantly affected by axial coordination of ligands, both in positive and negative ways. Gray *et al.* have exploited axial coordination in designing a hetero-TTA system in which a pyridine-donor functionalized DPA annihilator derivative has been tethered to a Zn(II) porphyrin triplet sensitizer with the aim of improving sensitizer-to-annihilator energy transfer.[49] Although axial coordination may be beneficial in some hetero-TTA systems as shown by Gray *et al*., Sugunan *et al.* have observed that axial coordination of solvents to Zn(II) porphyrins diminishes the yield of UC fluorescence produced by homo-TTA in the solution-state by a factor of ~20, reasoning that the presence of the axially coordinated ligand increases the distance between the porphyrin planes in a TTA encounter complex, reducing the probability of a sufficient degree of orbital overlap occurring between the porphyrins in the encounter complex that is required to facilitate Dexter electron transfer.[48]

1.6 Triplet Exciton Transport

1.6.1 Aggregation in TTA Systems

In order for two annihilating molecules to share a significant degree of orbital overlap and participate in Dexter electron transfer, it is necessary that they are in close proximity to each other. One of the most important mechanisms of association for annihilating species in TTA systems is through molecular aggregation. Annihilating species form aggregates due to their extended planar conjugated π-systems, which strongly interact with the conjugated π-systems of other porphyrin molecules through π-π stacking.[118] Porphyrins are well known to aggregate in both solution and in the solid state, even at concentrations as low as 10^{-8} M.[119] Aggregation of porphyrins is readily identifiable by the observation of bathochromic shifts and broadening of the Soret band in the absorption spectrum of the porphyrins. The effects of aggregation of porphyrins contributes to both constructive and destructive processes in TTA systems and will be discussed accordingly throughout the remainder of the Introduction chapter.

1.6.2 Solution-State TTA Systems

In the solution state, molecules in the triplet excited state are able to freely move through the bulk solvent, and therefore are able to effectively transport excited state energy to other molecules in solution, effectively facilitating both homo- and hetero-TTA. The collision of molecules in solution is diffusion-limited, which places upper bounds on the energy transfer rate between triplet acceptors. Solution state hetero-TTA-UC systems have been previously implemented as light-harvesting layers by Schulze *et al.* for improving solar cell efficiencies (Figure 1.17 below).[60] Solution-state TTA systems would have limited application for commercial use, as the solution layer would likely be sensitive to temperature, have limited flexibility, would not be able to be manufactured via printing methods and have greater restrictions than solid-state TTA systems on the concentration of triplet sensitizers that could be incorporated into the UC layer. It is of great interest to develop effective solid-state TTA systems for integration into modern solar energy harvesting devices. Regardless, solution state TTA provides a useful model system for the interactions between annihilator molecules, for which the

photophysical parameters and energy transfer rates of these molecules can be analyzed and characterized.

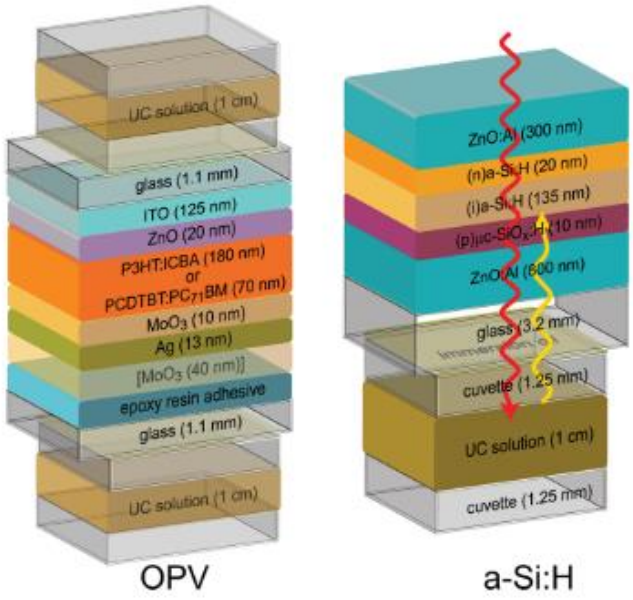

Figure 1.17: Solar cell architectures with integrated solution-state UC layer for organic photovoltaic cells (left) and amorphous silicon cells (right) as designed by Schulze *et al.*[60] The TTA-UC system employed was based on a solution of Pd(II) metalloporphyrin sensitizer and rubrene annihilator.

1.6.3 Solid-State TTA Systems

Molecules in their excited triplet state are in fixed locations in the solid state, and are not able to be transported through solid media in order to share orbital overlap with other molecules in their triplet excited state that are not in mutual immediate vicinity of each other. Triplet excitons must be able to migrate through solid media in order to interact with other triplets at distant locations to facilitate TTA. Steer *et al.* have argued that aggregation of the porphyrins in the solid state must occur in order to mediate triplet migration for the observation of TTA-UC.[70,120] Steer *et al.* have provided clear evidence for the aggregation of zinc(II) tetraphenylporphyrin in solid-state poly(methyl methacrylate) thin films exhibiting homo-TTA-UC fluorescence, as shown by the broadening and red-shifting of the absorption spectra of the films and the bi-exponential

fluorescence decay of the porphyrins in the films.[70] Triplet migration within aggregates in solid media occurs via a chain of sequential Dexter electron exchange steps (Figure 1.18 below). Triplet excitons (T_1 in Figure 1.18) can 'hop' between adjacent molecules in their singlet ground state (S_0; white circles in Figure 1.18) via triplet energy transfer (TET) steps until they come into contact with another triplet and decay via TTA (Path 1 in Figure 1.18), resulting in decay to the ground state via a combination of IC and upconverted emission (hν in Figure 1.18). Migrating triplets may also encounter a triplet trap site (green circle in Figure 1.18) or form an excimer (see section **1.7** of the Introduction chapter), decaying to the ground state via ISC (Path 2 in Figure 1.18).

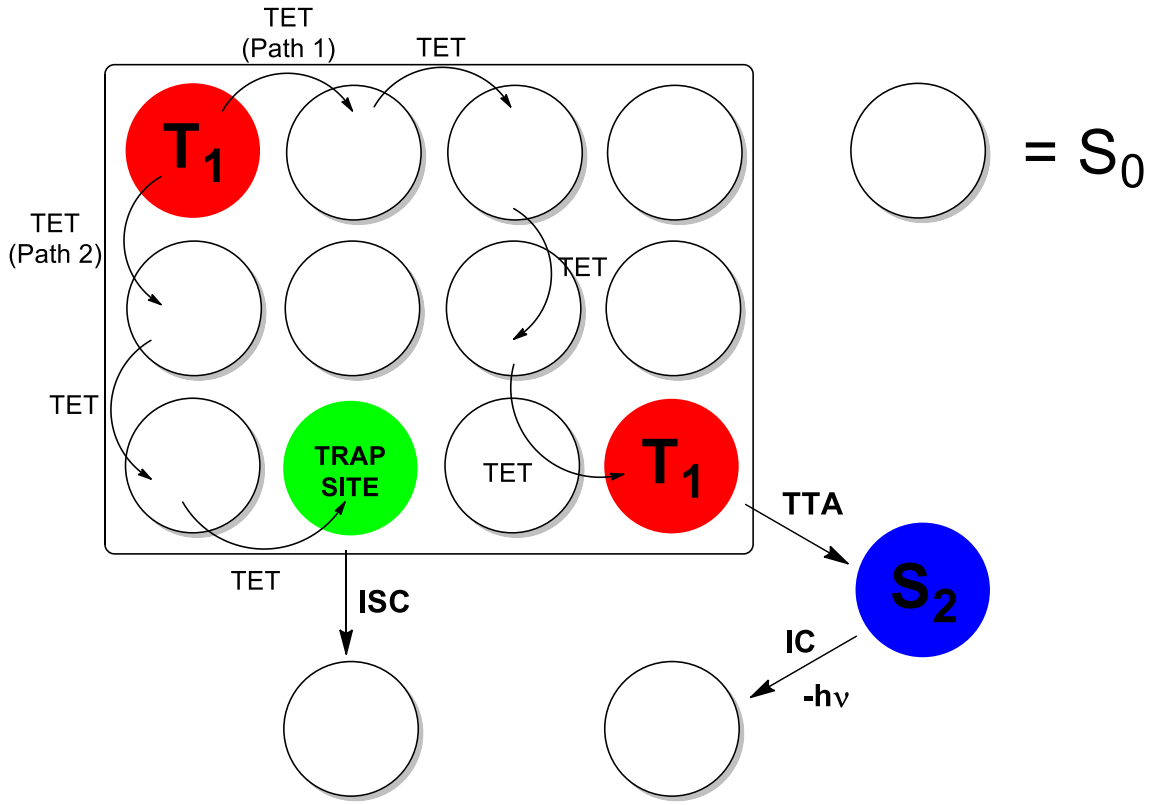

Figure 1.18: Triplet energy migration in a homomolecular multimolecular aggregate. The aggregate is outlined by the box in the diagram. Arrows leading outside of the box denote relaxation pathways of individual molecules located inside the aggregate and do not indicate energy transfer processes to molecules located outside of the aggregate cluster. Triplet migration from the triplet excited molecule in the top left of the aggregate may take either path 1 or path 2, but cannot take both simultaneously.

1.6.4 Hetero-TTA vs Homo-TTA in the Solid State

Most solid-state TTA systems currently in the literature have been based on hetero-TTA. The most commonly studied system employs a blend of metalloporphyrin triplet sensitizer such as PtOEP and polyacene derivative annihilator such as DPA.[71-73] The blend is typically a neat thin film of sensitizer in bulk annihilator,[71-73] or a blend of sensitizer and annihilator dispersed in an inert polymer matrix.[71] When two or more compounds are cast as films from solution, they phase separate as solvent is gradually removed, to form localized domains of each compound. The occurrence of unwanted TTA within the sensitizer domain itself between two metalloporphyrins is a source of triplet loss in hetero-TTA systems as the UC product state from homo-TTA between Pd and Pt metalloporphyrins is non-emissive (see **1.5.4.4**). Gouzardi and Keivanidis have estimated that maximum UC emission intensity in PtOEP/DPA TTA solid-state systems occurs at the upper limit of the bimolecular intra-sensitizer annihilation constant of 1.1×10^{-13} cm^3 s^{-1}.[71] The annihilation constant derived by Gouzardi and Keivanidis is proportional to the size of the PtOEP aggregates and thus an increase in PtOEP aggregate size beyond that at which the annihilation constant is optimized would induce a loss in DPA UC fluorescence intensity. Triplets migrating from within sensitizer domains must survive potential unwanted exciton quenching both within the sensitizer and annihilator domains in order to eventually meet another triplet, which requires long triplet exciton diffusion lengths to be achievable. Karpicz *et al.* have suggested that migration of triplets to the sensitizer-annihilator interface is a major rate limiting step in the production of TTA-UC fluorescence.[72] The triplet must be able to effectively cross the phase boundary between sensitizer and annihilator domains to continue migrating through the bulk annihilator medium. Additionally, the free triplet concentration in the annihilator bulk must be great enough that the likelihood of two triplets coming into contact within their lifetimes is high. The aforementioned triplet migration and quenching considerations place an upper limit on the sensitizer-to-annihilator ratio that can be employed in hetero-TTA systems. Baluschev *et al.* have demonstrated that the UC fluorescence yield of PdOEP/DPA degassed neat thin film blends drop cast from toluene reaches a maximum intensity at a sensitizer loading of 2% PdOEP.[73]

1.6.5 Future Outlook for Design of TTA-UC Based Light Harvesting Systems

Solid-state homo-TTA systems employing dual absorber-upconverter compounds bypass the issues discussed in section **1.6.4** of the Introduction chapter attributed to phase separation, as phase separation is not relevant when there is only one compound present in the active layer of a film. Ideally, an effective solid-state homo-TTA system could be formed from a pure layer of dual absorber-upconverter, maximizing the sensitization of light into triplet excitons and minimizing the need for long triplet diffusion lengths. The development of an effective UC layer for solar cells based on solid-state homo-TTA constructed from a single highly concentrated dual absorber-upconverter material would prove invaluable for the enhancement of solar cell efficiencies.

Several limitations with homo-TTA systems employing metalloporphyrins as dual absorber-upconverters currently exist that restrict their ability to be integrated as part of the design of effective UC layers for solar cells. The most significant drawback of homo-TTA remains the very low fluorescence quantum yield and short lifetime of the product S_2 state from the TTA encounter for even the most promising dual absorber-upconverter compound, ZnTPP ($\tau(S_2)$ = 1.45 ps, $\Phi_f(S_2) = 1.2 \times 10^{-3}$).[92] Regardless, ZnTPP derviatives currently provide the best model for understanding intermolecular interactions that dictate the effectiveness of homo-TTA processes.

Beyond the issues with S_2 fluorescence quantum yields and lifetimes, the major limitations in homo-TTA systems involve the quenching of exciton energy before the excitons can participate in TTA. Undesirable exciton decay in metalloporphyrin-based TTA systems can be manifested in the form of singlet excimer formation, efficient singlet deactivation via IC, quenching of triplet excitons by molecular oxygen, and through triplet excimer and triplet trap site formation resulting in non-radiative deactivation of triplets via ISC. The aforementioned exciton decay mechanisms present in metalloporphyrin-based homo-TTA systems decrease the free migrating triplet population in solid UC layers, and act to limit the distances for which those free triplets can migrate through the UC layer. Fluorescence from the product UC state of metalloporphyrin

homo-TTA can also be quenched by immediate excimer-type stabilization of the two molecules that participated in the TTA encounter. The exciton decay pathways that dictate the overall TTA-UC fluorescence quantum yield in metalloporphyin-based homo-TTA systems are discussed in section **1.7**.

1.7 Exciton Decay Pathways in Metalloporphyrin-Based Homo-TTA Systems

1.7.1 S_1 Singlet State Deactivation Pathways

Although the electronic association of chromophores is necessary for energy migration to occur, π-conjugated molecules that are in close contact with each other can become electronically associated in a manner that rapidly deactivates the excited state energy of the multi-molecular structure. In metalloporphyrins, this rapid exciton energy decay can even out-compete the rate of ISC within the monomeric porphyrin itself, hence lowering the quantum yield of triplet formation and shunting TTA.[70] Quenching of singlet excited state energy in aggregates and ordered molecular structures is often attributed to formation of excited state dimers, known as excimers. Evidence for singlet excimer formation has been well documented for chromophores such as perylene biismides[121] and pyrenes,[122] as well as metalloporphyrin derivatives.[123] The formation of excimers is driven by the increased stabilization of the excited state energy of the excimer with respect to the excited state monomer. Stabilization in the excimers results in lowering of the delocalized exciton energy within the excimer causing both an ISC shunt and restricted migration of the exciton through media, with the excited state energy eventually relaxing to the ground state via IC.

Susceptibility for the formation of singlet excimers and exciton traps has been shown to increase as a function of the loading of metalloporphyrins in solid state layers and thus singlet decay rates increase in regions of high local porphyrin concentration. Solomon *et al.* have demonstrated a decrease in the diffusion lengths of singlet excitons from 60 nm to 3.5 nm in zinc(II) protoporphyrin (ZnP): peptide-amphiphile (PA) blends upon using ultrafast transient photoluminesce techniques, attributed to enhanced singlet excimer formation, when increasing

the blend ratio from 1:120 ZnP:PA to 1:6 ZnP:PA.[123] O'Brien *et al.* have observed an increase in the rate of the fast component of the fluorescence decay traces of zinc(II) tetraphenylporphyrin aggregates immersed in PMMA films, as a function of increased porphyrin loading, corresponding to concentration-accelerated singlet decay via IC within aggregates, with subsequent reduction in homo-TTA-UC fluorescence yields.[70] The fact that aggregation and spatial association of porphyrins can act to both enhance exciton migration and inhibit exciton migration, necessitates a deeper understanding of the parameters and inter-chromophore structure-property relationships that contribute to both of these processes.

1.7.2 T_1 Triplet State Deactivation Pathways

1.7.2.1 Triplet Excimer Formation and Exciton Migration Trap Sites

Stabilization of exciton energy via the formation of excimers is applicable to triplet excitons in addition to singlet excitons discussed in **1.7.1**. Similarly to the singlet excited state deactivation of exciton energy in randomly oriented chromophore systems, triplet excimer formation is more frequent when the concentration of chromophore is increased. Callis *et al.*[124] and Sapunov[125,126] have attributed triplet excimer formation between triplet state and ground state molecules to be contributing to the increase in the rate of triplet decay of metalloporphyrins, seen in solution state flash photolysis experiments as a function of increasing metalloporphyrin concentration. Sapunov has suggested that the mechanism of formation of triplet excimers in solution is driven by an increase in a stabilizing dispersion interaction between triplet and ground state molecules, caused by increased solvatophobic interactions between the metalloporphyrin and the solvent upon formation of the triplet state.[125] Direct evidence for triplet excimer formation for Pd(II)TPP in toluene solution has been provided by the red-shifting of phosphorescence bands upon increasing the concentration of PdTPP,[125] and similar red-shifting of phosphorescence maxima are observed for neat solid films of PtOEP.[127] The presence of a broad, featureless band in the phosphorescence spectrum of PtOEP-doped polystyrene matrixes between 740 and 790 nm is indicative of triplet excimer emission in PtOEP aggregates in the solid-state, which become pronounced with increased PtOEP:polystyrene ratios.[128]

In rigid or semi-rigid disordered multi-chromophore systems, migration of triplet excitons proceed via local Dexter electron-exchange hopping interactions. Random orientations of molecules lead to random π-electron interactions, which variably modify the energy of electronic states at these sites. The energies of these variably-perturbed electronic states are modeled by site-energy distributions.[129] Triplet exciton energy will migrate through the system until it reaches the low-energy tail ends of the site-energy distribution, where triplet trap sites occur. A triplet trap site occurs when a migrating triplet possesses less energy than required to transfer its exciton energy to the molecules in its surroundings. Triplet excimers are referred to as 'deep' traps as the inter-chromophore interaction leading to excited state energy stabilization within the excimer is greater than the inter-chromophore interactions that contribute to excited states at the low-energy tail end of the density-of-states distribution. The excited states at the low-energy tail end of the density-of-states distibution are referred to as 'shallow' traps. Shallow triplet traps can be distinguished from triplet excimer trapping as phosphorescence emission from these trap sites will show a similar red-shifting of the maxima, with retention of vibronic features and peak shape unlike in the triplet excimer case, as shown by Ito *et al.* in the phosphorescence spectra of poly[(carbazolylethyl methacrylate)-co-(methyl methacrylate)] films[130] and poly[(9-phenanthrylmethyl methacrylate)-co-(methyl methacrylate)] films.[131] In the aforementioned studies by Ito *et al.*, shallow trap formation became more prominent with increasing chromophore loading. The presence of excimer and shallow triplet trap sites in rigid multi-chromophore systems may be worthy of consideration when maximization of triplet diffusion lengths is desirable in systems such as those designed for solid-state homo-TTA applications employing metalloporphyrin dual sensitizer-emitter chromophores.

1.7.2.2 Quenching of Triplet State Energy by Molecular Oxygen

Molecular oxygen in the atmosphere or dissolved in solution, exists as a ground state triplet biradical, and as such can participate in heteromolecular TTA with the triplet state of a metalloporphyrin, resulting in the formation of singlet oxygen.[132] The quenching of metalloporphyrins by triplet oxygen often out-competes desirable triplet deactivation processes such as triplet energy transfer or homo-TTA, with rate constants of singlet oxygen formation approaching the diffusion limit in solution.[133] Not only does the formation of singlet oxygen

deplete the triplet population intended for participation in TTA-UC, singlet oxygen also acts as a destructive agent in systems employing conjugated organic chromophores due to oxidation of the chromophores, permanently degrading the materials resulting in losses in desired photophysical function and efficiency.[134,135]

For TTA systems to operate at peak efficiency, oxygen must be excluded or prevented from interacting with the triplet state of sensitizers or annihilators as much as possible. In solution, triplet lifetimes of metalloporphyrins are highly subject to the degree of degassing of the solution. Callis *et al.* have explicitly stated that extensive freeze-pump-thaw cycles (10 or more) and degassing at pressures less than 10^{-6} torr are necessary to achieve accurate rate constants for bimolecular processes such as triplet excimer formation in metalloporphyrin solution and thin films.[124] This is often difficult to achieve in practice with common laboratory equipment, and as such, an unknown degree of persistent oxygen quenching may induce variance in quantitative data for triplet lifetimes, excimer formation rates and TTA processes. Various methods have been implemented for the purpose of protecting metalloporphyrin-based TTA systems from oxygen quenching. Blending of the metalloporphyrins into inert matrixes that act as oxygen barriers such as poly(vinyl alcohol) (PVA)[74] and hyperbranched unsaturated polyphosphates[75] has been investigated in solid state TTA systems. In solution based TTA systems, immersion of metalloporphyrins in low oxygen permeability viscous media such as soybean derived oils[76] and poly(ethylene glycol) (PEG) chains[77] have shown significant improvement in TTA quantum yields compared to TTA quantum yields in standard solvent systems such as toluene.

1.7.3 S_2 Singlet State Deactivation Pathways

The relative contributions to the decay pathways of the S_2 excited state of metalloporphyrins are highly dependent on the nature of the central metal ion and the local electronic environment of the metalloporphyrin. As discussed in **1.5.3.3**, increasing the size of the metal ion will increase the rate of non-radiative decay from the S_2 state and hence lower the S_2 fluorescence lifetime and quantum yield. Tripathy *et al.* have obtained overall rate constants for non-radiative decay ($k_{nr}(S_2)$) from the S_2 state as well as the rate constant for ISC from S_2 ($k_{ISC}(S_2)$) for Mg, Zn and

Cd tetraphenylporphyrin.[92] Tripathy *et al.* have shown that although $k_{ISC}(S_2)$ increases with metal ion size, the magnitude of the increase in $k_{ISC}(S_2)$ does not justify the relative increase in $k_{nr}(S_2)$ with increasing metal ion size, and ISC contributes only to a minor decay pathway for S_2, although many T_n vibrational energy levels may lie close to the S_2 state energy. For ZnTPP, the most studied metalloporphyrin for observing S_2 fluorescence, more than 90% of the monomeric ZnTPP S_2 population decays via IC.[92]

When metalloporphyrins are in close enough proximity to one another, IC can be further accelerated, resulting in quenching of the already-weak S_2 fluorescence. Zn(II) porphyrins that have been covalently linked by an ortho-phenylene bridge to form a cofacially-stacked dimer, have been shown by Cho *et al.* to participate in through-space electronic exchange interactions that induce strong charge-transfer transitions that contribute to 'ladder' type deactivation channels, which accelerate non-radiative decay from S_2 resulting in complete S_2 fluorescence quenching not observed in the meta-phenylene or para-phenylene-bridged dimer analogues.[136] Stevens *et al.* have reported that ZnTPP dimers and multimers formed via aggregation in solution, in contrast to their monomeric analogues, exhibit no S_2 fluorescence at all upon direct excitation in the Soret band, due to enhanced IC as observed by delayed S_1 fluorescence from the dimers and multimers.[137]

Interestingly, the rate of S_2 fluorescence is faster than the rate at which two molecules participating in TTA can diffuse away from each other in solution. Hence, within the S_2 fluorescence lifetime of the product singlet state of TTA, the ground state molecule produced from the TTA encounter is close enough to the S_2 excited molecule such that the ground state molecule and S_2 excited molecule can electronically interact in an excimer-type system, however complete quenching of S_2 excited state energy after TTA like that observed by Stevens *et al.* for aggregate dimers[137] clearly does not occur after TTA as S_2 fluorescence is detectable from ZnTPP. A dependence on the electronic coupling of the ground state and S_2 state products of a TTA encounter, on the S_2 fluorescence character has been documented by Ksenofontova *et al.*,[81] as the S_2 emission maximum in the fluorescence spectrum of ZnTPP produced from TTA is

somewhat red-shifted with respect to the S_2 emission maximum produced by direct one-photon absorption in the Soret band. The fluorescence quantum yield of S_2 emission obtained from the product state of ZnTPP-sensitized TTA per successful singlet produced has been shown to be more than 5 times lower than the emission obtained from the S_2 state created upon direct excitation of ZnTPP in solution.[82] Stevens *et al.* have suggested that the TTA efficiency of two molecules in a TTA encounter is affected by the average intermolecular separation distances between the two porphyrins, as the S_2 product of encounters that are too close may be rapidly deactivated, yet the molecules in the encounter must still be close enough to share the required orbital overlap necessary for Dexter energy-transfer to proceed.[78,137]

1.8 Ordered Molecular Systems in the Framework of TTA

1.8.1 Overview of Supramolecular Metalloporphyrin Assemblies and Polymeric Arrays

One of the most desirable aspects of rational design is to be able to introduce as many elements of control over the assembly of the system of concern, and to be able to correlate those elements of design to the observed properties of the system. In the context of designing TTA-UC systems based on organic sensitizers and emitters, several authors in the literature have suggested that the design elements to be carefully controlled are the degrees of overlap of π-orbitals between molecules participating in both TTET and TTA, intermolecular separation distance between molecules, and the relative spatial orientation of the molecules with respect to each other.[45,47,79,80]

Many synthetic approaches have been pursued in the literature to create multi-metalloporphyrin assemblies and arrays with controlled inter-porphyrin orientations, spatial separations and proximity control, with the aim of controlling and enhancing photophysical properties and exciton dynamics within oligomeric and supramolecular metalloporphyrin structures. Such synthetic methodologies include self-assembly of ordered porphyrin aggregates to form well-defined zinc(II) porphyrin meso-bridged oligomer dimers[138] and porphyrin nanorods.[139] Self-assembly via axial coordination to the zinc metal centre has been exploited to form cross-linked meso-bridged porphyrin polymer wires[140] exhibiting efficient charge transport, extended zinc(II)

porphyrin stacks with long exciton diffusion lengths,[141] and zinc(II) porphyrin 'boxes' (Figure 1.19) made from inter-coordinated series of N-donor functionalized porphyrin dimers.[142,143]

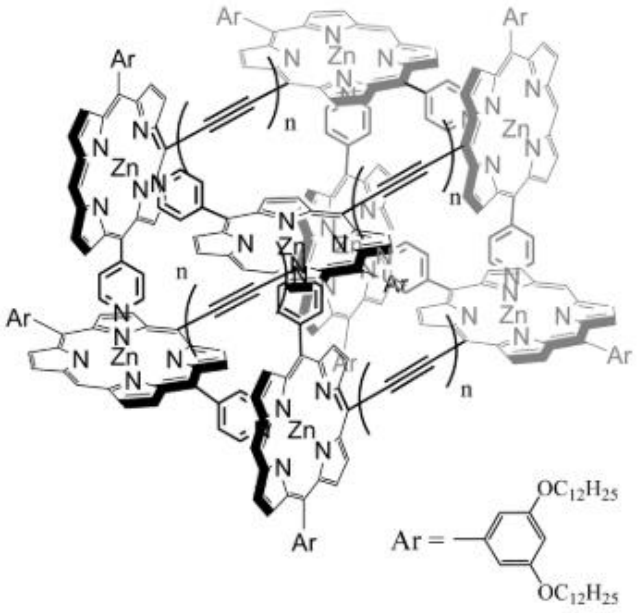

Figure 1.19: Zinc(II) porphyrin 'boxes' synthesized by Kim *et al.*[142]

By covalently linking zinc(II) porphyrin sub-units, several light-harvesting antennae systems possessing ultrafast inter-porphyrin energy transfer abilities have been developed, including meso-meso tethered porphyrin rings,[144] cyclic porphyrin arrays,[145] linear meso-meso bridged porphyrin oligomers[57] and tapes[146,147] and highly-branched dendrimers.[148,149] Although these multi-porphyrin arrays display efficient energy transfer, the exciton dynamics studied are largely restricted to singlet energy transfer under high excitation power conditions, and the arrays possess strong inter-porphyrin π-interactions manifesting in excitonic coupling as seen by splitting of the Soret bands in their absorption spectra.[57,145-147] Such strong inter-porphyrin π-interactions result in the photophysical properties and energy levels of the individual porphyrins sub-units in such a polymeric array, to be no longer reasonably modeled by their monomeric analogues, leading to a disturbance in the fine balance of electronic systems intended to participate in homo-TTA. For TTA systems in multi-molecular environments, it is important that the electronic environment of the annihilators is not significantly perturbed by proximal or spatial intermolecular interactions, as has been discussed throughout section **1.7**. Regardless, TTA applications have benefitted from the use of meso-meso bridged metalloporphyrin

oligomers, as seen in the improvement of sensitization of annihilators in hetero-TTA systems leading to higher TTA quantum yields.[57]

1.8.2 Photophysical Properties of Pendant Polymers

Of the synthetic methodologies explored in the literature, those that employ polymers bearing dual triplet sensitizer-upconverter moieties as regular pendant side-chain substituents, present some of the most promising avenues toward the optimization of chromophore orientation and proximity leading to beneficial photophysical properties in multi-porphyrin arrays for TTA applications. Chromophores in pendant polymers may be able to retain the majority of the photophysical character defined by their monomer analogues, yet still be in close enough proximity to each other to electronically communicate. Inter-pendant electronic communication has been definitively demonstrated by singlet energy transfer between pendant methoxy-ethylhexyloxy poly(phenylene vinylene) (MEH-PPV) oligomers as determined via fluorescence anisotropy techniques.[150] Tilley *et al.* have demonstrated triplet energy transfer between pendant DPA chromophores upon sensitization of the polymers with triplet energy from Ru(II) tris (4,4'-dimethyl-2,2'-bipyridine) in chloroform solution, as the rate of delayed fluorescence from the DPA pendant polymers within the first 5 μs after laser pulse excitation is rapid, being attributed to intramolecular TTA, and noticeably slows after 10 μs at which point intermolecular TTA begins to dominate the observed temporal UC fluorescence profile (Figure 1.20).[51] The increased rate of delayed fluorescence from intramolecular TTA in pendant chromophore systems as presented by Tilley *et al.* may be possible to emulate by polymers bearing zinc(II) porphyrin pendant substituents that could potentially participate in intramolecular homo-TTA.

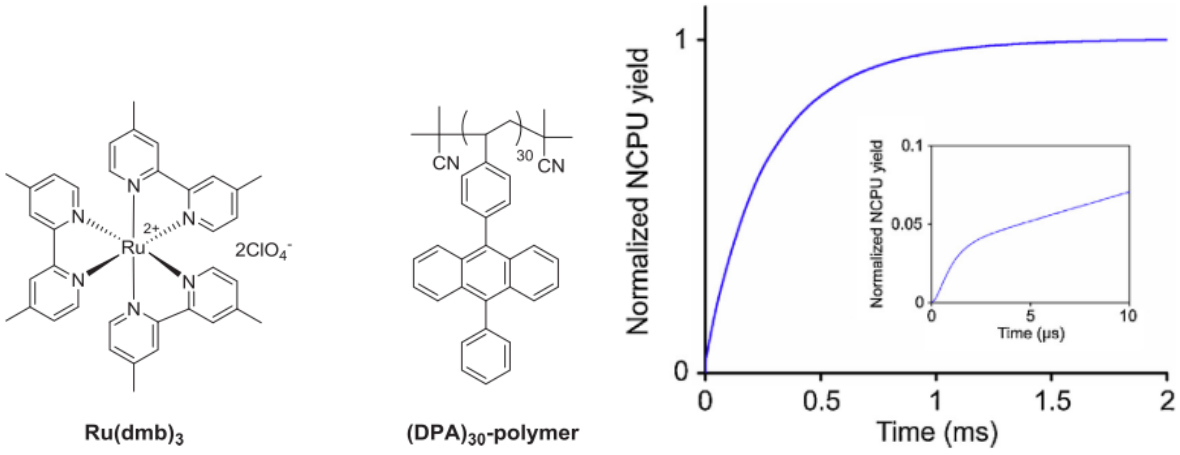

Figure 1.20: Structures of compounds used for intramolecular TTA studies by Tilley *et al.*[51] (left). Temporal evaluation of upconverted emission yield in DPA_{30} polymer studied by Tilley *et al.*,[51] exhibiting fast intramolecular TTA as shown by the steep slope of the curve at the short timescale (inset of figure on the right hand side).

The proximity and orientation of porphyrins in pendant polymers has proven to play an impactful role on their observed photophysical properties. Previous research on polymers with pendant porphyrin substituents has shown that polymers with cofacially oriented porphyrin pendants and/or minimal steric bulk outside of the plane of the porphyrin, exhibit strong intramolecular inter-porphyrin excitonic coupling due to increased π-electron overlap. These strong inter-pendant interactions seen in tetra-alkyl substituted pendant porphyrin polymers[151] and double-backbone bridged porphyrin ladderphanes,[152] are experimentally verified by excitonic splitting of Soret bands in the polymers and reduced fluorescence quantum yields, likely due to accelerated IC not present in the monomeric analogues. The use of meso-tetraaryl substituents on porphyrin pendants has shown no excitonic splitting,[151,153,154] and only minor reductions in fluorescence quantum yields,[151] yet broadening of the Soret absorption for these compounds suggests weaker intramolecular electronic interactions between pendants that would be potentially appropriate for TTA systems.

Fujitsuka *et al.* have systematically investigated the dependence of the orientation and density of communicating porphyrin pendants on intramolecular energy transfer processes by varying the ratios of *cis* and *trans* double bonds along a polymer backbone to which porphyrins are appended, thereby controlling the ratio of pendants that are cofacially stacked along the polymer chain (Figure 1.21 below).[155] Fujitsuka *et al.* report decreases in fast components of fluorescence decay due to singlet-singlet and singlet-triplet annihilation, with decreasing numbers of porphyrin pendants that are cofacially aligned in the polymers[155]. Although there exists multiple studies on photophysical properties and exciton dynamics on pendant porphyrin polymers, there is a lack of information available in the literature on the triplet exciton dynamics or TTA processes that occur within pendant porphyrin polymers. Prior to the commencement of work on the projects outlined in this thesis, no direct evidence has been presented for the occurrence of homo-TTA in pendant porphyrin polymers.

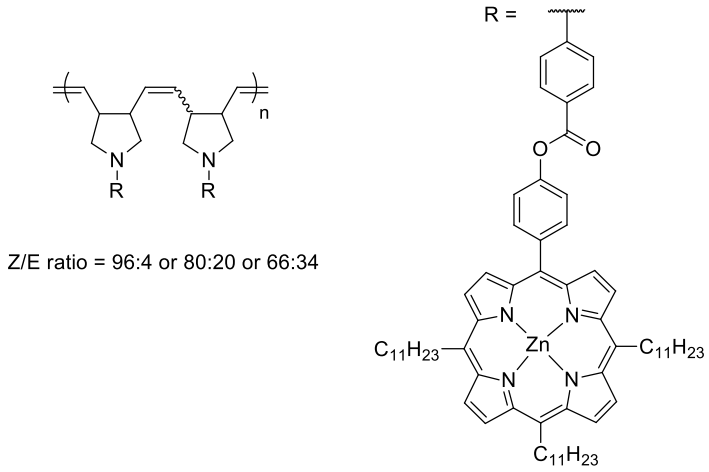

Figure 1.21: The generic structure of the pendant zinc porphyrin polymers synthesized by Fujitsuka *et al.*[155] The ratios of *cis* (Z) to *trans* (E) stereochemistry in the backbone polymer were varied in the study using ratios of 96:4, 80:20 and 66:34 Z/E respectively.

1.8.3 Techniques Toward the Synthesis of Pendant Polymers

1.8.3.1 Living Polymerization Methods

True 'living' polymerization techniques are those that lack the ability, for the propagating chain reaction whereby monomers continually add to growing polymer chains, to terminate. Because polymer chains cannot terminate, the rate of growth of the polymer chains throughout the polymerization reaction is close to uniform, and therefore the distribution of product polymer chain lengths is narrow. The distribution of chain lengths resulting from a polymerization reaction is quantified by the polydispersity index (PDI) (eqn. 1.7):

$$PDI = \frac{M_w}{M_n} \tag{1.7}$$

where M_w is the weight-average molecular mass of the polymer chain mixture and M_n is the number-average molecular mass. As high degrees of control over the structural and physical properties of chromophore-appended polymers are desirable for fine-tuning of photophysical properties, use of synthetic techniques for the formation of polymer backbone chains with low PDI values is essential. Ring Opening Metathesis Polymerization (ROMP)[156] is a living polymerization method that has been implemented in the synthesis of low PDI pendant polymers previously, however ROMP employs expensive rare metal-based catalysts that are able to polymerize a limited range of monomer materials.

Living polymerization techniques that employ radical reactions to propagate polymer chain growth have proven highly useful for the synthesis of polymers with well-defined chain lengths. Although Atom Transfer Radical Polymerization (ATRP)[157,158] and Nitroxide-Mediated Polymerization (NMP)[159] are living radical polymerization techniques capable of creating low PDI polymers, ATRP requires high ratios of metal-based catalysts that are difficult to remove from the polymer product, and the difficulty of nitroxide synthesis combined with the limited monomer compatibility of NMP, place considerable restrictions on both ATRP and NMP for laboratory and industrial scale synthesis.

1.8.3.2 RAFT Polymerization

The discovery of Reversible Addition-Fragmentation Chain-Transfer polymerization (RAFT) by Rizzardo *et al.*[160] in 1998 has proven to be revolutionary in the field of polymer science. RAFT polymerization is a living radical polymerization technique that employs thiocarbonylthio based chain transfer agents (CTAs) which act to reversibly capture living radical polymer chains, creating an equilibrium between the captured 'dormant' state and the 'living' state of the growing polymer chain. The rate of association or dissociation to or from the CTAs, in addition to the relative initiator:CTA:monomer ratio, exercises control over the length of the polymers upon total consumption of the monomer in the reaction, while keeping PDI values close to 1 throughout the course of a RAFT polymerization reaction. Because RAFT polymerization leaves the CTA intact upon completion of the polymerization reaction, the product polymers themselves are macro-CTAs, allowing for the straightforward synthesis of block copolymers.[161,162] When synthetically desirable, CTAs can be easily cleaved or deactivated by nucleophiles, radical reactions or oxidizing reagents.[163] The superiority of the RAFT polymerization method over other polymerization techniques is due to the vast range of monomers that are compatible with RAFT due to the ability to tune CTA properties by varying substituents on the thiocarbonylthio core,[164] the lack of expensive metal-based catalysts and the ability for RAFT to be performed under various reaction conditions and solvents including water.[165,166] As a result of the high versatility of RAFT polymerization, many exotic macromolecular structures have been created in addition to pendant polymers,[162] including star polymers,[167] hyperbranched polymers,[168] brush polymers[169] and dendrimers.[170]

1.8.3.3 Mechanism of RAFT Polymerization

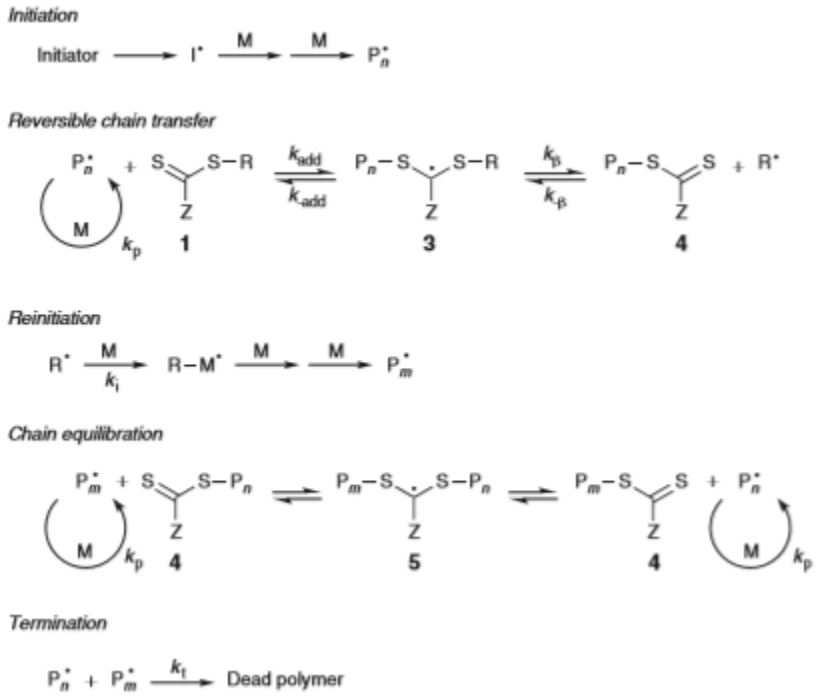

Figure 1.22: Mechanism of RAFT polymerization reproduced from the work of Moad *et al.*[171]

A radical source is required to begin the RAFT polymerization process (initiatior in Figure 1.22). Typically compounds that generate radicals upon exposure to heat or light under ambient conditions, such as 2,2-azobisisobutyronitrile (AIBN)[150] or benzoyl peroxide[172] (X and Y respectively in Figure 1.23), are added in small quantities (much less than CTA or monomer quantities) to RAFT reactions as radical initiators. The initiator radicals, I, react with monomers, M, to form a propagating active polymer chain, $P^{\bullet}_n$. Monomers used in RAFT polymerization reactions are vinylic species or compounds with double bonds susceptible to radical reactions, such as methacrylate[173] or styrene[150] derivatives (X and Y respectively in Figure 1.23).

Chain transfer then occurs where the CTA **1** captures the $P^{\bullet}_n$ radical to form the intermediate adduct radical **3**, for which the propagating $P^{\bullet}_n$ chain is said to be in the 'dormant' state. The R-CTA- $P^{\bullet}_n$ adduct radical **3** can then liberate the R group of the CTA by homolytic cleavage of the S-R bond followed by radical recombination to restore the thiocarbonylthio functionality and form CTA **4**. The choice of R and Z groups (shown in CTA **1** in Figure 1.22) dictate the stability of the CTA adduct radicals **3** and **5** and therefore rates of chain transfer,[174] which in turn controls

the effectiveness of the polymerization to form low PDI polymers. CTAs must be chosen to compliment the type of monomer used in the RAFT polymerization reaction, in order to minimize undesirable effects such as rate-retardation[175] which can result in higher termination rates and lower PDIs. Common CTAs used in RAFT polymerization are 2-(Dodecylthiocarbonothioylthio)propanoic acid **(**DoPAT)[150] and cumyl dithiobenzoate[176] (Figure 1.23).

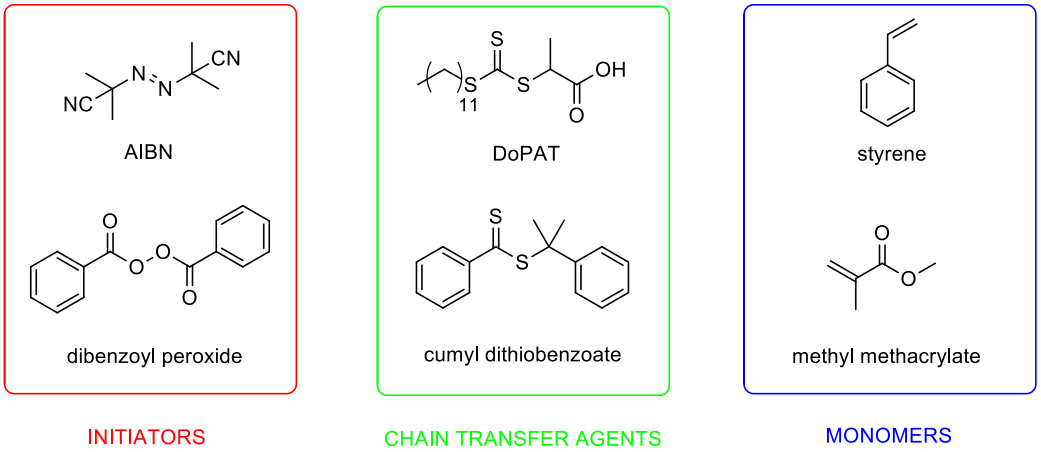

Figure 1.23: Examples of common initiators, chain transfer agents (CTAs) and monomers used in RAFT polymerization reactions.

When $P^{\bullet}_n$ is liberated from the CTA adduct **3** it is able to react with M, forming a polymer, $P^{\bullet}_m$, with chain length greater than $P^{\bullet}_n$. $P^{\bullet}_m$ can then react with the CTA **4** to form the CTA adduct **5**, and the main chain equilibrium in the polymerization reaction is established between the $P^{\bullet}_n$ - CTA- $P^{\bullet}_m$ adduct **5**, CTA **4**, $P^{\bullet}_n$ and $P^{\bullet}_m$ ('chain equilibration' in Figure 1.22). Termination of the propagating chains can occur via radical recombination or disproportionation (Figure 1.24).[177] As the monomer:initiator concentration ratio is typically in the range of 100 to hundreds of thousands, RAFT polymerization is able to proceed to almost 100% monomer-to-polymer conversion without significant termination occurring throughout the reaction.

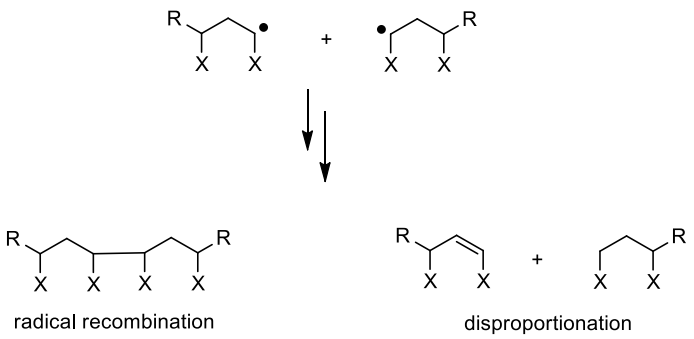

Figure 1.24: Termination via radical recombination (left) and disproportionation (right).

1.8.3.4 Post-Polymerization Functionalization (PPF)

Often the substituents of a polymer backbone chain contain reactive functional groups that are able to undergo further modification, allowing for the introduction of pendant groups by post-polymerization functionalization (PPF). The general PPF procedure is outlined in Figure 1.25. In many situations it is beneficial or necessary to employ PPF to introduce desired pendant groups onto a polymer backbone chain, where conventional polymerization of an analogous monomer species is problematic or not possible. An example of necessary implementation of PPF is in the synthesis of poly(N-allylacrylamide),[178] where conventional radical polymerization of the monomer N-allylacrylamide would yield uncontrolled branching and cross-linking of polymer chains due to the 2 double bonds present in the monomer susceptible to radical polymerization. The same batch of reactive polymer backbone chain can be separated into portions such that many different pendant groups can introduced via PPF onto backbone polymers that have the exact same M_n and PDI, eliminating the variable of polymer length in studies of structure-property relationships in a series of pendant polymers with varying pendant groups. The PPF step in the synthesis of a pendant polymer can provide a pathway for a convergent synthesis of desired pendant chromophores, providing a more efficient synthetic pathway than synthesizing the pendant chromophore completely itself prior to functionalization. The convergent synthesis of chromophore pendant units from a reactive polymer backbone and chromophore precursor has been demonstrated in the formation of poly-(phenylenevinylene) (PPV) pendants via Horner-Wadsworth-Emmons (HWE) reactions between poly(phosphonates) and aryl aldehydes,[150,179] and in the synthesis of phthalocyanine pendants by cyclizing the benzodinitrile substituents of

poly(benzodinitrile) with phthalonitrile derivatives.[180] Pendant porphyrin polymers have been synthesized using PPF methods by Friedel-crafts alkylation of the meso-phenyl groups of ZnTPP monomers with the backbone chloromethyl functionality of a poly(vinylbenzylchloride) polymer.[154]

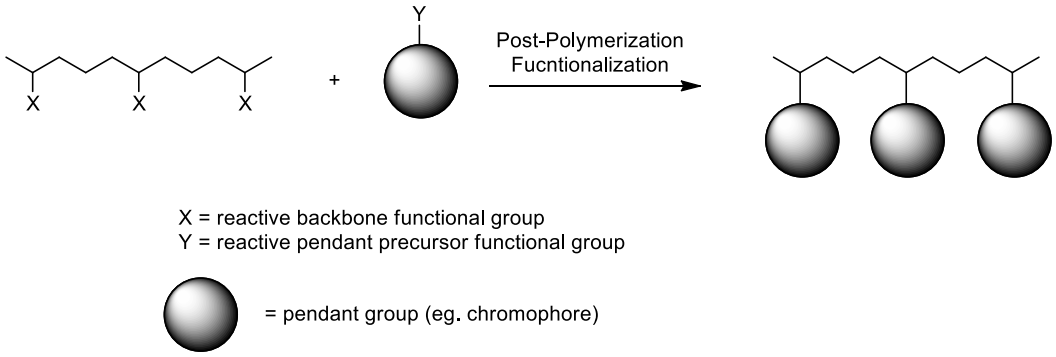

Figure 1.25: Post-polymerization functionalization of a reactive polymer backbone.

1.9 Sterically Bulky Substituents in Extended π-Conjugated Molecules

Solubility of chromophores in organic solvents is necessary for both the creation of solution-based TTA systems, and for ease of fabrication of solid-state TTA systems through solution-processing techniques such as drop-casting, solvent annealing, spin-coating and printing of thin films. π- π stacking of chromophores with extended conjugation, coupled with the often large size of the chromophore, results in increased aggregation of the chromophores, therefore decreasing the solubility of the chromophore aggregates. Large alkyl-branched or highly polar substituents are often introduced into the chromophore structure in order to increase the solubility of these chromophores in common laboratory solvents. As discussed in section **1.7** of the Introduction chapter, aggregation not only decreases the solubility of the chromophores, but induces intermolecular electronic interactions leading to excimer formation, energy trapping and increased rates of non-radiative relaxation of excitons which can limit the quantum yield of TTA in UC systems. The substituents used commonly as solubilizing groups in π-conjugated molecules can minimize degrees of self-aggregation by forcing the minimum distance between the planes of the π-conjugated molecules to increase using the steric bulk of the substituents as physical spacers. Ikeda *et al.* have integrated 2,4,6-tris(3,5-di-tert-butylphenoxy)phenyl

substituents into planar multi-porphyrin tapes (Figure 1.26), successfully conferring solubility of the porphyrin tapes, and preventing aggregation as seen in the minimization of Soret broadening and retention of vibronic features in the absorption spectra of the porphyrin tapes, in comparison to analogous porphyrin tapes with less bulky solubilizing groups.[146] N,N-2,6-bis(3,5-di-tert-butylphenyl)-4-butylphenyl substituents that are locked perpendicular to the plane of perylene diimides, investigated by Banal *et al.*, have proven effective in excluding the effects of excimer quenching between perylene diimide groups in the solid state (Figure 1.26 below).[181]

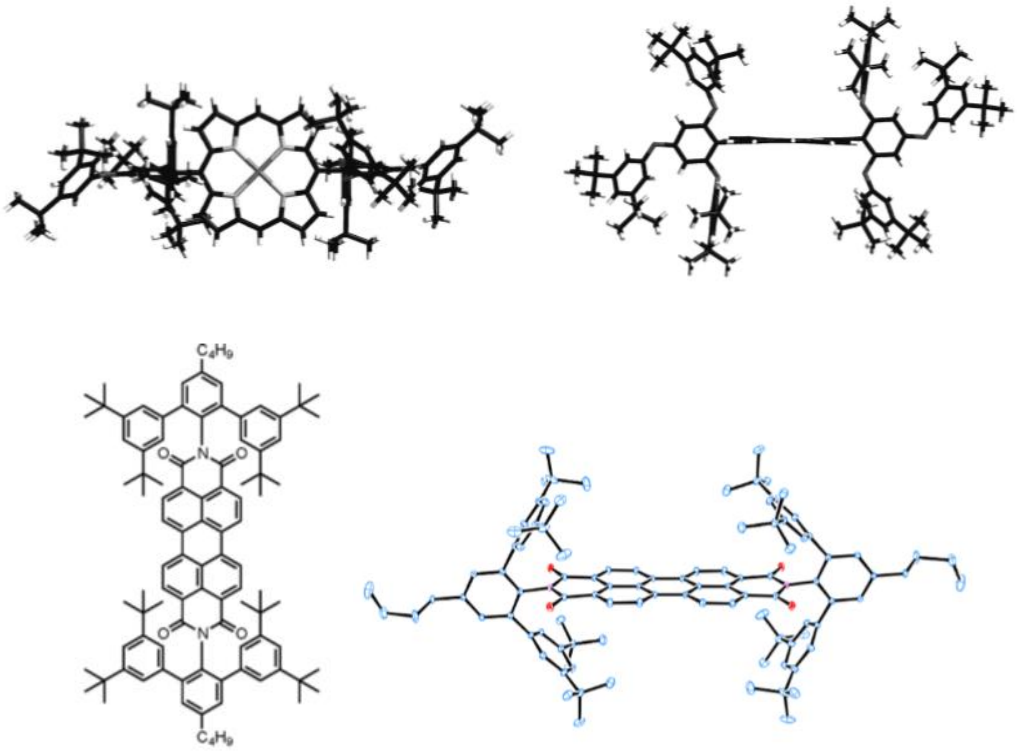

Figure 1.26: (top) X-ray crystal structure of bis-[2,4,6-tris(3,5-di-tert-butylphenoxy)phenylporphyrinato] zinc(II) monomer unit used in porphyrin tapes studied by Ikeda *et al.*,[146] view from above the porphyrin plane (top left) and eye-level to the porphyrin plane (top right). (bottom) X-ray crystal structure of N,N-(2,6-bis(3,5-di-tert-butylphenyl)-4-butylphenyl) perylene diimide studied by Banal *et al.*,[181] 2D structure from above the porphyrin plane (bottom left) and 3D structure at eye-level to the porphyrin plane (bottom right).

1.10 Thesis Outline and Objectives

The design of sunlight-harvesting TTA-UC systems requires easy integration into both industrial and everyday applications and devices, and requires compatibility with large scale commercial production. Effective homo-TTA-UC in the solid state would provide the ideal conditions for future widespread manufacture of TTA-based light harvesting systems. Currently, both homo-TTA and solid-state TTA systems suffer from limitations that restrict their viability for use in photon upconverting systems. Much research effort has been directed toward developing TTA-UC materials and controlled TTA systems in general, however there are few studies that have rigorously explored the parameters that contribute to the efficiency of solid-state TTA, and in particular homo-TTA processes. Although the derivatives of zinc(II) metalloporphyrins currently suffer from restricted fluorescence quantum yields from their S_2 state, they remain the best model compound to study as a dual absorber-upconverter for use in homo-TTA-UC. The vast pool of available literature on metalloporphyrins and porphyrins in general makes the use of porphyrins in homo-TTA systems highly appealing.

The research presented in this thesis aims to elucidate the physical mechanisms and inter-chromophore interactions that contribute to both beneficial and detrimental phenomena that affect the ability of multi-chromophore systems to participate in homo-TTA resulting in UC fluorescence from zinc(II) porphyrin derivatives, in both the solution and solid-state. Focus will be directed in particular to the effects of inter-porphyrin proximity, orientation, and aggregation, on the exciton dynamics of multi-porphyrin systems. A greater understanding of the parameters that influence the success of TTA-UC, are developed in the work outlined in this thesis through systematic structure-property relationships. In this regard, the effects of substituent size on the TTA characteristics of small molecule zinc(II) porphyrin systems are investigated. The inter-pendant interactions and triplet exciton dynamics of zinc(II) porphyrin appended polymers are discussed in the framework of homo-TTA using transient absorption techniques. Additional studies into the effects of the nature of the backbone-to-pendant linking moiety are conducted to gain further insight toward rational design of pendant porphyrin polymer-based homo-TTA systems.

The topics discussed in the chapters of this thesis are as follows:

Chapter 1 – Introduction. The use and relevance of TTA in solar energy harvesting systems is outlined and various methods to overcome the Shockley-Queisser Limit are reviewed. The characteristics of metalloporphyrins are listed in detail. Exciton decay pathways are discussed in the framework of TTA. Molecular architectures as candidates for use in energy transfer and TTA processes are reviewed.

Chapter 2 – Photon Upconversion of Sterically-Bulky Zn(II) Porphyrins in Solution and Solid-State PVA Films. The synthesis and photophysical characterization of a series of zinc(II) porphyrin small molecules with meso-substituents that incrementally increase in steric bulk are discussed. The effects of the spatial separation and relative orientation between porphyrins participating in homo-TTA encounters on their observed UC fluorescence yields are investigated in the solution and solid state.

Chapters 3 and 4 constitute related studies within a broader project investigating pendant zinc porphyrin polymers.

Chapter 3 – Synthesis and Photophysics of Oligo-Phenylenevinylene Linked Pendant Porphyrin Polymers. The synthesis of a series of pendant polymers linked by oligo-phenylenevinylene (oligo-*p*-PV) backbone-to-pendant linking groups and their monomeric analogues is outlined. The photophysical properties of the polymers are rationalized in terms of inter-pendant association phenomena and electronic effects introduced by conjugation extension of the porphyrin core. The potential of the polymers for TTA applications are summarized.

Chapter 4 – Synthesis and Exciton Dynamics of Pendant Zinc Porphyrin Polymers with Stilbene and Benzyl Ether Linking Groups. The synthesis and photophysical characterization of a series of pendant polymers and their monomeric analogues, with varying linker group

flexibility and limited degrees of through-linker conjugation extension are presented. Singlet and triplet exciton dynamics are probed using fluorescence decay and transient absorption techniques respectively. Mechanistic models are proposed for the observed exciton decay behavior. The homo-TTA-UC efficiency of the polymers and their model compounds are determined in both coordinating and non-coordinating solvents.

Chapter 5 – Experimental. All general and specific experimental procedures for synthesis and photophysical analyses are listed in detail. All structural characterization data for the compounds synthesized as part of the work in this thesis is included in this chapter.

1.11 References

(1) IEA "2019 Snapshot of Global PV Markets," 2019.

(2) IRENA "Renewable Energy Generation Costs in 2018," 2019.

(3) https://energyinformative.org/solar-cell-comparison-chart-mono-polycrystalline-thin-film/. accessed 14/03/2019

(4) https://es-media-prod.s3.amazonaws.com/media/components/panels/spec-sheets/Sunpower%20SPR-X22-360%20Datasheet.pdf. *accessed 14/03/2019*

(5) https://www.nrel.gov/pv/cell-efficiency.html. *accessed 05/08/2020*

(6) Shockley, W.; Queisser, H. J. *J. Appl. Phys.* **1961,** *32*, 510.

(7) Richards, B. S. *Sol. Energ. Mat. Sol. C* **2006,** *90*, 2329.

(8) Polman, A.; Atwater, H. A. *Nat. Mater.* **2012,** *11*, 174.

(9) Rühle, S. *Sol. Energy* **2016,** *130*, 139.

(10) ASTM G173-03, *Standard Tables for Reference Solar Spectral Irradiances: Direct Normal and Hemispherical on 37° Tilted Surface*, ASTM International, West Conshohocken, PA, **2012**

(11) Meng, L.; Zhang, Y.; Wan, X.; Li, C.; Zhang, X.; Wang, Y.; Ke, X.; Xiao, Z.; Ding, L.; Xia, R.et al. *Science* **2018,** *361*, 1094.

(12) Jain, N.; Schulte, K. L.; Geisz, J. F.; Friedman, D. J.; France, R. M.; Perl, E. E.; Norman, A. G.; Guthrey, H. L.; A., S. M. *Appl. Phys. Lett.* **2018,** *112*, 053905.

(13) http://www.sharp-world.com/corporate/news/130614.html. *accessed 25/01/2019*

(14) https://www.ise.fraunhofer.de/en/press-media/press-releases/2014/new-world-record-for-solar-cell-efficiency-at-46-percent.html. *accessed 25/01/2019*

(15) Dimroth, F.; Grave, M.; Beutel, P.; Fiedeler, U.; Karcher, C.; Tibbits, T. N. D.; Oliva, E.; Siefer, G.; Schachtner, M.; Wekkeli, A.et al. *Prog. Photovolt: Res. Appl.* **2014,** *22*, 277.

(16) Zhang, Y.; Wang, Q.; Zhang, X.-B.; Liu, Z.-Q.; Chen, B.-Z.; Huang, S.-S.; Peng, N.; Wang, Z.-Y. *Chin. Phys. Lett.* **2016,** *33* (10), 108801.

(17) Dai, P.; Ji, L.; Tan, M.; Uchida, S.; Wu, Y.; Abuduwayiti, A.; Heini, M.; Guo, Q.; Bian, L.; Lu, S.et al. *Sol. Energ. Mat. Sol. C* **2017,** *171*, 118.

(18) Bonnet-Eymard, M.; Boccard, M.; Bugnon, G.; Sculati-Meillaud, F.; Despeisse, M.; Ballif, C. *Sol. Energ. Mat. Sol. C* **2013,** *117*, 120.

(19) Trupke, T.; Green, M. A.; Würfel, P. *J. Appl. Phys.* **2002,** *92*, 1668.

(20) Wegh, R. T.; Donker, H.; Oskam, K. D.; Meijerink, A. *Science* **1999,** *283*, 663.

(21) Sun, J.; Sun, Y.; Zhu, J.; Zeng, J.; Du, H. *Adv. Mater. Res.* **2012,** *502*, 136.

(22) Tsai, M.-L.; Tu, W.-C.; Tang, L.; Wei, T.-C.; Wei, W.-R.; Lau, S.-P.; Chen, L. J.; He, J.-H. *Nano Lett.* **2016,** *16*, 309.

(23) Huang, C.-Y.; Wang, D. Y.; Wang, C.-H.; Chen, Y.-T.; Wang, Y.-T.; Jiang, Y.-T.; Yang, Y.-J.; Chen, C.-C.; Chen, Y.-F. *ACS Nano* **2010,** *4* (10), 5849.

(24) Aebischer, A.; Gumy, F.; Bünzli, J.-C. G. *Phys. Chem. Chem. Phys.* **2009,** *11*, 1346.

(25) Masoomi-Godarzi, S.; Liu, M.; Tachibana, Y.; Goerigk, L.; Ghiggino, K. P.; Smith, T. A.; Jones, D. J. *Adv. Energy Mater.* **2018,** *8*, 1801720.

(26) Levine, A. M.; Schierl, C.; Basel, B. S.; Ahmed, M.; Camargo, B. A.; Guldi, D. M.; Braunschweig, A., B. *J. Phys. Chem. C* **2019,** *123*, 1587.

(27) Lubert-Perquel, D.; Salvadori, E.; Dyson, M.; Stavrinou, P. N.; Montis, R.; Nagashima, H.; Kobori, Y.; Heutz, S.; Kay, C. W. M. *Nat. Commun.* **2018,** *9*, 4222.

(28) MacQueen, R. W.; Liebhaber, M.; Niederhausen, J.; Mews, M.; Gersmann, C.; Jäckle, S.; Jäger, K.; Tayebjee, M. J. Y.; Schmidt, T. W.; Rech, B.et al. *Mater. Horiz.* **2018,** *5*, 1065.

(29) Andreani, L. C.; Bozzola, A.; Kowalczewski, P.; Liscidini, M.; Redorici, L. *Advances in Physics: X* **2019,** *4* (1), 1548305.

(30) Trupke, T.; Green, M. A.; Würfel, P. *J. Appl. Phys.* **2002,** *92*, 4117.

(31) Bianchi, G. S.; Zanuto, V. S.; Astrath, F. B. G.; Malacarne, L. C.; Terra, I. A. A.; Catunda, T.; Nunes, L. A. O.; Jacinto, C.; Andrade, L. H. C.; Lima, S. M.et al. *Opt. Lett.* **2013,** *38* (22), 4667.

(32) Babu, P.; Martín, I. R.; Venkata Krishnaiah, K.; Hyo Jin Seo; Venkatramu, V.; Jayasankar, C. K.; Lavín, V. *Chem. Phys. Lett.* **2014,** *600*, 34.

(33) Weingarten, D. H.; LaCount, M. D.; Van de Lagemaat, J.; Rumbles, G.; Lusk, M. T.; Shaheen, S. E. *Nat. Commun.* **2017,** *8*, 14808.

(34) Song, P.; Zhang, C. M.; Zhu, P. F. *J. Opt.* **2016,** *18*, 015901.

(35) Shalav, A.; Richards, B. S.; Trupke, T.; Krämer, K. W.; Güdel, H. U. *Appl. Phys. Lett.* **2005,** *86*, 013505.

(36) Ramasamy, P.; Manivasakan, P.; Kim, J. *RSC Adv.* **2014,** *4*, 34873.

(37) Cheng, X.; Pan, Y.; Yuan, Z.; Wang, X.; Su, W.; Yin, L.; Xie, X.; Huang, L. *Adv. Funct. Mater.* **2018,** *28*, 1800208.

(38) Wang, B.; Wang, J.; Huang, G.; Li, S.; Mei, Y. *Chem. Nano Mat.* **2018,** *4*, 348.

(39) Li, D.; Ågren, H.; Chen, G. *Dalton Trans.* **2018,** *47*, 8526.

(40) Parker, C. A.; Hatchard, C. G. *P. Roy. Soc. A - Math. Phy.* **1962,** *269* (1339), 147.

(41) Wu, W.; Guo, H.; Wu, W.; Ji, S.; Zhao, J. *J. Org. Chem.* **2011,** *76*, 7056.

(42) Bachilo, S. M.; Weisman, R. B. *J. Phys. Chem. A* **2000,** *104* (33), 7711.

(43) Chen, K.; Yang, W.; Wang, Z.; Iagatti, A.; Bussotti, L.; Foggi, P.; Ji, W.; Zhao, J.; Di Donato, M. *J. Phys. Chem. A* **2017,** *121*, 7550−7564.

(44) Gertsen, A. S.; Koerstz, M.; Mikkelsen, K. V. *Phys. Chem. Chem. Phys.* **2018,** *20*, 12182.

(45) Steer, R. P. *Dalton Trans.* **2017,** *47* (26), 8517.

(46) Stevens, A. L.; Novakovic, S.; White, J. M.; Wong, W. W. H.; Smith, T. A.; Ghiggino, K. P.; Paige, M. F.; Steer, R. P. *J. Phys. Chem. A* **2018,** *122*, 9605−9614.

(47) Steer, R. P. *Can. J. Chem.* **2017,** *95*, 1025.

(48) Sugunan, S. K.; Tripathy, U.; Brunet, S. M. K.; Paige, M. F.; Steer, R. P. *J. Phys. Chem. A* **2009,** *113*, 8548.

(49) Gray, V.; Börjesson, K.; Dzebo, D.; Abrahamsson, M.; Albinsson, B.; Moth-Poulsen, K. *J. Phys. Chem. C* **2016,** *120*, 19018−19026.

(50) Dzebo, D.; Börjesson, K.; Gray, V.; Moth-Poulsen, K.; Albinsson, B. *J. Phys. Chem. C* **2016,** *120*, 23397−23406.

(51) Tilley, A. J.; Robotham, B. E.; Steer, R. P.; Ghiggino, K. P. *Chem. Phys. Lett.* **2015,** *618*, 198.

(52) Islangulov, R. R.; Kozlov, D. V.; Castellano, F. N. *Chem. Commun.* **2005,** *30*, 3776.

(53) Chen, Y.; Zhao, J.; Xie, L.; Guo, H.; Li, Q. *RSC Adv.* **2012,** *2*, 3942.

(54) Singh-Rachford, T. N.; Castellano, F. N. *J. Phys. Chem. A* **2009,** *113* (33), 9266.

(55) Boutin, P. C.; Ghiggino, K. P.; Kelly, T. L.; Steer, R. P. *J. Phys. Chem. Lett.* **2013,** *4*, 4113−4118.

(56) Baluschev, S.; Miteva, T.; Yakutkin, V.; Nelles, G.; Yasuda, A.; Wegner, G. *Phys. Rev. Lett.* **2006,** *97* (14), 143903.

(57) Xun, Z.; Zeng, Y.; Chen, J.; Yu, T.; Zhang, X.; Yang, G.; Li, Y. *Chem. Eur. J.* **2016,** *22*, 8654

(58) Lissau, J. S.; Gardner, J. M.; Morandeira, A. *J. Phys. Chem. C* **2011,** *115*, 23226.

(59) Liu, Q.; Yang, T.; Feng, W.; Li, F. *J. Am. Chem. Soc.* **2012,** *134*, 5390−5397.

(60) Schulze, T. F.; Czolk, J.; Cheng, Y.-Y.; Fückel, B.; MacQueen, R. W.; Khoury, T.; Crossley, M. J.; Stannowski, B.; Lips, K.; Lemmer, U.et al. *J. Phys. Chem. C* **2012,** *116*, 22794−22801.

(61) Nattestad, A.; Cheng, Y.-Y.; MacQueen, R. W.; Schulze, T. F.; Thompson, F. W.; Mozer, A. J.; Fückel, B.; Khoury, T.; Crossley, M. J.; Lips, K.et al. *J. Phys. Chem. Lett.* **2013,** *4*, 2073−2078.

(62) Zhao, W.; Castellano, F. N. *J. Phys. Chem. A* **2006,** *110*, 11440.

(63) Latterini, L.; Massaro, G.; Penconi, M.; Gentili, P. L.; Roscini, C.; Ortica, F. *Dalton Trans.* **2018,** *47*, 8557.

(64) Singh-Rachford, T. N.; Castellano, F. N. *J. Phys. Chem. Lett.* **2010,** *1*, 195.

(65) Durandin, N. A.; Isokuortti, J.; Efimov, A.; Vuorimaa-Laukkanen, E.; Tkachenko, N. V.; Laaksonen, T. *Chem. Commun.* **2018,** *54*, 14029.

(66) Eisenberger, H.; Nickel, B.; Ruth, A. A.; Steer, R. P. *J. Chem. Soc. Faraday Trans.* **1996,** *92* (5), 741.

(67) Nickel, B. *Chem. Phys. Lett.* **1979,** *68*, 17.

(68) Nickel, B.; Klemp, D. *Chem. Phys.* **1993,** *174*, 297.

(69) Kray, H.-J.; Nickel, B. *Chem. Phys.* **1980,** *53*, 235.

(70) O'Brien, J. A.; Rallabandi, S.; Tripathy, U.; Paige, M. F.; Steer, R. P. *Chem. Phys. Lett.* **2009,** *475*, 220.

(71) Goudarzi, H.; Keivanidis, P. E. *ACS Appl. Mater. Interfaces* **2017,** *9*, 845−857.

(72) Karpicz, R.; Puzinas, S.; Gulbinas, V.; Vakhnin, A.; Kadashchuk, A.; Rand, B. P. *Chem. Phys.* **2014,** *429*, 57.

(73) Baluschev, S.; Yakutkin, V.; Wegner, G.; Minch, B.; Miteva, T.; Nelles, G.; Yasuda, A. *J. Appl. Phys.* **2007,** *101*, 023101.

(74) Mori, T.; Mori, T.; Saito, A.; Koishi, H.; Nakamoto, C.; Fujii, A.; Saomoto, H. *Mol. Syst. Des. Eng.* **2018,** *3*, 908.

(75) Marsico, F.; Turshatov, A.; Peköz, R.; Avlasevich, Y.; Wagner, M.; Weber, K.; Donadio, D.; Landfester, K.; Baluschev, S.; Wurm, F. R. *J. Am. Chem. Soc.* **2014,** *136*, 11057−1106.

(76) Liu, Q.; Yin, B.; Yang, T.; Yang, Y.; Shen, Z.; Yao, P.; Li, F. *J. Am. Chem. Soc.* **2013,** *135*, 5029−5037.

(77) Mongin, C.; Golden, J. H.; Castellano, F. N. *ACS Appl. Mater. Interfaces* **2016,** *8*, 24038−24048.

(78) Rautela, R.; Joshi, N. K.; Novakovic, S.; Wong, W. W. H.; White, J. M.; Ghiggino, K. P.; Paige, M. F.; Steer, R. P. *Phys. Chem. Chem. Phys.* **2017,** *19*, 23471.

(79) Sato, R.; Kitoh-Nishioka, H.; Kamada, K.; Mizokuro, T.; Kobayashi, K.; Shigeta, Y. *J. Phys. Chem. Lett.* **2018,** *9*, 6638−6643.

(80) Yanai, N.; Kimizuka, N. *Chem. Commun.* **2016,** *52*, 5354.

(81) Ksenofontova, N. M.; Stel'makh, G. F.; Tsvirko, M. P. *Dokl. Akad. Nauk. SSSR.* **1986,** *289*, 405.

(82) Stel'makh, G. F.; Tsvirko, M. P. *J. Appl. Spectrosc.* **1982,** *36*, 430−435.

(83) Bünzli, J.-C. G.; Piguet, C. *Chem. Soc. Rev.* **2005,** *34*, 1048.

(84) Williams, R. *J. Chem. Phys.* **1958,** *28*, 577.

(85) Kee, H. L.; Bhaumik, J.; Diers, J. R.; Mroz, P.; Hamblin, M. R.; Bocian, D. F.; Lindsey, J. S.; Holten, D. J Photochem. Photobiol. A **2008,** *200*, 346.

(86) Dexter, D. L. *J. Chem. Phys.* **1953,** *21*, 836.

(87) Forster, L. S.; Livingston, R. *J. Chem. Phys.* **1952,** *20*, 1315.

(88) Heinrich, G.; Schoof, S.; Gusten, H. *J. Photochem.* **1974,** *3*, 315

(89) Fujiwara, Y.; Ozawa, R.; Onuma, D.; Suzuki, K.; Yoza, K.; Kobayashi, K. *J. Org. Chem.* **2013,** *78*, 2206−2212.

(90) Robinson, G. W.; Frosch, R. P. *J. Chem. Phys.* **1963,** *38*, 1187.

(91) Kasha, M. *Discuss. Faraday Soc.* **1950,** *9*, 14.

(92) Tripathy, U.; Kowalska, D.; Liu, X.; Velate, S.; Steer, R. P. *J. Phys. Chem. A* **2008,** *112*, 5824.

(93) Robotham, B.; Lastman, K. A.; Langford, S. J.; Ghiggino, K. P. *J. Photochem. Photobiol. A* **2013,** *251*, 167.

(94) Harada, K.; Fujitsuka, M.; Sugimoto, A.; Majima, T. *J. Phys. Chem. A* **2007,** *111*, 11430.

(95) Schechter, A. N. *Blood* **2008,** *112* (10), 3927.

(96) Yella, A.; Lee, H.-W.; Tsao, H. N.; Yi, C.; Chandiran, A. K.; Nazeeruddin, M.; Diau, E. W.-G.; Yeh, C.-Y.; Zakeeruddin, S. M.; Grätzel, M. *Science* **2011,** *334*, 629.

(97) Gao, K.; Li, L.; Lai, T.; Xiao, L.; Huang, Y.; Huang, F.; Peng, J.; Cao, Y.; Liu, F.; Russell, T. P.et al. *J. Am. Chem. Soc.* **2015,** *137*, 7282−7285.

(98) Čeklovský, A.; Takagi, S. *Cent. Eur. J. Chem.* **2013,** *11* (7), 1132.

(99) Mroz, P.; Bhaumik, J.; Dogutan, D. K.; Aly, Z.; Kamal, Z.; Khalid, L.; Kee, H. L.; Bocian, D. F.; Holten, D.; Lindsey, J. S.et al. *Cancer Lett.* **2009,** *282*, 63.

(100) Poorter, B.; Meunier, B. *Tetrahedron Lett.* **1984,** *25* (18), 1895.

(101) Simpson, W. T. *J. Chem. Phys.* **1949,** *17*, 1218.

(102) Niewodniczanski, H. *Physica* **1967,** *33* (1), 92.

(103) *The Porphyrin Handbook*; 1st ed.; Kadish, K. M.; Guilard, R.; Smith, K. M., Eds.: Academic Press, 2012; Vol. 16.

(104) Gouterman, M. *J. Mol. Spectrosc.* **1961,** *6*, 138.

(105) Prendergast, K.; Spiro, T. G. *J. Am. Chem. Soc.* **1992,** *114*, 3793.

(106) *The Porphyrin Handbook*; Kadish, K. M.; Smith, K. M.; Guilard, R., Eds.; Academic Press: San Diego, CA, 2000; Vol. 8.

(107) J., C. H. *Tetrahedron* **1973,** *29*, 899.

(108) Bonfantini, E. E.; Burrell, A. K.; Campbell, W. M.; Crossley, M. J.; Gosper, J. J.; Harding, M. M.; Officer, D. L.; Reid, D. C. W. *J. Porphyrins Phthalocyanines* **2002,** *6*, 708.

(109) *Advances in Inorganic Chemistry*; 1st ed.; van Eldik, R.; Stochel, G., Eds.; Academic Press: San Diego, CA, 2011; Vol. 63.

(110) Gouterman, M. *J. Chem. Phys.* **1959,** *30*, 1139.

(111) Gouterman, M.; Hanson, L. K.; Khalil, G.-E.; Buchler, J. W.; Rohbock, K.; Dolphin, D. *J. Am. Chem. Soc.* **1975,** *97* (11), 3142.

(112) Gurinovich, G. P.; Jagarov, B. M. *Luminescence of Crystals, Molecules, and Solutions*; Springer: Boston, MA, 1973.

(113) Spellane, P. J.; Gouterman, M.; Antipas, A.; Kim, S.; Liu, Y. C. *Inorg. Chem.* **1980,** *19*, 386.

(114) *The Porphyrin Handbook*; 1st ed.; Kadish, K. M.; Smith, K. M.; Guilard, R., Eds.; Academic Press: San Diego, CA, 2000; Vol. 3.

(115) Favereau, L.; Cnossen, A.; Kelber, J. B.; Gong, J. Q.; Oetterli, R. M.; Cremers, J.; Herz, L. M.; Anderson, H. L. *J. Am. Chem. Soc.* **2015,** *137*, 14256−14259.

(116) Rogers, J. E.; Nguyen, K. A.; Hufnagle, D. C.; McLean, D. G.; Su, W.; Gossett, K. M.; Burke, A. R.; Vinogradov, S. A.; Pachter, R.; Fleitz, P. A. *J. Phys. Chem. A* **2003,** *107*, 11331.

(117) Waiters, W. A.; de Paula, J. C.; Jackson, B.; Nutaitis, C.; Hall, K.; Lind, J.; Cardozo, K.; Chandran, K.; Raible, D.; Phillips, C. M. *J. Phys. Chem.* **1995,** *99*, 1166.

(118) Abraham, R. J.; Eivazi, F.; Pearson, H.; Smith, K. M. *J. Chem. Soc., Chem. Commun.* **1976,** (17), 699.

(119) O'Brien, J. A.; Lu, Y.; Hooley, E. N.; Ghiggino, K. P.; Steer, R. P.; Paige, M. F. *Can. J. Chem.* **2011,** *89*, 122.

(120) Steer, R. P. *J. Appl. Phys.* **2007,** *102*, 076102.

(121) Son, M.; Park, K. H.; Shao, C.; Würthner, F.; Kim, D. *J. Phys. Chem. Lett.* **2014,** *5*, 3601−3607.

(122) Hoche, J.; Schmitt, H.-C.; Humeniuk, A.; Fischer, I.; Mitrić, R.; Röhr, M. I. S. *Phys. Chem. Chem. Phys.* **2017,** *19*, 25002.

(123) Solomon, L. A.; Sykes, M. E.; Wu, Y. A.; Schaller, R. D.; Wiederrecht, G. P.; Fry, H. C. *ACS Nano* **2017,** *11*, 9112−9118.

(124) Callis, J. B.; Knowles, J. M.; Gouterman, M. *J. Phys. Chem.* **1973,** *77* (2), 154.

(125) Sapunov, V. V. *Opt. Spectrosc.* **2000,** *88* (3), 359.

(126) Sapunov, V. V. *J. Appl. Spectrosc.* **1998,** *65* (6), 898.

(127) Bansal, A. K.; Holzer, W.; Penzkofer, A.; Tsuboi, T. *Chem. Phys.* **2006,** *330*, 118.

(128) Nifiatis, F.; Su, W.; Haley, J. E.; Slagle, J. E.; Cooper, T. M. *J. Phys. Chem. A* **2011,** *115*, 13764.

(129) Hisada, K.; Ito, S.; Yamamoto, M. *J. Phys. Chem. B* **1997,** *101*, 6827.

(130) Ito, S.; Katayama, H.; Yamamoto, M. *Macromolecules* **1988,** *21*, 2456.

(131) Ito, S.; Numata, N.; Katayama, H.; Yamamoto, M. *Macromolecules* **1989,** *22*, 2207.

(132) Schweitzer, C.; Schmidt, R. *Chem. Rev.* **2003,** *103*, 1685−1757.

(133) Ventura, B.; Flamigni, L.; Marconi, G.; Lodato, F.; Officer, D. L. *New J. Chem.* **2008,** *32*, 166.

(134) Perthué, A.; Domínguez, I. F.; Verstappen, P.; Maes, W.; Dautel, O. J.; Wantz, G.; Rivaton, A. *Sol. Energ. Mat. Sol. C* **2018,** *176*, 336.

(135) Rabek, J. F.; Ranby, B. *Polym. Eng. Sci.* **1975,** *15* (1), 40.

(136) Cho, S.; Yoon, M.-C.; Kim, C. H.; Aratani, N.; Mori, G.; Joo, T.; Osuka, A.; Kim, D. *J. Phys. Chem. C* **2007,** *111*, 14881.

(137) Stevens, A. L.; Joshi, N. K.; Paige, M. F.; Steer, R. P. *J. Phys. Chem. B* **2017,** *121*, 11180−11188.

(138) Kärnbratt, J.; Gilbert, M.; Sprafke, J. K.; Anderson, H. L.; Albinsson, B. *J. Phys. Chem. C* **2012,** *116*, 19630−19635.

(139) Kim, T.; Ham, S.; Lee, S. H.; Hong, Y.; Kim, D. *Nanoscale* **2018,** *10*, 16438.

(140) Grozema, F. C.; Houarner-Rassin, C.; Prins, P.; Siebbeles, L. D. A.; Anderson, H. L. *J. Am. Chem. Soc.* **2007,** *129*, 13370.

(141) Huijser, A.; Suijkerbuijk, B. M. J. M.; Gebbink, R. J. M. K.; Savenije, T. J.; Siebbeles, L. D. A. *J. Am. Chem. Soc.* **2008,** *130*, 2485.

(142) Kim, P.; Lim, J. M.; Yoon, M.-C.; Aimi, J.; Aida, T.; Tsuda, A.; Kim, D. *J. Phys. Chem. B* **2010,** *114*, 9157.

(143) Hwang, I.-W.; Kamada, T.; Ahn, T. K.; Ko, D. M.; Nakamura, T.; Tsuda, A.; Osuka, A.; Kim, D. *J. Am. Chem. Soc.* **2004,** *126*, 16187.

(144) Nakamura, Y.; Hwang, I.-W.; Aratani, N.; Ahn, T. K.; Ko, D. M.; Takagi, A.; Kawai, T.; Matsumoto, T.; Kim, D.; Osuka, A. *J. Am. Chem. Soc.* **2005,** *127*, 236.

(145) Yoon, M.-C.; Cho, S.; Kim, P.; Hori, T.; Aratani, N.; Osuka, A.; Kim, D. *J. Phys. Chem. B* **2009,** *113*, 15074.

(146) Ikeda, T.; Tsuda, A.; Aratani, N.; Osuka, A. *Chem. Lett.* **2006,** *35* (8), 946.

(147) Song, N. W.; Cho, H. S.; Yoon, M.-C.; Aratani, N.; Osuka, A.; Kim, D. *Bull. Korean Chem. Soc.* **2002,** *23* (22), 271.

(148) Larsen, J.; Brüggemann, B.; Polívka, T.; Sundström, V.; Åkesson, E.; Sly, J.; Crossley, M. J. *J. Phys. Chem. A* **2005,** *109*, 10654.

(149) Larsen, J.; Brüggemann, B.; Khoury, T.; Sly, J.; Crossley, M. J.; Sundström, V.; Åkesson, E. *J. Phys. Chem. A* **2007,** *111*, 10589.

(150) Tilley, A. J.; Chen, M.; Danczak, S. M.; Ghiggino, K. P.; White, J. M. *Polym. Chem.* **2012,** *3*, 892.

(151) Wang, H.-W.; Liu, Z.-C.; Chen, C.-H.; Lim, T.-S.; Fann, W.; Chao, C.-G.; Yu, J.-Y.; Lee, S.-L.; Chen, C.-H.; Huang, S.-L.et al. *Chem. Eur. J.* **2009,** *15*, 5719

(152) Chou, C.-M.; Lee, S.-L.; Chen, C.-H.; Biju, A. T.; Wang, H.-W.; Wu, Y.-L.; Zhang, G.-F.; Yang, K.-W.; Lim, T.-S.; Huang, M.-J.et al. *J. Am. Chem. Soc.* **2009,** *131*, 12579.

(153) Fujitsuka, M.; Okada, A.; Tojo, S.; Takei, F.; Onitsuka, K.; Takahashi, S.; Majima, T. *J. Phys. Chem. B* **2004,** *108*, 11935.

(154) Wang, R.; Gao, B.; Jiao, W.; Yu, L.; Pan, W. *J. Appl. Polym. Sci.* **2014,** *131* (15), 40516.

(155) Fujitsuka, M.; Satyanarayana, K.; Luh, T.-Y.; Majima, T. *J. Photochem. Photobiol. A* **2016,** *331*, 56.

(156) Nguyen, S. B. T.; Johnson, L. K.; Grubbs, R. H.; Ziller, J. W. *J. Am. Chem. Soc.* **1992,** *114*, 3974.

(157) Kato, M.; Kamigaito, M.; Sawamoto, M.; Higashimura, T. *Macromolecules* **1995,** *28*, 1721—1723.

(158) Wang, J.-S.; Matyjaszewski, K. *J. Am. Chem. Soc.* **1995,** *117*, 5614.

(159) Moad, G.; Rizzardo, E. *Macromolecules* **1995,** *28*, 8722.

(160) Chiefari, J.; Chong, Y. K.; Ercole, F.; Krstina, J.; Jeffery, J.; Le, T. P. T.; Mayadunne, R. T. A.; Meijs, G. F.; Moad, C. L.; Moad, G.et al. *Macromolecules* **1998,** *31*, 5559.

(161) Li, Z.; Ma, J.; Cheng, C.; Zhang, K.; Wooley, K. L. *Macromolecules* **2010,** *43*, 1182.

(162) Häussler, M.; Lok, Y. P.; Chen, M.; Jasieniak, J.; Adhikari, R.; King, S. P.; Haque, S. A.; Forsyth, C. M.; Winzenberg, K.; Watkins, S. E.et al. *Macromolecules* **2010,** *43*, 7101.

(163) Moad, G.; Rizzardo, E.; Thang, S. H. *Polym. Int.* **2011,** *60*, 9.

(164) Destarac, M. *Polym. Rev.* **2011,** *51* (2), 163.

(165) Albertin, L.; Stenzel, M. H.; Barner-Kowollik, C.; Foster, L. J. R.; Davis, T. P. *Macromolecules* **2005,** *38*, 9075.

(166) McKenzie, T. G.; Colombo, E.; Fu, Q.; Ashokkumar, M.; Qiao, G. G. *Angew. Chem. Int. Ed.* **2017,** *56*, 12302

(167) Stenzel-Rosenbaum, M.; Davis, T. P.; Chen, V.; Fane, A. G. *J. Polym. Sci., Part A: Polym. Chem.* **2001,** *39*, 2777.

(168) Thurecht, K. J.; Blakey, I.; Peng, H.; Squires, O.; Hsu, S.; Alexander, C.; Whittaker, A. K. *J. Am. Chem. Soc.* **2010,** *132*, 5336.

(169) Wei, Z.; Zhu, S.; Zhao, H. *Polym. Chem.* **2015,** *6*, 1316.

(170) Patton, D. L.; Taranekar, P.; Fulghum, T.; Advincula, R. *Macromolecules* **2008,** *41*, 6703.

(171) Moad, G.; Rizzardo, E.; Thang, S. H. *Aust. J. Chem.* **2005,** *58*, 379.

(172) Chen, J.; Zhao, X.; Zhang, L.; Cheng, Z.; Zhu, X. *J. Polym. Sci., Part A: Polym. Chem.* **2015,** *53*, 1430.

(173) Foster, J. C.; Matson, J. B. *Macromolecules* **2014,** *47*, 5089−5095.

(174) Keddie, D. J.; Moad, G.; Rizzardo, E.; Thang, S. H. *Macromolecules* **2012,** *45*, 5321−5342.

(175) Moad, G. *Macromol. Chem. Phys.* **2014,** *215*, 9−26.

(176) Nguyen, M. N.; Bressy, C.; Margaillan, A. *Polymer* **2009,** *50*, 3086.

(177) Odian, G. *Principles of polymerization*; John Wiley & Sons: Hoboken, NJ, 2004.

(178) Ferruti, P.; Bettelli, A.; Fere, A. *Polymer* **1972,** *13*, 462.

(179) Wuyts, C.; Dermaut, W.; Hoefnagels, R.; Aerts, G.; Goovaerts, E.; Geise, H. J. *Polym. Int.* **2003,** *52*, 1660.

(180) Wang, L.; Li, J.; Zhang, W.; Chen, G.; Zhang, W.; Zhu, X. *Polym. Chem.* **2014,** *5*, 2872.

(181) Banal, J. L.; Soleimaninejad, H.; Jradi, F. M.; Liu, M.; White, J. M.; Blakers, A. W.; Cooper, M. W.; Jones, D. J.; Ghiggino, K. P.; Marder, S. R.et al. *J. Phys. Chem. C* **2016,** *120*, 12952−12958.

Chapter 2

Photon Upconversion of Sterically-Bulky Zn(II) Porphyrins in Solution and Solid-State PVA Films

2.1 Introduction

2.1.1 Background

Zn(II) porphyrin derivatives are unique as they are one of the few chromophores that can produce fluorescence via NCPU-TTA without need for triplet energy transfer to another emitting species i.e. homomolecular NCPU-TTA. Homomolecular TTA systems that rely on triplet sensitizers based on Zn(II) porphyrin derivatives have recently been shown to successfully participate in NCPU in the solid state, both when the sensitizer has been deposited as pure thin film[1] and when the sensitizer has been immersed in an inert polymer matrix.[2] Solid-state NCPU-TTA systems would likely be more desirable for commercial use compared to their solution-based NCPU-TTA system counterparts, as they would have a greater potential to be fabricated into everyday appliances and light harvesting devices in a practical manner.

As mentioned in the Introduction, porphyrins readily become spatially associated via aggregation. A degree of aggregation of the porphyrins is necessary for homomolecular TTA to occur in solid films,[2] however, ground state porphyrins in close proximity to the product higher excited singlet (S_2) state from TTA such as those in aggregates, including the resultant ground state porphyrin produced from the TTA encounter, can provide additional radiationless deactivation pathways for the higher excited state (S_2) porphyrin which diminishes the NCPU fluorescence yield of the TTA system.[3,4]

In order to minimize the effects of aggregation quenching on NCPU-TTA, it may be necessary to reduce the degree of aggregation of the porphyrins by spatially separating the π-electron rich porphyrin planes from one another. A common approach taken to reduce aggregation between porphyrins and increase their solubility in organic solvents has been to install relatively inert bulky side chain groups, such as 3,5-di-*tert*-butylphenyl[5] (Figure 2.1) and mesityl[6] at the meso-positions of the porphyrin ring. Sterically bulky di-tert butyl groups have proven successful in preventing excimer quenching in TTA systems previously.[7] Side groups such as (3,5-trihexylsilyl)phenyl[8] and 2,4,6-tris(3,5-di-tert-butylphenoxy)phenyl[9] have previously been incorporated into the structures of porphyrins in extreme cases where any chance of aggregation between porphyrins needed to be eliminated.

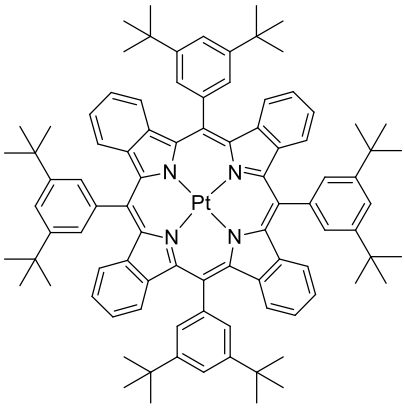

Figure 2.1: 3,5-di-*tert*-butylphenyl substituents used to decrease aggregation and increase solubility of a porphyrin-based triplet sensitizer.[5]

It has been shown that Soret excitation of Zn(II) porphyrin aggregates results in no emission from the S_2 state, in contrast to the widely documented S_2 emission observed from TTA between two triplet state Zn(II) porphyrins.[10] As the porphyrins in the encounter complex cannot diffuse from each other faster than the S_2 lifetime in solution, and are rigidly fixed in the solid state, it has been postulated that the spatial separation between porphyrins that successfully produce observable UC fluorescence is sufficient to inhibit access of the S_2 state to the S_1 potential surface in the excited-state dimer product of TTA.

Although strong aggregation between porphyrins may present problems for homomolecular TTA systems as discussed above, increasing the separation of the porphyrins beyond a certain limit may not allow for sufficient orbital overlap between two porphyrins in their triplet state such that TTA can occur effectively. Inclusion of 2,4,6-triethylphenyl substituents at the meso-positions of Pt(II) tetraphenylporphyrin (PtTPP) has been shown to sterically protect the electronic environment of the porphyrin core, increasing the triplet lifetime of the 2,4,6-triethylphenyl-substituted porphyrin with respect to the parent PtTPP and inhibiting oxygen quenching, but consequently reducing the rate of homomolecular TTA in solution compared to the TTA rate observed for PtTPP.[11] A increased Pt-Pt distance of 10.8 Å is observed in the crystal structure of the 2,4,6-triethylphenyl-substituted compound (Figure 2.2) compared to 8.3 Å in PtTPP. Although reduction in TTA mediated self-quenching rate has been attributed to steric shielding of the π-orbitals in the porphyrin ring when employing ethyl groups in the ortho positions of the meso-phenyl substitutents, prior to this work no study was present in the literature that explored the optimization of homomolecular NCPU-TTA as a function of the steric bulk of the peripheral substituents on the porphyrin macrocycle. Considering the widespread use of various side-chain groups in metalloporphyrin structures used in both hetero- and homomolecular TTA applications, an understanding of the structure-property relationship between steric bulk of annihilating species and their TTA-mediated UC fluorescence yields is therefore of immense value and interest to furthering the development of commercially viable NCPU-TTA based devices.

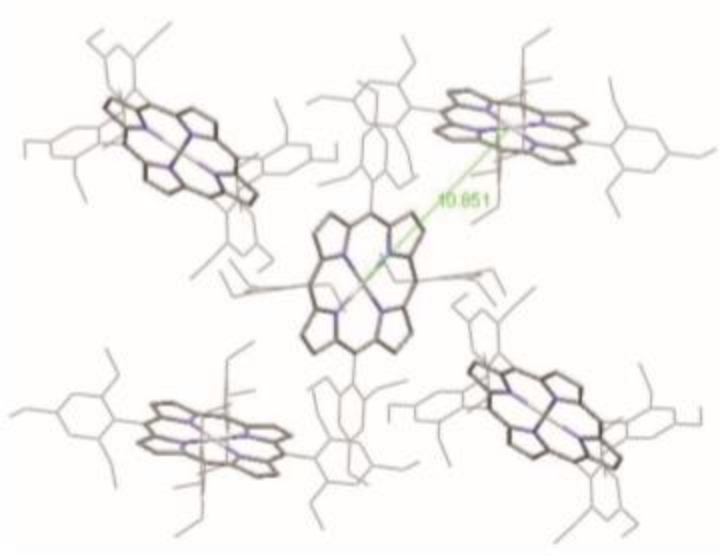

Figure 2.2: Crystal structure of [5,10,15,20-tetrakis(2,4,6-triethylphenyl)porphyrinato] platinum(II) reproduced from the work of Moiseev *et al.*[11]

One of the major limitations of TTA systems is that they must remain oxygen-free, as atmospheric oxygen exists as a triplet biradical and can undergo TTA with triplets present in the system to form singlet oxygen,[12] which quenches triplets intended to be producing upconverted fluorescence and can potentially degrade the annihilating species in the system. Poly(vinyl alcohol) (PVA) thin films have been previously utilized for development of photovoltaic device encapsulation systems due to their low oxygen permeability.[13] The ability for PVA to act as an oxygen barrier may be similarly applicable to maintaining air-free conditions in solid-state homomolecular UC systems.

2.1.2 Chapter Overview and Objectives

The work presented in this chapter was part of a collaboration led by the research group of Professor Ronald P. Steer, University of Saskatchewan, Canada, and resulted in a joint publication entitled "Determinants of the Efficiency of Photon Upconversion by Triplet-Triplet Annihilation in the Solid State: Zinc Porphyrin Derivatives in PVA".[14] The objective of the work presented in this chapter is to explore and rationalize the changes in fluorescence upconversion

yields of NCPU-TTA systems in both solution and solid-state PVA matrices, that employ Zn(II) porphyrin derivatives as dual absorber-upconverter molecules, when systematic modifications to the steric bulk of the porphyrin substituents are introduced. The contribution outlined in this chapter to the published work was to design and synthesize the molecules for study and collaborate in the interpretation of theory and additional spectroscopic results obtained by collaborators at the University of Saskatchewan. Additional triplet state analysis of the compounds was performed after publication. A series of di- and tetra-substituted Zn(II) porphyrin derivatives were synthesized with side-groups of varying steric bulk introduced at the meso-positions of the porphyrin macrocycle, as outlined below in Figure 2.3. NCPU-TTA fluorescence yields, PVA thin film fabrication and computational data were obtained in collaboration with the Steer research group from the University of Saskatchewan, Canada.

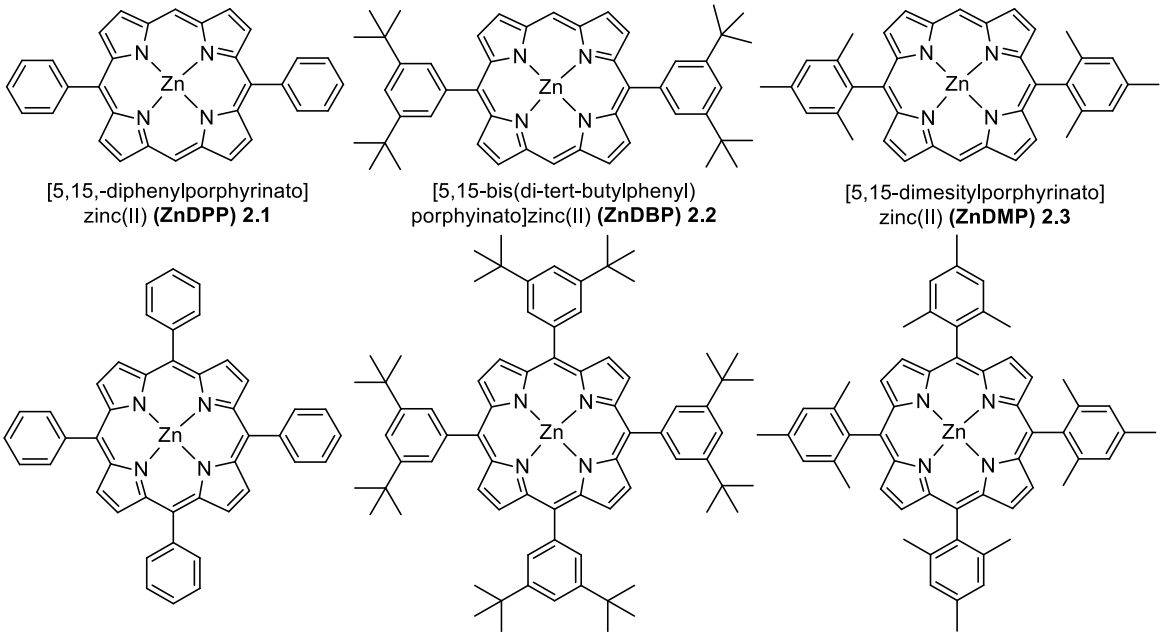

Figure 2.3: Zn(II) porphyrins synthesized and studied in chapter 2.

2.2 Synthetic Approach and Design

As Zn(II) tetraphenylporphyrin is one of the most commonly studied triplet sensitizers employed in both homo- and heteromolecular TTA systems, it was chosen as the model compound in this work upon which additional steric bulk would be incorporated progressing through the series of synthesized compounds. As discussed in the Introduction chapter section **1.5.3.3**, the use of Zn(II) as the central metal ion in the porphyrin ligand is necessary to produce observable fluorescence from the S_2 state, as Pd and Pt porphyrins are non-emissive from the S_2 state. The meso-substituents chosen to increase steric bulk were 3,5-di-tert-butylphenyl and mesityl (2,4,6-trimethylphenyl) groups, as they provide suitable incremental increases in steric bulk with respect to Zn(II) tetraphenylporphyrin. Porphyrins with 2,6-di-ortho substituted phenyl groups at the meso positions, such as the mesityl and 2,4,6-triethylphenyl groups, lock the meso-phenyl plane perpendicular to the porphyrin plane, hence increasing porphyrin-to-porphyrin plane separation compared to meso-phenyl groups with the same substituents in other places. The most common method of synthesizing tetra-substituted porphyrins is via the acid-catalysed condensation-cyclization of an aldehyde and pyrrole in the presence of atmospheric oxygen, outlined by Adler's method[15] (Figure 2.4). This method has been successfully implemented in the syntheses of 5,10,15,20-tetraphenylporphyin[15] (TPP) **2.10** and 5,10,15,20-tetrakis(3,5-di-*tert*-butylphenyl)porphyrin[16] (TBP) **2.11** previously. Adler's method for the synthesis of porphyrins was followed in order to obtain the aforementioned compounds **2.10** and **2.11** for use in the work studied in this chapter.

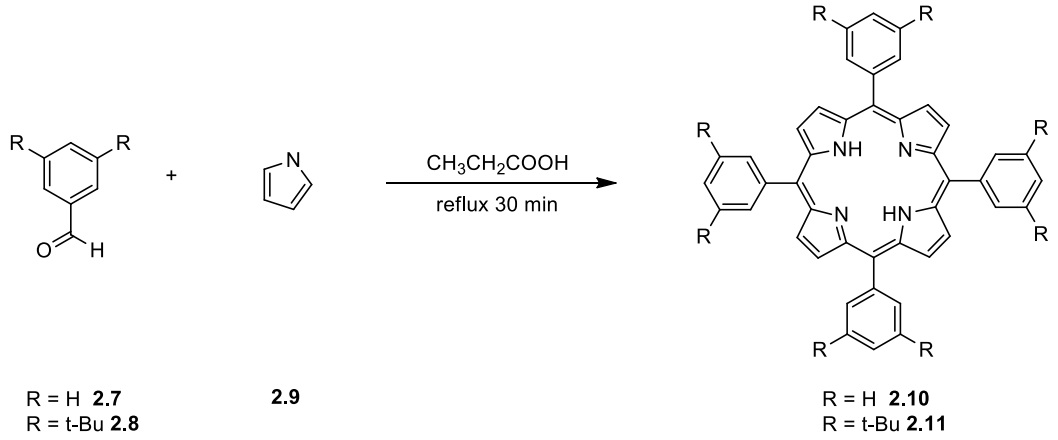

Figure 2.4: Adler's synthesis of tetraarylporphyrins TPP **2.10** and TBP **2.11**.[15,16]

Ortho-substituted benzaldehyde derivatives such as mesitaldehyde, yield almost no porphyrin under Adler's conditions; Lindsey and Wagner[17] have reasoned that this is because the kinetic barrier due to steric repulsion between the ortho-substitutents and the meso-hydrogen present in the porphyrinogen resulting from condensation between the aldehyde and pyrrole, is too high for Adler's conditions to overcome. Some ortho-substituents larger than methyl may also prove too large to fit inside the groove below the tetrahedral meso-carbon of the theoretical porphyrinogen. The steric interactions of the ortho-substituents with the porphyrinogen are outlined in Figure 2.5.

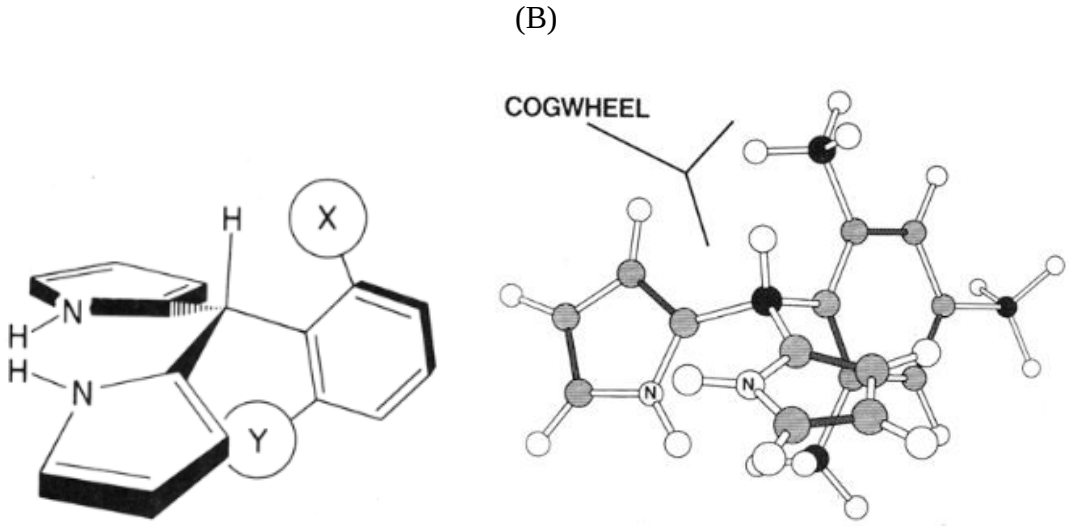

Figure 2.5: (A) Segment of tetraarylporphyrinogen with ortho-substituents X (above the groove) and Y (below the groove) labeled. (B) Ball-and-stick model of segment of tetramesitylporphyrinogen, with the cogwheeling interaction of the ortho-methyl protons about the meso-hydrogen outlined. Porphyrinogen segment figures (A) and (B) above reproduced from the work of Lindsey and Wagner.[17]

Lindsey and Wagner found that a combination of BF_3 and EtOH provided catalytic conditions necessary for the formation of the porphyrinogen from mesitaldehyde to yield tetramesitylporphyrin (TMP) **2.13** in appreciable yield. Part of the rationale in the improvement of the reaction yield was due to the increased basicity of mesitaldehyde due to steric

destabilization of resonance, with BF_3 exhibiting a 100 fold increase in binding affinity to mesitaldehyde compared to benzaldehyde.[17] The inclusion of ethanol in the reaction mixture is necessary to displace the highly stable BF_3-mesitaldehyde complex. Upon formation of the porphyrinogen under Lindsey's conditions, the use of DDQ as an oxidant is required to induce aromatization of the macrocycle. The synthetic procedures outlined in Lindsey and Wagner's work (Figure 2.6) were replicated in order to achieve the compound 5,10,15,20-tetramesitylporphyrin[17] (TMP) **2.13** desired for use in the work studied in this chapter.

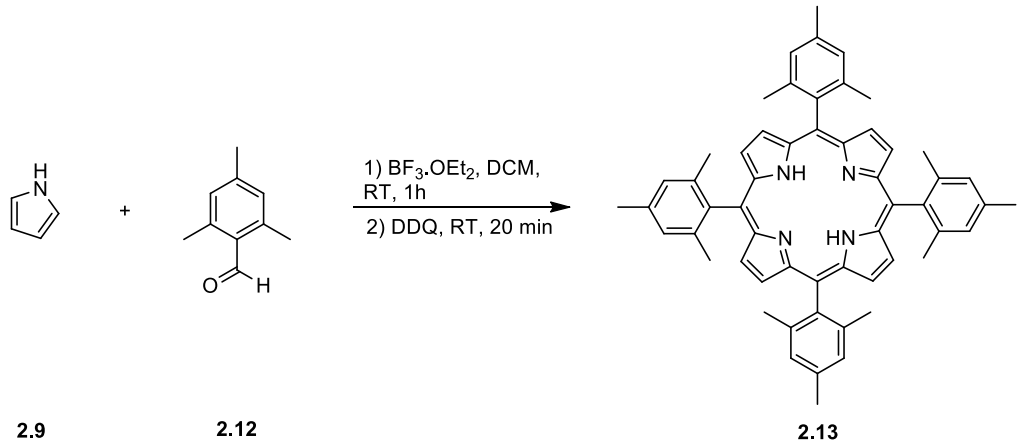

Figure 2.6: Lindsey's synthesis of tetramesitylporphyrin **2.13**.[17]

The general approach in the literature toward the synthesis of meso- di-substituted porphyrins, is to perform acid-catalysed condensation cyclizations between dipyrromethane and a substituted aldehyde to form a porphyrinogen, followed by oxidation with DDQ in order to introduce aromaticity into the macrocycle.[18-20] The central methylene in dipyrromethane introduces an unsubstituted meso- carbon upon incorporation into the porphyrinogen macrocycle. In this manner, planes of D_{2h} symmetry are introduced into the porphyrin structure. As discussed for the synthesis of tetramesitylporphyrin, BF_3/EtOH co-catalysis is necessary to form the dipyrrin fragment of the porphyrinogen that contains the ortho-substituted meso-phenyl group .This methodology has been successfully implemented in the synthesis of the compound 5,15-dimesitylporphyrin[18] (DMP) **2.16**, desired for use in the work presented in this chapter. Stirring dipyrromethane and either benzaldehyde or 3,5-di-tert-butylbenzaldehyde with TFA as an acid catalyst have proven appropriate conditions for the synthesis of the desired compounds in this

study, 5,15-diphenylporphyrin[19] (DPP) **2.14** and 5,15-bis(3,5-di-tert-butylphenyl)porphyrin[20] (DBP) **2.15**.

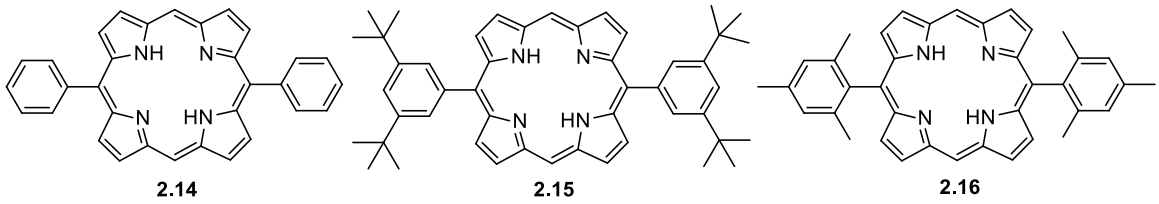

Figure 2.7: Di-substituted free-base porphyrins **2.14 -2.16** synthesized in the work discussed in chapter 2.

2.3 Synthesis

Although the precursors benzaldehyde, mesitylaldehyde and pyrrole were readily obtainable from chemical suppliers, it was practical to synthesize multi-gram amounts of 3,5-di-tert-butylbenzaldehyde **2.8** and dipyrromethane **2.19** in the laboratory. In order to synthesize 3,5-di-tert-butylbenzaldehyde **2.8**, 3,5-di-*tert*-butyltoluene and NBS were refluxed with AIBN to yield the intermediate 1-(bromomethyl)-3,5-di-*tert*-butylbenzene **2.18**. Without further purification, the 1-(bromomethyl)-3,5-di-*tert*-butylbenzene **2.18** was formylated via the Sommelet reaction following literature procedures[21] to give 3,5-di-tert-butylbenzaldehyde **2.8** in 52% yield after recrystallization from EtOH (Figure 2.8).

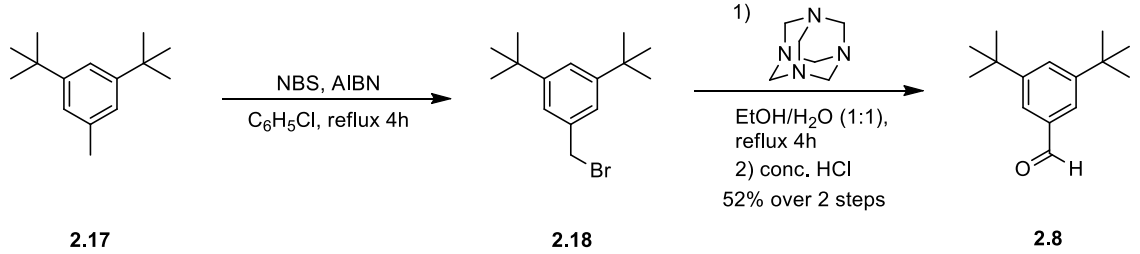

Figure 2.8: Synthesis of 3,5-di-tert-butylbenzaldehyde **2.8**.

Dipyrromethane **2.19** was synthesized in accordance with literature[22] from paraformaldehyde and pyrrole in the presence of $InCl_3$ Lewis-acid catalyst in 66% after silica gel column chromatography purification (Figure 2.9). Care was taken in order to prevent exposure of the dipyrromethane to light and oxygen throughout the work up, purification and when storing the compound, as it is susceptible to oxidation under ambient conditions.

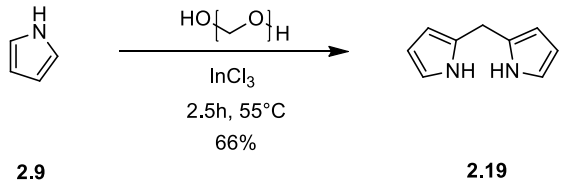

Figure 2.9: Synthesis of dipyrromethane **2.19**.

Chelation of the inner ring nitrogens to Zn^{2+} ions was achieved for all porphyrins by stirring the desired free-base porphyrin in a 3:1 DCM/MeOH solution with zinc acetate dihydrate overnight. The general scheme for the synthesis of all compounds studied in this chapter is outlined in Figure 2.10 below. The synthetic conditions and yields for each reaction step are outlined in Table 2.1.

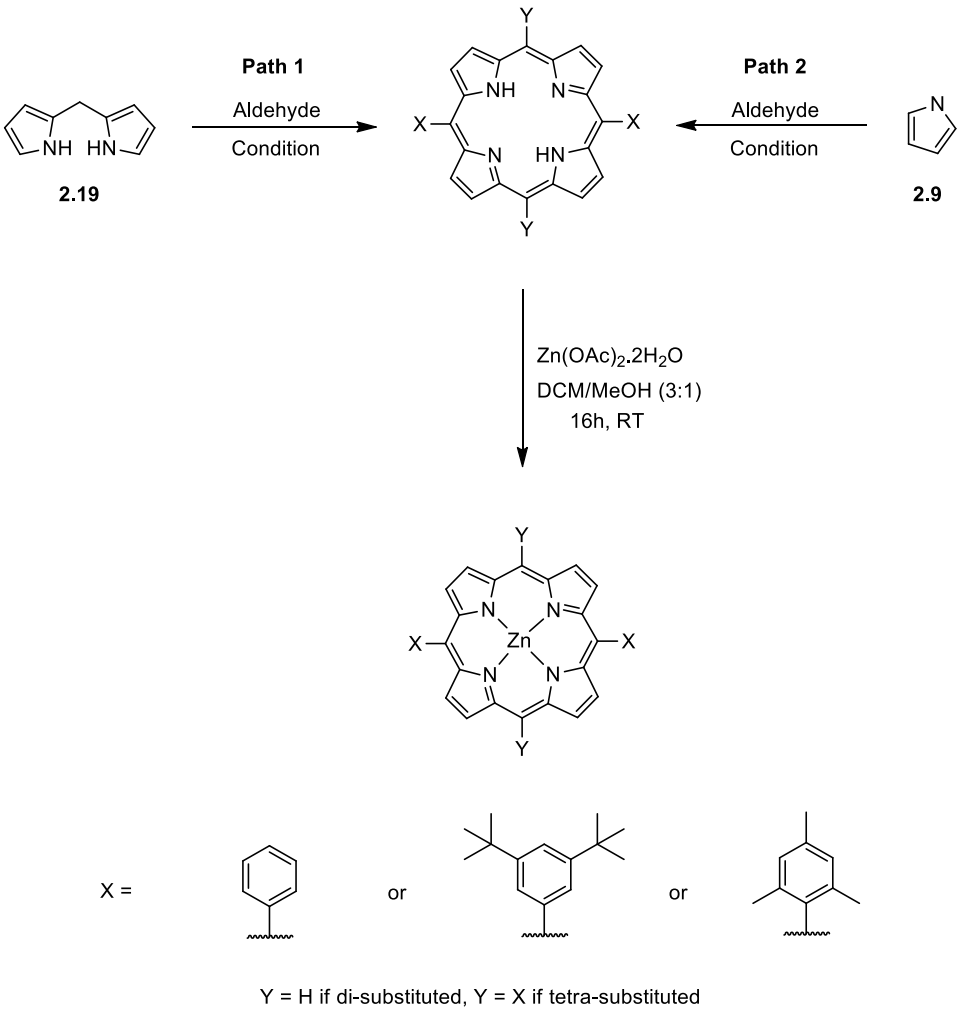

Figure 2.10: Synthetic pathways for the synthesis of tetra- and di-substituted Zn(II) porphyrins **2.1 – 2.6**.

Table 2.1: Synthetic conditions and yields for the synthesis of the tetra- and di-substituted porphyrins **2.10, 2.11, 2.13** and **2.14 – 2.16** and their Zn(II) metalated analogues **2.1**-**2.6**.

Desired Final Product	**Aldehyde**	**Conditions**	**Free-base Porphyrin yield**	**Reaction Path**	**Porphyrin metalation yield**
ZnDPP **2.1**	Benzaldehyde **2.7**	1)TFA, DCM, RT, 3h 2) DDQ, RT, 20 min	(compound **2.14**) 21%	1	98%
ZnDBP **2.2**	3,5-(Di-*tert*-butyl) benzaldehyde **2.8**	1)TFA, DCM, RT, 3h 2) DDQ, RT, 20 min	(compound **2.15**) 17%	1	94%
ZnDMP **2.3**	Mesitaldehyde **2.12**	1) BF_3•OEt_2, 1% EtOH in DCM, RT, 1h 2)DDQ, RT, 20 min	(compound **2.16**) 27%	1	90%
ZnTPP **2.4**	Benzaldehyde **2.7**	CH_3CH_2COOH, Reflux 30 min	(compound **2.10**) 15%	2	71%
ZnTBP **2.5**	3,5-(Di-*tert*-butyl) benzaldehyde **2.8**	CH_3CH_2COOH, Reflux 30 min	(compound **2.11**) 8%	2	94%
ZnTMP **2.6**	Mesitaldehyde **2.12**	1) BF_3•OEt_2, 1% EtOH in DCM, RT, 1h 2)DDQ, RT, 20 min	(compound **2.13**) 29%	2	98%

The low yields of the free-base porphyrins were expected due to a significant portion of polypyrrolic oligomers of variable length that did not cyclise in the porphyrin-forming reactions, and were observed upon column chromatography as a slow-moving, thick black band. The yields for TPP **2.10**,[15] TMP **2.13**[17] and DMP **2.16**[18] were consistent with the literature however the yields of TBP **2.11**,[16] DPP **2.14**[19] and DBP **2.15**[20] were lower than expected. Due to the small mass of each porphyrin required for photophysical analysis, it was deemed unnecessary to optimize the yields of the free-base porphyrins for the purposes of the work presented in this chapter. Regardless, a repeat iteration of the synthesis of TMP was performed as reported in this chapter (yield of 29%, Table 2.1), which improved upon the yield reported in the corresponding publication (11% yield).[14] The metalation of the free-base porphyrins was near-quantitative, with the yield of metalation of TPP being an anomaly due to loss of product upon work-up.

Successful synthesis of tetra-substituted porphyrins was confirmed by the large singlets observed around 8.5-9.0 ppm in their respective ^{1}H NMR spectra, corresponding to the β-pyrrolic protons in identical environments due to their D_{4h} symmetry. The di-susbtituted porphyrins show splitting in the β-pyrrolic proton peaks in their respective ^{1}H NMR spectra due to loss of symmetry, and a peak at approx. 10.20 – 10.40 ppm due to the 2 meso- protons not present in the tetra-substituted porphyrins. The absence of the broad singlet between -2.40 and -3.10 ppm in the ^{1}H NMR spectra of all Zn(II) metalated porhyrins, present in their respective parent free-base porphyrins, is indicative of loss of inner ring N-H protons upon chelation to zinc(II). An example of ^{1}H NMR spectra for free-base tetra- and di-substituted porphyrins and their metalated derivatives are shown below for ZnDMP **2.3** (Figure 2.11) and ZnTPP **2.4** (Figure 2.12).

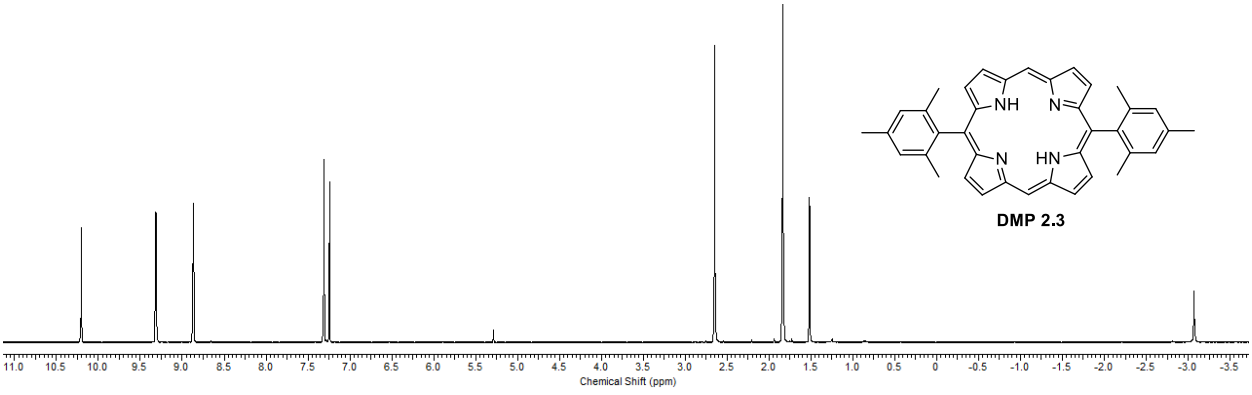

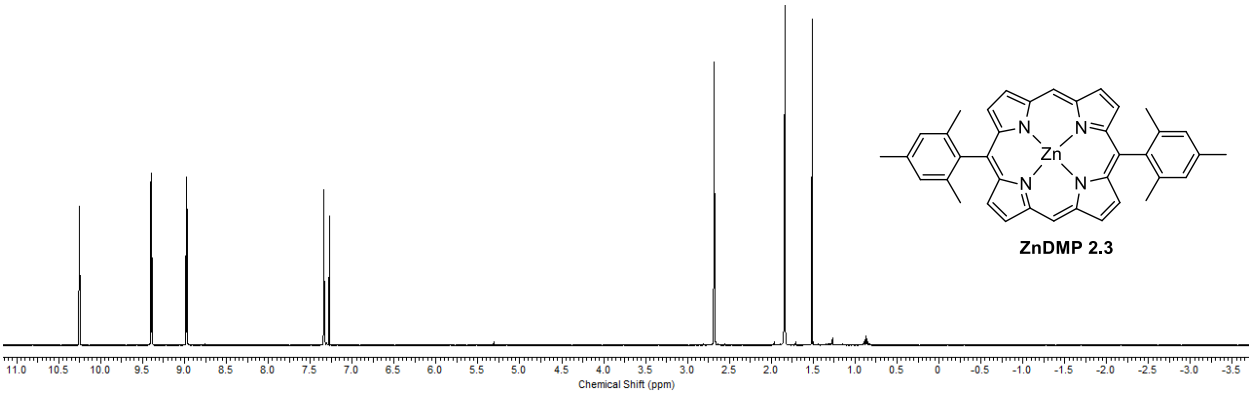

Figure 2.11: ^{1}H NMR spectra depicting characteristic peaks of di-substituted free-base and metalated porphyrins. DMP **2.16** is shown at the top and ZnDMP **2.3** is shown at the bottom.

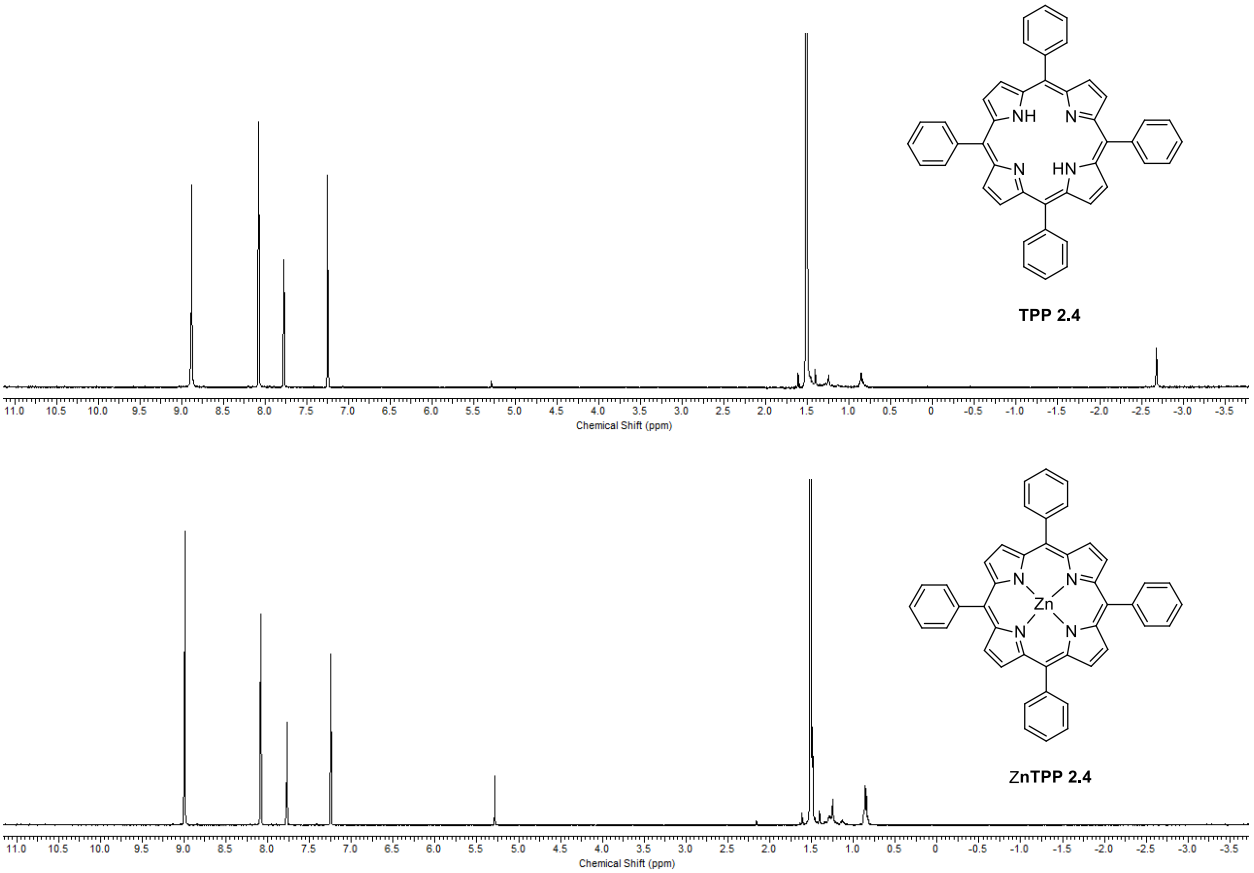

Figure 2.12: ^{1}H NMR spectra depicting characteristic peaks of tetra-substituted free-base and metalated porphyrins. TPP **2.10** is shown at the top and ZnTPP **2.4** is shown at the bottom.

2.4 Steady-State Solution Photophysics

2.4.1 Absorbance Measurements

The UV-visible absorption and fluorescence spectra for the tetra- and di- substituted porphyrins were obtained from solutions in toluene at room temperature (Figure 2.13). The concentration of all solutions used to obtain the absorption spectra was 3.3 μM. Absorption maxima for the Soret and Q-bands as well as the molar extinction coefficients (ε) for all compounds are listed in Table 2.2. ZnDPP **2.1** and ZnTPP **2.4** were synthesized in house but were only used for comparative purposes in the steady-state photophysical studies and transient absorption spectra presented in this chapter; all TTA-UC experiments in the publication corresponding to the work in this chapter were performed on commercially sourced ZnDPP **2.1** and ZnTPP **2.4**.[14]

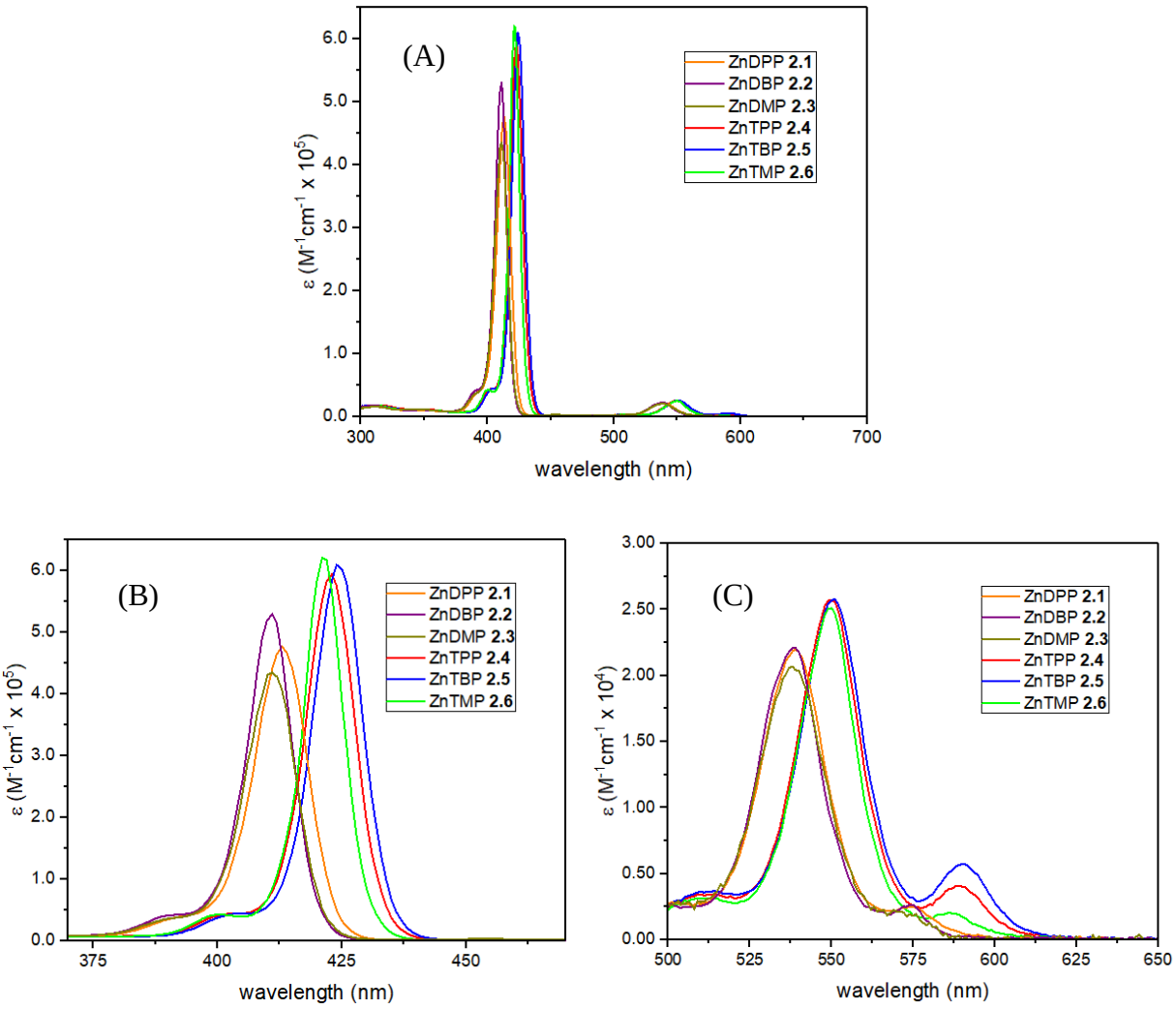

Figure 2.13: (A) Absorption spectra of the tetra- and di- substituted porphyrins **2.1-2.6** in toluene. (B) Spectra in (A) zoomed into Soret region for clarity. (C) Spectra in (A) zoomed into Q-band region for clarity.

Table 2.2: Absorption data for the tetra- and di-substituted porphyrins **2.1-2.6** in toluene.

Compound	λ_{max} Soret (nm)	ε Soret (10^5 $M^{-1}cm^{-1}$)	λ_{max} Q-band abs (nm) [(1,0),(0,0)]	ε Q-band (10^4 $M^{-1}cm^{-1}$) [(1,0),(0,0)]	ε Q-band at 532 nm (10^3 $M^{-1}cm^{-1}$)
ZnDPP **2.1**	411	4.35	538, 570	2.07, 0.20	17.3
ZnDBP **2.2**	413	4.77	539, 575	2.20, 0.25	17.7
ZnDMP **2.3**	411	5.30	539 [(1,0)]	2.21 [(1,0)]	18.8
ZnTPP **2.4**	423	5.94	550, 589	2.56, 0.41	6.83
ZnTBP **2.5**	424	6.10	551, 590	2.58, 0.58	6.48
ZnTMP **2.6**	421	6.21	550, 586	2.51, 0.21	6.32

The absorption maxima and the molar extinction coefficients for both the Soret and Q-bands within the set of all tetra-substituted Zn(II) porpyhrins were almost identical, and within the set of all di-substituted Zn(II) porphyrins again all maxima were identical. These results are corroborated by measurements recorded by the Steer group as part of the publication associated with this work.[14] The similarity was to be expected, as substitution of the meso-phenyl groups with various alkyl substitutents should not introduce any significant inductive effects into the molecular orbitals of the porphyrin aromatic ring such that shifts in absorption maxima should occur, nor do they extend the conjugation of π-orbitals in the porphyrin, which could increase the observed extinction coefficients of the porphyrins. The similarity in absorption properties allows for the assumption to be made that any differentiation in TTA properties or NCPU fluorescence yields between the studied porphyrins would not arise due to a mismatch between the amount of incident light energy being absorbed by the TTA systems under comparison.

The observed trends in relative absorption intensities in the zinc porphyrin series are consistent with theory in the literature. According to Gouterman's four orbital theory,[23] inclusion of electron-donating substitutents at the meso-positions is known to alter the a_{2u} orbital such that the HOMO increases, explaining the red-shifting of the Q-band absorption maxima of the tetra-substituted porphyrins, which contain additional electron donating aryl substituents at the meso-positions compared to the di-substituted porphyrins. The Q(1,0) band extinction coefficients remain similar within the sets of tetra- and di-substituted porphyrins as relatively consistent degrees of vibronic intensity borrowing from the Soret bands are in effect.[24] Modification of the HOMO by virtue of variation of the nature of the donating substituents at the meso-positions lifts the accidental degeneracy of the two HOMO orbitals a_{1u} and a_{2u}, and the ideally forbidden Q(0,0) transition becomes more allowed with greater mismatch between a_{1u} and a_{2u} orbital energies.[25] The ratio of the absorption intensities of the Q(0,0) to Q(1,0) vibronic bands is represented by the equation:

$$\frac{A[Q(0,0)]}{A[Q(1,0)]} = (constant)[E(a_{2u}, e_g) - E(a_{1u}, e_g)]^2 \qquad (2.1)$$

where A[Q(0,0)] and A[Q(1,0)] represent the absorption intensities of the Q(0,0) and Q(1,0) bands respectively, and $E(a_{2u},e_g)$ and $E(a_{1u},e_g)$ represent the energy gap between the HOMO and HOMO-1 respectively.[25] The fact that equation 2.1 relates the vibronic intensities of the Q-band to the energy difference between the two allowed transitions via a square relationship means small shifts from degeneracy in the a_{2u} and a_{2u} orbitals will result in more pronounced increases in the Q(0,0) extinction coefficients. The slight variance in the extinction coefficients of the (0,0) vibronic transitions are therefore potentially due to the degree of freedom of rotation in the meso-aryl substituents due to their steric bulk and substitution pattern, allowing for different degrees of orbital overlap and electron donating ability of the aromatic aryl group with the porphyrin macrocycle. This is evident in the observation that the mesityl substituted compounds have the weakest Q(0,0) transition as they are completely locked perpendicular to the porphyrin plane. The dihedral angle between the porphyrin plane and the meso-phenyl rings has previously been shown to play a role in determining the electronic properties of meso-aryl substituted porphyrins due to meso-phenyl-to-porphyrin conjugation effects and subsequent distortion of macrocycle planarity.[26]

2.4.2 Fluorescence Measurements

The fluorescence spectra are shown in Figure 2.14 below. The fluorescence spectra in Figure 2.14 were corrected for the photomultiplier detector wavelength response. Fluorescence quantum yields of all tetra- and di- substituted porphyrins were calculated relative to ZnTPP ($\Phi = 0.033$ in toluene)[27] and are listed in Table 2.3. Data obtained for Soret excited emission, fluorescence lifetimes (τ_1), and both radiative and non-radiative rate constants for S_1 fluorescence decays (k_r and k_{nr} respectively) were obtained by Dr. Ranjana Rauleta and Dr. Neeraj K. Joshi of the University of Saskatchewan, Canada.

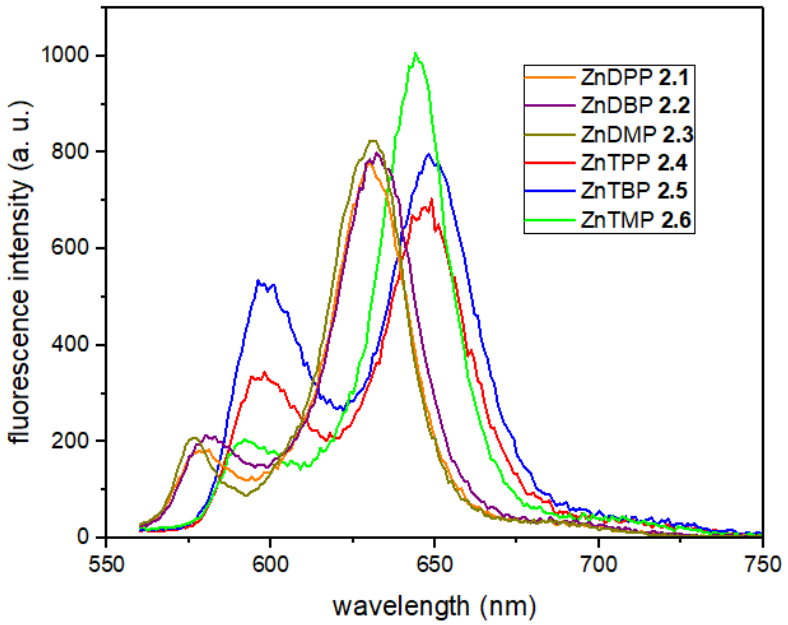

Figure 2.14: Fluorescence spectra of the tetra- and di-substituted porphyrins **2.1-2.6** in toluene. Samples were diluted to have a 0.05 absorbance at the Q-band maximum.

Table 2.3: Fluorescence data for the tetra- and di-substituted porphyrins **2.1-2.6** in toluene.

Compound	λ_{max} Soret band (nm)	λ_{max} Q-band (nm)	Φ_f Q-band	τ_1 (ns)	k_r ($x10^9$ s^{-1})	k_{nr} ($x10^9$ s^{-1})
ZnDPP **2.1**	418	581, 630	0.027	2.3 ± 0.1	0.012 ± 0.002	0.423 ± 0.021
ZnDBP **2.2**	419	580, 632	0.030	2.4 ± 0.1	0.013 ± 0.002	0.405 ± 0.020
ZnDMP **2.3**	417	577, 630	0.027	2.3 ± 0.1	0.012 ± 0.002	0.418 ± 0.021
ZnTPP **2.4**	426	598, 649	0.033	1.9 ± 0.1	0.017 ± 0.003	0.489 ± 0.029
ZnTBP **2.5**	426	596, 648	0.041	2.1 ± 0.1	0.018 ± 0.004	0.456 ± 0.026
ZnTMP **2.6**	423	592, 644	0.033	2.4 ± 0.1	0.013 ± 0.003	0.401 ± 0.020

Similarly to the absorption data, no major differences were observed in the fluorescence properties in both the tetra- and di-substituted sets of porphyrins contributing to the data in Table 2.3. A slight reduction in quantum yield and radiative decay rate constants of the di-substituted compounds compared to the tetra-substituted compounds is observed. A similar Stokes shift is observed for the tetra- and di-substituted porphyrins in both the Soret and Q-bands, at around 2-6 nm in the Soret band and 40 nm in the Q-bands. Fluorescence lifetimes, radiative and non-radiative decay rate constants are similar across all compounds suggesting that the substitution pattern at the meso position has minimal effects on the excited state relaxation dynamics as previously reported by Liu *et al.*[28] As was the case for the absorption properties of the porphyrins, the fluorescence data provides no evidence to suggest that any major differences between the NCPU-TTA properties of the porphyrins in solution are a direct result of differences in the inherent properties of the singlet states of the porphyrins or due to quenching of excited states before ISC can occur.

2.5 Triplet Transient Absorption Specroscopy

Transient Absorption Spectroscopy (TAS) is a technique used to gain photophysical information about species that exist on short timescales, ranging from milliseconds to femtoseconds. Transient absorption of a photoactive molecule is achieved by employing a primary excitation source (pump, (1) in Figure 2.15) that generates the transient species, and a secondary excitation source (probe, (2) in Figure 2.15) that excites the transient species to a higher excited state. For nanosecond flash photolysis systems used for TAS, typical pump sources are solid-state lasers such as Nd:YAG lasers, and probe beams are derived from continuous white light sources such as xenon arc lamps. The pump and probe lamps intersect at the sample chamber ((3) in Figure 2.15), and the transmitted light from the probe beam is detected either by an ICCD camera ((4) in Figure 2.15) or digital oscilloscope ((5) in Figure 2.15). Information about the transient species is obtained by analysis of the difference in absorption by a sample of the probe pulse, before and after the sample is subject to excitation from the pump pulse. This difference in absorbance is usually expressed as the change in optical density (ΔOD). Plotting ΔOD as a function of wavelength gives rise to the transient absorption spectrum.

The transient absorption spectra provide information on ground-state bleaching, absorption by excited states or reaction intermediates to higher excited states, stimulated emission and potential charge transfer states in the sample compound. Assignment of the peaks and troughs in the transient absorption spectra to physical processes is often achieved by measuring spectra at varied delay times between the pump and probe pulses. The temporal resolution afforded by the TAS technique allows kinetic data such as excited state lifetimes and excited state quenching rates to be determined for many compounds. TAS is particularly useful in exploring triplet state behavior in organic chromophores as the triplet state is not accessible by direct absorption of light and often is non-emissive or exhibits weak phosphorescence under ambient conditions.

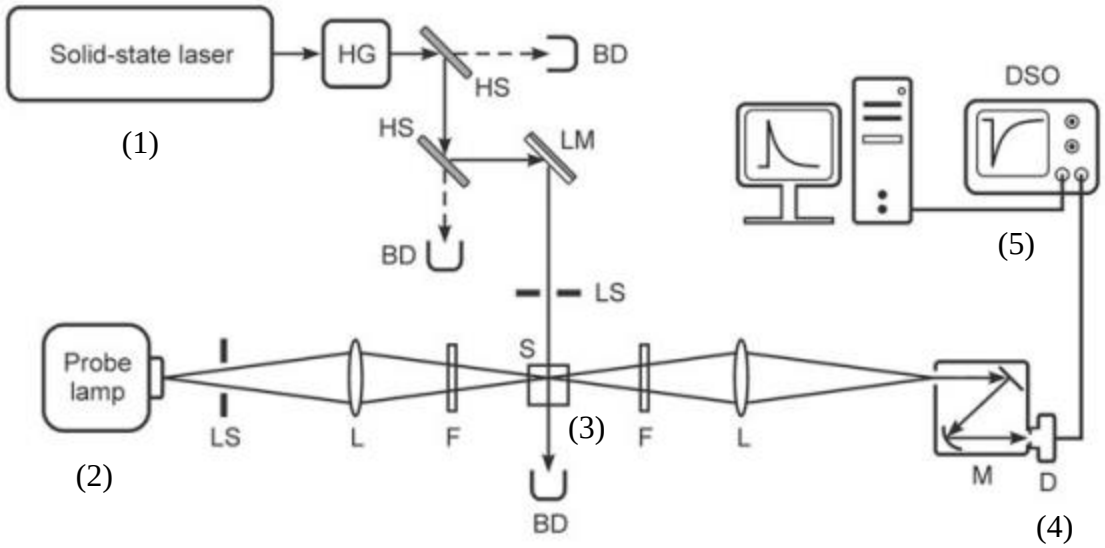

Figure 2.15: Typical Nanosecond Laser Flash Photolysis system employed in triplet-triplet transient absorption spectroscopy. Figure adapted from Chemical Neurobiology Methods and Protocols.[29]

All solutions used in the transient absorption analysis and triplet decay kinetics were prepared in spectroscopic grade toluene and degassed thoroughly prior to measurements. Solutions of porphyrin were prepared to have the same OD at the desired excitation wavelength (532 nm) so that the concentration of the singlet excited state upon excitation would be the same across all samples. The samples were prepared with an OD of 0.02 at the excitation wavelength in order to minimize intermolecular quenching of excited states in the sample by aggregation-induced internal conversion or excessive TTA. A gate delay time of 200 ns was set in order to capture the absorption spectrum of the triplet state porphyrins while the population of triplets was still relatively high, and such that the delay sufficiently exceeded the time scale in which stimulated emission or excitation scatter from the laser pump pulse would be observed in the transient absorption spectrum. The transient absorption spectroscopic data and triplet decay kinetic experiments were obtained after the publication of the work detailed in this chapter and were conducted in order to characterize the triplet state of the compounds **2.1**-**2.6**. The triplet-triplet transient absorption spectra for compounds **2.1**-**2.6** are shown in Figure 2.16 below.

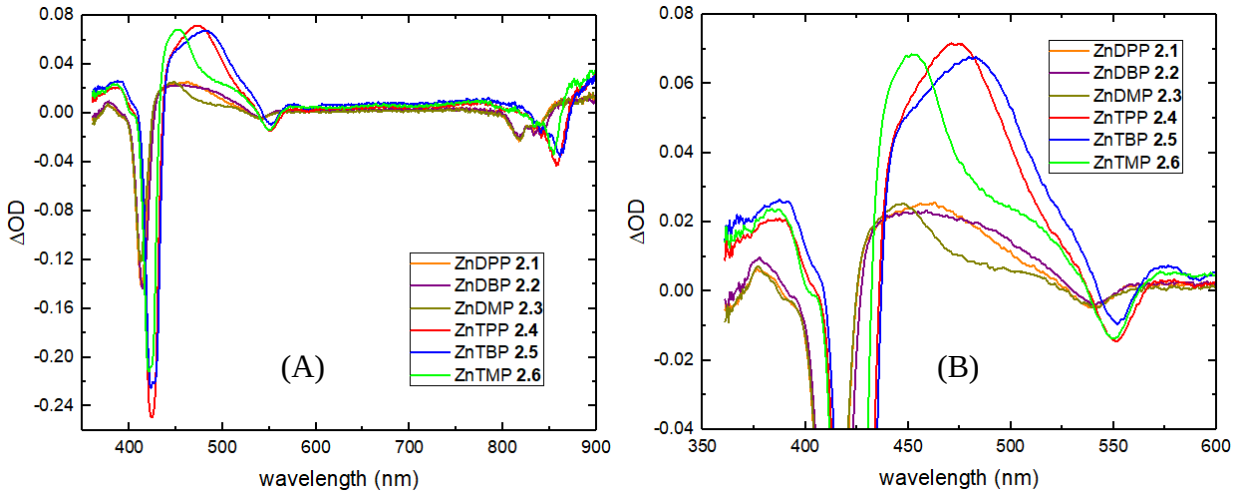

Figure 2.16: (A) Triplet-triplet transient absorption spectra for compounds **2.1-2.6** in degassed toluene solution. (B) Spectra in (A) zoomed in for clarity in the $T_1 \rightarrow T_s$ triplet absorption region.

The triplet absorption spectra in Figure 2.16 exhibit strong ground state bleaching for all compounds at approximately 420 nm corresponding to the intense Soret band singlet absorption. The triplet absorptions at 460 – 490 nm in Figure 2.16 are characteristic of the $a_{2u} \rightarrow e_g^*$ ($^3(\pi,\pi^*)$) transition by Zn porphyrins in the triplet manifold (T_1) upon excitation with the probe beam to the T_s state, where T_s represents the doubly excited triplet state.[30,31] The triplet absorption maxima are listed in Table 2.4. An additional bleaching and absorption begins to appear in the 800-950 nm range for all compounds in Figure 2.16, which has been attributed in metalloporphyrin triplet absorption spectra to a weakly allowed $e_g^* \rightarrow b_{1u}^*$ or b_{2u}^* ($^3(\pi^*,\pi^*)$) transition to a higher excited triplet state T_n where n>1.[30,31] The triplet absorption maximum for ZnTPP **2.4** in toluene (471 nm) closely matches previous literature reports by Waiters *et al.* (474 nm).[32]

Bathochromic shifting of the triplet absorption maxima in Figure 2.16 is consistent with the electron donating ability of the meso-substitution pattern for both the di- and tetra substituted porphyrins. The dihedral angle of meso-aryl porphyrin substituents becomes smaller in the T_s excited state as the energy barrier for phenyl rotation becomes smaller, thereby allowing for greater degrees of conjugation by the aryl substituents into the porphyrin plane, resulting in reduction of the $T_1 \rightarrow T_s$ energy gap and consequent bathchromic shifting in triplet-triplet absorption maxima.[32] As discussed for the singlet state properties and absorption spectra in section **2.4.1**, the degree of meso-aryl rotation and associated aryl-to-porphyrin conjugation in the triplet excited state of porphyrins and metalloporphyrins can also variably affect the porphyrin macrocycle degree of planarity which may further broaden the triplet absorption profile.[33] The observation that the meso-mesityl substituted compounds exhibit shorter absorption maxima and more well-defined vibronic features in the triplet absorption spectra than the other porphyrins is consistent with the fact that the rotation of the phenyl group is forcibly restricted in ZnDMP **2.3** and ZnTMP **2.6**. The magnitude of ΔOD for the $T_1 \rightarrow T_s$ absorption is significantly larger in the tetra-substituted porphyrin series than in the di-substituted series.

Table 2.4: Triplet-triplet absorption and triplet decay parameters for compounds **2.1**-**2.6** in degassed toluene solution.

Compound	Triplet-triplet absorption $\lambda_{(max)}$ (nm)	ΔOD at $\lambda_{(max)}$ (10^{-2})
ZnDPP **2.1**	463	2.56
ZnDBP **2.2**	459	2.33
ZnDMP **2.3**	448	2.53
ZnTPP **2.4**	471	7.17
ZnTBP **2.5**	480	6.77
ZnTMP **2.6**	452	6.85

2.6 Solution State Upconversion Measurements

Solution-state NCPU experiments were performed in order to assess the ability of the porphyrins to partake in homomolecular TTA. The NCPU-TTA experiments were performed by Dr. Ranjana Rauleta and Dr. Neeraj K. Joshi of the University of Saskatchewan, Canada. Further experimental details on all solution state and solid state NCPU-TTA experiments can be found in the publication corresponding to the work studied in this chapter.[14] All Zn(II) porphyrins produced clearly observable amounts of UC fluorescence upon excitation in the Q-band. The samples ZnTMP **2.6** and ZnDBP **2.2** shown in Figure 2.18 below exhibited the largest UC fluorescence intensities from their respective subgroups of tetra- and di-substituted Zn(II) porphyrins.

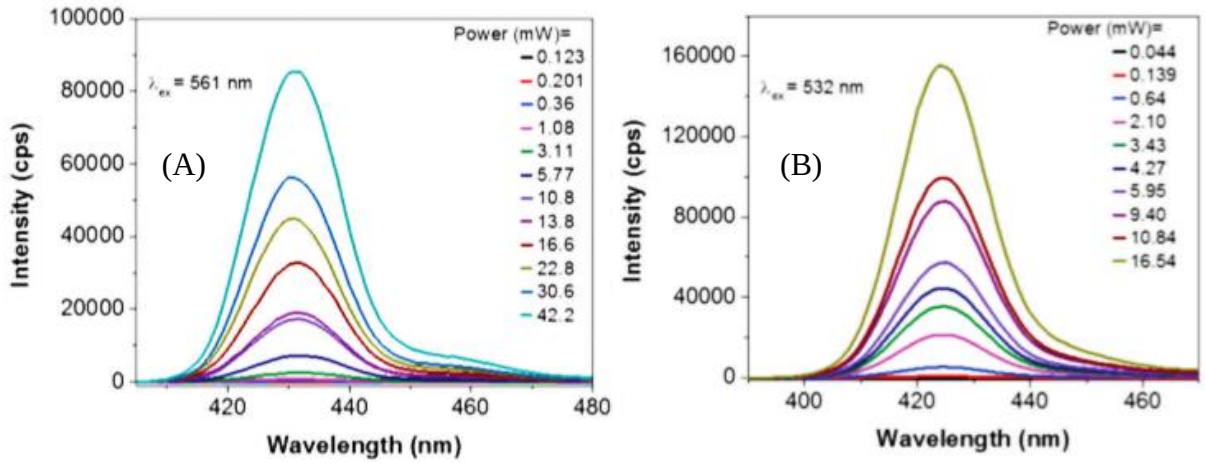

Figure 2.17: Upconverted emission from (A) ZnTMP **2.6** and (B) ZnDBP **2.2** in degassed toluene.

The dependence of the absorbed power of the sample on the UC fluorescence intensity was determined via double logarithmic plots of UC S_2 fluorescence intensity vs residual S_1 fluorescence intensity shown in Figure 2.18 below, the latter providing an auxiliary measure of the amount of power absorbed by the sample. Calculation of the slope of the plots showed that the kinetics of the process resulting in the observed emission peaks around 430 nm in Figure 2.18 and for all porphyrins were second order. The second-order kinetic relationship between absorbed power and UC fluorescence was more prominent at lower excitation powers, with the slope decreasing in gradient as the excitation powers increased.

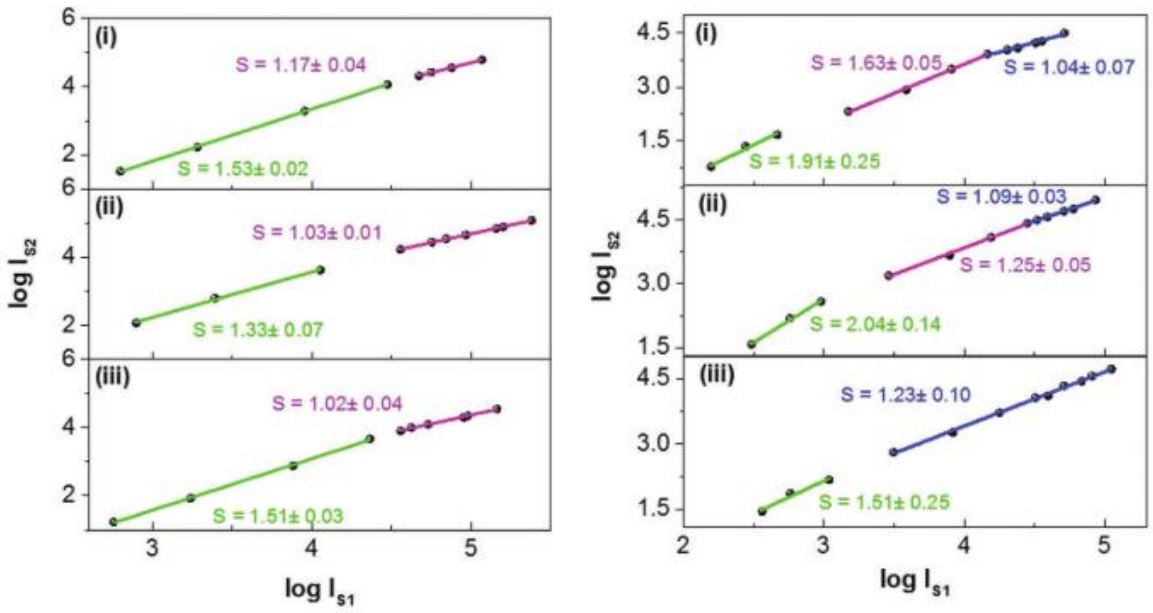

Figure **2.18:** Double logarithmic plots of UC S_2 emission intensity vs S_1 fluorescence for (A)(i) ZnDPP **2.1**, (ii) ZnDBP **2.2**, (iii) ZnDMP **2.3** and (B)(i) ZnTPP **2.4**, (ii) ZnTBP **2.5**, (iii) ZnTMP **2.6**. Excitation wavelength for (A) was 532 nm and for (B) was 561 nm. All samples had an absorbance of 0.10 at their respective excitation wavelengths.

Comparison of the relative UC fluorescence yields of the Zn(II) porphyrins in solution was achieved by dividing the integrated areas of the UC emission spectra by the absorption at the wavelength of excitation, for UC emission spectra obtained using the same excitation power across the samples to be compared, shown in Figure 2.19 below.

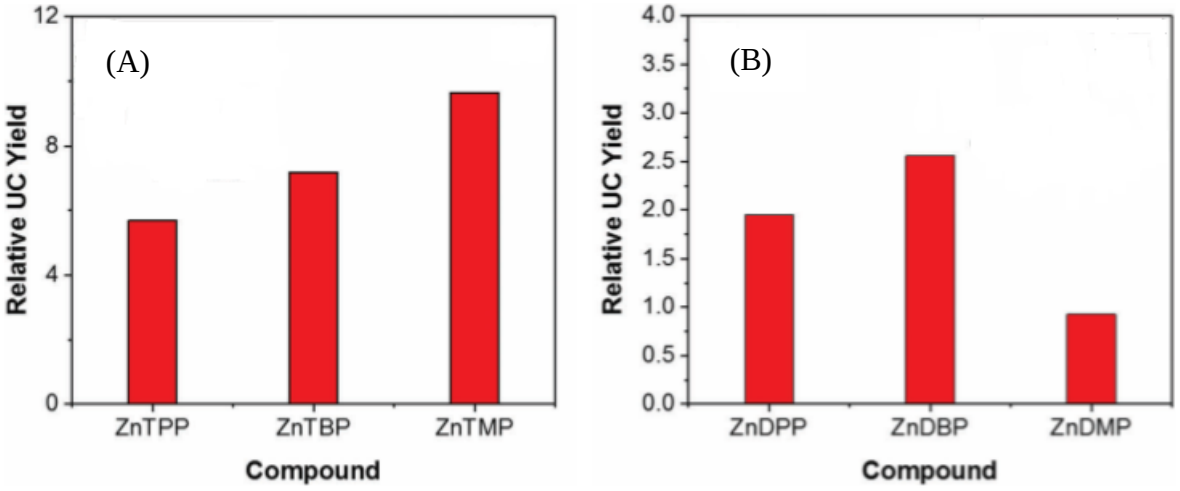

Figure 2.19: Relative UC fluorescence yields for the (A) tetra-substituted Zn(II) porphyrins **2.4-2.6** and (B) di-substituted Zn(II) porphyrins **2.1**-**2.3** in degassed toluene.

A small but observable increase in UC fluorescence yield is present in the samples upon increase of steric bulk introduced at the meso-phenyl substituents, with the exception of the ZnDMP sample. For any given meso-phenyl substituent, the tetra-substituted Zn(II) porphyrin had a higher overall UC yield in solution than its di-substituted counterpart. The relative ΔOD values of the $T_1 \rightarrow T_s$ triplet absorption values in Table 2.4 provide an explanation for the discrepancy in relative UC yields between the di- and tetra-substituted compounds. The ΔOD values in Table 2.4 for the di-substituted compounds are significantly smaller than those for the tetra-substituted compounds. Although the formal triplet molar extinction coefficients were not obtained in this study, the relative ΔOD values of the $T_1 \rightarrow T_s$ triplet absorption values in Table 2.4 provide a good approximation of the triplet concentration upon excitation by the pump laser flash, as the samples were all prepared with identical absorbances at the excitation wavelength, the triplet quantum yields of the di- and tetra substituted compounds are expected to be similar and the depletion of the ground state is expected to be substantial in all compounds at the moderately high excitation powers employed in Figure 2.16.

2.7 Solid-State Photophysics

The solid-state absorption and NCPU-TTA experiments were performed by Dr. Ranjana Rauleta and Dr. Neeraj K. Joshi of the University of Saskatchewan, Canada.

2.7.1 Absorbance Measurements

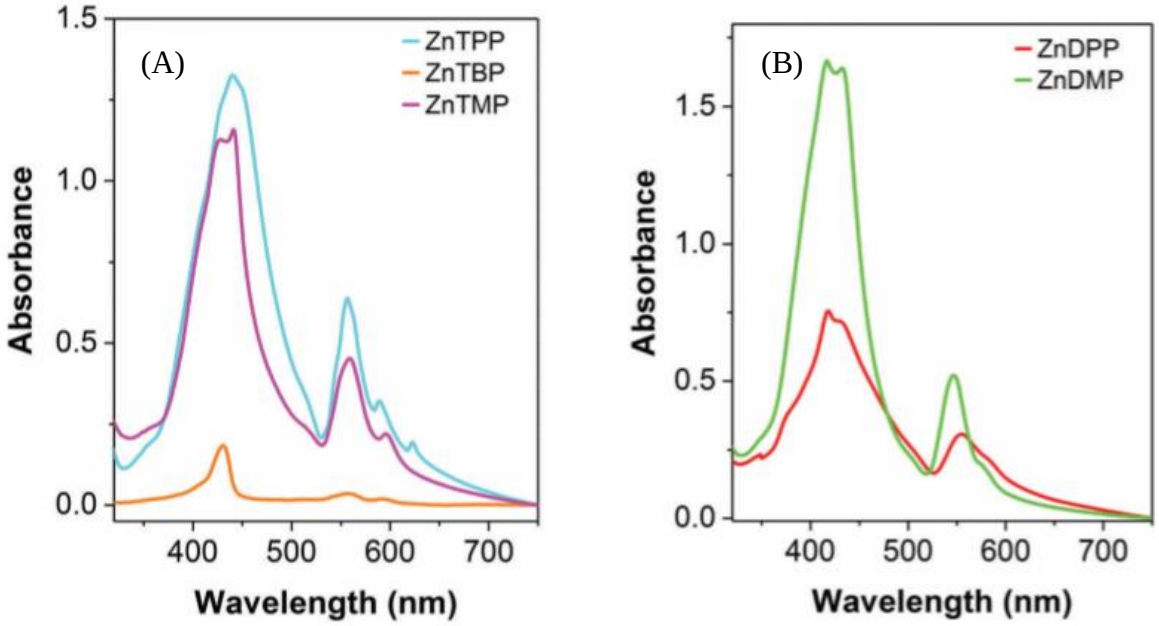

Figure 2.20: Absorption spectra of the (A) tetra- substituted Zn(II) porphyrins **2.4-2.6** and (B) di-substituted Zn(II) porphyrins **2.1-2.3** as 0.1% dispersions in PVA films.

The solid state absorption spectra of the zinc porphyrins in PVA films (Figure 2.20) displayed significant broadening of the absorption maxima, especially in the Soret band. The fluorescence decays of all porphyrins in PVA were bi-exponential, with the faster component contributing to the majority of the decay, indicating that enhanced internal conversion was occurring in the porphyrins in the solid state compared to the solution state. The bi-exponential decays and the severe broadening of the Soret band demonstrate aggregation of the porphyrins occurring within the PVA matrix. Bathochromic shifting of the Soret maxima is indicative of J-aggregate formation between porphyrins. As mentioned in the Introduction chapter section **1.6.3**, aggregation of porphyrins in the solid state is necessary for homomolecular-TTA to occur.

2.7.2 Solid State Upconversion Measurements

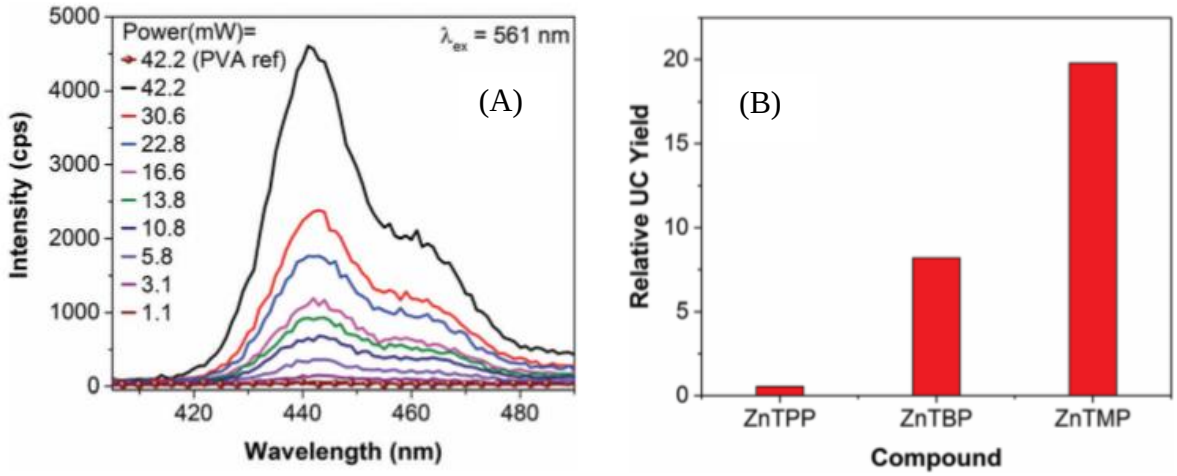

Figure 2.21: (A) Power dependent NCPU-TTA emission of ZnTMP **2.6** in PVA (0.01 w/w%). (B) Relative UC S_2 emission of tetra-substituted Zn(II) porphyrin derivatives **2.4-2.6** in aerated PVA films.

The UC fluorescence intensity of ZnTMP **2.6** at various laser excitation intensities are shown in Figure 2.21 (A), with relative UC emission yields of the tetra-substituted compounds Figure 2.21 (B). The tetra-substituted zinc porphyrins all produced observable UC emission when immersed in PVA films, however the di-substituted zinc porphyrins did not produce any significant UC emission in the PVA films. Additionally, the relative UC yields of the tetra-substituted porphyrins were similar when under degassed and aerated conditions, providing further evidence for the oxygen-barrier properties of the PVA solid-state matrix. In contrast to the relative UC yields observed in degassed solution, increasing the steric bulk of the meso-aryl substituents had a significant effect on the relative UC yields in the PVA films, with a large increase in relative UC yield occurring when the steric bulk of the meso-aryl group incrementally increases from phenyl to 3,5-di-tert-butyl to mesityl. The ratios of the relative UC yields of the tetra-substituted zinc porphyrins in PVA films was approximately 1:7:20 for ZnTPP:ZnTBP:ZnTMP respectively (Figure 2.21 (B)). The relative UC yields indicate that the number of meso-aryl substituents and the steric bulk of the meso-aryl substituents play an important role in optimizing the relative orientations and inter-porphyrin distances within the zinc porphyrin aggregates in PVA films for the production of NCPU-TTA fluorescence.

2.8 Computational Analysis of Zinc Porphyrin Dimer Aggregates

In order to gain insight into the orientations of the zinc porphyrins in their aggregated form, computational calculations using density functional theory (DFT) were performed on the ZnDPP and ZnTPP structures to determine the minimum energy orientation of dimeric aggregates in the gas phase. All DFT calculations and analyses were performed by Dr. Ranjana Rauleta of the University of Saskatchewan, Canada, and detailed experimental parameters are outlined in the publication on the work outlined in this chapter.[14] Although the porphyrin aggregate structures in the PVA films are expected to be complex, dimeric aggregates provide a model system for which the minimum energies of a series of fixed orientation aggregates can be calculated that represent the environment of an annihilating porphyrin pair in the solid state. A series of fixed input geometries were chosen as plausible starting orientations for the formation of the aggregate dimers which were then optimized to yield minimum energy output structures, in order to model the formation of the aggregates in the PVA matrix. The input geometries of the porphyrins modeled in the calculations were face-to-face (F-F), slipped-stacked and head-to-tail (H-T, side-by-side in plane), which could additionally be parallel (∥) or perpendicular (⊥) to the plane of the meso-aryl substituents in the case of the di-substituted porphyrins (Figure 2.23) due to decreased symmetry compared to the tetra-substituted compounds (Figure 2.24).

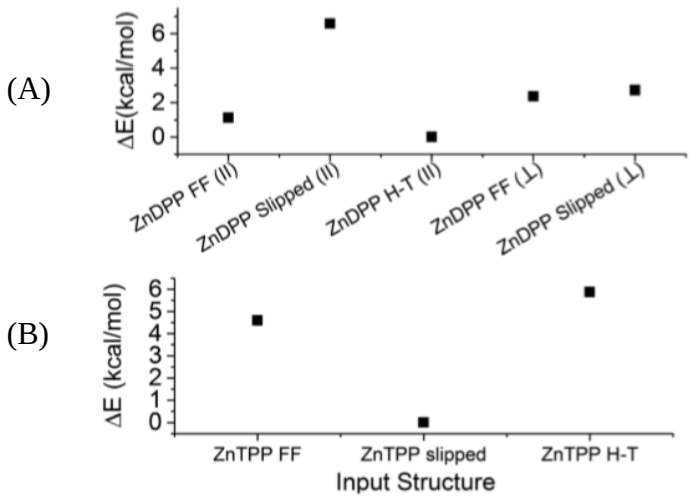

Figure 2.22: Relative stabilities of the optimized local minimum energy structures of the (A) ZnDPP **2.1** dimers and (B) the ZnTPP **2.4** dimers obtained at the B97D/6-31G(d,p) level in the gas phase.

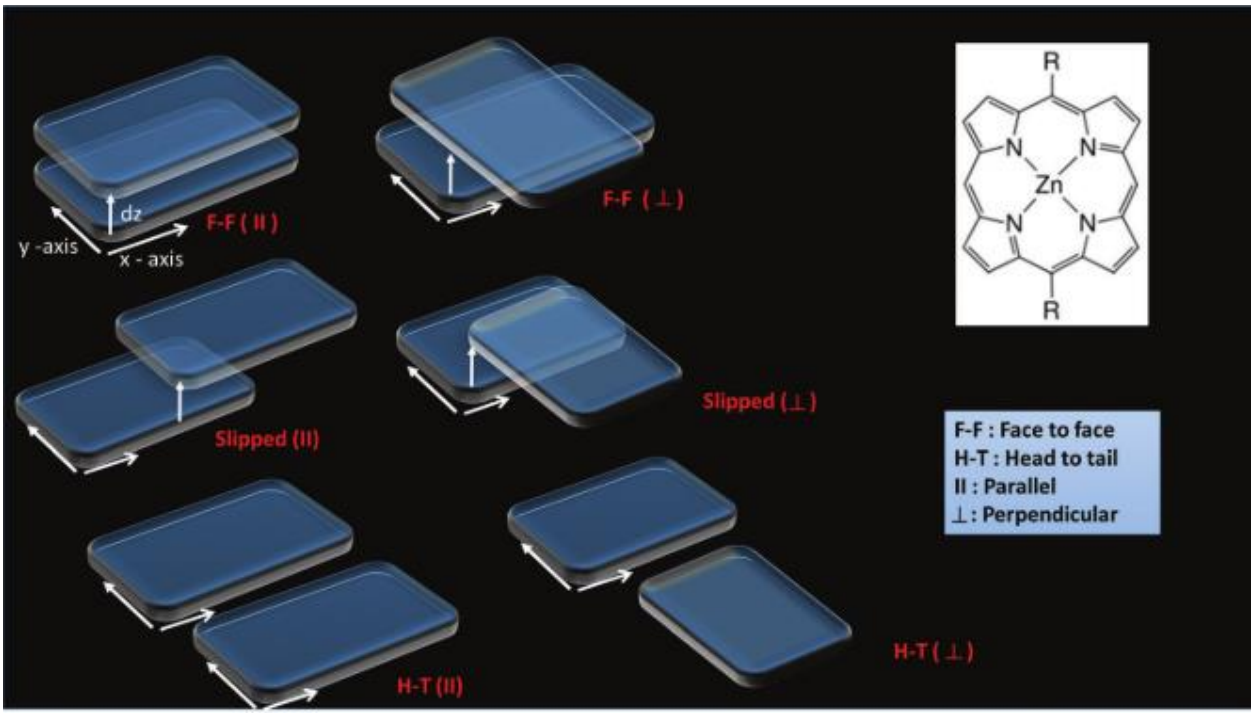

Figure **2.23:** Input structures of ZnDPP **2.1** dimers subject to energy minimization.

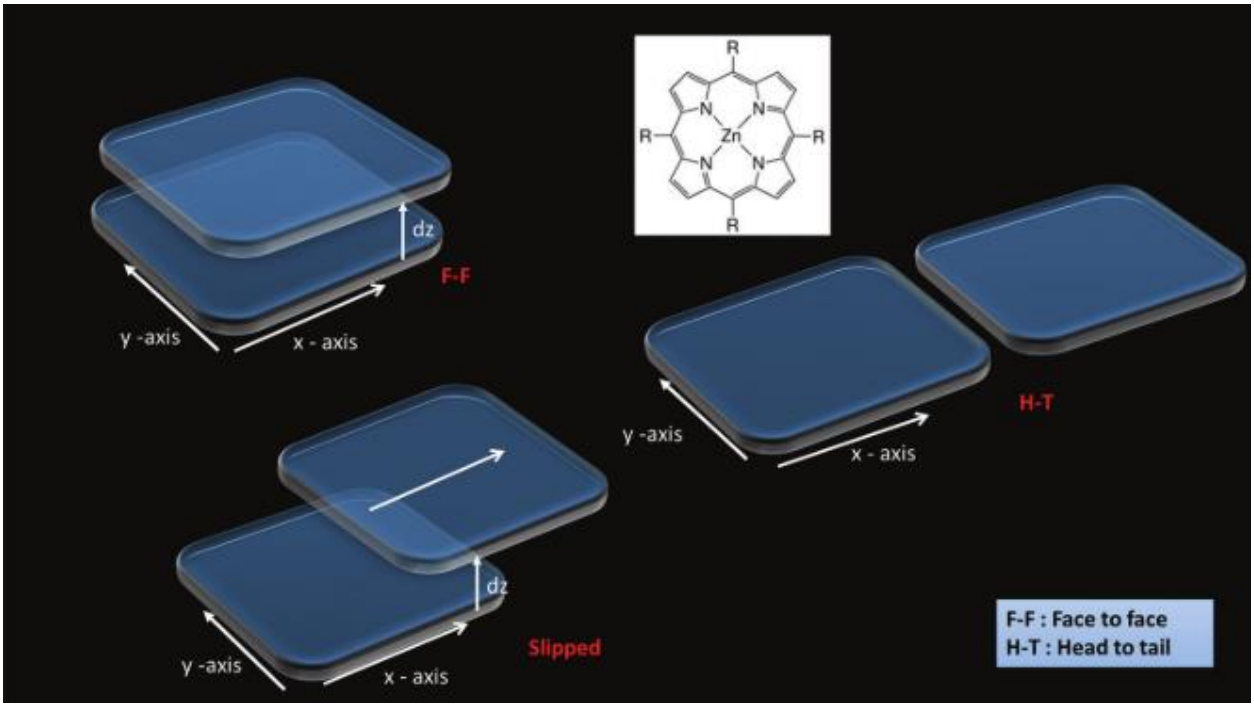

Figure **2.24:** Input structures of ZnTPP **2.4** dimers subject to energy minimization.

From the calculations in Figure 2.22, the lowest energy dimeric input geometry for ZnDPP **2.1** is the parallel head-to-tail structure, with the lowest energy input geometry for ZnTPP **2.4** being the slipped stacked dimer. In all cases, the geometry of the output dimers was slipped-stacked and hence the assumption was made that the aggregates formed in PVA films would tend toward forming this minimum energy dimer geometry.

Further calculations were conducted in order to understand the lack of NCPU-TTA occurring in the PVA films for the di-substituted compounds. A plot of the potential energy surface of the lowest energy input dimeric geometry of ZnDPP **2.1** (H-T in Figure 2.22) against the intermolecular Zn-Zn distance between the porphyrins in the dimer, varied along a one-dimensional coordinate, (black dots in Figure 2.25) shows a broad minimum energy region with two distinguishable local minima at around 3.3Å and 4.0Å. The Lennard-Jones function for the ZnDPP dimer **2.1** was calculated using the average minimum Zn-Zn distance for the dimer geometries (red curve in Figure 2.25) in order to demonstrate the relative span of the dimer binding potential. The broad minimum energy region as a function of intermolecular Zn-Zn distance has been attributed to the concept that the binding energies of the metalloporphyrin dimers may be similar at different slip parameters.

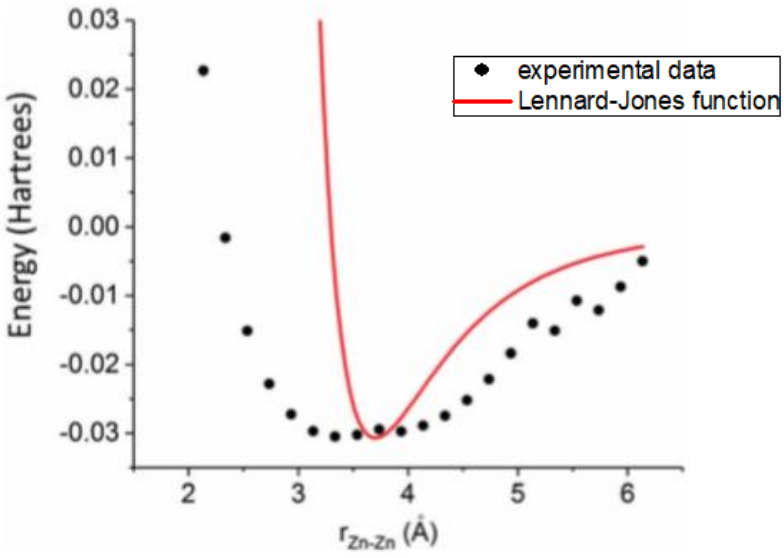

Figure 2.25: Potential energy of the ZnDPP **2.1** dimer as a function of intermolecular Zn-Zn distance (experimental data plotted as black dots). The Lennard-Jones function for the ZnDPP dimer **2.1** is shown by the red curve.

It was proposed that at varied slip parameters of the input geometries (shown in Figures 2.23 and 2.24 above) to obtain the optimized minimum energy output geometries of the dimers, the input geometries with the shortest intermolecular Zn-Zn distance would result in the most efficient TTA due to increased orbital overlap as predicted by the Dexter energy transfer mechanism governing the TTA process. The intermolecular Zn-Zn distance r_{Zn-Zn} was calculated for the output geometries for both ZnDPP **2.1** and ZnTPP **2.4** for varying input geometries as shown in Table 2.5 below.

Table 2.5: Distance between the two Zn atoms r_{Zn-Zn} in the output structures of the porphyrin dimers of **2.1** and **2.4** obtained by optimization at the B97D/6-31G(d,p) level in the gas phase.

Compound	Input Geometry	Output Geometry	r_{Zn-Zn} (Å)
ZnDPP **2.1**	F-F (∥)	Slipped	3.93
	Slipped (∥)	Slipped	4.59
	H-T (∥)	Slipped	4.11
	F-F (⊥)	Slipped	3.20
	Slipped (⊥)	Slipped	3.36
ZnTPP **2.4**	F-F	Slipped	3.23
	Slipped	Slipped	4.65
	H-T	Slipped	4.96

The data presented in Table 2.5 shows that the slipped dimer output geometries with face-to-face input geometries in both ZnDPP **2.1** and ZnTPP **2.4** experience the shortest intermolecular Zn-Zn distances at 3.20Å and 3.23Å respectively. These input geometries would thus be expected to lead to the formation of dimeric aggregates with the most optimal orientation and separation for participating in TTA in the PVA films.

Considering the results from the data in Figures 2.22 and 2.25 and Table 2.5, a rationale was proposed for the lack of NCPU-TTA for the di-substituted porphyrin series in PVA films. Although Dexter energy transfer is assumed to be most efficient at the shortest Zn-Zn distances, non-radiative relaxation of S_2 may be enhanced at these smaller intermolecular separation distances as discussed in section **1.7.3**, however the output geometries obtained for the optimum input geometries of the dimers produced intermolecular Zn-Zn distances that were similar (3.20Å and 3.23Å for F-F input geometries, Table 2.5), and thus would play a negligible role in dictating the relative yield of NCPU-TTA fluorescence between ZnDPP **2.1** and ZnTPP **2.4** in PVA films. Upon formation of the PVA films, the di-substituted porphyrins must form a distribution of orientations within their local aggregate domains that provide unfavourable conditions for TTA, which the tetra-substituted porphyrins do not experience. The di-substituted porphyrins possess a wide variety of dimeric orientations that lie at local potential energy minima (seen in Figure 2.22) compared to the tetra-substituted porphyrins due to their difference in symmetries. The orientations and Zn-Zn distances at the local minima of the di-substituted porphyrins that are non-optimal for TTA are therefore greater. Upon formation the PVA films, the non-optimal dimeric aggregates in the PVA in their local potential energy minima are trapped in the matrix, and are therefore unable to access the optimum orientations required for participating in effective TTA. This phenomenon may not necessarily be generalized to other polymer matrixes but is assumed to be active formation of the PVA matrix employed in the NCPU-TTA experiments. The cause of the large differences in the NCPU-TTA yields observed within the set of tetra-substituted zinc porphyrins in PVA (Figure 2.21 (B)) still require further investigation, however it is interpreted from the data in Figure 2.21 (B) and the computational results above, that increasing the steric bulk of the meso-aryl substitutents on the metalloporphyrin macrocycle allows for the greatest proportion of low-energy slipped dimeric aggregates to be produced upon formation of the PVA film, therefore producing the greatest NCPU-TTA fluorescence with increasing steric bulk in PVA films.

2.9 Conclusion

The synthesis of a series of di-substituted and tetra-substituted zinc metalloporphyrins was performed for the purpose of determining the effects of substitution pattern of zinc porphyrins on the NCPU-TTA fluorescence in solution and solid-state PVA films. The steady state solution photophysics, triplet-triplet transient absorption spectroscopy and triplet decay kinetics were investigated in order to characterize the singlet state and triplet state behavior of the zinc porphyrins and identify potential differences in photophysical properties that may lead to observed differences in NCPU-TTA fluorescence yields. The absorption and fluorescence data for all compounds exhibited minor differences that were able to be rationalized by theory available in the literature. No significant deviation in NCPU-TTA yields are expected to be caused by differences in the steady state photophysical properties observed within the series of zinc porphyrins, as was intended in the design of the compounds studied in this chapter. The triplet transient absorption spectroscopy predicted that a smaller population of triplets would be available to participate in solution-state TTA for the di-substituted compounds compared to the tetra-substituted porphyrins, which was corroborated in the data for the relative NCPU-TTA yields in the solution state. The solution-state NCPU-TTA fluorescence yields exhibited a small but observable increase as a function of increasing steric bulk on the meso-aryl substituents of the porphyrins. The relative increase in NCPU-TTA fluorescence yields within the set of tetra-substituted zinc porphyrins was far more pronounced in PVA films than in solution, and the di-substituted porphyrins produced no observable NCPU-TTA fluorescence in the PVA films. Computational studies revealed that the most stable dimer configurations were those oriented in a slipped-stacked manner, and that the di-substituted porphyrins did not produce NCPU-TTA fluorescence in PVA films as their dimeric aggregates were likely to be trapped in local potential energy minima that corresponded to dimer configurations that were less optimal for producing TTA than their higher symmetry tetra-substituted porphyrin analogues. The fact that NCPU-TTA can be facilitated with substantial S_2 fluorescence yields in aerated PVA films when the steric bulk of the zinc metalloporphyrin dual-absorber upconverter is large may allow for improvements in future design of solar energy light harvesting systems employing homomolecular TTA processes.

2.10 References

(1) Giri, N. K.; Ponce, C. P.; Steer, R. P.; Paige, M. F. *Chem. Phys. Lett.* **2014,** *598*, 17.

(2) O'Brien, J. A.; Rallabandi, S.; Tripathy, U.; Paige, M. F.; Steer, R. P. *Chem. Phys. Lett.* **2009,** *475*, 220.

(3) Stel'makh, G. F.; Tsvirko, M. P. *J. Appl. Spectrosc.* **1982,** *36* (4), 430.

(4) Ksenofontova, N. M.; Stel'makh, G. F.; Tsvirko, M. P. *Dokl. Akad. Nauk SSSR* **1986,** *289*, 405.

(5) Schulze, T. F.; Czolk, J.; Cheng, Y.-Y.; Fückel, B.; MacQueen, R. W.; Khoury, T.; Crossley, M. J.; Stannowski, B.; Lips, K.; Lemmer, U.et al. *J. Phys. Chem. C* **2012,** *116*, 22794.

(6) Huang, C.; Wang, N.; Li, Y.; Li, C.; Li, J.; Liu, H.; Zhu, D. *Macromolecules* **2006,** *39*, 5319.

(7) Zhao, W.; Castellano, F. N. *J. Phys. Chem. A* **2006,** *110*, 11440.

(8) Mol, J. A.; Lau, C. S.; Lewis, W. J. M.; Sadeghi, H.; Roche, C.; Cnossen, A.; Warner, J. H.; Lambert, C. J.; Anderson, H. L.; Briggs, G. A. D. *Nanoscale* **2015,** *7* (31), 13181.

(9) Ikeda, T.; Tsuda, A.; Aratani, N.; Osuka, A. *Chem. Lett.* **2006,** *35* (8), 946.

(10) Stevens, A. L.; Joshi, N. K.; Paige, M. F.; Steer, R. P. *J. Phys. Chem. B* **2017,** *121*, 11180.

(11) Moiseev, A. G.; Margulies, E. A.; Schneider, J. A.; Bélanger-Gariépy, F.; Perepichka, D. F. *Dalton. Trans.* **2014,** *43*, 2676.

(12) Schweitzer, C.; Schmidt, R. *Chem. Rev.* **2003,** *103*, 1685.

(13) Gaume, J.; Wong-Wah-Chung, P.; Rivaton, A.; Thérias, S.; Gardette, J.-L. *RSC Adv.* **2011,** *1*, 1471.

(14) Rautela, R.; Joshi, N. K.; Novakovic, S.; Wong, W. W. H.; White, J. M.; Ghiggino, K. P.; Paige, M. F.; Steer, R. P. *Phys. Chem. Chem. Phys.* **2017,** *19*, 23471.

(15) Adler, A. D.; Longo, F. R.; Finarelli, J. D.; Goldmacher, J.; Assour, J.; Korsakoff, L. *J. Org. Chem.* **1967,** *32*, 476.

(16) Hasegawa, T.; Miyamoto, T. K.; Sasaki, Y. *J. Coord. Chem.* **1996,** *37*, 299.

(17) Lindsey, J. S.; Wagner, R. W. *J. Org. Chem.* **1989,** *54* (4), 828.

(18) Yu, L.; Muthukumaran, K.; Sazanovich, I. V.; Kirmaier, C.; Hindin, E.; Diers, J. R.; Boyle, P. D.; Bocian, D. F.; Holten, D.; Lindsey, J. S. *Inorg. Chem.* **2003,** *42* (21), 6629.

(19) DiMagno, S. G.; Lin, V. S.-Y.; Therien, M. J. *J. Org. Chem.* **1993,** *58*, 5983.

(20) Plater, M. J.; Aiken, S.; Bourhill, G. *Tetrahedron* **2002,** *58*, 2405.

(21) Megiatto Junior, J. D.; Spencer, R.; Schuster, D. I. *J. Mater. Chem.* **2011,** *21*, 1544.

(22) Laha, J. K.; Dhanalekshmi, S.; Taniguchi, M.; Ambroise, A.; Lindsey, J. S. *Org. Process Res. Dev.* **2003,** *7*, 799−812.

(23) Gouterman, M. *J. Mol. Spectrosc.* **1961,** *6*, 138.

(24) Perrin, M. H.; Gouterman, M.; Perrin, C. L. *J. Chem. Phys.* **1969,** *50*, 4137.

(25) Spellane, P. J.; Gouterman, M.; Antipas, A.; Kim, S.; Liu, Y. C. *Inorg. Chem.* **1980,** *19*, 386.

(26) Rosa, A.; Ricciardi, G.; Baerends, E. J. *J. Phys. Chem. A* **2006,** *110*, 5180.

(27) Strachan, J.-P.; Gentemann, S.; Seth, J.; Kalsbeck, W. A.; Lindsey, J. S.; Holten, D.; Bocian, D. F. *J. Am. Chem. Soc.* **1997,** *119*, 11191.

(28) Liu, X.; Tripathy, U.; Bhosale, S. V.; Langford, S. J.; Steer, R. P. *J. Phys. Chem. A* **2008,** *112*, 8986.

(29) Banghart, M. R., Ed.; Springer: New York, 2013.

(30) Gouterman, M. *J. Chem. Phys.* **1960,** *33*, 1523.

(31) Rodriguez, J.; Kirmaier, C.; Holten, D. *J. Am. Chem. Soc.* **1989,** *111*, 6500.

(32) Waiters, V. A.; de Paula, J. C.; Jackson, B.; Nutaitis, C.; Hall, K.; Lind, J.; Cardozo, K.; Chandran, K.; Raible, D.; Phillips, C. M. *J. Phys. Chem.* **1995,** *99*, 1166.

(33) Gorski, A.; Knyukshto, V.; Zenkevich, E.; Starukhin, A.; Kijak, M.; Solarski, J.; Semeikin, A.; Lyubimova, T. *J. Photochem. Photobiol. A* **2018,** *354*, 101.

Chapter 3

Synthesis and Photophysics of Oligo-Phenylenevinylene Linked Pendant Porphyrin Polymers

3.1 Introduction

Triplet-triplet annihilation (TTA) mediated photon upconversion (UC) is one of the leading methodologies currently being pursued in research toward improving solar energy harvesting systems by exceeding the Shockley-Queisser (SQ) limit. TTA systems employing dual absorber-upconverter species for homo-TTA, in particular zinc(II) porphyrin derivatives, show promise for both solution and solid state TTA systems as they avoid energy transfer limitations due to phase separation of components of different molecular nature seen in hetero-TTA systems. Homo-TTA systems currently fall behind hetero-TTA systems when comparing TTA-UC fluorescence quantum yields in general, therefore demand exists for research attention toward the optimization of the photophysical properties of dual-absorber upconverter systems. As such, an understanding of the mechanisms and parameters that constructively and destructively contribute to facilitation of homo-TTA is necessary.

As mentioned in the Introduction chapter section 1.8.1, some of the most important parameters for facilitating effective UC between the two annihilating species participating in a TTA encounter event are the degrees of overlap of π-orbitals, proximity, and the relative spatial orientation of the molecules, with respect to each other in the TTA encounter complex. It is envisioned that polymers with pendant ZnTPP units, such as those synthesized previously by Wang *et al.* (Figure 3.1),[1] may potentially provide favourable conditions for mediating intramolecular homo-TTA-UC by providing a structural environment that optimizes the aforementioned parameters. Incorporation of ZnTPP pendant units onto a polymer backbone chain affords control over the proximity of the ZnTPP dual absorber-upconverter units, allowing for inter-pendant electronic communication. Pendant chromophore polymers have previously demonstrated the ability to facilitate intramolecular TTA-UC when employing DPA units as the pendant upconverter species in hetero-TTA systems (discussed in section 1.8.2).[2]

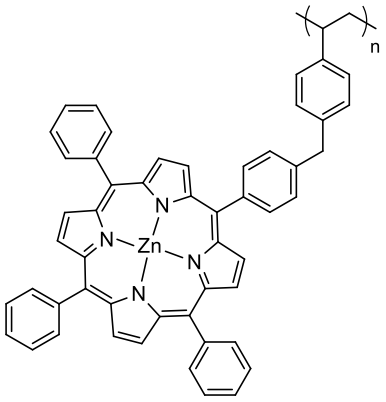

Figure 3.1: Example of a pendant zinc porphyrin polymer synthesized by Wang *et al.*[1]

Porphyrins in pendant polymers may be in sufficient proximity to provide orbital overlap required for the Dexter energy-exchange process through which TTA proceeds, however the local electronic environment created by the interaction of porphyrins in close proximity with each other may in fact be detrimental to the production of TTA-UC fluorescence if the electronic coupling and orbital overlap of the pendant porphyrins is too strong, as discussed in the Introduction chapter section 1.7.3. The consideration of effects of strong inter-pendant interaction on TTA comes into focus especially when porphyrins are employed as the pendant units in pendant polymers. Porphyrins have extended π-conjugation systems and therefore are

subject to porphyrin-porphyrin π-π stacking interactions, which could potentially lead to greater degrees of intramolecular aggregation and excitonic quenching in pendants when porphyrins are chosen as the pendant units in pendant polymers. Although a degree of aggregation in solid state TTA systems is necessary for TTA to proceed as discussed in section 1.6.3, aggregation in metalloporphyrins is well-known to play a significant role in the quenching of excitons at all stages of the TTA process (as discussed in the Introduction chapter sections 1.6.4, 1.7.1 and 1.7.3).

There may however be potential benefits in creating porphyrins with extended π-conjugated systems for solar-powered NCPU-TTA applications. Tetraannulation at the β-pyrollic positions on the porphyrin macrocycle periphery has been employed as a method for π-conjugation extension in the design of TTA sensitizers such as platinum(II) tetraphenyltetrabenzoporphyrin[3] and palladium(II) tetraquinoxaline porphyrin derivatives.[4,5] These vast π-systems exhibit increased molar absorption coefficients and bathochromic shifts in the Q-band, both of which increase the ability of the porphyrins to harvest light from the rich red region of the solar irradiation distribution. Because these tetraannulated porphyrins possess significant π-electron area in the plane capable of effective orbital overlap with other π-conjugated chromophores, large alkyl substituents are required to decrease strong aggregation and improve the solubility of these compounds. Expanding the size of the initially large annulated porphyrin with substituents that occupy space perpendicular to the porphyrin plane in order to decrease aggregation may prove difficult for incorporation into pendant polymer structures due to steric considerations.

Some of the most effective methods of increasing the porphyrin macrocycle conjugation have been reported in the works of the Officer group, in which the β-position of the porphyrin periphery has been extended using *para*-phenylenevinylene (*p*-PV) oligomers in order to create conjugated porphyrin-porphyrin dyads[6,7] and β-conjugation-extended metalloporphyrin electron donors for dye-sensitized solar cells.[8,9] As part of the library of work by the Officer group, Ventura *et al.* have synthesized β-oligo-*p*-PV substituted porphyrins with 0, 1 and 2 *p*-PV units in order to investigate structure-property relationships between the degree of conjugation in the

monomeric porphyrin units and their photophysical properties (Figure 3.2).[10] Incrementally increasing the conjugation length of the porphyrin chromophore using the synthetic design outlined by Ventura *et al.*[10] could be not only performed to make understood modifications to the photophysical properties of the single molecule porphyrins, but could be performed in order to study the intermolecular interactions between porphyrins as a function of increasing conjugation that may play a role in facilitating or inhibiting NCPU-TTA. As discussed above, understanding the nature of these intermolecular interactions would be highly valuable for designing TTA systems when porphyrins with extended conjugation are in close proximity in pendant polymer environments.

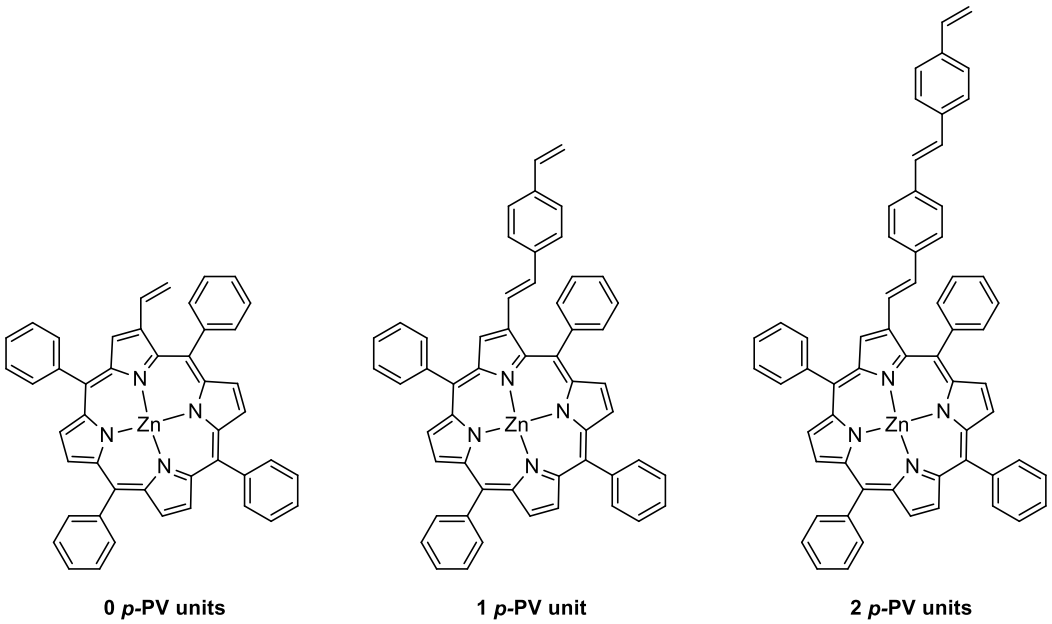

Figure 3.2: Vinyl-capped β-oligo-*p*-PV substituted porphyrins with 0, 1 and 2 *p*-PV units (left to right) synthesized by Ventura *et al.*[10]

The intention of the work presented in this chapter is to synthesize and characterize a series of pendant porphyrin polymers with variable degrees of π-conjugation extension in their zinc porphyrin pendant units, in order to study structure-property relationships between the conjugation length of the pendant porphyrin unit and the photophysical properties of the pendant polymers. The conjugation of the porphyrin π-network of the monomeric units of pendant porphyrin polymers were systematically extended in a well-defined manner by increasing the

number of *para*-phenylene vinylene (*p*-PV) units that are directly conjugated to ZnTPP pendants at the β-position of the porphyrin macrocycle (Figure 3.3). The oligomeric phenylene vinylene moieties were designed to function as backbone-to-pendant linking groups. Monomeric model compounds were synthesized in addition to the pendant polymers in order to identify properties introduced in the pendant environment by comparison of monomer and polymer photophysics. The effects of inter-pendant electronic association on both the singlet and triplet states of ZnTPP pendant chromophores were able to be elucidated using spectrophotometric and fluorescence measurement techniques, in addition to transient absorption spectroscopy.

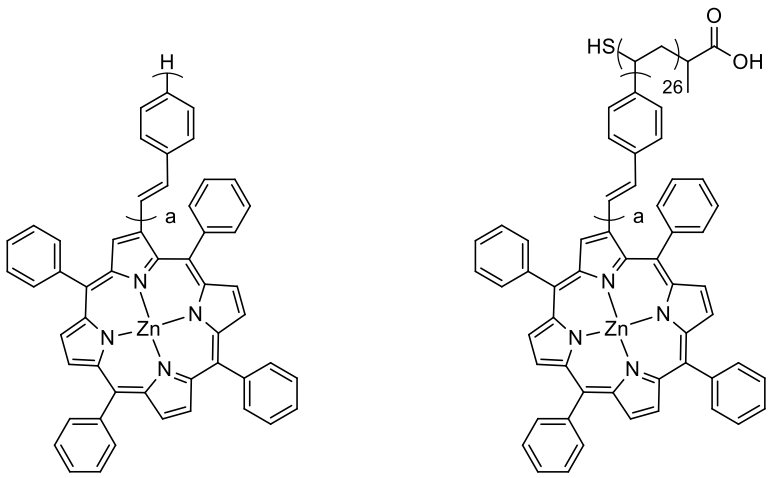

3.1; a = 1
3.2; a = 2
3.3; a = 3

3.4; a = 1
3.5; a = 2
3.6; a = 3

Figure 3.3: Target pendant porphyrin polymers (right) and their monomeric model analogues (left) investigated in chapter 3.

3.2 Synthetic methodology

3.2.1 Horner-Wadsworth-Emmons Olefination

In order to extend the conjugation of the porphyrin core using oligomeric *p*-PV units, it was necessary to ensure that the double bond geometry that resulted from the olefin formation steps was exclusively *trans*. Ventura *et al.* successfully introduced *p*-PV units with *trans* geometry using Horner-Wadsworth-Emmons (HWE) olefination reactions in a step-wise manner, such that one phenylene vinylene unit can be introduced per HWE reaction at the terminus of the β-substituent until the desired length of the *p*-PV oligomer is obtained.[10] Although the formation of the precursor aldehyde-phosphonate adduct intermediate to the *cis*-isomer (*erytho* adduct) is kinetically favoured in the HWE reaction over the adduct intermediate to the *trans*-isomer (*threo* adduct), the intermediate *cis*-oxaphosphetane from the *erytho* adduct has been calculated to be about 3 kcal mol^{-1} higher in energy than for the *trans* stereoisomer of the intermediate oxaphosphetane formed from the *threo* adduct.[11] Considering that the carbon-carbon bond formation step for the aldehyde-phosphonate adduct is reversible, the *trans* stereoisomer of the intermediate oxaphosphetane, and thus the product olefin with *trans* stereochemistry, is exclusively formed by thermodynamic equilibration of the aldehyde-phosphonate adduct in HWE reactions. HWE has been used for the synthesis of *trans*-*p*-PV conjugated oligomers,[12,13] polymers[14,15] and dendrimers[16] in a range of previous photophysical studies. In the syntheses of β-oligo-*p*-PV substituted porphyrins performed by Ventura *et al.*, β-aldehyde-functionalized porphyrins were coupled to benzylphosphonate derivatives using HWE reactions.[10]

3.2.2 Post-Polymerization Functionalization

Synthetic techniques towards the synthesis of pendant polymers in general have been outlined in the Introduction chapter section 1.8.3. Polymers with pendant porphyrin units have been synthesized previously by polymerization of norbornene-functionalized porphyrin monomers using ROMP,[17,18] living polymerization of isocyanide-functionalized porphyrin monomers using Pd-Pt μ-ethynediyl heterodinuclear complex catalysts[19] and radical polymerization of vinyl-functionalised porphyrins.[20] The synthesis of such porphyrin monomers with complex functionality is tedious and low-yielding by mass, which introduces risk into the polymerization

step as the monomers from unsuccessful or incomplete polymerization reactions are typically not recoverable as they form a distribution of oligomers. Additionally, the chromophore itself may be incompatible with some polymerization techniques which limits the scope of the design of the polymers. Although the terminal vinyl substitutents on the oligo-*p*-PV conjugation extended porphyrins synthesized by Ventura *et al.*[10] (Figure 3.2) may seem appealing for use in living radical polymerization reactions, the central vinylene moieties in the *p*-PV oligomers may be susceptible to attack by radicals in addition to the terminal vinyl group. Addition to the phenylene vinylene double bonds of arylstyrene derivatives has been observed previously for radical polymerizations of styrene and methyl methacrylate performed previously in the presence of arylstyrene small molecules.[21]

Post-polymerization functionalization (discussed in section 1.8.3.4) bypasses the difficulties of synthesizing and polymerizing porphyrin monomers, as the polymerization step is performed typically on an easily-synthesized monomer that behaves predictably under the chosen polymerization conditions. Any unreacted functionalized chromophore intended to be appended to the polymer backbone that may remain after a reaction can be simply recovered and used in subsequent reactions. Post-polymerization functionalization has been utilized previously as an effective technique for the synthesis of polymers with pendant oligo-*p*-PV units previously by employing HWE olefination in the PPF reaction step.[22-24] In order to synthesize these pendant oligo-PV polymers, aldehyde-functionalized PPV oligomer precursors were appended to a backbone polymer functionalized with benzylphosphonate groups (Figure 3.4). The backbone polymers were themselves synthesized by RAFT polymerization (RAFT polymerization is discussed in section 1.8.3.2). Backbone polymers synthesized using RAFT polymerization are highly desirable for use in photophysical applications as they can be made as short-chain oligomers with low PDI, increasing solubility in organic solvents and minimizing variance in photophysical properties that may be caused due to the length of the backbone polymer.

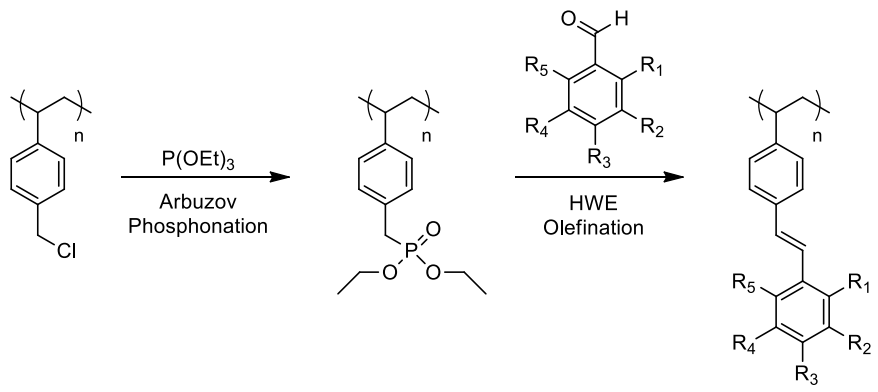

Figure 3.4: General HWE-PPF methodology utilized by Tilley *et al.*,[22] Wuyts *et al.*[23] and Belfield *et al.*[24] for the synthesis of polymers with pendant oligo-*p*-PV side chains. R_1 to R_5 represent substituents that vary between the studies of Tilley *et al.*, Wuyts *et al.* and Belfield *et al.*

Using the combined HWE – PPF methodology outlined in Figure 3.4, the synthesis of the desired *p*-PV chromophore pendant unit is achieved upon completion of the *p*-PV reaction step, which simplifies the synthesis of the necessary pendant chromophore precursor. As PPF allows for the polymerization of a porphyrin-functionalized chromophore to be avoided, and has been demonstrated on many occasions to be effective for the installation of *p*-PV oligomer derivatives on polymer backbones using HWE olefination, the combined HWE-PPF technique was employed in the synthesis of the pendant porphyrin polymers **3.4 – 3.6** studied in this chapter (outlined in Figure 3.7). The syntheses of the oligo-PPV functionalized porphyrin precursor aldehydes **3.14**, **3.15** and **3.18** are outlined in Figure 3.5 and have been reported by Ventura *et al.* previously.[10] The syntheses of the monomeric oligo-*p*-PV functionalized porphyrins **3.1 – 3.3** are outlined in Figure 3.6.

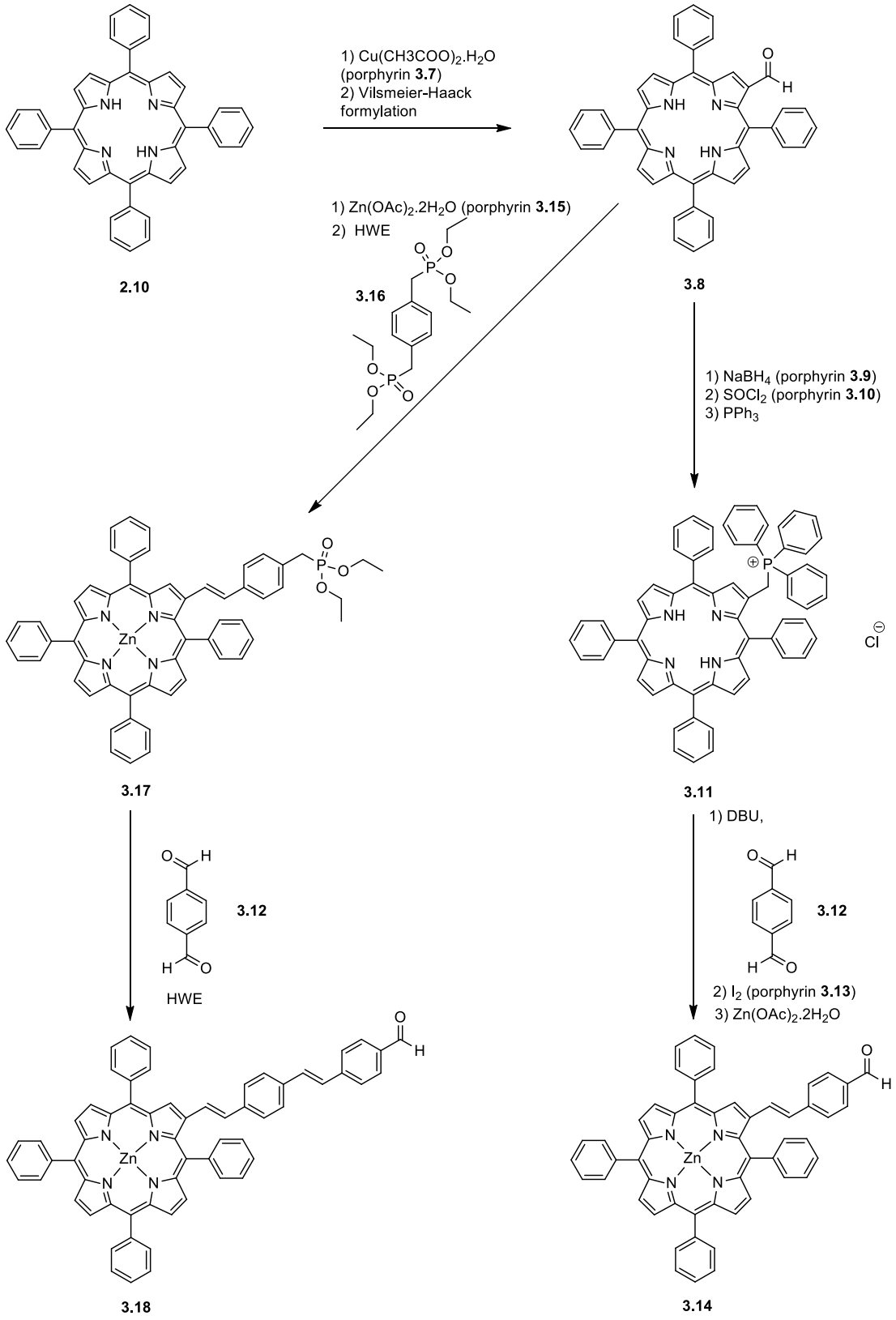

Figure 3.5: Proposed synthesis of oligo-*p*-PV series precursor aldehydes **3.14, 3.15** and **3.18**.

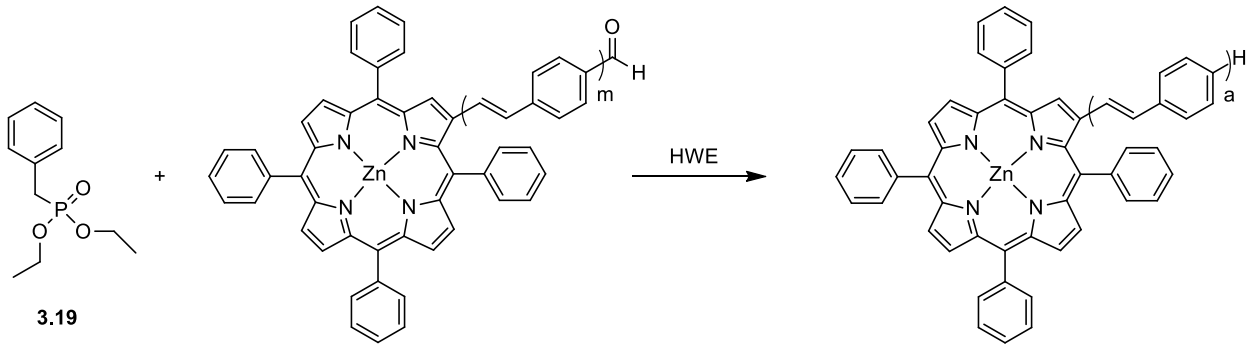

3.15; m = 0
3.14; m = 1
3.18; m = 2

3.1; a = 1
3.2; a = 2
3.3; a = 3

Figure 3.6: Proposed synthesis of oligo-*p*-PV series model monomeric compounds **3.1**, **3.2** and **3.3**.

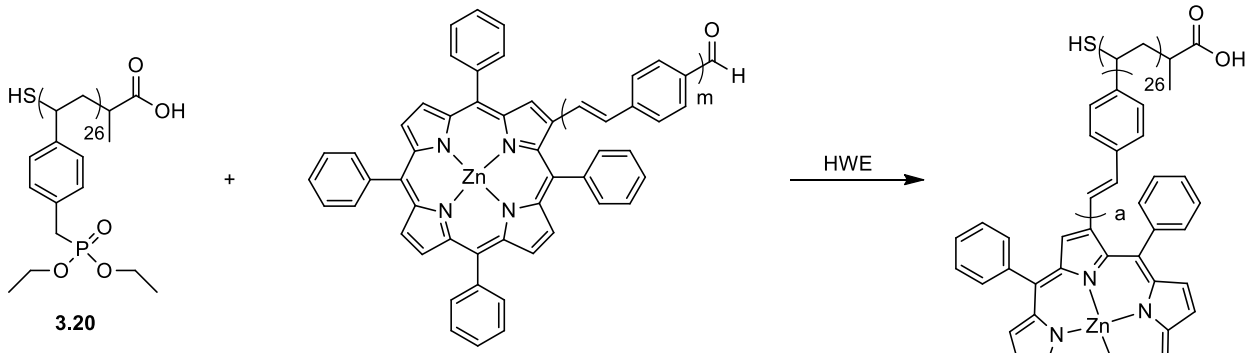

3.15; m = 0
3.14; m = 1
3.18; m = 2

3.4; a = 1
3.5; a = 2
3.6; a = 3

Figure 3.7: Proposed synthesis of oligo-*p*-PV series polymers **3.4**, **3.5** and **3.6**.

3.3 Synthesis

3.3.1 Synthesis of 2-formyl-5,10,15,20-tetraphenylporphyrin precursor 3.15

Several methods have been developed to introduce the formyl group at the β-position of tetraarylporphyrins by employing variations of the Vilsmeier-Haack reaction using the reagents

DMF and $POCl_3$,[25-27] however the most effective of these Vilsmeier-Haack β-formylation reactions to date was developed by Bonfantini *et al.*[25] The formylation reaction outlined by Bonfantini *et al.* utilized [5,10,15,20-tetraphenylporphyrinato] copper(II) (CuTPP **3.7**) as the starting material porphyrin and involves demetalation of the intermediate Cu(II)porphyrin iminium salt *in situ* rather than demetalation following hydrolysis to form the formyl group. Demetalation prior to hydrolysis of the Vilsmeier salt allows for prevention of exposure of the β-formyl-porphyrin to strong acidic conditions which can result in unwanted intramolecular Friedel-Crafts cyclisation reactions between the β-formyl-group and the adjacent meso-phenyl substituent.[28] The use of Cu(II) as the central metal ion allows for both relatively labile removal of the central metal ion to form the free-base porphyrin and activation of the β-position of the porphyrin toward electrophilic attack by the Vilsmeier reagent.

Thus, in order to obtain the copper-chelated precursor to aldehyde **3.15**, $Cu(CH_3COO)_2.H_2O$ was stirred with TPP to give CuTPP **3.7** in 91% yield (Figure 3.8). CuTPP **3.7** was subsequently formylated under Vilsmeier-Haack conditions outlined by Bonfantini *et al.*,[25] using DMF and $POCl_3$ to form the reactive chloroiminium species, followed by electrophilic attack of the Vilsmeier reagent at the β-position of Cu(II)-TPP, demetalation of the metalloporphyrin iminium salt upon addition of conc. H_2SO_4 and iminium hydrolysis. The product 2-formyl-tetraphenylporphyrin **3.8** was obtained in 78% yield after purification via silica gel column chromatography (Figure 3.8). The presence of the singlet at 9.41 ppm in the ^{1}H NMR spectrum of **3.8** indicated the introduction of the aldehyde, with corresponding loss of β-pyrrolic proton doublet and gain of downfield-shifted β-pyrrolic proton singlet at 9.21 ppm indicating the aldehyde was introduced at the β-position. The presence of the singlet at -2.54 ppm integrating to 2H in the ^{1}H NMR spectrum of **3.8**, corresponding to the inner ring N-H protons of the product free-base porhyrin, provides evidence for effective demetalation of the parent Cu(II) porphyrin *in situ*. Free-base 2-formyl-TPP **3.8** was then chelated to zinc by stirring with $Zn(CH_3COO)_2.2H_2O$ to give aldehyde **3.15** in 99% yield. Lack of a singlet at -2.54 ppm in the ^{1}H NMR spectrum of **3.15**, in addition to a peak at 704.1546 *m/z* in the mass spectrum centered in a cluster of peaks characteristic of the zinc isotope distribution, confirmed effective chelation of the porphyrin free-base to the Zn(II) metal ion.

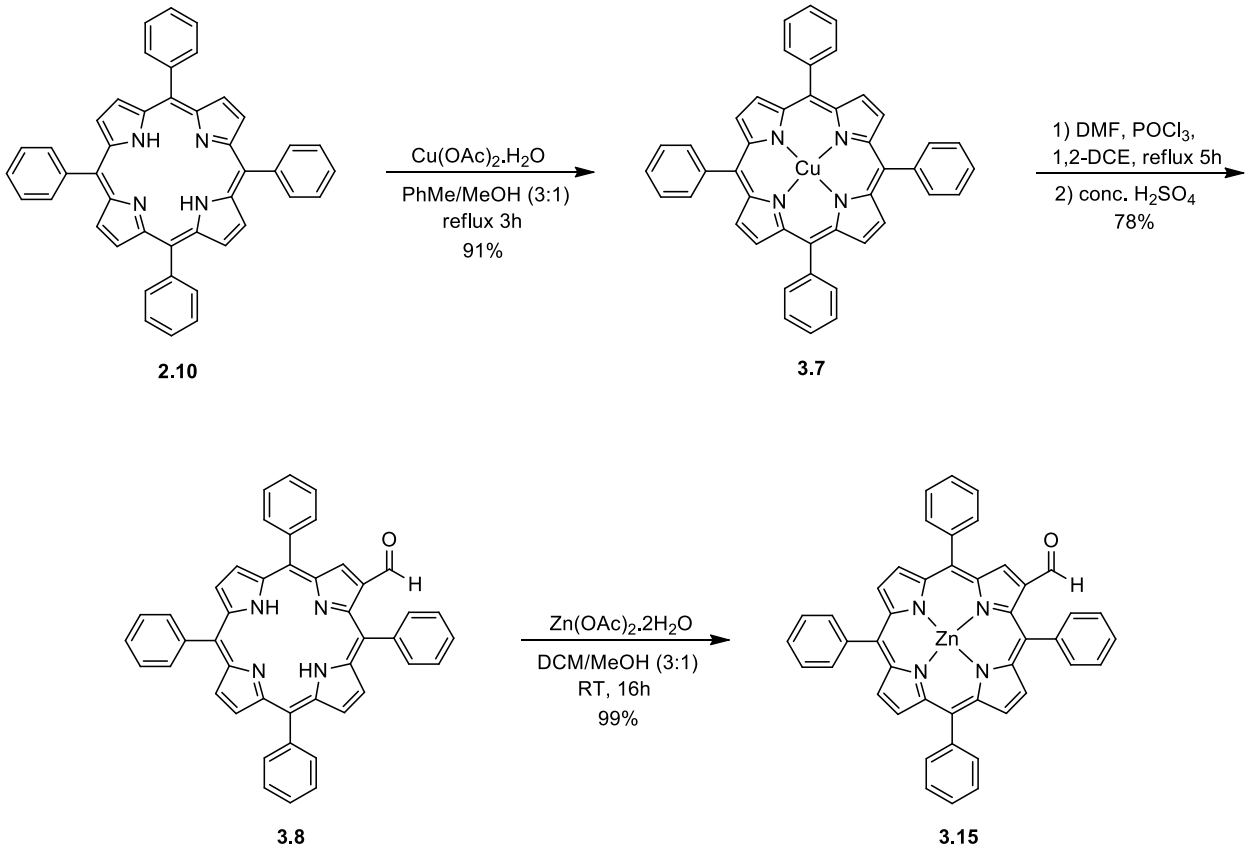

Figure 3.8: Synthesis of [2-formyl-5,10,15,20-tetraphenylporphyrinato] zinc(II) **3.15**.

3.3.2 Synthesis of [2-((E)-4'-formylstyryl)-5,10,15,20-tetraphenylporphyrinato] zinc(II) precursor 3.14

To achieve the synthesis of the aldehyde precursor 3.14, the synthesis of an intermediate porphyrin capable of reacting with terephthaldehyde to produce a *trans*-olefinic bond at the β-position was required. Ventura *et. al* achieved this by creating a β-triphenylmethylphosphonium functionalized porphyrin, which could then undergo a Wittig-type olefination reaction to form a double bond.[10] The double bond formed in the Wittig reaction forms a mixture of *cis* and *trans* stereoisomers which requires stirring with I_2 to form 100% of the thermodynamically favoured *trans* isomer. Although this method proved successful in achieving predominantely *trans* olefinic double bonds at the β-position, it was of interest to investigate the possibility of using the Arbuzov reaction to form a β-methylphosphonate-functionalized porphyrin that could potentially

participate in HWE olefination to exclusively form *trans*-vinylic bonds at the β-position of porphyrins. To the best of our knowledge, there were no prior literature reports on the synthesis of a β-methylphosphonate-functionalized porphyrin by direct Arbuzov phosphonation.

To form either the β-triphenylmethylphosphonium or β-methylphosphonate functionalized porphyrins, a β-chloromethyl porphyrin precursor was required. 2-formyl-TPP **3.8** was reduced to β-hydroxymethyl-TPP **3.9** in 97% yield after stirring with $NaBH_4$ (Figure 3.9). Conversion of β-hydroxymethyl-TPP **3.9** to β-chloromethyl-TPP **3.10** was achieved using $SOCl_2$ in 92% yield (Figure 3.9). The presence of the $[M+H]^+$ molecular ion peak at 663.2310 *m/z* in the mass spectrum of **3.10** and the disappearance of a broad triplet at 1.95 ppm in the ^1H NMR spectrum of **3.10** corresponding to the hydroxyl proton of **3.9** confirmed the successful synthesis of **3.10**. Purification of **3.10** was not possible as the product material from the reaction quickly decomposed on silica and both basic and neutral alumina, however the crude product was deemed sufficiently pure by ^1H NMR spectroscopic analysis to continue through to the subsequent synthetic steps.

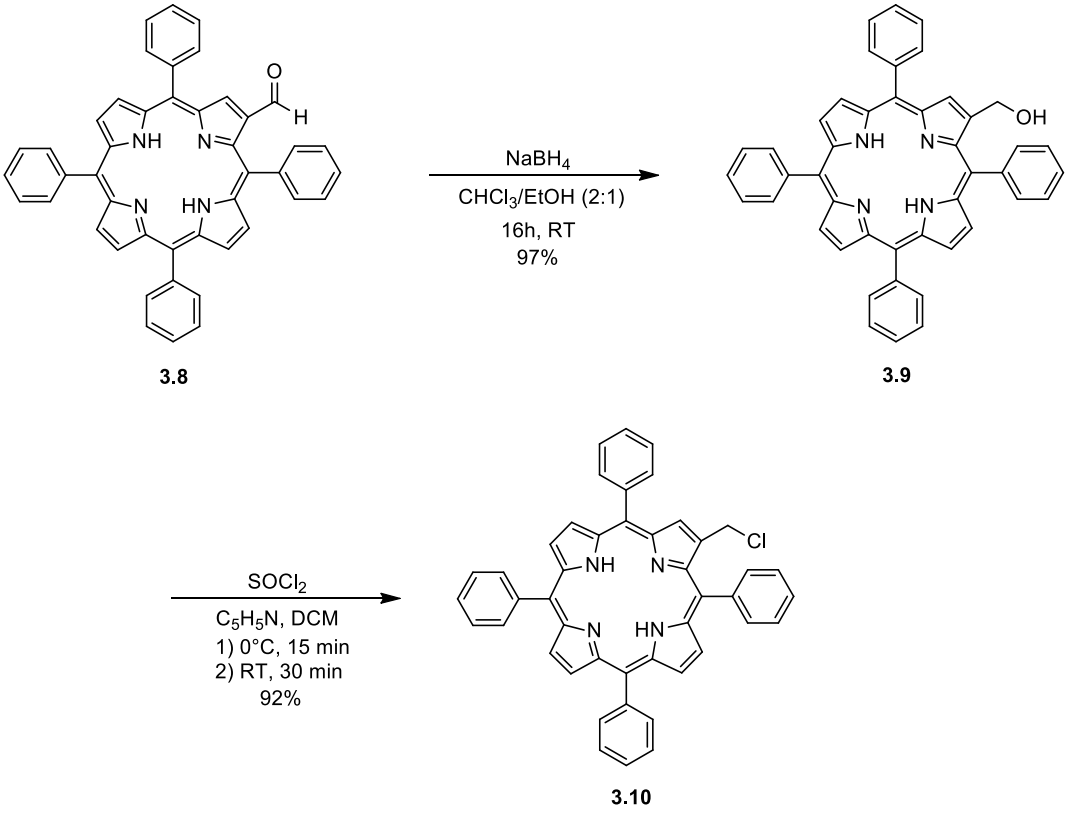

Figure 3.9: Synthesis of 2-chloromethyl-TPP **3.10**.

To obtain the β-methylphosphonate-functionalized porphyrin **3.21**, 2-chloromethyl-TPP **3.10** was refluxed in triethylphosphite. Porphyrin **3.21** was thus obtained in 49% yield after purification using column chromatography (Figure 3.10). The introduction of the phosphonate into **3.21** was confirmed by ^{1}H NMR spectroscopy, with a doublet at 3.38 ppm with H-P coupling constant of 21.8 Hz confirming the presence of a β-methylene group which is bonded to a phosphorus atom and a triplet at 1.06 ppm integrating to 6 protons corresponding to the terminal methyl groups on the ethyl groups of the diethyl phosphonate. The mass spectrum of **3.21** displayed an abundant peak at 765.3002 *m/z* consistent with the presence of the $[M+H]^{+}$ molecular ion peak of **3.21**. A large portion of the crude material remaining after refluxing **3.10** in triethylphosphite degraded on both silica and basic alumina into a green substance which was unable to be definitively characterized by straightforward mass spectrometry or ^{1}H NMR spectroscopic analysis. The reaction was repeated to obtain reproducible yield results, with subsequent attempts yielding less than 50% of the β-methylphosphonate- functionalized porphyrin **3.21**. Although the Arbuzov reaction proved successful in forming **3.21**, the yields were significantly lower than the 90% yield reported for the formation of β-triphenylmethylphosphonium chloride **3.11**.[10] Considering the low yields of the precursor **3.21**, it was decided not to pursue the use of **3.21** as the precursor for *trans*-olefinic bond formation, even though an isomerization step to convert the mixture of geometric isomers formed to the pure *trans* product would be required when employing the Wittig reaction.

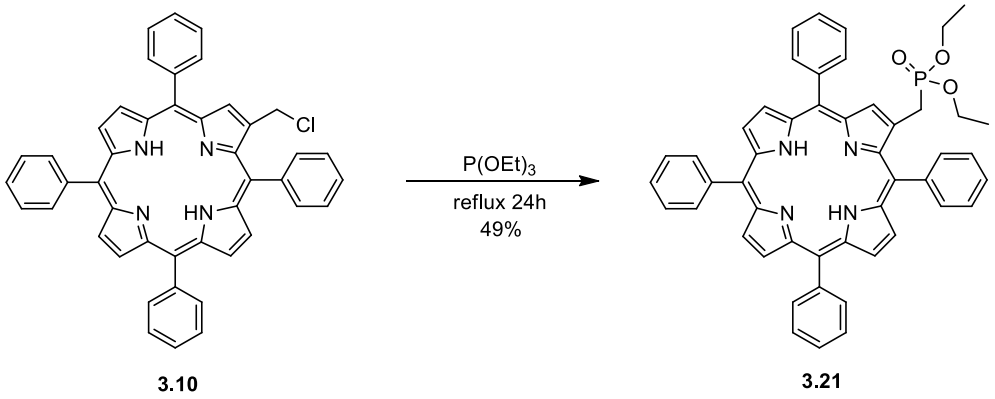

3.10 **3.21**

Figure 3.10: Synthesis of β-methylphosphonate-functionalized porphyrin **3.21**.

In pursuing the synthetic methodology detailed by Ventura *et al.*[10] toward the synthesis of aldehyde **3.14**, **3.10** was refluxed with PPh_3 to give triphenyl[(5,10,15,20-tetraphenylporphyrin-2-yl)methyl]phosphonium chloride **3.11** in near quantitative yield (98%, Figure 3.11). Formation of the phosphonium salt was confirmed by the doublet in the ^{1}H NMR spectrum of **3.11** at 5.34 ppm with J-coupling constant of 15.0 Hz, indicative of strong coupling between the β-methylene protons and the phosphorus atom separated by two bonds in the methylphosphonium moiety. The mass spectrum of the product displays an abundant peak at 889.3457 *m/z* representative of the $[M\text{-}Cl]^+$ molecular ion peak of **3.11**.

Wittig olefination of **3.11** was then performed using terephthaldehyde **3.12** and DBU as base. The crude product was immediately subject to *cis-trans* isomerization by stirring with 0.7 eq. I_2 for 16h, and the *trans*-isomer aldehyde **3.13** was obtained in 86% yield (Figure 3.11). The ^{1}H NMR spectrum of **3.13** displayed two sets of doublets with a roofing pattern integrating to one proton each at 7.15 ppm and 7.31 ppm, both with vicinal coupling constants of 15.9 Hz, confirming the presence of a vinylic bond with *trans* stereoisomerism. No doublets with coupling constants of less than 14 Hz were observed below 7.30 ppm in the ^{1}H NMR spectrum of **3.13**, suggesting that the product did not contain any *cis* double bonds. Although only a small excess of terephthaldehyde **3.12** was used in the Wittig olefination, formation of any conjugated bisporphyrin side-products were suppressed due to the reduced electrophilicity of the resultant aldehyde **3.13** because of electron donation from the porphyrin into the aldehyde moiety and the short reaction time (1 min). Aldehyde **3.13** was then stirred with $Zn(CH_3COO)_2.2H_2O$ to give the HWE precursor aldehyde **3.14** in 98% yield (Figure 3.11).

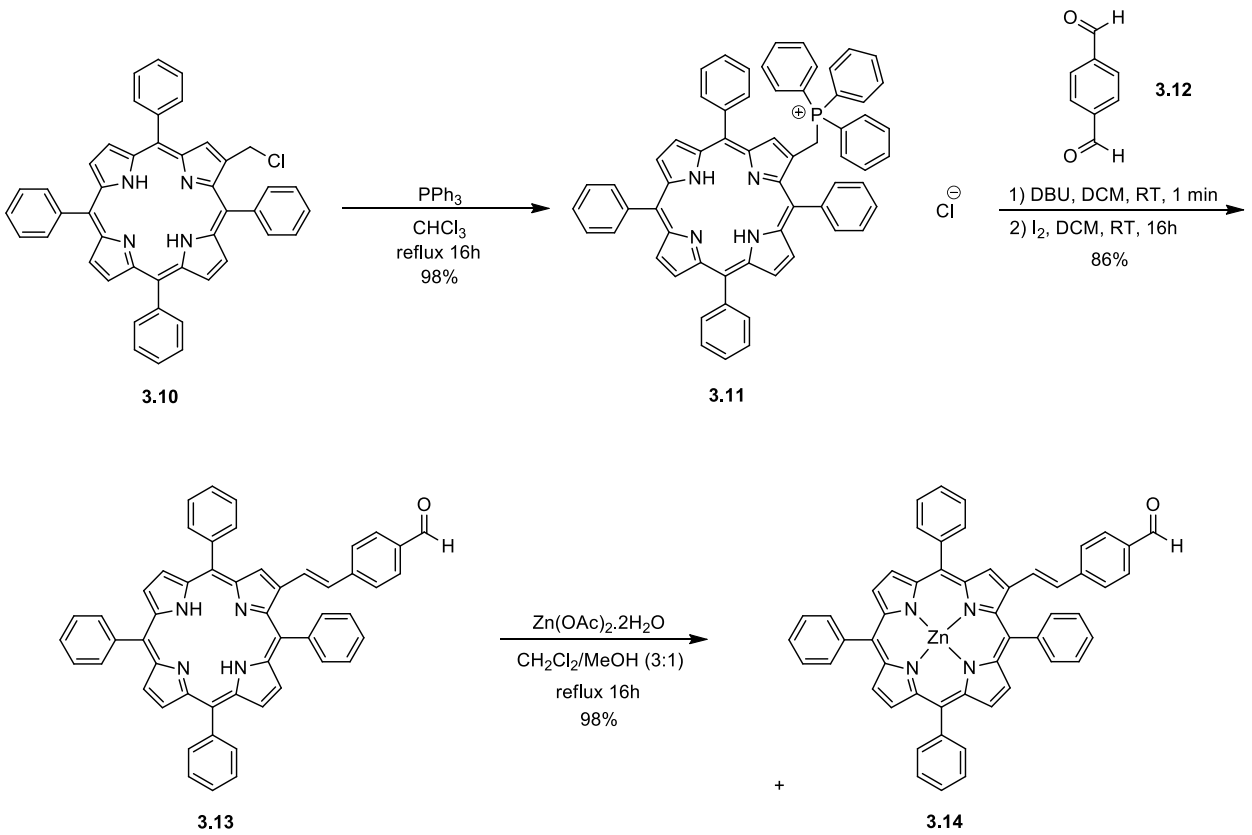

Figure 3.11: Synthesis of HWE precursor aldehyde **3.14**.

3.3.3 Synthesis of [2-((E)-4'-((E)-4''-formylstyryl)styryl)-5,10,15,20-tetraphenylporphyrinato] zinc(II) precursor 3.18

The final precursor required for the HWE synthesis of the oligo-PPV substituted model compounds and polymers was [2-((E)-4'-((E)-4''-formylstyryl)styryl)-5,10,15,20-tetraphenylporphyrinato] zinc(II) **3.18**. The synthetic route to aldehyde **3.18** proceeded via 2 sequential HWE olefination steps. Before proceeding with the HWE steps, it was necessary to synthesize the para-disubstituted bis-phosphonate diethyl ester **3.16**, hence α,α-dichloro-*p*-xylene **3.22** was refluxed in triethylphosphite to give 1,4-xylenebis(diethylphosphonate) **3.16** in 99% yield (Figure 3.12).

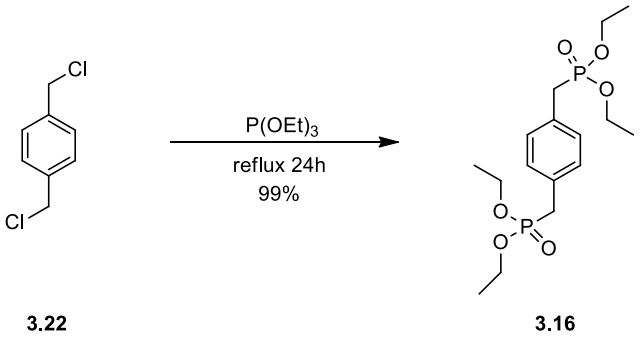

3.22 **3.16**

Figure 3.12: Synthesis of 1,4-xylenebis(diethylphosphonate) **3.16**.

HWE coupling using aldehyde **3.15** and 1,4-xylenebis(diethylphosphonate) **3.16** was performed using *t*-BuOK as base to give phosphonate ester functionalized porphyrin **3.17** in 46% yield after purification via column chromatography (Figure 3.13). An excess (4 eq.) of 1,4-xylenebis(diethylphosphonate) **3.16** was used in order to ensure minimal by-product conjugated bisporphyrin **3.23** (Figure 3.14) was formed as a byproduct of the HWE reaction. A substantial amount of non-product compounds were isolated after column chromatography. Starting material aldehyde **3.15** (23%) was recovered in the first major fraction from the crude reaction mixture. The UV-visible absorption spectrum of the second side product fraction somewhat resembled that of the conjugated bisporphyrin **3.23** previously reported by Ventura *et al.*,[6] with similar Soret and Q-band absorption maxima and a shoulder at 495 nm, however these side products produced broad peaks in the ^{1}H NMR spectrum and the mass spectrum did not exhibit any peaks representing possible molecular ions for the conjugated bisporphyrin **3.23**, therefore a definitive characterization of the side product could not be made. Some highly insoluble material remained trapped on the silica bed after isolation of the phosphonate **3.17** was complete. Formation of product **3.17** was confirmed by observation of the $[M+H]^+$ molecular ion peak in the mass spectrum at 929.2589 *m/z* and the presence of broad peaks at 1025 cm^{-1} and 1231 cm^{-1} in the FT-IR spectrum corresponding to the phosphonate P-O and P-O-C stretches respectively. ^{1}H NMR spectroscopy was difficult to perform even using d_8-THF in accordance with literature[10] due to the very poor solubility of **3.17**.

The phosphonate ester functionalized porphyrin **3.17** was then stirred with *t*-BuOK and terephthaldehyde **3.12** in THF to give the aldehyde **3.18** in 46% yield after column chromatography as seen in Figure 3.13 (literature yield obtained by Ventura *et al.* - 68%).[10] An

excess (4 eq.) of terephthaldehyde **3.12** was used in an attempt to minimize the formation of conjugated bisporphyin **3.24** (Figure 3.14) as a byproduct of the HWE reaction. After prolonged reaction time from 1h to 2h, no appreciable increase in the formation of the desired product **3.18** was observed qualitatively by TLC analysis. A large amount of starting material phosphonate **3.17** (40% of starting material mass) was recovered after column chromatography purification of the crude reaction mixture. No appreciable amount of conjugated bisporphyrin **3.24** was isolated from the reaction mixture. Although the solvent volume was scaled up proportionally with the increase in starting material phosphonate **3.17**, the very low solubility of **3.17** in most solvents, including THF, may have led to variance in the conversion of the starting material **3.17** to product **3.18** in the HWE reaction compared to the previous yield obtained by Ventura *et al.*[10] Evidence for the formation of **3.18** was present in the ^{1}H NMR spectrum of **3.18**, which showed a singlet at 10.03 ppm corresponding to inclusion of an aldehyde. The mass spectrum of **3.18** displayed a peak at 909.2559 *m/z* consistent with the presence of the $[M+H]^+$ molecular ion peak.

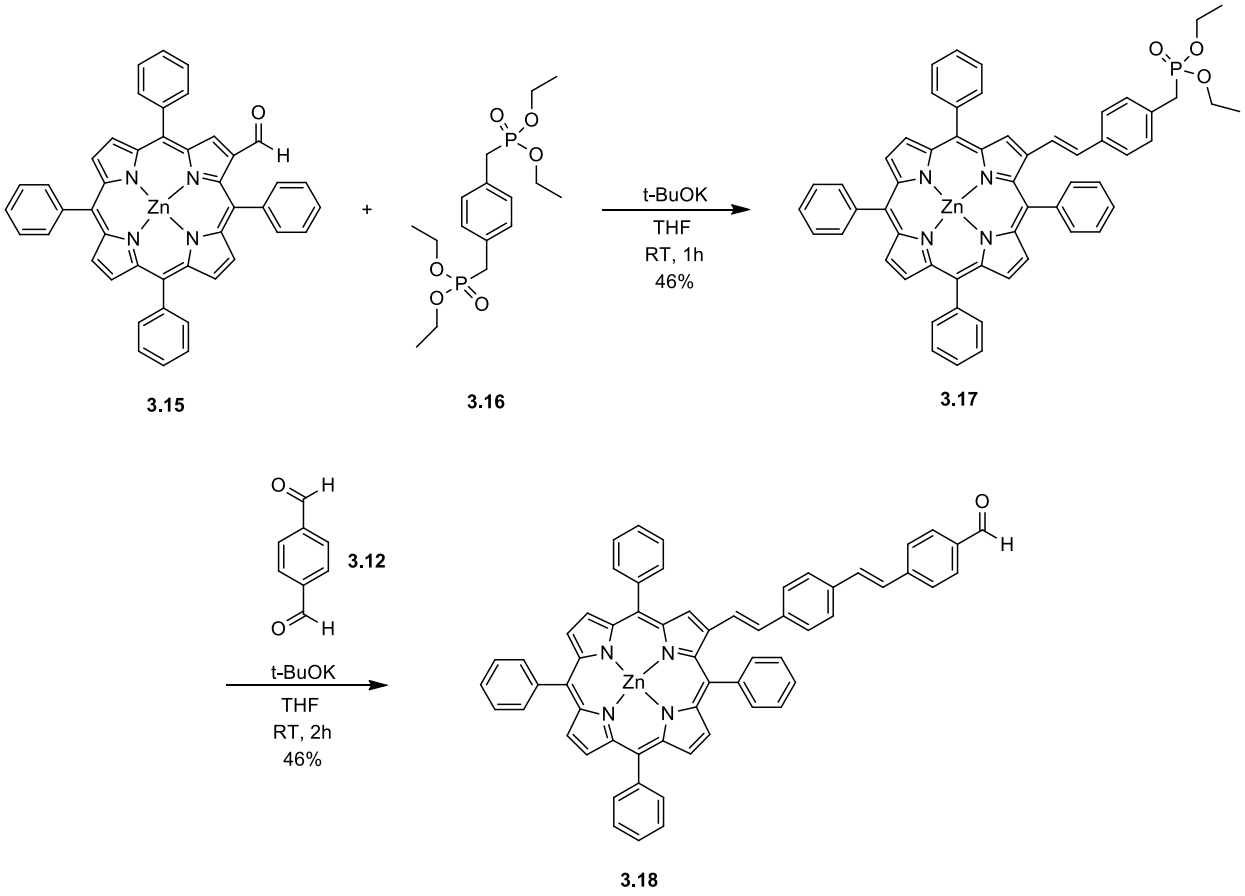

Figure 3.13: Synthesis of aldehyde-functionalised porphyrin precursor **3.18**.

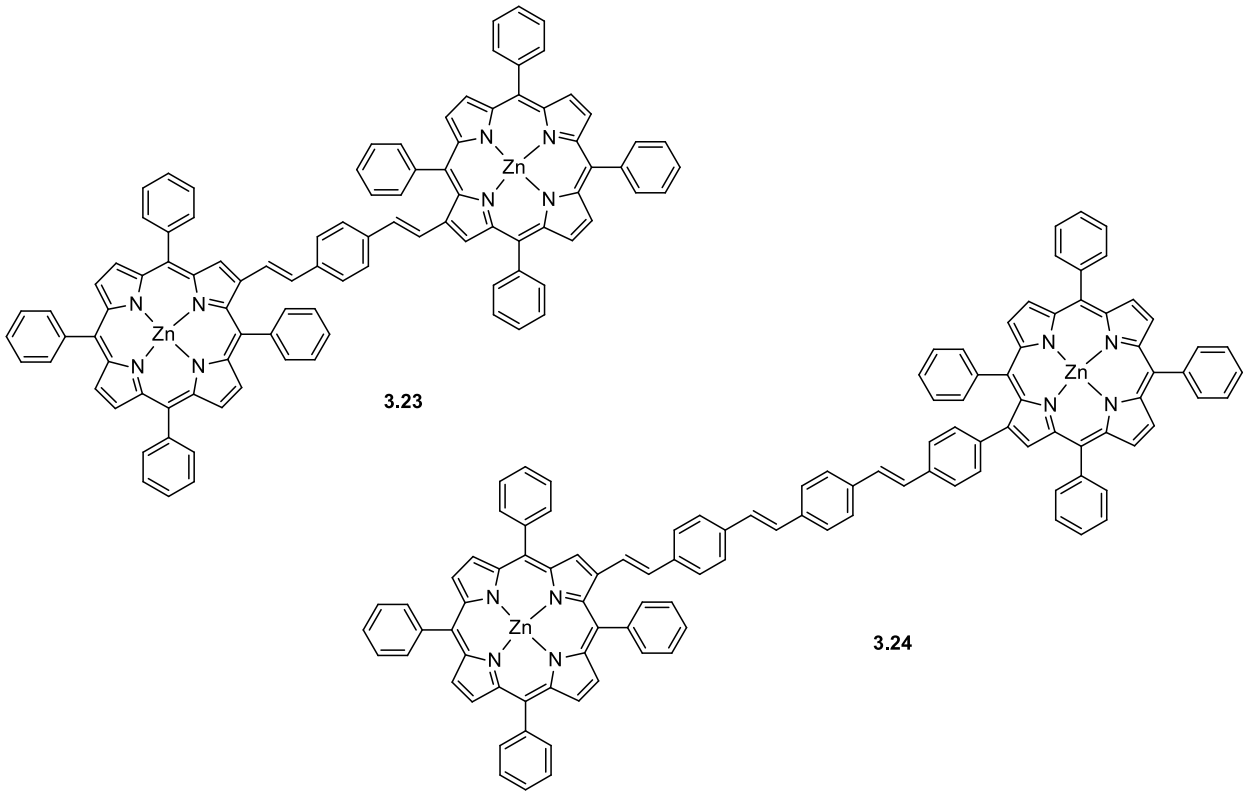

Figure 3.14: Possible conjugated bisporphyrin side products **3.23** and **3.24** from the syntheses of **3.17** and **3.18**.

3.3.4 Synthesis of monomeric model compound porphyrins with varied length oligo-*p*-PV β-substituents

A series of model compounds that represent close analogues of the monomer units present in the polymer series were desired in order to rationalize and make comparisons to the polymer photophysical data. The synthesis of compound **3.1** has been previously reported by Mitchell *et al*. using a slightly different synthetic methodology to that outlined in Figure 3.6.[8] The synthesis of the free-base analogue of **3.1** was reported earlier by Bonfantini et al.[29] The synthesis of these compounds was envisaged to proceed via HWE olefination of aldehyde-functionalised porphyrin precursors **3.14**, **3.15**, and **3.18**, with benzyl diethylphosphonate **3.19** (Figure 3.16). In order to obtain benzyl diethylphosphonate **3.19**, benzyl bromide **3.25** was subject to Arbuzov phosphonation with triethlyphosphite to give **3.19** in 93% yield (Figure 3.15).

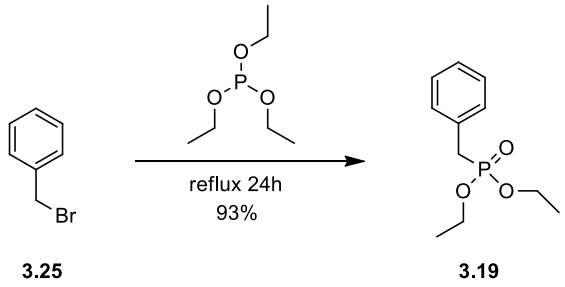

Figure 3.15: Synthesis of diethyl benzylphosphonate **3.19**.

It was decided that NaH would be used as base instead of *t*-BuOK to improve the yield of the HWE coupling step in the formation of the monomer compounds in comparison to the reactions for the formation of **3.17** and **3.18**, as NaH would more effectively deprotonate the benzylic protons of **3.19**. Hydride salts have been previously used to deprotonate phosphonates in HWE reactions for the synthesis of pendant oligo-*p*-PV polymers.[22] HWE olefination between diethyl benzylphosphonate **3.19** and aldehydes **3.15**, **3.14** and **3.18** using NaH as base gave the β-oligo-*p*-PV substituted monomers **3.1**, **3.2** and **3.3** in 85%, 83% and 85% yields respectively (Figure 3.16). The aldehyde protons between 9.50 – 10.10 ppm in the ^{1}H NMR spectra of the precursor aldehyde compounds **3.15**, **3.14** and **3.18** disappeared in the ^{1}H NMR spectra of all respective model compounds **3.1 – 3.3** indicating functionalization at the terminus of the β-oligo-PV substituent. ^{1}H NMR spectral resolution of all doublets due to the formation of *trans*-vinylic protons in the HWE reactions was not possible due to overlap of both phenylene proton peaks and overlap with other vinylene peaks, however the overall integration in the chemical shift region of 7.00 – 7.50 ppm was consistent with the addition of two protons due to olefin formation and five more protons due to the inclusion of the terminal phenyl group on the β-oligo-PV substituent. The ESI positive mode mass spectra of model compounds **3.1 – 3.3** exhibited peaks at 778.2602, 881.2603 and 983.3075 m/z, corresponding to the M^+ molecular ion of **3.1** and the $[M+H]^+$ ions of **3.2** and **3.3** respectively.

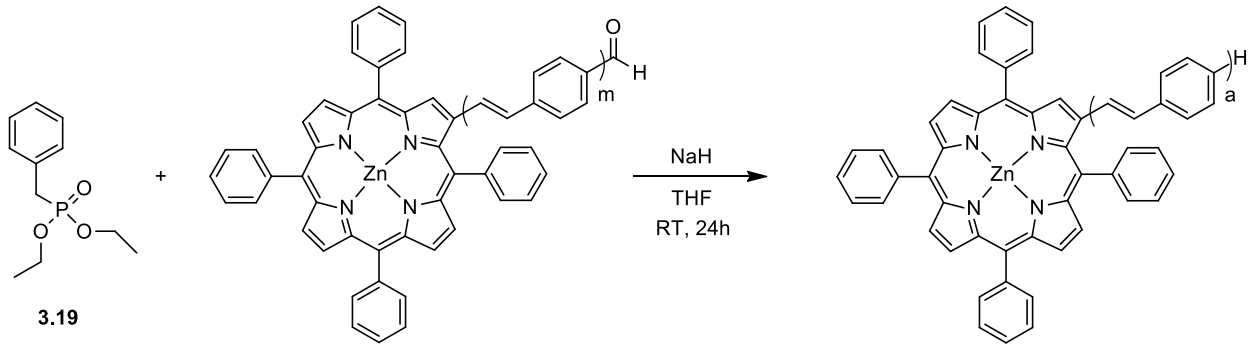

3.15; m = 0
3.14; m = 1
3.18; m = 2

3.1; a = 1, 85%
3.2; a = 2, 83%
3.3; a = 3, 85%

Figure 3.16: Synthesis of oligo-*p*-PV substituted monomeric model compounds **3.1 – 3.3**.

3.3.5 Synthesis of pendant porphyrin polymers with varying length oligo-*p*-PV backbone-to-pendant linking moieties

3.3.5.1 Synthesis of functionalized backbone polymer 3.20

For the HWE post-polymerization functionalization to proceed, it was necessary to synthesize a polymer chain with pendant benzyl phosphonate groups. α-(dodecylthiocarbonothioylthio)-ω-(1-carboxyethyl)-poly(4-vinylbenzylchloride) (poly(VBC)-DoPAT **3.26**) with well-defined chain length (M_n = 4273, PDI = 1.07, 26 vinylbenzylchloride units per chain average) was donated by Dr. John Li from the White group, hence being readily available for use as a backbone chain for the creation of the poly(vinylbenzylphosphonate) precursor polymer via post-polymerization functionalization using Arbuzov phosphonation. The trithiocarbonate moiety linked to the end of the poly(VBC)-DoPAT **3.26** as part of the chain-transfer agent used in the synthesis of the polymer requires removal prior to photophysical experimentation, as the trithiocarbonate moiety is known to quench excited states of chomophores.[30] The trialkyl phosphite used in the Arbuzov phosphonation was proposed to act as a nucleophile and thus cleave the trithiocarbonate *in situ* resulting in a terminal thiol, in a manner similar to that seen previously for such thiocarbonates in the presence of various nucleophiles.[31,32] Arbuzov phosphonation of poly(VBC)-DoPAT **3.26** using triethyl phosphite resulted in complete conversion of the benzyl chloride group to the benzyl diethylphosphonate, as indicated by the disappearance of the chloromethyl protons at 4.55 ppm and the appearance of the broad peaks at 3.06 and 3.95 ppm corresponding to the methylene

protons on the β-methylphosphonate and the ethyl $–CH_2$ groups present respectively in the ^1H NMR spectra of poly(4-vinyldiethylbenzylphosphonate) **3.20** (Figure 3.18). The yield of the phosphonation PPF reaction was 82% (Figure 3.17).

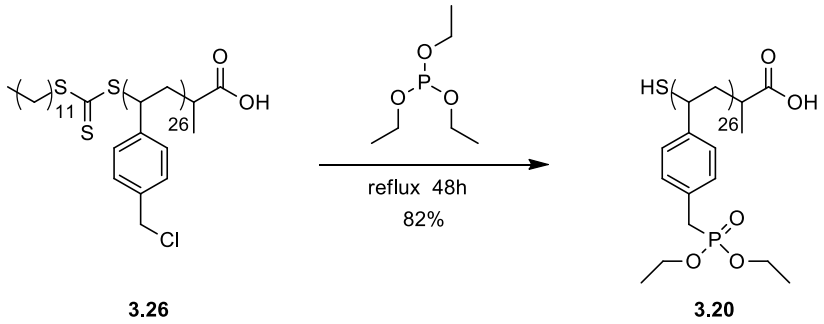

Figure 3.17: Synthesis of poly(4-vinyldiethylbenzylphosphonate) **3.20**.

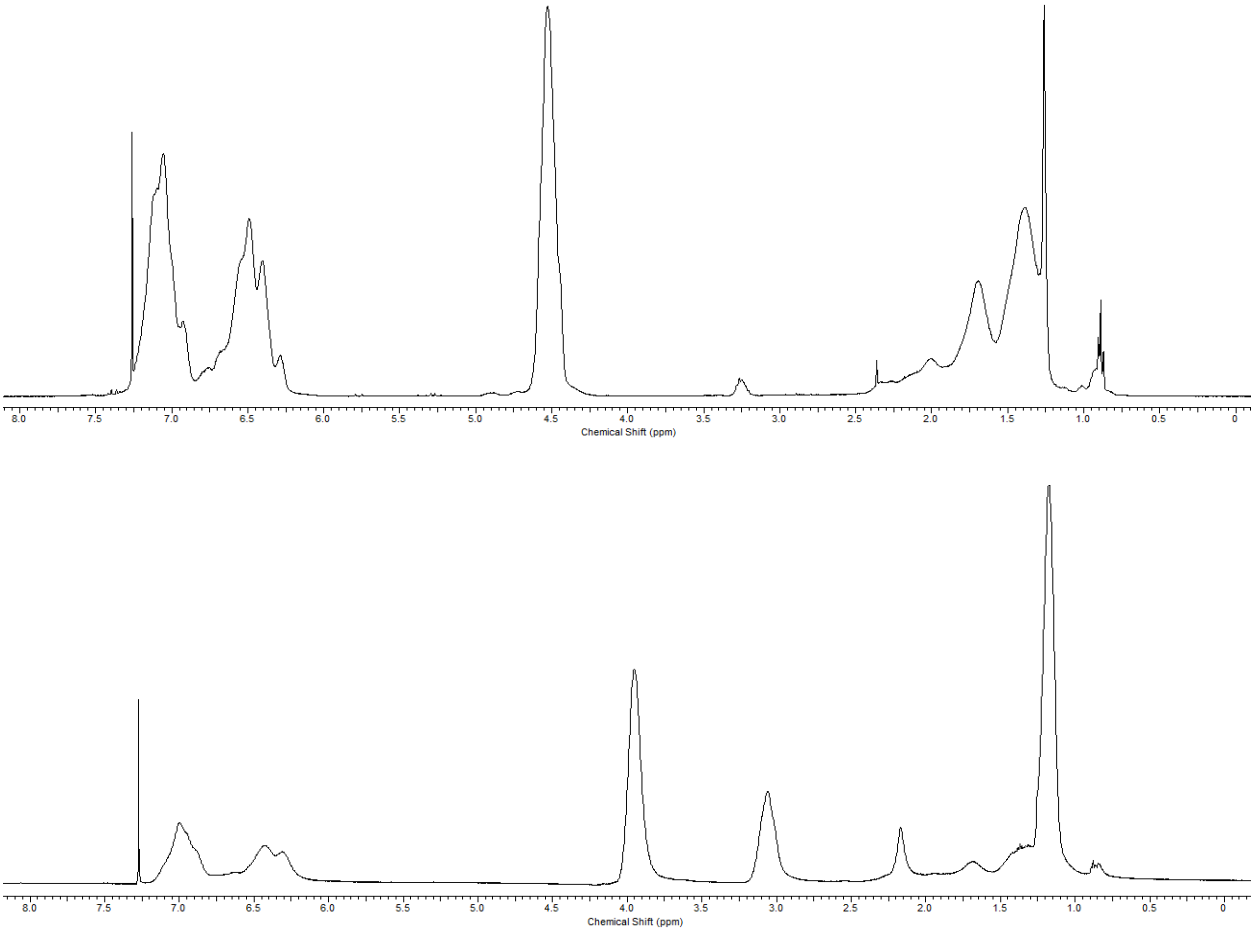

Figure 3.18: ^1H NMR spectra of poly(VBC)-DoPAT **3.26** (top) and poly(4-vinyldiethylbenzylphosphonate) **3.20** (bottom).

Evidence for the cleavage of the trithiocarbonate group is provided in the comparison of the ^{1}H NMR spectra of the poly(4-vinyldiethylbenzylphosphonate) **3.20** with Poly(VBC)-DoPAT **3.26** (Figure 3.18), as the sharp triplet at 0.89 ppm in the spectrum of **3.26** corresponding to the terminal $–CH_3$ protons on the dodecyl chain of the chain-transfer agent is missing in the poly(4-vinyldiethylbenzylphosphonate) spectrum. Additional evidence for the removal of the trithiocarbonate group is present in the comparison of the UV-visible absorption spectra of **3.20** with **3.26** (Figure 3.19). The clear absorption at 311 nm in the absorption spectrum of Poly(VBC)-DoPAT **3.26** due to the trithiocarbonate group is no longer present in the absorption spectrum of poly(4-vinyldiethylbenzylphosphonate) **3.20**.

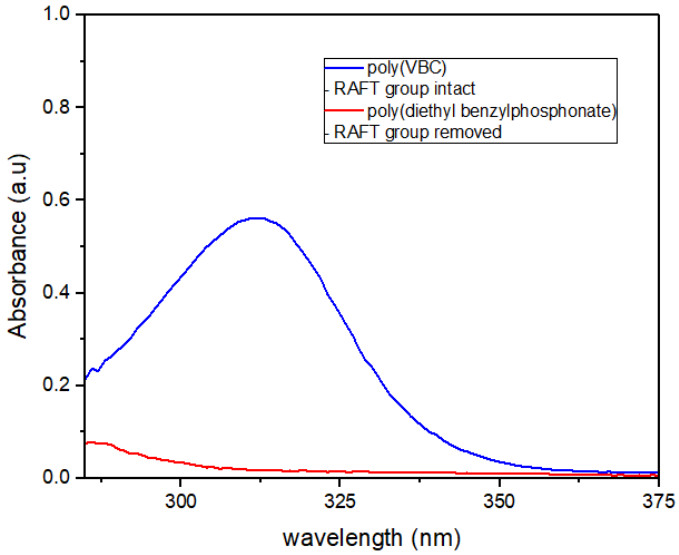

Figure 3.19: UV-visible absorption spectra of poly(VBC)-DoPAT **3.26** and poly(4vinyldiethyl benzylphosphonate) **3.20**, both as 49 µM solutions in toluene.

3.3.5.2 Pendant Porphyrin Polymer Synthesis

With the phosphonate-functionalized backbone polymer in hand, post-polymerization functionalization was able to proceed to form the oligo-PPV linked pendant porphyrin polymers **3.4 – 3.6**. 2 eq. of aldehydes **3.15**, **3.14** and **3.18** were stirred with poly(4-vinyldiethyl benzylphosphonate) **3.20** and NaH under N_2 to give polymers **3.4 – 3.6** in 52%, 90%, and 73% yields respectively (Figure 3.20). The use of excess aldehyde and an extended reaction time of 5 days were implemented in order to guarantee the maximum degree of backbone functionalization

possible. The yields stated here are considered after size-exclusion chromatography (SEC) over bio-S-X beads using THF as eluent, repetitive washings of the polymers with distilled petroleum spirits and subsequent high-vacuum drying in order to remove as much of the residual small molecule and solvent impurities as possible from the polymer bulk material. SEC was used as the purification technique for the polymers as it was not possible to find a suitable solvent system that could easily wash the monomers from the polymer sediment without also causing the polymer to remain in solution. Washing of the polymers with the petroleum spirits was likely to have led to reduction and variability in the perceived yields of the polymers after completion of the purification process, as it proved difficult to avoid disperse fine particles of polymer being carried with the supernatant upon separation from the bulk sediment within a reasonable sedimentation time frame of approximately 1h sedimentation wait time per wash cycle, with 4 wash cycles per polymer sample.

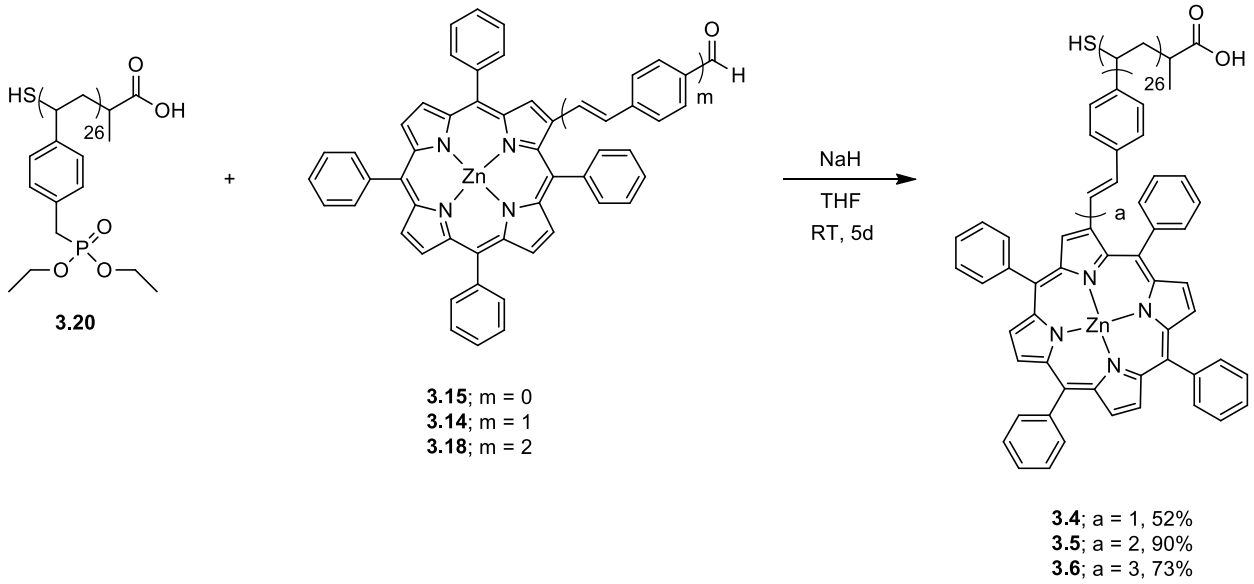

Figure 3.20: Synthesis of pendant porphyrin polymers **3.4 – 3.6**.

The ^{1}H NMR spectra of polymers **3.4 – 3.6** (Figure 3.21) display complete disappearance of the broad peaks at 3.06 and 3.95 ppm corresponding to the methylene protons on the β-methylphosphonate and the ethyl $–CH_2$ groups present respectively in the ^{1}H NMR spectra of poly(4-vinyldiethylbenzylphosphonate) **3.20** (Figure 3.18 top), indicating that all phosphonate groups present in the backbone starting material polymer **3.20** have been consumed in the post-

polymerization functionalization reactions. $C_2D_2Cl_4$ was used as solvent for the ^1H NMR spectroscopy of all pendant porphyrin polymers, as this solvent allowed for NMR spectra to be run at high temperature, allowing for better resolution of the characteristic regions of porphyrinic protons when incorporated into the polymer structure. The high solvation power of $C_2D_2Cl_4$ additionally allows for a higher concentration of polymer sample in the NMR sample tubes, which improves the signal-to-noise ratio in the polymer NMR spectra. The peaks seen furthest downfield between 8.30-9.20 ppm in ^1H NMR spectra of **3.4 – 3.6** (Figure 3.21) represent the β-pyrollic protons of the pendant porphyrin groups, and furthermore, the broad shape of these peaks corroborates the idea that the β-pyrollic protons of porphyrins in the sample compounds have been incorporated into polymeric structures. The prominent peaks at 1054 cm^{-1} and 1247 cm^{-1} seen in the FT-IR spectra of poly(diethybenzylphosphonate) **3.20** representing P-O-C and P-O stretching frequencies respectively, completely disappear in the FT-IR spectra of all polymers **3.4 – 3.6**, further suggesting that a large proportion of phosphonate side groups on the polymer backbones were replaced with pendant oligo-*p*-PV porphyrins upon completion of the HWE reactions. Such disappearance of strong peaks between 1000 – 1100 cm^{-1} and 1200 – 1300 cm^{-1} in the FT-IR spectrum upon HWE reaction of poly(phosphonate) derivatives with aldehydes is consistent with analyses performed previously by Belfield *et al.*[24]

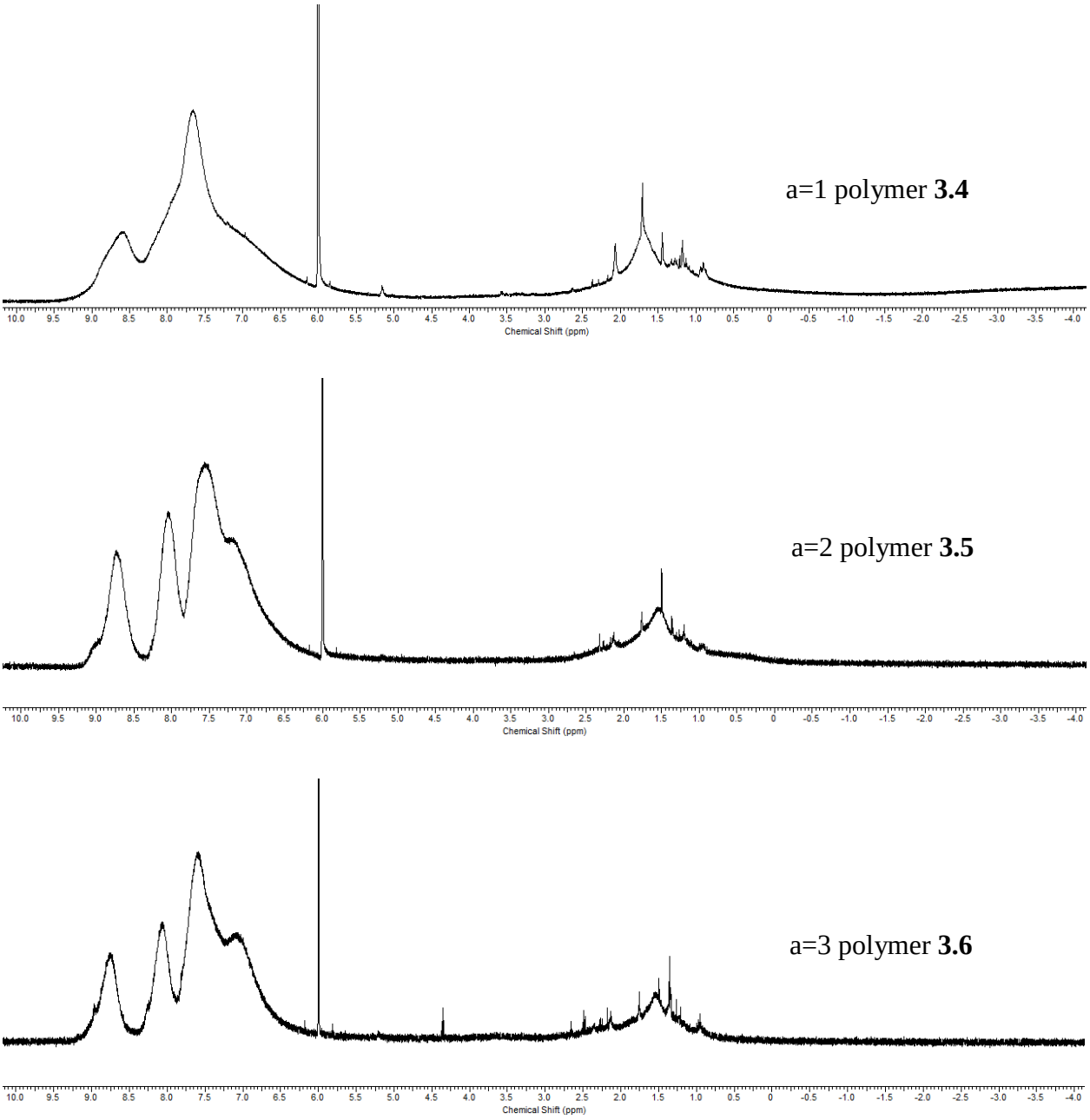

Figure 3.21: ^{1}H NMR spectra of pendant porphyrin polymers **3.4 – 3.6** in $C_2D_2Cl_4$.

3.4 Analysis of the Degree of Polymer Backbone Functionalisation

Several analytical methods were pursued in order to determine the degree of functionalization of the polymers **3.4 – 3.6**. Although no analysis method was able to provide an accurate quantitative value for the extent of backbone functionalization, the use of synthetic yields and UV-visible absorption data provided approximations to the minimum thresholds of functionalization. The methods used for calculation of the functionalization degrees are outlined in sections 3.4.1 and 3.4.2, while the functionalization yields are compared and discussed in section 3.4.3 below.

3.4.1 Approximation of Minimum Functionalization Degrees using Synthetic Yields

In order to approximate the minimum degree of functionalization from synthetic yields, an assumption must be made that 100% of the starting material polymer backbone will contribute to the final mass of polymer obtained. This implies a 100% yield of polymer recovery, therefore the synthetic yield can now be interpreted as the percentage molecular weight in the synthesized polymer of the expected maximum molecular weight of the polymer if 100% functionalization was afforded. If this assumption is not made, it is not possible to determine whether variation in the final mass obtained is due to either a highly functionalized polymer with loss of product in work-up or a poorly functionalized polymer for which most of the polymer backbone chain has been recovered in the work-up. In practice, the former is most likely the case and significant losses of polymer product due to work-up and purification have been noted earlier in the thesis. The functionalization degrees derived from the synthetic yields according to calculations outlined below therefore give a good approximation of the lower bound of backbone functionalization assuming there are no small molecule impurities present in the samples.

The average molecular weight of a polymer with known average polymer chain length and variable degree of functionalization is given by the following equation:

$$Cx + By + z = M_w \qquad 3.1$$

Where M_w is the average molecular weight of a polymer with known polymer chain length, C is the pendant chromophore monomer unit molar mass, x is the average number of chromophore pendant units in the polymer, B is the molar mass of the unfunctionalized pendant precursor unit, y is the average number of unfunctionalized pendant precursor units in the polymer and z is the residual mass due to end groups and non pendant groups. In the case where the polymers discussed in this thesis are fully functionalized, x = 26, y = 0, z = 106 and the fully functionalized polymer molecular weight, MW_{FF}, can be easily calculated. Upon assuming 100% polymer backbone recovery, the following equation can be used to determine x and y:

$$Cx + By + z = S_y MW_{FF} \tag{3.2}$$

Where S_y denotes the synthetic yield as a fraction. Given that the polymer chain average length is known to be 26 units for all polymers used for syntheses in this thesis:

$$x + y = 26 \tag{3.3}$$

which can be rearranged to give

$$26 - x = y \tag{3.4}$$

Substituting eq. 3.4 into eq. 3.2 and rearranging gives the solution for the number of chromophore units x in the pendant backbone:

$$\frac{S_y MW_{FF} - z - 26B}{C - B} = x \tag{3.5}$$

The degree of functionalization F can then be determined using the following equation:

$$\frac{100x}{26} = F \tag{3.6}$$

3.4.2 Approximation of Minimum Functionalization Degrees using UV-Visible Absorption Ratios

Although measurement of extinction coefficients of polymers cannot be used to estimate the true degree of functionalization of the polymers, as polymers with full porphyrin pendant inclusion have been reported to experience variable reduction of extinction coefficients,[17] measurement of extinction coefficients can provide a reasonable estimate for the lower threshold for the minimum degree of inclusion of pendants into the backbone. As the Q(1,0) band absorption maxima of the porphyrins have considerable extinction coefficient magnitudes however are generally less perturbed by local neigbouring electronic environments that the Soret band maxima, they were used in the following analyses of polymer backbone functionalization degrees.

In order to approximate degrees of polymer functionalization using spectrophotometric techniques, the assumption must be made that the extinction coefficient of the monomeric compounds are the same as the extinction coefficients of the monomeric chromophore units when included into the polymer structure. Thus, solutions of polymer and model compounds were prepared with the same concentrations per chromophore unit given the initial assumption that the polymers were fully functionalized. If fully functionalized, the polymers should have the same absorbances as the monomers at the same sample prepared chromophore unit concentrations. If this is not the case, the true concentration of absorbing chromophore units in the polymer sample can be obtained using the equation

$$\frac{A_p c_m}{A_m} = c_p \qquad 3.7$$

Where A_p is the polymer absorption, A_m is the model compound absorption, c_p is the concentration of chromophore units in the polymer sample and c_m is the concentration of chromophore units in the model compound sample, which for all compounds is 3.3µM. The molar concentration c_p can be used to calculate the concentration of chromophore in the polymer sample in units of mass per unit volume, V_c, through eq. 3.8. This is because the relationship c_p / c_m can be interpreted as a mol ratio rather than a concentration ratio as the subject of analysis in

the absorption is the chromophore unit only and not the combination of partially functionalized polymer backbone plus chromophore units. Equation 3.8 is shown below, where C is the pendant chromophore monomer unit molar mass.

$$C \times c_p = V_c \tag{3.8}$$

The concentration of total polymer in the initially prepared sample, in units of mass per unit volume, V_p, can be easily determined as both the mass of polymer used to prepare the sample and the volumes used to dilute the sample are known. Thus the fraction of the chromophore monomer unit mass contributing to the total polymer mass, F_c, can be obtained via eq. 3.9 below.

$$\frac{V_c}{V_p} = F_c \tag{3.9}$$

Considering eq. 3.1 mentioned previously for the synthetic yield calcluations

$$Cx + By + z = M_w \tag{3.1}$$

And that the fraction of residual mass in the polymer sample contributing to unfunctionalized backbone units and mass due to end groups combined, F_R, is given by

$$F_R = 1 - F_c \tag{3.10}$$

It can be determined that

$$F_c M_w = Cx \tag{3.11}$$

And

$$F_R M_w = By + z \tag{3.12}$$

And thus combining and rearraging eq. 3.11 and 3.12 gives

$$\frac{Cx}{F_c} = \frac{By + z}{F_R} \tag{3.13}$$

Eq. 3.4 can be substituted into eq. 3.13 above and rearranged to give the solution for the number of chromophore units present in the polymer chain, x, shown in eq. 3.14 below.

$$\frac{26F_cB + F_cz}{CF_R + F_cB} = x \qquad 3.14$$

Substitution of x into eq. 3.6 above yields the degree of functionalization based on the relative UV-visible absorption ratios.

3.4.3 Comparison of Functionalization Yields Derived from Synthetic Yields and UV-Visible Absorption Spectrophotometry

Table 3.1: Degrees of functionalization (F) of the polymer backbones of polymers **3.4 – 3.6** derived from synthetic yields and UV-visible spectrophotometry.

Compound	% Minimum functionalization (F) derived from synthetic yield	% Minimum functionalization (F) derived from UV-visible absorption
a=1 polymer **3.4**	30	23
a=2 polymer **3.5**	86	31
a=3 polymer **3.6**	64	29

The F values derived from both synthetic yield and UV-visible spectrophotometry data, as seen in Table 3.1, indicate that functionalization of polymer compounds **3.4 – 3.6** by inclusion of porphyrin pendants is highly incomplete. As expected, the F values obtained using UV-visible absorption data were significantly lower than the F values obtained uing synthetic yield data. This is likely due to inter-pendant interactions, discussed further in section 3.5, that have been shown to lead to variable reduction of extinction coefficients in the polymers.[17] The F values determined using synthetic yield data are more reliable that those determined using UV-visible absorption data as the purity of the samples can be inferred by lack of phosphonate proton peaks in ^{1}H NMR spectra shown in Figure 3.21 and lack of chromophoric precursor artifacts in the

photophysical spectra. It is important to note that the F values presented in Table 3.1 are minimum functionalization degrees and due to the complexity of extraneous parameters, such as the aforementioned potential inter-pendant electronic interactions, do not truly reflect the functionalization degrees of polymers **3.4 – 3.6**. Regardless, the functionalization degrees calculated were highly inconsistent between analytical methods and were thus deemed inappropriate or inconclusive in determining accurate degrees of polymer backbone functionalization for any of the polymers studied.

3.4.4 Alternative Techniques for Approximating the Degree of Backbone Functionalization

Gel Permiation Chromatography (GPC) and Inductively Coupled Plasma Optical Emission Spectroscopy (ICP-OES) were also attempted in an effort to characterize the degree of backbone functionalization. The comparison of ^{1}H NMR integrals of characteristic peaks was deemed inappropriate for determining functionalization degrees as no clearly resolved peaks were present in the polymer spectra (Figure 3.21) that could be attributed solely to unfunctionalized pendant units or backbone proton environments.

Data obtained by GPC analysis for the polymers **3.4 – 3.6** yielded broad retention peaks that corresponded to PDI values greater than 3 and M_n values that varied between 4000 to several million g mol^{-1}, from which meaningful molecular weight analysis could not be extracted. GPC molecular weight distribution analysis has however been successfully performed previously by Wang *et al.* on pendant zinc porphyrin polymers using similar calibration with polystyrene standards.[17] ICP-OES was attempted on polymer **3.5** in order to relate the zinc content in the polymers to the number of pendant units present in the backbone (appendix A2). The analyses determined that the zinc content of 2 samples of **3.5** were 7.4 and 9.2 parts per thousand (ppk), with the zinc content in a fully-functionalized sample of **3.5** expected to be 72 ppk. This functionalization degree of approximately 10 – 13% is highly inconsistent with the functionalization degrees obtained in Table 3.1 for polymer **3.5**. The use of ICP-OES for functionalization analysis was abandoned as it was evident that choice of appropriate solvent, poor polymer digestion and low zinc extraction efficiency all contributed to the low zinc contents obtained for **3.5**.

3.5 Absorption Spectra

The UV-visible absorption spectra for the oligo-PV linked model compounds and polymers (Figure 3.22) were obtained from solutions of the respective porphyrins in toluene at room temperature. The concentration of all solutions used to obtain the absorption spectra was 3.3 µM. For polymers, the concentration was approximated based on the total number of repeat units in the polymer chains rather than the total number of polymer chains, with an assumption of 100% backbone functionalization. Molar extinction coefficients (ε) were calculated for all compounds, as listed in Table 3.2.

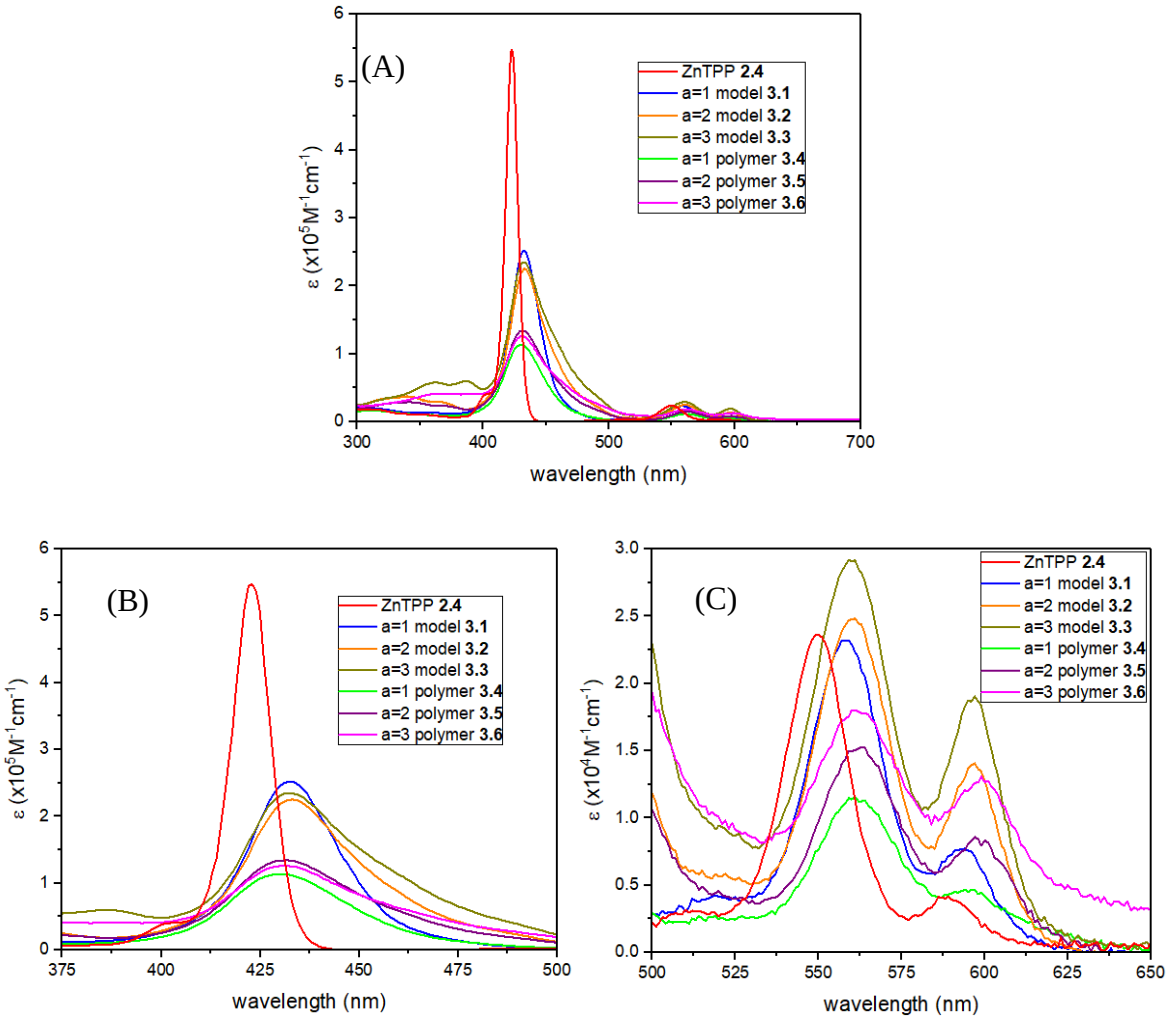

Figure 3.22: (A) UV-visible absorption spectra of ZnTPP **2.4**, the model compounds **3.1 – 3.3**, and the polymers **3.4 – 3.6** in toluene. (B) Spectra in (A) zoomed into Soret absorption region for clarity. (C) Spectra in (A) zoomed into Q-band absorption region for clarity.

Table 3.2: UV-visible absorption data for ZnTPP **2.4**, the model compounds **3.1 – 3.3**, and the polymers **3.4 – 3.6** in toluene at 3.3μM. The absorption transitions to the first and second vibronic quanta of the Q-band are indicated by (0,0) and (1,0) respectively.

Compound	λ_{max} Soret (nm)	ε Soret (10^5 $M^{-1}cm^{-1}$)	λ_{max} Q-band (nm) [(1,0),(0,0)]	ε Q-band (10^4 $M^{-1}cm^{-1}$) [(1,0),(0,0)]	ε Q-band at 532 nm (10^3 $M^{-1}cm^{-1}$)
ZnTPP **2.4**	423	5.48	550, 589	2.36, 0.41	6.05
a=1 model **3.1**	433	2.52	559, 593	2.32, 0.77	4.40
a=2 model **3.2**	433	2.25	561, 597	2.48, 1.41	5.13
a=2 model **3.3**	432	2.35	560, 597	2.92, 1.90	7.73
a=1 polymer **3.4**	431	1.13	561, 594	1.16, 0.47	2.59
a=2 polymer **3.5**	431	1.34	563, 597	1.53, 0.86	3.61
a=3 polymer **3.6**	430	1.26	562, 599	1.80, 1.31	8.26

The absorption spectra of all β-oligo-*p*-PV substituted compounds **3.1 – 3.6** in Figure 3.22 exhibit a bathochromic shift close to 10 nm in their Soret and Q-band maxima with respect to ZnTPP **2.4**. Such bathochromic shifting has been observed by Ventura *et al.* for analogous monomeric β-oligo-*p*-PV substituted zinc porphyrins and was reasoned to be due to delocalization-induced destabilization of the HOMOs and stabilization of LUMOs leading to a smaller HOMO-LUMO gap upon conjugation extension of the porphyrin macrocycle at the β-position.[8,10] Broadening of the Soret bands generally increases for compounds **3.1 – 3.6** as a function of conjugation extension. The absorption maxima of all β-oligo-*p*-PV substituted zinc porphyrins **3.1 – 3.6** are found within a 6 nm range for each respective absorption band, indicating that the number of phenylene vinylene units in the conjugated β-substituent does not play a large role in determining the Soret and Q-band energies after inclusion of the first *p*-PV unit.

The Soret band molar extinction coefficients of all compounds **3.1 – 3.6** decrease substantially with increased β-conjugation length with respect to ZnTPP **2.4**, while the Q(0,0) molar extinction coefficients incrementally increase as a function of increasing β-conjugation length, again consistent with absorption data on the analogous monomeric β-oligo-*p*-PV substituted zinc porphyrins studied by Ventura *et al.*[10] As the conjugation increases at the β-position, the difference in the energies of the HOMO and HOMO-1 becomes larger. According to equation 2.1, the intensity of the Q(0,0) vibronic quantum with respect to the Q(1,0) vibronic quantum will increase proportional to the square of the difference in the $a_{2u} \rightarrow e_g$ and $a_{1u} \rightarrow e_g$ transition energies, thus an increase in β-conjugation length will decrease the Q(1,0)/Q(0,0) extinction coefficient ratio (see section 2.4.1).

The bathochromic shifting of the Q-band absorption maxima of the polymers **3.4 – 3.6** of approximately 2 nm with respect to their monomeric analogues, observed in Figure 3.22 (C), is consistent with inter-pendant electronic interactions of porphyrins in pendant polymer environments and has been observed previously for pendant porphyrin polymer systems.[17] In addition, the absorption spectra of the polymers **3.4 – 3.6** in Figure 3.22 (B) show Soret band maxima that are hypsochromically shifted approximately 2 nm with respect to their monomeric analogues. The molar extinction coefficients of both the Soret and Q-bands of polymers **3.4 – 3.6** are approximately half the intensity of their monomeric analogues. As mentioned in section 3.4, reduction in molar extinction coefficients has been previously observed for porphyrins upon inclusion into a pendant polymer environment, even when full pendant inclusion is guaranteed because the polymers are synthesized through polymerization of a porphyrin-appended monomer.[17]

Increasing the number of *p*-PV units on the β-conjugated backbone-to-pendant linking moiety in the polymers **3.4 – 3.6** introduces no splitting of their Soret bands due to excitonic coupling, which would indicate strong inter-pendant electronic coupling or inter-pendant aggregation that would likely guarantee rapid non-radiative relaxation of excited states in the polymers. Such strong inter-pendant interactions leading to excitonic splitting may be expected due to the

increased size of the planar π-electron systems of the pendant units in **3.4 – 3.6** which are in close proximity to each other. Excitonic splitting has been demonstrated for pendant porphyrin polymers with *meso*-dodecyl substituents, which allow for shorter plane-to-plane distances between pendant porphyrin units and thus greater π-π interaction than pendant porphyrin polymers with *meso*-aryl substituents.[17]

3.6 Fluorescence Spectra

The fluorescence spectra in Figure 3.23 below were obtained from solutions of the respective porphyrins in toluene at room temperature and corrected for the photomultiplier detector wavelength response. Fluorescence quantum yields of all model compounds and polymers were calculated relative to ZnTPP **2.4** ($\Phi = 0.033$)[33] and are listed in Table 3.3. All solutions used in the fluorescence spectra measurements had an absorbance of 0.05 ± 0.005 at their respective Q(1,0) absorption maxima in order to minimize inner filter effects such as reabsorption and quenching due to intermolecular porphyrin aggregation.

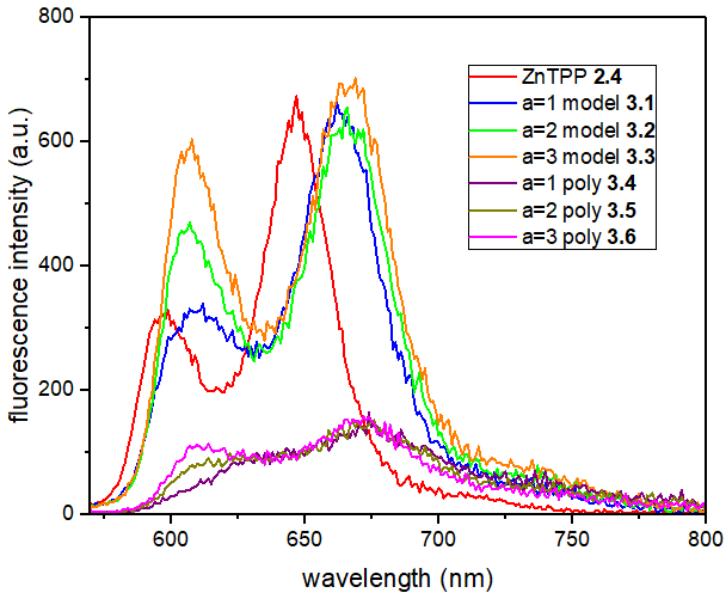

Figure 3.23: Fluorescence spectra of ZnTPP **2.4**, the model compounds **3.1 – 3.3** and the polymers **3.4 – 3.6** in toluene. All porphyrin samples were excited at their respective absorption maxima, listed in Table 3.2.

Table 3.3: Fluorescence parameters for ZnTPP **2.4**, the model compounds **3.1 – 3.3** and the polymers **3.4 – 3.6** in toluene.

Compound	λ_{max} Q-band (nm)	Φ_f Q-band
ZnTPP **2.4**	599, 647	0.033
a=1 model **3.1**	612, 662	0.045
a=2 model **3.2**	607, 666	0.052
a=2 model **3.3**	608, 669	0.061
a=1 polymer **3.4**	674	0.017
a=2 polymer **3.5**	676	0.016
a=3 polymer **3.6**	614, 672	0.017

The model compounds **3.1 – 3.3** have emission maxima with Stokes shifts of approximately 50 nm for the emission from the Q(1,0) vibronic peak which are similar to ZnTPP **2.4** and those previously reported for analogous compounds.[10] The magnitude of the shifts in emission maxima for all compounds **3.1 – 3.6** with respect to ZnTPP **2.4** are essentially proportional to the shifts in their respective absorption maxima with respect to ZnTPP **2.4**. The trend of increasing fluorescence quantum yield with increasing number of *p*-PV units at the β-conjugated substituent observed for the monomer series is also consistent with the literature.[10] Bathochromic shifting of emission maxima in the pendant polymers **3.4 – 3.6** is likely due to the majority emission of photons from energy states lower than the lowest energy vibrational state of S_1 of an independent monomeric chromophore, brought about by orbital mixing of chromophores in a variety of structural conformations in the local pendant chromophore environment.

The polymers **3.4 – 3.6** exhibit a significant reduction in fluorescence quantum yields in comparison to their monomeric analogues, suggesting that there is significant competition by non-radiative relaxation mechanisms due to inter-pendant orbital interactions brought about by the proximity of the pendant chromophores. The relative degree of fluorescence quantum yield reduction with respect to their parent monomeric compounds in the polymer series **3.4 – 3.6** (28 – 37% quantum yield reduction) is similar to those pendant *meso*-phenyl substituted porphyrin

polymers reported by Wang *et al.* with a short linking group (24% quantum yield reduction).[17] The S_1 fluorescence quantum yields of **3.4 – 3.6** (0.016 – 0.017) are greater than that of those pendant porphyrin polymers reported by Fujitsuka *et al.* (0.0058 – 0.0080),[34] suggesting that the inter-pendant electronic communication is greater between pendants in the polymers studied by Fujitsuka *et al.* even though the conjugation is extended further in the pendant units of **3.4 – 3.6**. This is likely due however to the fact that the pendant units in the polymers studied by Fujitsuka *et al.* are more closely electronically associated with one another than for the pendants in polymers **3.4 – 3.6** as a result of the restriction of conformational freedom in the helical polyisocyanide backbone, indicated by hypsochromic shifts of up to 14 nm in the Soret band maxima with respect to the monomeric pendant unit (compared to approximately 2 nm for polymers **3.4 – 3.6**).

In contrast to the monomeric porphyrins **3.1 – 3.3**, the fluorescence quantum yield of the pendant polymers **3.4 – 3.6** exhibited almost no overall change upon extension of the conjugation of the porphyrin core by addition of *p*-PV units to the β-position, however a slight increase in the intensity of the Q(0,0) band emission from the polymers was observed. The contribution of the small increase in Q(0,0) emission intensity in the polymer series **3.4 – 3.6** with increasing number of *p*-PV units is not large enough to significantly change the overall fluorescence intensity from the polymers, as there is a large relative contribution to the emission profile from wavelengths lower than the Q(0,0) emission maxima, which itself is almost identical in shape and intensity regardless of *p*-PV unit length within the series **3.4 – 3.6**.

3.7 Triplet Transient Absorption Spectroscopy

All solutions used in the transient absorption analysis were prepared in spectroscopic grade toluene and degassed thoroughly prior to measurements. Solutions of porphyrin were prepared to have the same OD (0.02) at the desired excitation wavelength (532 nm) so that the concentration of the singlet excited state upon excitation would be similar across all samples. The excitation pulse energy used for all triplet transient absorption spectra in section **3.6** was 8.2 mJ. A gate delay time of 200 ns was set in order to capture the absorption spectrum of the triplet state

porphyrins while the population of triplets was still relatively high, and such that the delay comfortably exceeded the time scale in which excitation scatter would be observed in the transient absorption spectrum. The triplet transient absorption spectra for the model and polymer compounds **3.1 – 3.6** are shown in Figure 3.24 below. Triplet absorption maxima for the spectra in Figure 3.24 and their peak ΔOD values are listed in Table 3.4.

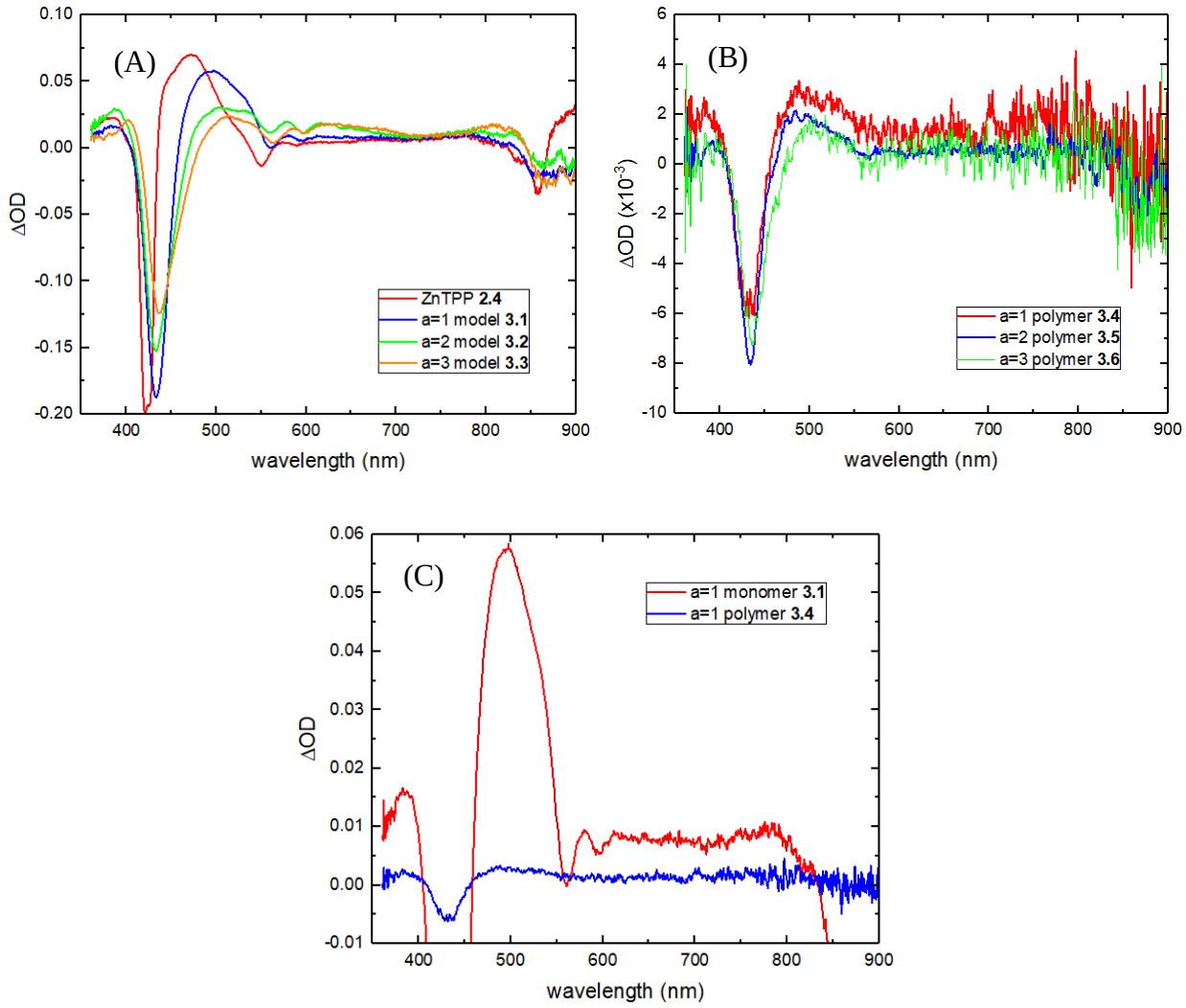

Figure 3.24: (A) Triplet transient absorption spectra of ZnTPP **2.4** and the model compounds **3.1 – 3.3** in toluene. (B) Triplet transient absorption spectra of pendant polymers **3.1 – 3.3** in toluene. (C) Triplet transient absorption spectra in toluene of the model compound **3.1** and polymer **3.4** containing one *p*-PV unit at the β-position, overlaid for comparison.

Table 3.4: Triplet absorption parameters for ZnTPP **2.4**, the model compounds **3.1 – 3.3** and the polymers **3.4 – 3.6** in degassed toluene.

Compound	λ_{max} (nm)	ΔOD λ_{max} (x10^{-2})
ZnTPP **2.4**	471	7.01
a=1 model **3.1**	497	5.76
a=2 model **3.2**	502	3.04
a=2 model **3.3**	514	2.34
a=1 polymer **3.4**	488	0.33
a=2 polymer **3.5**	485	0.22
a=3 polymer **3.6**	505	0.20

The transient absorption spectra of compounds **3.1 – 3.6** in Figure 3.24 all display a large trough between 420 – 440 nm due to ground state bleaching in the Soret band absorption region. Broad peaks due to the T_1-T_s excited state electronic transition appear in the spectra in Figure 3.24 with maxima between 470 – 520 nm. Although the ΔOD intensity of the triplet absorption spectra in Figure 3.24 do not necessarily reflect the true triplet molar extinction coefficients of the compounds **3.1 – 3.6**, they provide a qualitative estimate of the relative triplet populations at the delay time after excitation of the samples and thus a parameter for determining if excited state quenching or non-radiative relaxation is occurring in the compounds. The trend of bathochromic shifting of triplet absorption maxima and reduction in ΔOD values at the triplet absorption maxima, upon addition of *p*-PV units at the β-position, is consistent with the triplet absorption spectra obtained by Ventura *et al.* for analogous β-oligo-p-PV substituted zinc porphyrins.[10] A similar trend is was observed by Rogers *et al.* when conjugation of the macrocycle is increased by subsequent iterations of benzo-annulation at the β-pyrrolic positions.[35] Rogers *et al.* have calculated that the measured reduction in the rate of ISC from the singlet to the triplet state is due to greater mismatch of the S_1 energy level with any of the triplet state energies T_1 to T_4 upon extension of the porphyrin macrocycle conjugation via annulation. The reduction in the rate of ISC upon conjugation extension likely contributes to decreased triplet populations, which may

explain the reduction in ΔOD intensity with increased conjugation observed for the compounds studied by Officer *et al.*, Rogers *et al.* and in this chapter.

The ΔOD values at the triplet absorption maxima of the pendant polymers **3.4 – 3.6** are significantly lower than those for their respective monomeric analogues **3.1 – 3.3**. Fujitsuka *et al.* have shown that the ISC quantum yields decrease 5 – 10 fold for pendant zinc porphyrin polymers compared to their monomeric analogues, with a corresponding relative reduction in ΔOD in their respective triplet absorption spectra.[34] The fact that both the S_1 fluorescence quantum yields and the ΔOD values in the triplet absorption spectra decrease in polymers **3.4 – 3.6** compared to model compounds **3.1 – 3.3** suggest that reduced ISC quantum yields such as those calculated by Fujitsuka *et al.* are likely in the polymers. If this is not the case, then the reduction in ΔOD values in Table 3.4 implies there is rapid quenching of triplet excitons after ISC occurs in the polymers, however, such a triplet exciton quenching mechanism may still be active regardless of the ISC quantum yield. The polymer **3.4** with one *p*-PV unit (a=1) at the β-position has a ΔOD value of approximately $1/17^{th}$ of its monomeric analogue **3.1** (Figure 3.24 (C)). Considering the magnitude of the reduction in ΔOD between **3.1** and **3.4**, it is likely both reduced ISC quantum yield and triplet exciton quenching are occurring in the polymer pendant units, which are accelerated by increased inter-pendant orbital interactions due to the extended conjugation of the porphyrin core upon incorporation of the β-oligo-*p*-PV substituent.

3.8 Conclusion

A series of pendant zinc porphyrin polymers with β-oligo-*p*-PV backbone-to-pendant linking groups, along with their monomeric analogues, were synthesized in order to investigate effects of extending the conjugation of the porphyrin core on inter-pendant interactions that may alter the photophysical properties of the polymers. The pendant polymers were synthesized by performing post-polymerization functionalization on a polymer backbone previously synthesized using RAFT polymerization. Broadening of ^{1}H NMR signals and UV-visible absorption peaks of the polymers provided evidence for effective inclusion of the zinc porphyrin pendant units into the polymeric structure.

An overall increase in the net Q-band extinction coefficient was observed in both the monomeric compounds and the polymers with increasing number of *p*-PV units as expected, with a reduction in extinction coefficient being observed upon inclusion of the porphyrin units into the pendant structure. The lack of excitonic splitting in the absorption spectra of the polymers **3.4 – 3.6** may be promising for the design of polymers with pendant dual-absorber upconverter units with extended π-conjugation, however the broad Soret absorption of the extended conjugation porphyrins studied in this chapter that extend into the Q-band, may accelerate IC from S_2 to S_1 thus quenching the product S_2 state of a homo-TTA event.

The S_1 fluorescence quantum yields of the polymers decreased compared to the monomer model compounds, indicating enhanced non-radiative relaxation to the ground state in the polymers due to electronic interaction with neighbouring pendant chromophores. The quantum yields of the polymers remained relatively similar regardless of the *p*-PV length of the linker group. The reduction in the exciton population due to efficient IC in the polymer series with the respect to the monomeric compounds is likely to substantially reduce the ISC quantum yield of the pendant polymers, thus restricting their viability as absorber compounds for use in TTA-UC applications. Further studies are required to elucidate the photophysical properties of the S_2 excited state of both the model compounds and polymers.

The T_1-T_s triplet absorption was almost completely suppressed for the polymers in comparison to their monomeric analogues, further suggesting ineffective conversion of singlet excitons to triplet excitons and possible quenching of triplet excitons in the polymers due to enhanced interaction with pendant chromophores in the local environment brought about by the extended π-conjugation system of the pendant units. The low triplet population observed for the polymers likely renders them poor dual absorber-upconverters for use in homo-TTA systems.

3.9 References

(1) Wang, R.; Gao, B.; Jiao, W.; Yu, L.; Pan, W. *J. Appl. Polym. Sci.* **2014,** *131* (15), 40516.

(2) Tilley, A. J.; Robotham, B. E.; Steer, R. P.; Ghiggino, K. P. *Chem. Phys. Lett.* **2015,** *618*, 198.

(3) Singh-Rachford, T. N.; Castellano, F. N. *J. Phys. Chem. Lett.* **2010,** *1*, 195.

(4) Schulze, T. F.; Czolk, J.; Cheng, Y.-Y.; Fückel, B.; MacQueen, R. W.; Khoury, T.; Crossley, M. J.; Stannowski, B.; Lips, K.; Lemmer, U.et al. *J. Phys. Chem. C* **2012,** *116*, 22794−22801.

(5) Nattestad, A.; Cheng, Y.-Y.; MacQueen, R. W.; Schulze, T. F.; Thompson, F. W.; Mozer, A. J.; Fückel, B.; Khoury, T.; Crossley, M. J.; Lips, K.et al. *J. Phys. Chem. Lett.* **2013,** *4*, 2073−2078.

(6) Ventura, B.; Barigelletti, F.; Lodato, F.; Officer, D. L.; Flamigni, L. *Phys. Chem. Chem. Phys.* **2009,** *11*, 2166.

(7) Belcher, W. J.; Burrell, A. K.; Officer, D. L.; Reid, D. C. W.; Scott, S. M. *J. Porphyrins Phthalocyanines* **2002,** *6*, 720.

(8) Mitchell, R.; Wagner, K.; Barnsley, J. E.; van der Salm, H.; Gordon, K. C.; Officer, D. L.; Wagner, P. *Eur. J. Org. Chem.* **2017**, 5750.

(9) Wang, Q.; Campbell, W. M.; Bonfantani, E. E.; Jolley, K. W.; Officer, D. L.; Walsh, P. J.; Gordon, K.; Humphry-Baker, R.; Nazeeruddin, M. K.; Grätzel, M. *J. Phys. Chem. B* **2005,** *109*, 15397.

(10) Ventura, B.; Flamigni, L.; Marconi, G.; Lodato, F.; Officer, D. L. *New J. Chem.* **2008,** *32*, 166.

(11) Ando, K. *J. Org. Chem.* **1999,** *64*, 6815.

(12) Tilley, A. J.; Danczak, S. M.; Browne, C.; Young, T.; Tan, T.; Ghiggino, K. P.; Smith, T. A.; White, J. *J. Org. Chem.* **2011,** *76*, 3372.

(13) Norris, B. N.; Zhang, S.; Campbell, C. M.; Auletta, J. T.; Calvo-Marzal, P.; Hutchison, G. R.; Meyer, T. Y. *Macromolecules* **2013,** *46*, 1384−1392.

(14) Page, Z. A.; Liu, Y.; Puodziukynaite, E.; Russell, T. P.; Emrick, T. *Macromolecules* **2016,** *49*, 2526−2532.

(15) Nitti, A.; Debattista, F.; Abbondanza, L.; Bianchi, G.; Po, R.; Pasini, D. *J. Polym. Sci. Pol. Chem.* **2017,** *55*, 1601.

(16) García-Martínez, J. C.; Díez-Barra, E.; Rodríguez-López, J. *Tetrahedron Lett.* **2012,** *53*, 2752.

(17) Wang, H.-W.; Liu, Z.-C.; Chen, C.-H.; Lim, T.-S.; Fann, W.; Chao, C.-G.; Yu, J.-Y.; Lee, S.-L.; Chen, C.-H.; Huang, S.-L.et al. *Chem. Eur. J.* **2009,** *15*, 5719

(18) Lin, N.-T.; Satyanarayana, K.; Chen, C.-H.; Tsai, Y.-F.; Yu, S. S.-F.; Chan, S. I.; Luh, T.-Y. *Macromolecules* **2014,** *47*, 6166−6172.

(19) Takei, F.; Nakamura, S.; Onitsuka, K.; Ishida, A.; Tojo, S.; Majima, T.; Takahashi, S. *Chem. Lett.* **2003,** *32* (6), 506.

(20) Kajiwara, A.; Aramata, K.; Kamachi, M.; Sumi, K. *Polym. J.* **1994,** *26* (2), 215.

(21) Bevington, J. C.; Brener, S. W.; Huckerby, T. N. *Macromolecules* **1989,** *22*, 55.

(22) Tilley, A. J.; Chen, M.; Danczak, S. M.; Ghiggino, K. P.; White, J. M. *Polym. Chem.* **2012,** *3*, 892.

(23) Wuyts, C.; Dermaut, W.; Hoefnagels, R.; Aerts, G.; Goovaerts, E.; Geise, H. J. *Polym. Int.* **2003,** *52*, 1660.

(24) Belfield, K. D.; Wang, J. *J. Polym. Sci. Pol. Chem.* **1995,** *33*, 1235.

(25) Bonfantini, E. E.; Burrell, A. K.; Gosper, J. J.; Campbell, W. M.; Harding, M. M.; Officer, D. L.; Crossley, M. J.; Reid, D. C. W. *J. Porphyrins Phthalocyanines* **2002,** *6*, 708.

(26) Momenteau, M.; Loock, B.; Bisagni, E.; Rougee, M. *Can. J. Chem.* **1979,** *57*, 1804.

(27) Ponomarev, G. V.; Maravin, B. *Khim. Geterotsikl. Soedin.* **1982**, 59.

(28) Henrick, K.; Owston, P. G.; Peters, R.; Tasker, P. A.; Dell, A. *Inorg. Chim. Acta.* **1980,** *45*, L161.

(29) Bonfantini, E. E.; Burrell, A. K.; Officer, D. L.; Reid, D. C. W.; McDonald, M. R.; Cocks, P. A.; Gordon, K. C. *Inorg. Chem.* **1997,** *36*, 6270.

(30) Farinha, J. P. S.; Relógio, P.; Charreyre, M.-T.; Prazeres, T. J. V.; Martinho, J. M. G. *Macromolecules* **2007,** *40*, 4680.

(31) Moad, G.; Rizzardo, E.; Thang, S. H. *Polym. Int.* **2011,** *60*, 9.

(32) Willcock, H.; O'Reilly, R. K. *Polym. Chem.* **2010,** *1*, 149.

(33) Strachan, J.-P.; Gentemann, S.; Seth, J.; Kalsbeck, W. A.; Lindsey, J. S.; Holten, D.; Bocian, D. F. *J. Am. Chem. Soc.* **1997,** *119*, 11191.

(34) Fujitsuka, M.; Okada, A.; Tojo, S.; Takei, F.; Onitsuka, K.; Takahashi, S.; Majima, T. *J. Phys. Chem. B* **2004,** *108,* 11935.

(35) Rogers, J. E.; Nguyen, K. A.; Hufnagle, D. C.; McLean, D. G.; Su, W.; Gossett, K. M.; Burke, A. R.; Vinogradov, S. A.; Pachter, R.; Fleitz, P. A. *J. Phys. Chem. A* **2003,** *107,* 11331.

Chapter 4

Synthesis and Exciton Dynamics of Stilbene and Benzyl Ether-Linked Pendant Porphyrin Polymers

4.1 Introduction

Development of photovoltaic devices that integrate non-coherent photon upconversion systems employing triplet-triplet annihilation mechanisms (NCPU-TTA) is currently one of the leading areas of research directed towards improving solar energy harvesting efficiencies. Optimization of NCPU-TTA in both solution and solid state media requires an in-depth understanding of the dynamic character of excitons intended to participate in TTA over the course of their lifetimes. The behavior and excited state decay processes that excitons in TTA systems are subject to are highly dependent on the electronic environment of the chromophores at all stages of the TTA process. As discussed in the Introduction chapter section 1.8.2 and chapter 3 section 3.1, control over the relative chromophore electronic environment can be achieved by introducing chromophores as pendant units linked to a polymer backbone. For homomolecular TTA systems such as those based on zinc metalloporphyin dual absorber-upconverter chromophores, the close proximity of porphyrins in a pendant polymer structure may increase orbital overlap leading to improved Dexter electron exchange, thus facilitating effective NCPU-TTA.

Drawbacks of including dual absorber-upconverter chromophores into a pendant polymer structure may however override the benefits of increased Dexter electron exchange between pendant units. As discussed in the Introduction chapter section 1.7.1, the high local chromophore concentrations that may be simulated in pendant chromophore environments could potentially cause inter-pendant excimer formation[1,2] or enhanced internal conversion,[3] lowering the ISC and therefore decreasing the triplet population available for TTA. As outlined in the introduction chapter 1.7.2, triplet excitons formed in pendant chromophore polymer systems may be subject to quenching by formation of intramolecular triplet excimers[4,5] or energy trapping,[4,5] which both shunt triplet exciton migration and lowers the energy levels of the triplet states such that formation of the upconverted TTA product states becomes unlikely. It is therefore highly desirable to be able to link structural and environmental modifications in TTA systems to excited state decay processes through mechanistic models, in order to implement rational synthetic design of TTA dual absorber-upconverters in future studies. Thorough investigation of the excited state decay behavior at all stages of exciton lifetimes would allow for identification of process that could impede effective TTA.

The nature of the backbone-to-pendant linking group, in particular the linker length and flexibility, can influence inter-pendant electronic interactions and thus introduce variation in the photophysical properties of the pendant polymers. Wang *et al.* have demonstrated that pendant porphyrins linked to the polymer backbone with aliphatic chains, have greater extinction coefficients and larger fluorescence quantum yields compared to those pendants fused to the backbone with no aliphatic linker, indicating reduced intramolecular aggregation or electronic coupling in the pendant porphyrins that have greater conformational freedom and spatial separation due to the aliphatic linker groups (Figure 4.1).[6] Wuyts *et al.* have observed that the efficiency of energy transfer from polymers with pendant stilbene chromophore units to an energy acceptor material in thin film blends varies when the backbone-to-pendant linking group changed from a flexible ether linking group to a direct rigid single bond from the backbone to the stilbene unit ie. no linking group.[7] In pendant polymer-related multi-chromophoric systems such as porphyrin dendrimers, the efficiency of dynamic exciton decay processes such as singlet-

singlet annihilation have exhibited significant increases when the aliphatic dendrimer linking chains increased by just one methylene unit.[8]

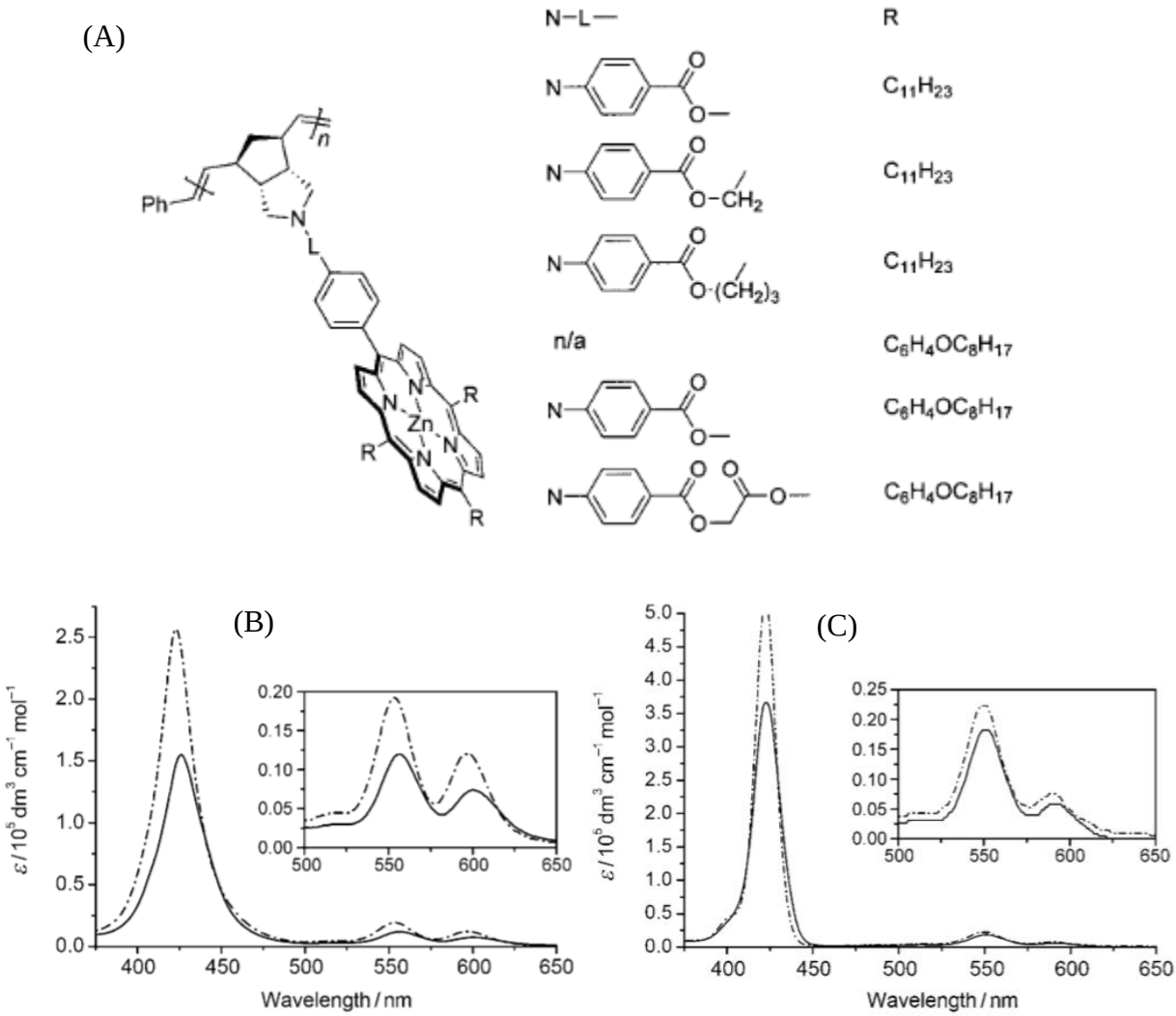

Figure 4.1: (A) Pendant porphyrin polymers synthesized by Wang et al. using ROMP techniques, with the various linking groups employed shown at the top right. Absorption spectra at known concentrations of the monomeric unit (dotted line) and polymer (solid line) of the pendant porphyrin polymer compounds with no flexible linker group (B) and a flexible linking group of extended length (C). Figures reproduced from Wang et al.[6]

The work presented in this chapter was part of a collaboration with the research group of Professor Ronald P. Steer, University of Saskatchewan, Canada, and resulted in a joint publication entitled "Exciton Dynamics of Photoexcited Pendant Porphyrin Polymers in Solution and Thin Flims".[9] The objective of the work presented in this chapter was to explore structure-property relationships between excited state decay processes and proximity of zinc porphyrin chromophores in pendant polymers and evaluate the viability of employing pendant zinc porphyrin polymers as TTA-mediated dual absorber-upconverters. To this end, a series of porphyrin-appended polymers were synthesized and characterized along with their monomeric analogues. The backbone-to-pendant linking group was varied in order to investigate possible changes in photophysical characteristics of the polymers due to the nature of the linking group.

The effect of the degree of rotation-induced conjugation that may lead to photophysical properties similar to those outlined in chapter 3 was studied by incorporating chromophoric stilbene linkers. Outside of the electronic association of the stilbene and porphyrin via rotation-induced conjugation, the stilbene linkers were expected not to introduce significant energy transfer from the porphyrin to the stilbene as the spectral overlap between the stilbene fluorescence[10] and zinc porphyrin absorption[11] is minimal. Electron transfer from oligo-*para*-phenylenevinylene (oligo-*p*-PV) chromophores covalently linked to porphyrins at the β-position has however been observed previously by Davis *et al.*[12] The oligo-*p*-PV-to-porphyrin electron transfer observed by Davis *et al.* was shown to be sensitive to the degree of rotation of the plane of the oligo-*p*-PV substituent with respect to the porphyrin π-conjugated plane. The observation of electron and energy transfer between zinc porphyrins and covalently linked chromophores has been of frequent interest in previous literature studies[12-15] and therefore it may be of interest in the future to create pendant porphyrin polymer systems that incorporate chromophores as backbone-to-pendant linking groups for dynamic energy transfer applications. Although no linker-to-porphyrin energy transfer studies were investigated in this chapter, the photophysical effects introduced into the zinc porphyrin by covalently linking independent chromophores at the β-position may provide useful considerations when designing complex porphyrin-based energy transfer systems.

In contrast to the compounds studied in chapter 3, the linking groups were predicted to have a lesser effect on the electronic states of the zinc porphyrin moieties and were predicted to participate in a lesser degree of inter-pendant aggregation or electronic interaction. Time-resolved analysis of singlet and triplet exciton dynamics of the compounds studied in this chapter was performed using fluorescence decay and triplet transient absorption decay techniques. Experiments were conducted in order to assess the viability of the pendant porphyrin polymers to be used as dual absorber-upconverters for producing intramolecular homo-NCPU-TTA fluorescence. The target polymers and model compounds studied in this chapter are shown below in Figure 4.2.

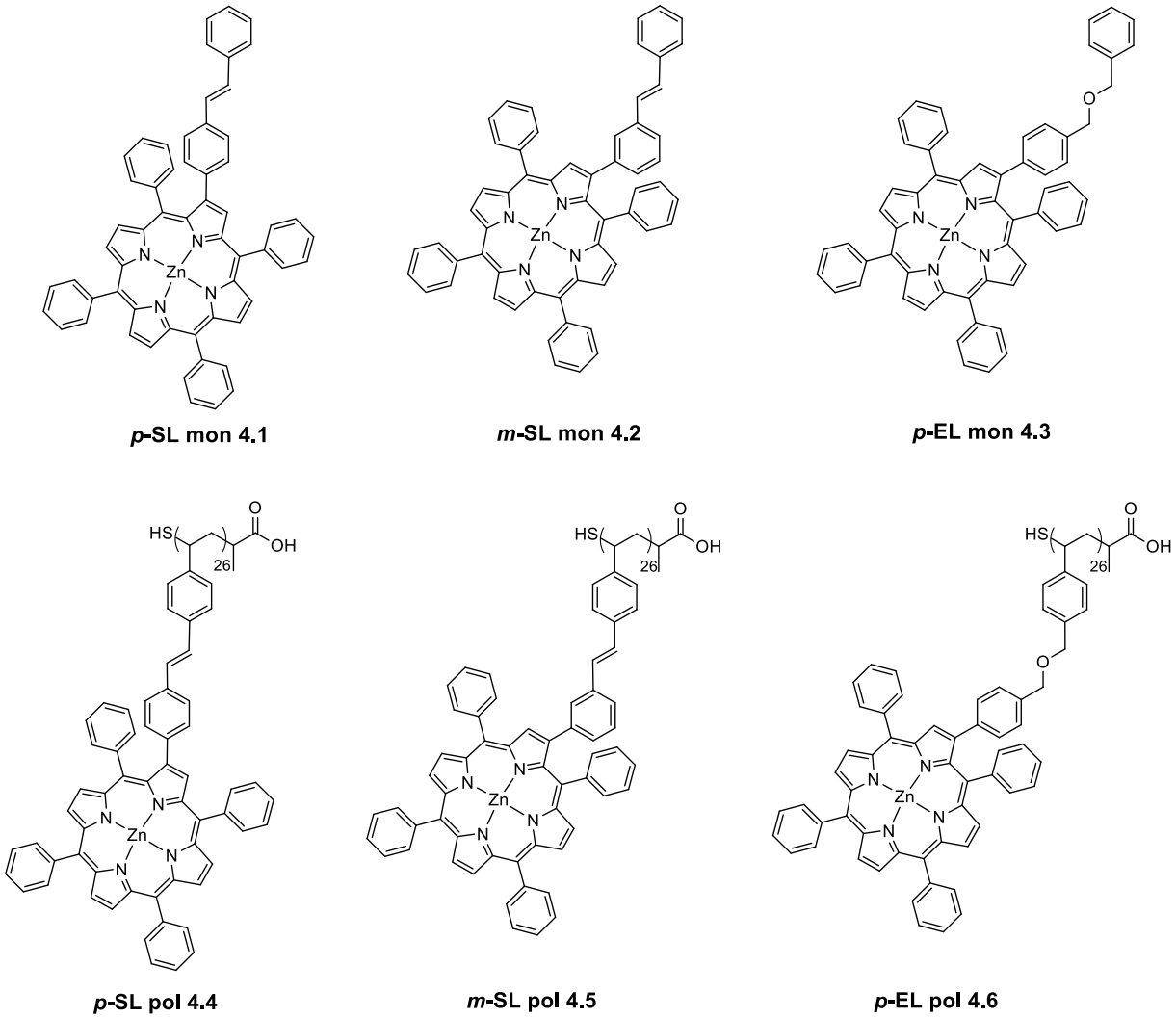

Figure 4.2: Pendant porphyrin polymers **4.4 – 4.6** and monomeric model compounds **4.1 – 4.3** studied in chapter 4.

4.2 Synthetic Outline and Design

Relatively inert pendant-to-backbone linking groups can be introduced either at the meso- or β-positions of the porphyrin core structure. Introduction of a functional meso-aryl substituent at the porphyrin ring formation step has been predominantly used for creating the monomer pendant-to-backbone linking group in previously synthesized pendant porphyrin polymers.[3,6,16] Obtaining porphyrins with one meso-aryl substituent that differs from the other three typically proceeds by a one-pot synthesis of a statistical distribution of porphyrins based on the reagent ratios, yielding 0-4 meso-substituents of identical nature on the porphyrin core. Tedious separation of these porphyrins is required to obtain the target porphyrin with one meso-substituent that differs from three other identical meso-substituents, in very low yields (<10%).[6,17,18] β-Functionalization of a tetraphenylporphyrin precursor was chosen as the methodology for introducing a pendant-to-backbone linking moiety for the target compounds in this chapter as the porphyrin ring formation step was predicted to be far more straight forward and easier to purify for large scale syntheses. β-Functionalization of porphyrins can be achieved by simple aromatic reactions such as Vilsmeier-Haack formylation[19] (employed in Chapter 3 and by Ventura *et al.*[20] for synthesis of extended conjugation linkers), copper(I)-catalysed nitration,[21] and bromination with N-bromosuccinimide (NBS).[22,23]

The methods of introducing rigid and flexible linking groups in pendant polymer structures were closely influenced by the following post-polymerisation techniques outlined in the work of Wuyts *et al.*[7] In the work of Wuyts *et al.*, the rigidly linked pendant stilbene units were directly covalently bound to the polymer backbone by the aromatic positions *para* to the vinyl moiety of the stilbene, and were formed by Horner-Wadsworth-Emmons olefination reactions similar to those implemented in the synthesis of the monomers and polymers outlined in Chapter 3. Wuyts *et al.* introduced flexible linking groups by nucleophilic substitution of a poly(vinylbenzylchloride)backbone with a hydroxyl-functionalised derivative of a stilbene chromophore to form benzyl ether linkages.

An additional polymer linker group that was covalently bound to the porphyrin core at the *meta*-position of the stilbene-adjoining β-phenyl substituent was designed. The meta-linked stilbene unit was expected to contribute minimally to the conjugation extension of the porphyrin macrocycle regardless of the degree of rotation-induced co-planarity of the β-stilbene group, as *meta*-linkages disrupt the conjugation of extended π-systems. *Meta*-linkages have been previously exploited for the segmentation of chromophore π-conjugated systems such as those observed in *meta*-linked spirobifluorene polymers.[24] Additionally, a decrease in the extent of face-to-face π-stacking interactions has previously been observed in chromophores incorporating *meta*-linkages.[25] Introducing *meta*-linkages into the β-stilbene unit may therefore potentially inhibit intramolecular aggregation of the stilbene-linked pendant porphyrin chromophores when the stilbene units are in close proximity within the pendant polymer molecular architectures. The synthetic pathway for the compounds studied in this chapter is outlined in Figure 4.3.

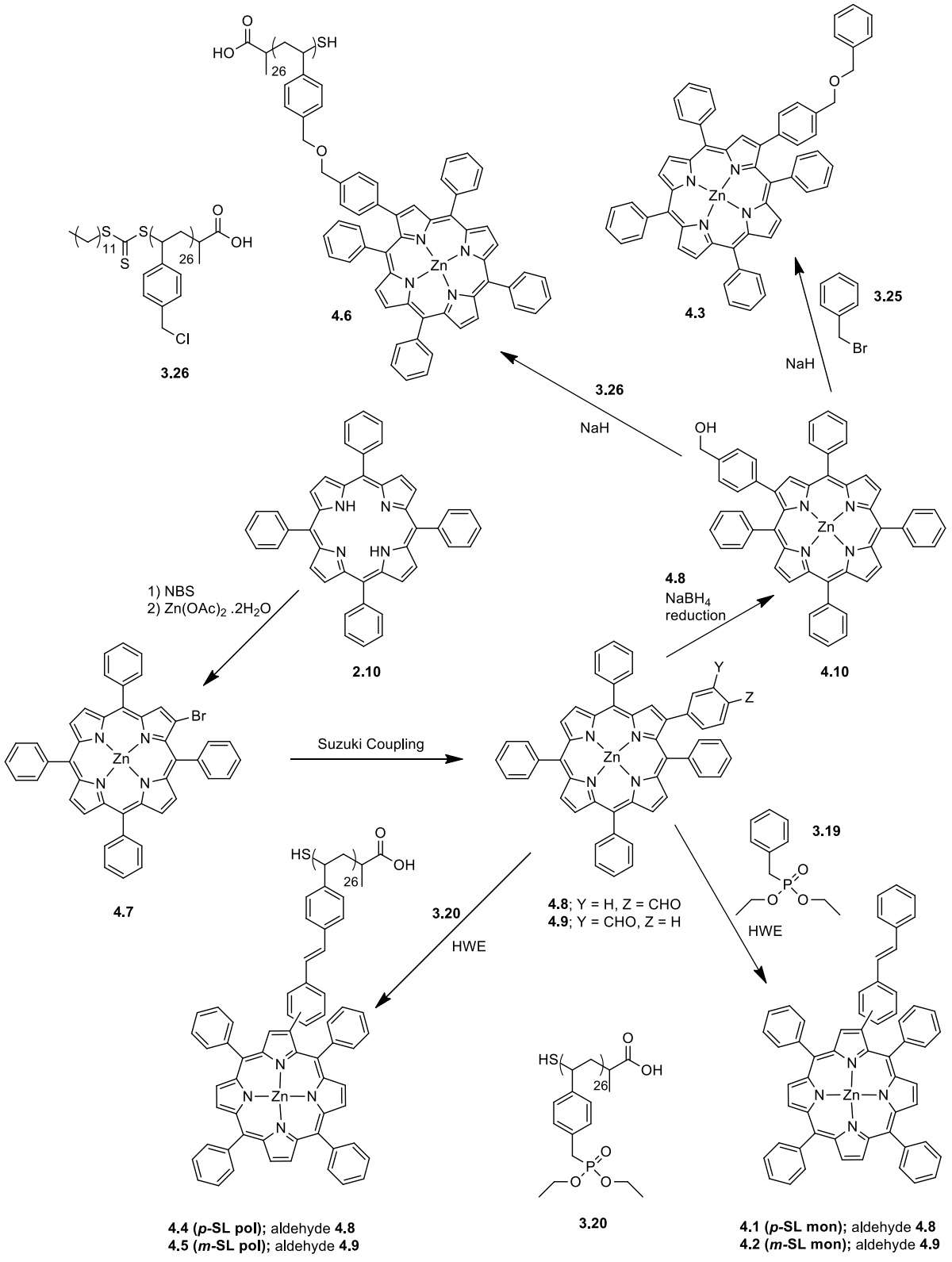

Figure 4.3: Proposed synthesis of pendant polymers **4.4 – 4.6** and monomeric model compounds **4.1 – 4.3**.

4.3 Synthesis

4.3.1 Functionalization of porphyrin macrocycle

The synthesis of the TPP **2.10** starting material was described previously in Chapter 2 section 2.3. Functionalization of the β-position of TPP **2.10** was achieved via bromination using NBS as the brominating agent. The bromination of tetraphenylporphyrin derivatives with NBS is known to give distributions of porphyrins with varying degrees of bromination, to which the degree of bromination depends on the number of equivalents of NBS, solvent, duration of reaction and addition method of the NBS.[22,23] The most effective method for obtaining predominantly mono-bromo substituted free-base tetraphenylporphyrin involves drop-wise addition of the NBS in $CHCl_3$ solution to a refluxing solution of 5,10,15,20-tetraphenylporphyin in $CHCl_3$ containing 1-2% pyridine.[22] Initially 2-bromo-5,10,15,20-tetraphenylporphyin **4.11** was isolated from this synthetic step using gravity-assisted silica gel column chromatography to give a yield of 42% (Figure 4.4).

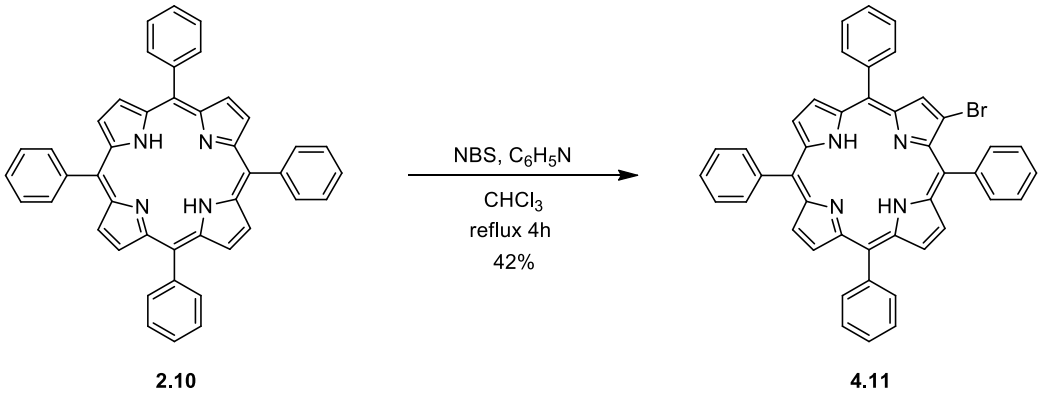

2.10 **4.11**

Figure 4.4: Synthesis of 2-bromo-tetraphenylporphyrin **4.11**.

The chromatographic separation of the mono-bromo derivative from the di-bromo derivative proved to be tedious and time-costly to perform on large-scale batches, and a significant portion of the mono-brominated porphyrin was lost or needed further purification to recover due to overlap/co-elution of part of the mono- and di-bromo bands with each other, even under strict eluent solubility gradient control and using gravity-assisted elution methods to slow the elution rate of the mono- and di-bromo-TPP bands. Due to the aforementioned purification difficulties, a different approach to the synthesis of the formylphenyl-substituted zinc porphyrin intermediates

4.8 and **4.9** was pursued, whereby the separation of the multi-functionalized derivatives would potentially be easily performed once the Suzuki coupling to introduce aldehyde groups to the brominated positions had been achieved hence increasing the solubility of the porphyrin derivatives and the increasing the relative polarity difference between the multi-functionalized porphyrin derivatives. Following the optimized route towards the synthesis of the formylphenyl-substituted zinc porphyrin intermediates **4.8** and **4.9** outlined in Figure 4.6, TPP **2.10** was first brominated at the β- position using NBS (Figure 4.6). Bromination of the porphyrin was confirmed by the abundant peaks in the high-resolution mass spectrum of the crude material at 695.1640 and 773.0729 m/z corresponding to the $[M+H]^+$ pseudo-molecular ions of the mono- and di- substituted derivatives (Figure 4.5). The mass spectrum (Figure 4.5) indicated that the predominant components of the crude mixture of brominated TPP derivatives were TPP molecules with 0, 1, or 2 bromine substituents, with the mono-bromo-TPP most abundant, as desired for further synthetic transformation. The $[M+H]^+$ ions of the multi-brominated species in Figure 5 exhibited the characteristic isotope patterns consistent with inclusion of bromine into the molecular ion structure. The crude mixture of porphyrins with various degrees of bromination was then metalated with a 5 fold excess of zinc(II) acetate dihydrate (Figure 4.6). Efficient chelation of the inner ring nitrogens of zinc(II) was confirmed by the ^{1}H NMR spectrum of the crude mixture of the zinc metalated brominated TPP derivatives, as complete disappearance of the peaks that appear between -2.6 and -3.0 ppm in the ^{1}H NMR spectrum of the free-base brominated TPP mixture was observed, corresponding to the loss of the inner ring N-H protons of the free-base porphyrin upon coordination to zinc.

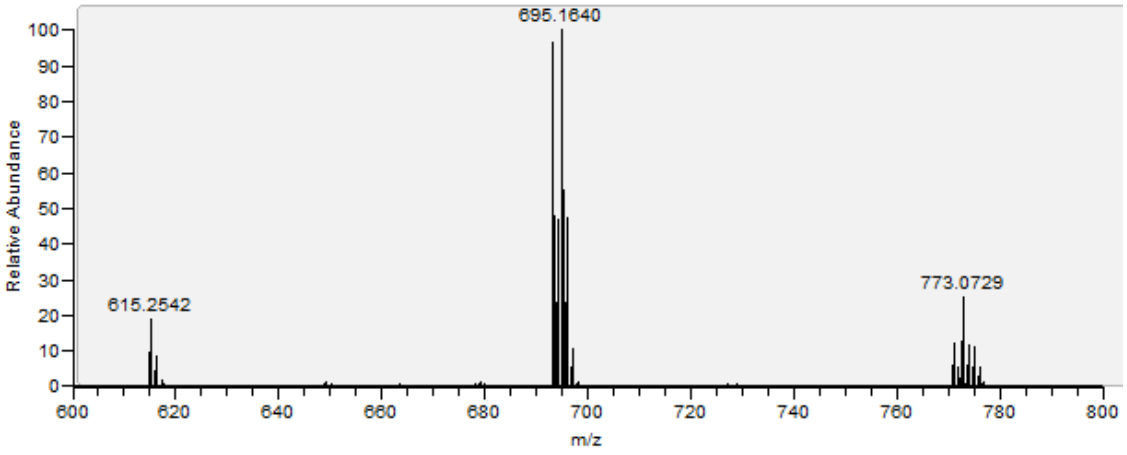

Figure 4.5: Mass spectrum (ESI+ mode) of the mixture of brominated TPP derivatives of **4.11**.

In order to obtain the desired aldehydes **4.8** and **4.9**, palladium-catalysed cross-coupling (Suzuki coupling) of aldehyde-substituted phenylboronic acid derivatives with the zinc metalated mixture of brominated porphyrin derivatives was then performed in a mixture of THF and 2M aqueous saturated Na_2CO_3, using $Pd(PPh_3)_4$ as the palladium catalyst, in accordance with a literature procedure adapted from the Suzuki coupling of mono-brominated porphyrins.[26] Reaction of 4-formylphenylboronic acid pinacol ester with the zinc metalated mixture of brominated porphyrin derivatives gave [2-(4-formylphenyl)-5,10,15,20-tetraphenylporphyrinato] zinc(II) **4.8** in 45% yield over 3 steps upon separation of the product mixture using silica gel column chromatography (Figure 4.6). As predicted, the chromatographic separation of the crude mixture of compounds with varied β-functionality proved to be much more straightforward than the isolation of the mono-bromo-TPP from the mixture of multi-brominated free-base TPP derivatives.

A repeat iteration of the synthesis of the zinc metalated mixture of brominated porphyrin derivatives was carried out, to be used in the formation of **4.9**. To this end, reaction of 3-formylphenylboronic acid with the second batch of zinc metalated brominated porphyrin derivatives gave [2-(3-formylphenyl)-5,10,15,20-tetraphenylporphyrinato] zinc(II) **4.9** in 52% yield over 3 steps upon separation of the product mixture using silica gel column chromatography (Figure 4.6). Evidence for the formation of **4.8** and **4.9** is present through identification of their molecular ion peaks in their mass spectra. For both **4.8** and **4.9**, $[M+H]^+$ requires m/z = 781.1946, while m/z = 781.1917 and m/z = 781.1937 were observed for **4.8** and **4.9** respectively in their mass spectra. Additionally, the most abundant peaks corresponding to the $[M+H]^+$ ions of **4.8** and **4.9** were both located in clusters of peaks that resemble the isotope pattern of zinc, which is consistent with the metalated porphyrin structure of **4.8** and **4.9**.

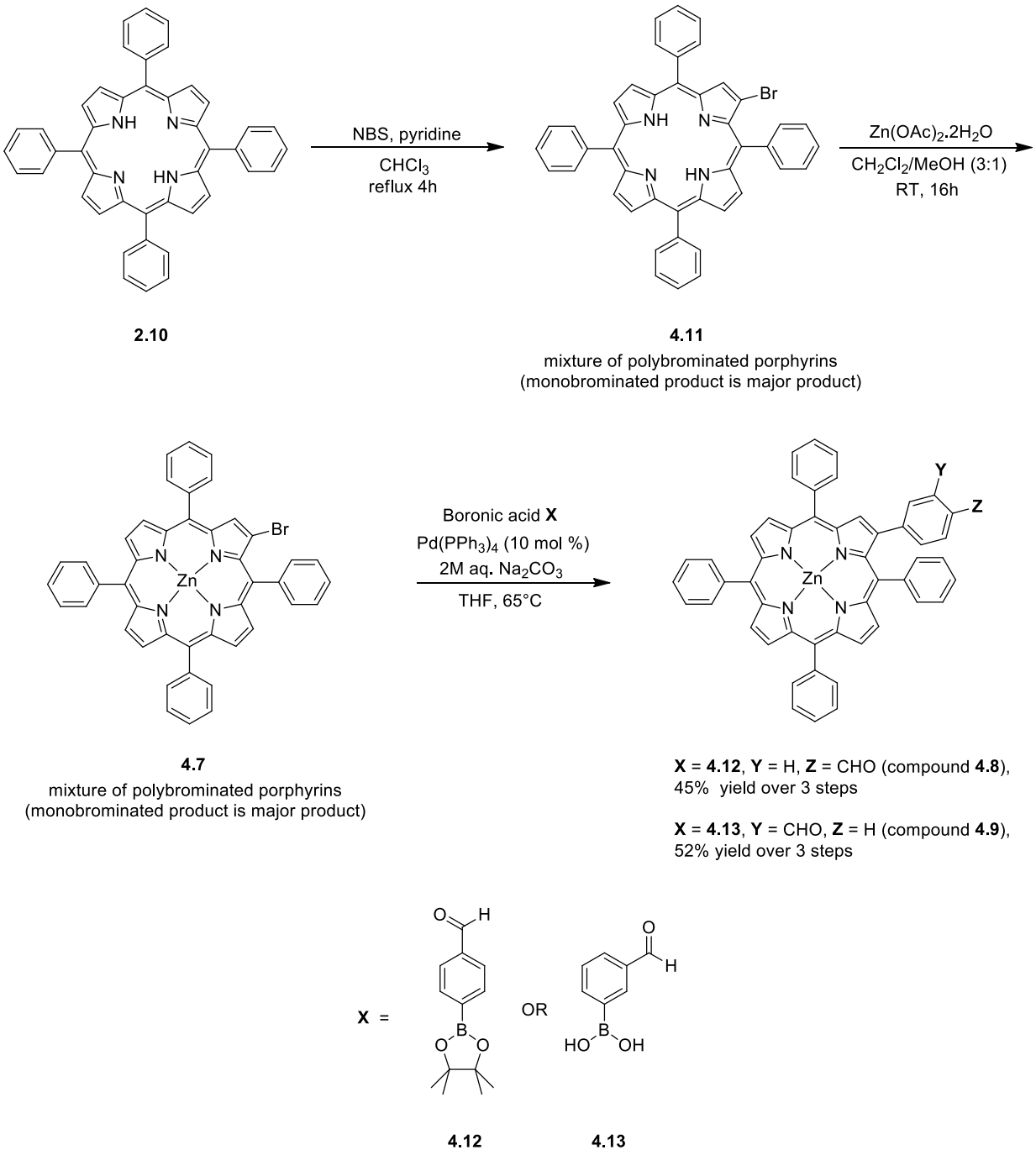

Figure 4.6: Synthesis of intermediate aldehydes **4.8** and **4.9** from tetraphenylporphyrin **2.10**.

4.3.2 Synthesis of Stilbene-Linked Model Compounds

The monomeric analogues of the stilbene-linked porphyrin-appended polymers **4.1** and **4.2** were synthesized as reference compounds for photophysical comparison to the polymers. Under similar synthetic conditions to those outlined for the syntheses of compounds **3.1 – 3.3** in Chapter 3, Horner-Wadsworth-Emmons olefination was employed to create the β-stilbene functionality using aldehydes **4.8** and **4.9**. Aldehyde **4.8** or **4.9** was stirred with benzyl diethylphosphonate **3.19** in THF using excess sodium hydride as base to give 2-((E)-4-(4-vinylstyryl)phenyl)-5,10,15,20-tetraphenylporphyrinato] zinc(II) (*p*-SL mon **4.1**) and 2-((E)-3-(4-vinylstyryl)phenyl)-5,10,15,20-tetraphenylporphyrinato] zinc(II) (*m*-SL mon **4.2**) (Figure 4.7) in 88% and 77% yields respectively.

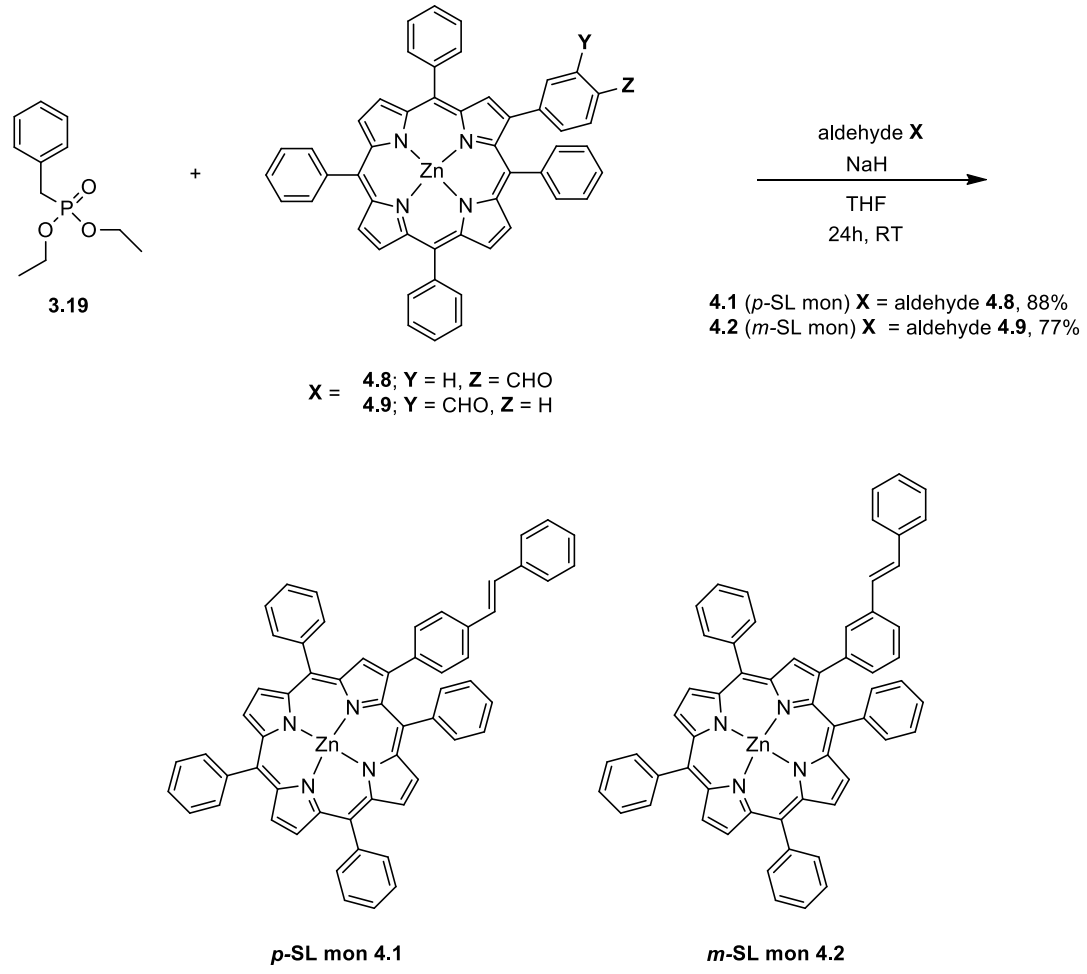

Figure 4.7: Synthesis of *p*-SL mon **4.1** and *m*-SL mon **4.2**.

Formation of the β-stilbene moieties in *p*-SL mon **4.1** and *m*-SL mon **4.2** were confirmed by ^{1}H NMR spectroscopy. The doublets observed in the region between 7.0-7.2 ppm in both the spectra of **4.1** and **4.2** exhibit vicinal coupling constants of 16.3/16.4 Hz (Figure 4.9 top) and 16.6 Hz (Figure 4.9 bottom) for **4.1** and **4.2** respectively, characteristic of the presence of a vinyl group with *trans*- geometry in both model compound structures. Additional structural elucidation was obtained through X-ray crystallography of **4.1** and **4.2**, which clearly display the stilbene moiety linked to the porphyrin β-position in the crystal structures of **4.1** ((A) in Figure 4.8) and **4.2** ((B) in Figure 4.8).

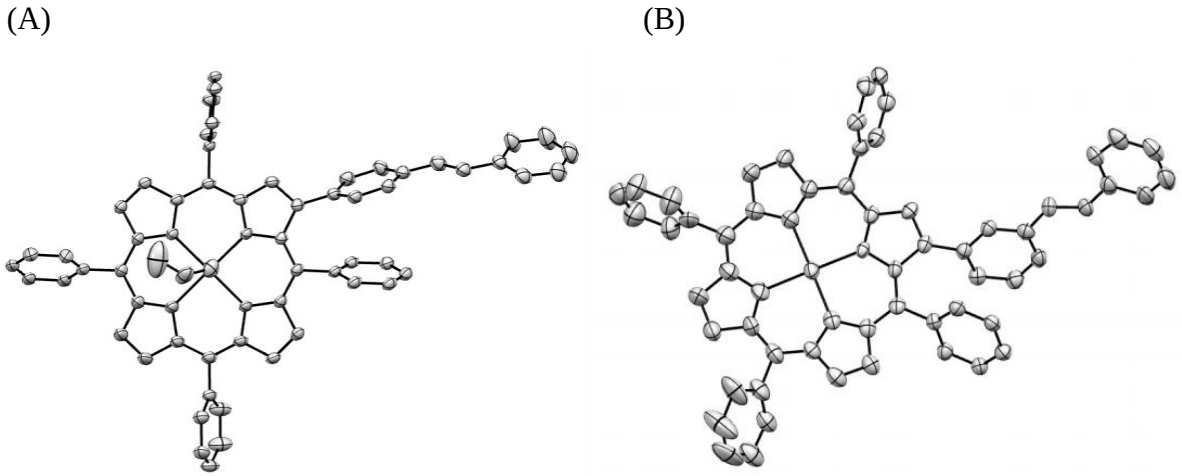

Figure 4.8: X-ray crystal structures of *p*-SL mon **4.1** (A) and *m*-SL mon **4.2** (B). Crystal structure of *p*-SL mon **4.1** (A) includes ethanol molecules coordinated to the zinc metal centres of the porphyrins, as ethanol was present as stabilizer in the chloroform solvent used in the vapour diffusion crystallization process. Crystal structures were obtained by Prof. Jonathan White of the University of Melbourne.

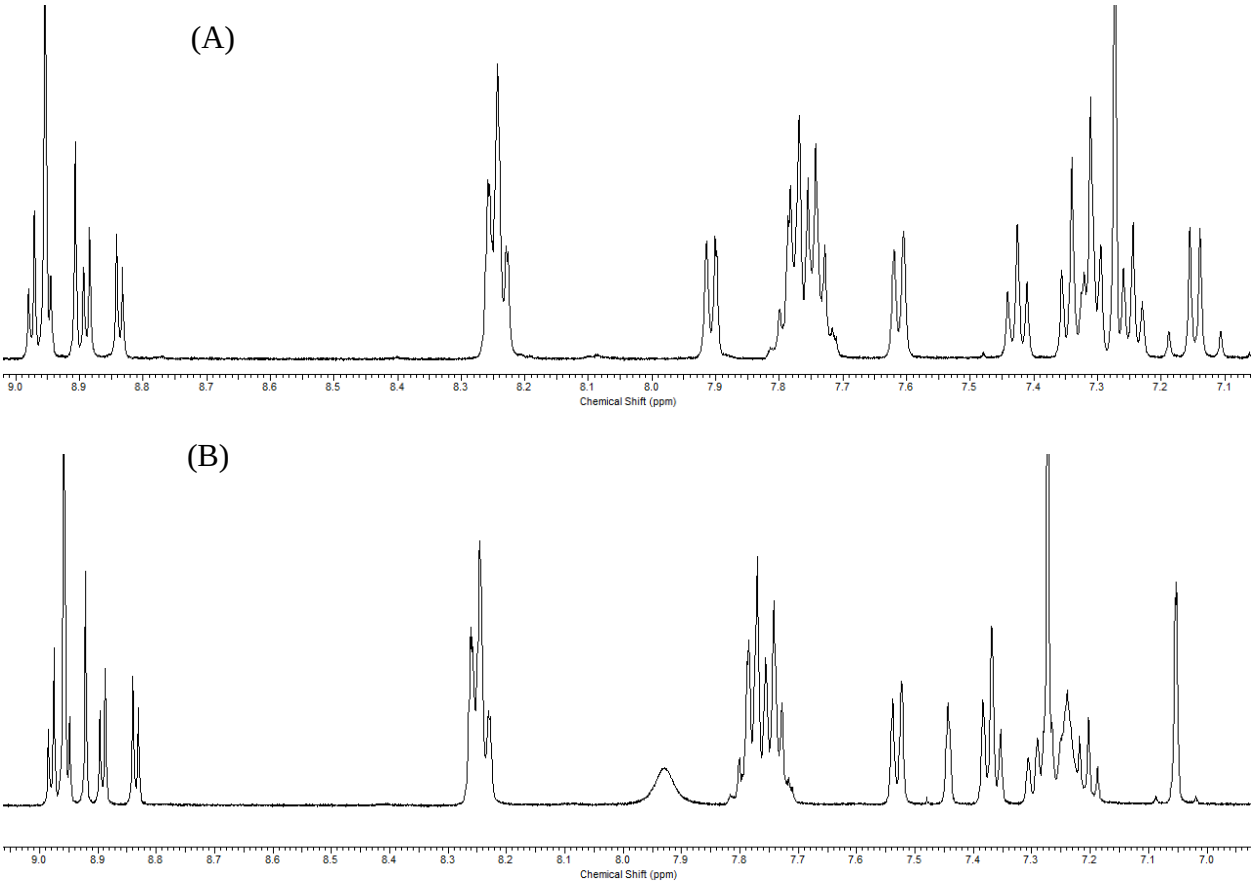

Figure 4.9: ^{1}H NMR spectra of *p*-SL mon **4.1** (A) and *m*-SL mon **4.2** (B).

4.3.3 Synthesis of Stilbene-Linked Porphyrin-Appended Polymers

Following the synthesis the appropriate precursors, the polymers *p*-SL pol **4.4** and *m*-SL mon **4.5** were synthesized. HWE coupling between poly(diethyl benzylphosphonate) **3.20** and 2 equivalents of aldehydes **4.8** or **4.9** in THF using excess sodium hydride as base, stirring at RT under N_2 for 5 days, gave poly{[2-((E)-4-(4-vinylstyryl)phenyl)-5,10,15,20-tetraphenylporphyrinato] zinc(II)} (*p*-SL pol **4.4**) and poly{[2-((E)-3-(4-vinylstyryl)phenyl)-5,10,15,20-tetraphenylporphyrinato] zinc(II)}(*m*-SL mon **4.5**) in 50% and 69% yields respectively (Figure 4.10). Similarly to the polymers outlined in Chapter 3 section 3.3.5.2, the polymers yields here are considered after size-exclusion chromatography (SEC) over bio-S-X beads using THF as eluent, repetitive washings of the polymers with distilled petroleum spirits and extensive high-vacuum drying.

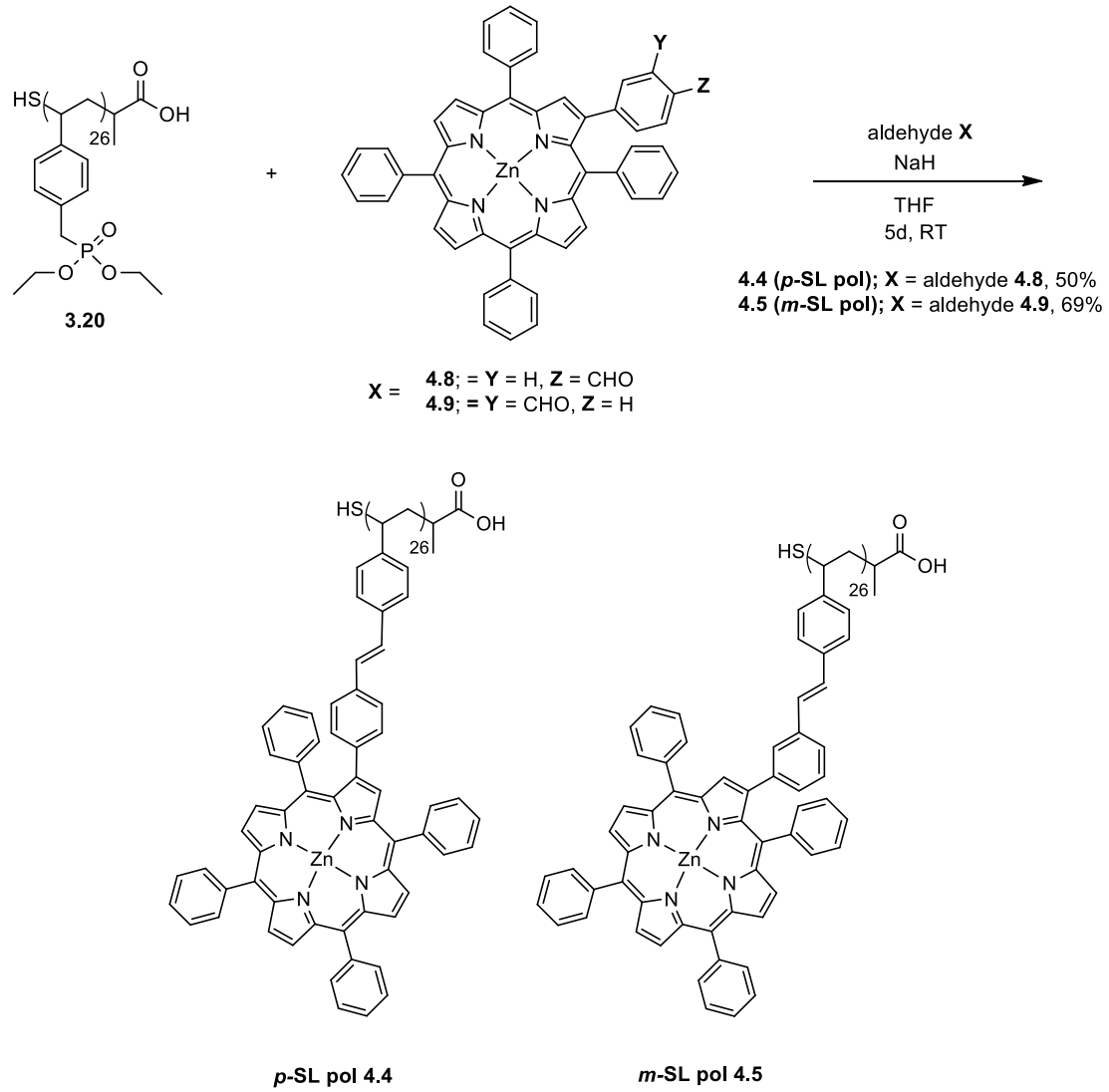

Figure 4.10: Horner-Wadsworth-Emmons Olefination for the post-polymerization functionalization of poly(diethyl benzylphosphonate) **3.20** to form the polymers *p*-SL pol **4.4** and *m*-SL mon **4.5**.

The ^{1}H NMR spectra of *p*-SL pol **4.4** and *m*-SL mon **4.5** (Figure 4.11 middle and bottom) display complete disappearance of the broad peaks at 3.06 and 3.95 ppm corresponding to the ethyl groups present in the ^{1}H NMR spectra of poly(diethybenzylphosphonate) **3.20** (Figure 4.11 top), indicating that all phosphonate groups present in the backbone starting material polymer **3.20** have been consumed in the post-polymerization functionalization reactions. The peaks appearing

furthest downfield between 8.30-9.10 ppm in ^{1}H NMR spectra of *p*-SL pol **4.4** and *m*-SL mon **4.5** (Figure 4.11 middle and bottom) represent the β-pyrollic protons of the porphyrin groups in **4.1** and **4.2**, and furthermore, the broad shape of these peaks corroborates the fact that the β-pyrollic protons of porphyrins in the sample compounds have been incorporated into polymeric structures.

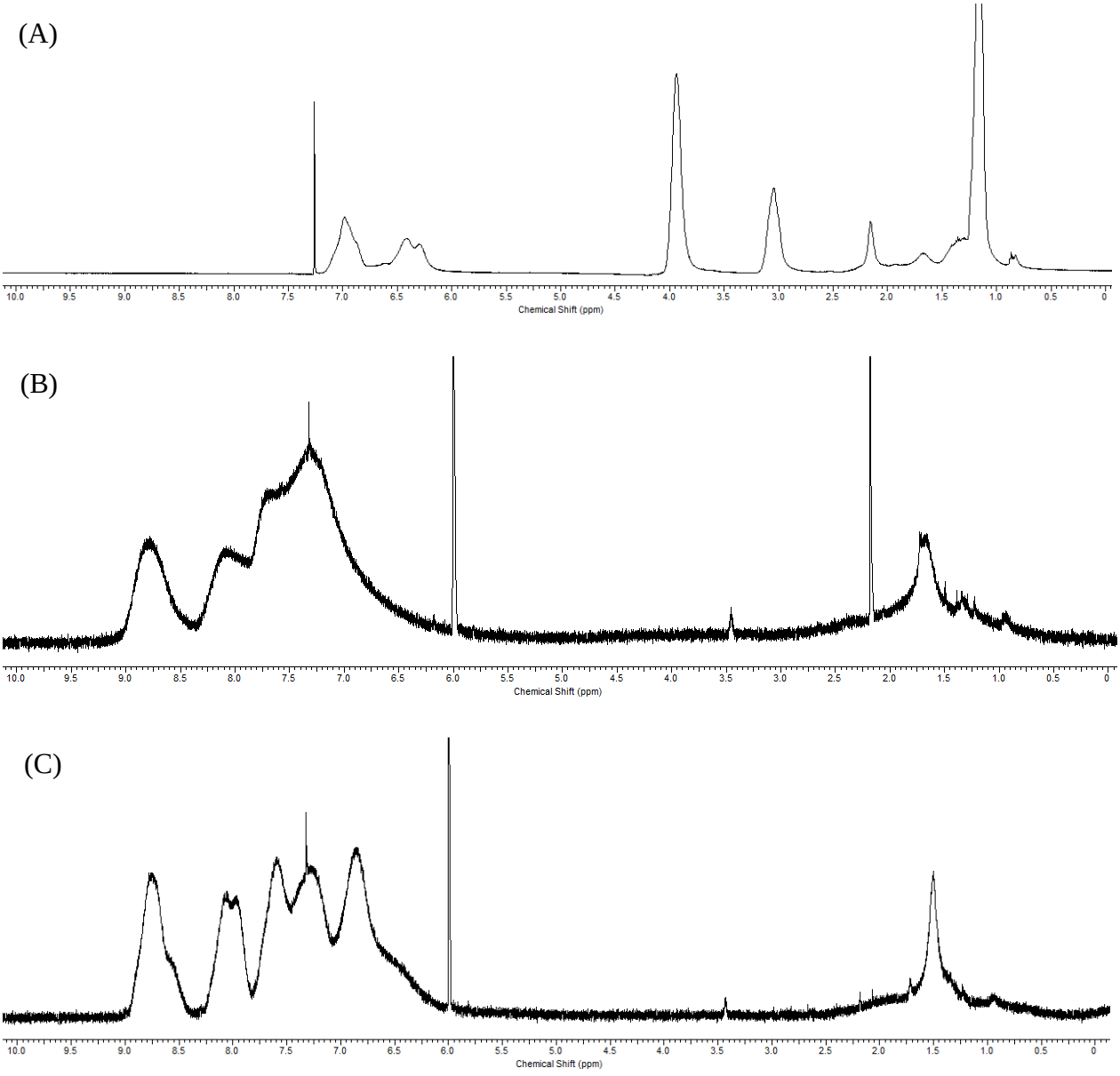

Figure 4.11: ^{1}H NMR ($CDCl_3$) spectra of poly(diethybenzylphosphonate) **3.20** (A), *p*-SL pol **4.4** ($C_2D_2Cl_4$, (B)) and *m*-SL mon **4.5** ($C_2D_2Cl_4$, (C)).

4.3.4 Synthesis of Ether-Linked Model Compound

It was envisaged that reaction of poly(4-vinylbenzylchloride) **3.26** with an alcohol-functionalized porphyrin derivative under basic conditions would be a viable approach to achieving a flexibly-linked porphyrin-appended polymer without extended linker group conjugation. As such, the necessary precursor alcohol-functionalized porphyrin was conveniently available via reduction of aldehyde **4.8**. Aldehyde **4.8** was thus reduced with $NaBH_4$ to give [2-((4-hydroxymethyl)phenyl)-5,10,15,20-tetraphenylporphyrinato] zinc(II) **4.10** in 96% yield (Figure 4.12). A model compound resembling the monomer unit in the desired polymer **4.6** was synthesized for photophysical comparison, as had been synthesized for *p*-SL mon **4.4** and *m*-SL mon **4.5**. Porphyrin alcohol **4.10** and benzyl bromide **3.25** were subject to Williamson ether synthetic conditions to yield the ether linked model compound [2-((4-benzyloxymethyl)phenyl)-5,10,15,20-tetraphenylporphyrinato] zinc(II) *p*-EL mon **4.3** in 86% yield (Figure 4.12).

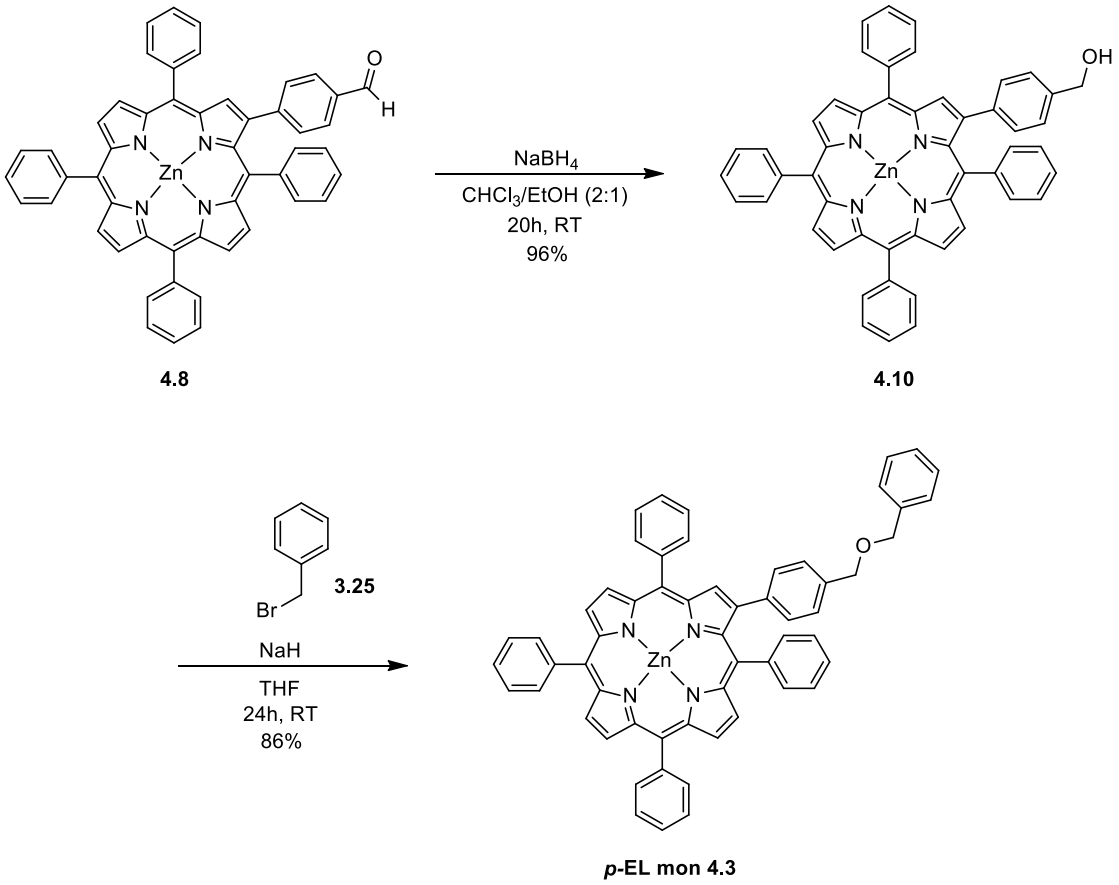

Figure 4.12: Synthesis of *p*-EL mon **4.3**.

Formation of the benzyl ether linkage in *p*-EL mon **4.3** is confirmed by using the integral of the β-pyrrolic proton doublet at 8.78 ppm (assigned as 1H) as a reference to compare to the integral region of the overlapping singlets at 4.55 ppm in the ^{1}H NMR spectrum, which correspond to the 2 sets of benzyl ether protons in the β-substituent of *p*-EL mon **4.3**. Setting the integral of the doublet at 8.78 ppm to 1H gives an integration corresponding to 3.81H at 4.55 ppm, closely matching the expected 4H integration for the overlapping peaks (Figure 4.15). The X-ray crystal structure of *p*-EL mon **4.3** is shown in Figure 4.13 below.

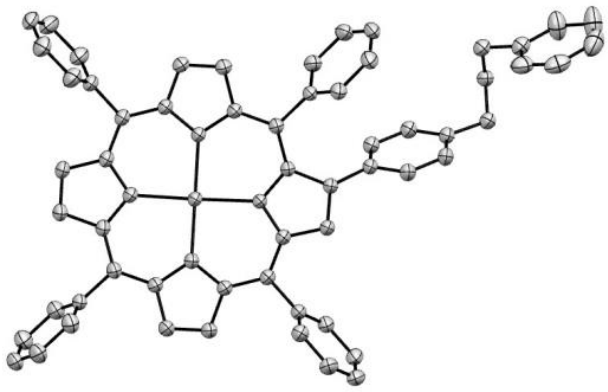

Figure 4.13: X-ray crystal structure of *p*-EL mon **4.3**. Crystal structure was obtained by Prof. Jonathan White of the University of Melbourne.

4.3.5 Synthesis of Ether-Linked Porphyrin-Appended Polymer

Porphyrin alcohol **4.10** and the polymer backbone poly(4-vinylbenzylchloride) **3.26** were subject to Williamson ether synthetic conditions to yield the ether linked porphyrin-appended polymer α-mercapto-ω-(1-carboxyethyl)-poly{[2-(4-(4-vinylbenzyloxymethyl)phenyl)-5,10,15,20-tetraphenylporphyrinato] zinc(II)} (*p*-EL pol **4.6**) in 70% yield (Figure 4.14).

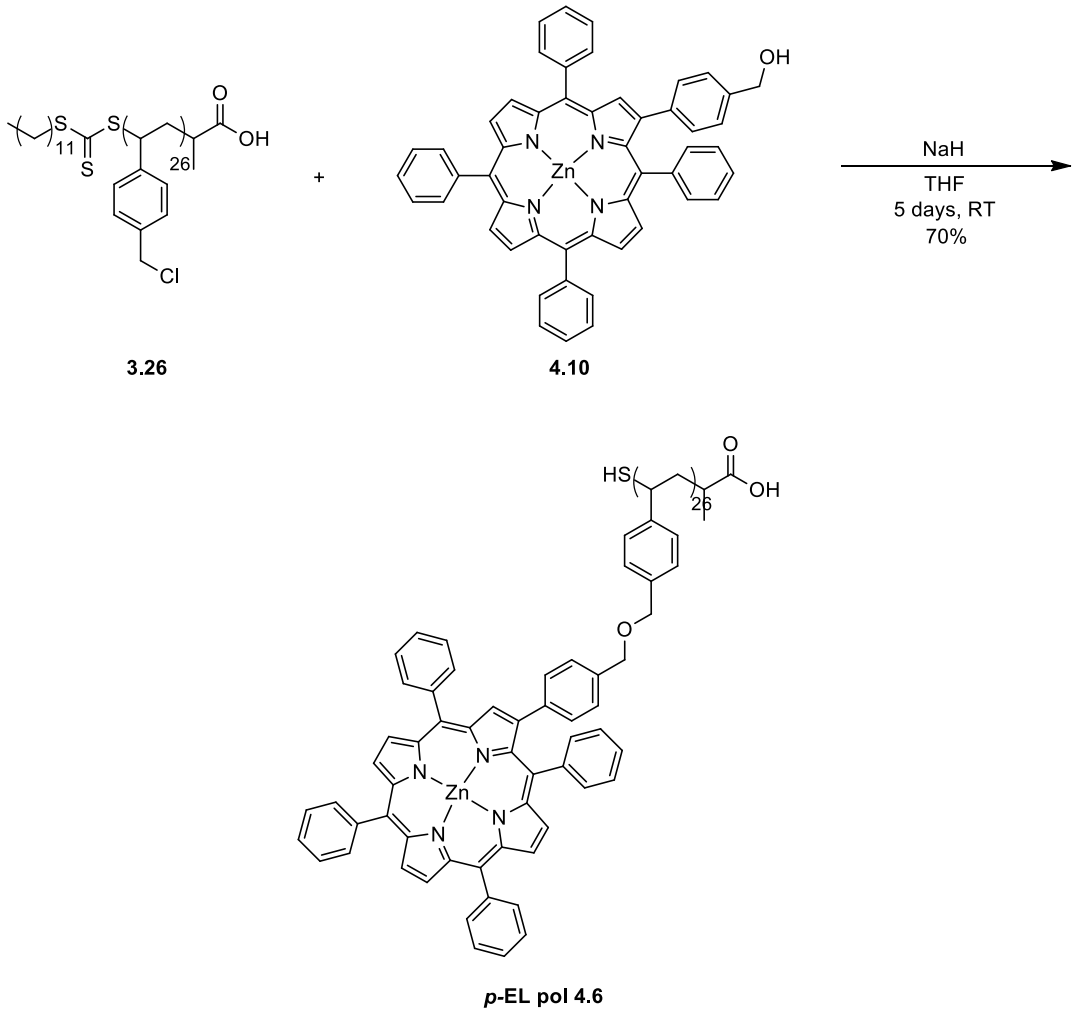

Figure 4.14: Synthesis of *p*-EL pol **4.6**.

As was the case for *p*-SL pol **4.4** and *m*-SL mon **4.5**, broadening of the peaks seen furthest downfield between 8.60-9.00 ppm in ^{1}H NMR spectra of *p*-EL pol **4.6** (Figure 4.15 (B)), which can be clearly assigned to the β-pyrollic protons of the porphyrins, indicates inclusion of the porphyrins as pendant chromophores in a polymeric structure. Complete disappearance of the chloromethyl peak in the ^{1}H NMR spectra of poly(vinylbenzylchloride) **3.26** upon formation of *p*-EL pol **4.6**, and thus complete functionalization of the polymer backbone, was difficult to confirm due to the small difference in chemical shift between the chloromethyl peak in the starting material and the methylene protons in the product ether linkage.

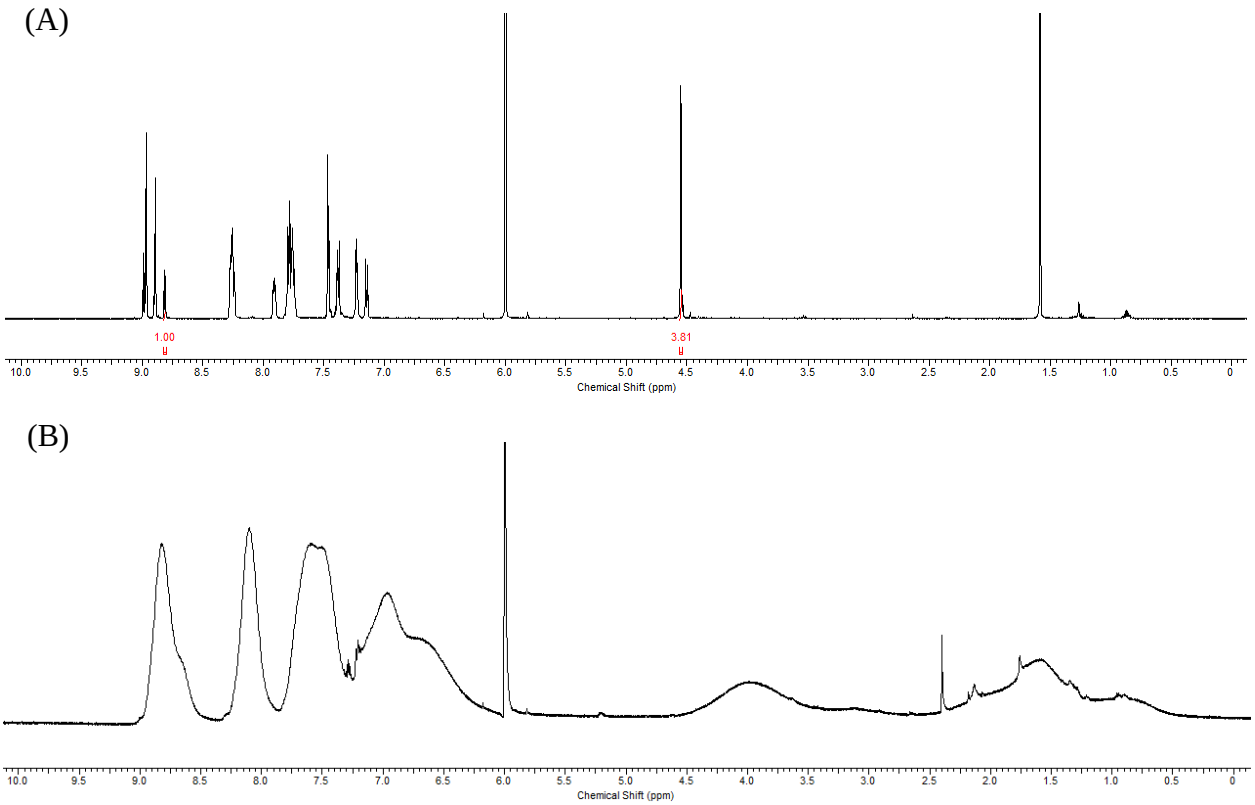

Figure 4.15: ^{1}H NMR spectra of *p*-EL mon **4.3** (A) and *p*-EL pol **4.6** (B) in $C_2D_2Cl_4$.

Cleavage of the RAFT trithiocarbonothioylthio moiety upon formation of *p*-EL pol **4.6** was unable to be confirmed definitively by UV-visible absorption techniques as was the case for cleavage of the RAFT group for poly(diethyl vinylbenzylphosphonate) **3.20** in Figure 3.19, as the absorption spectrum of the monomeric zinc porphyrin chromophore contained a broad absorption region that overlapped with the expected trithiocarbonothioylthio absorption maximum at 311 nm. Removal of the terminal RAFT chain transfer group is desirable for polymers designed for photophysical applications as it is known that the trithiocarbonothioylthio moiety can participate in non-radiative relaxation of chromophores in excited states.[27] It was expected however that under the highly nucleophilic reaction conditions in which excess alkoxide was present over a reaction period of several days, the trithiocarbonothioylthio RAFT group would be cleaved quantitatively. As discussed in chapter 3 in regard to the cleavage of the trithiocarbonothioylthio RAFT group in the presence of triethyl phosphite, literature reports corroborate the efficient end group removal of RAFT chain transfer agents under a variety of nucleophilic conditions including cleavage in the presence of alkoxides.[28,29]

Table 4.1: Degrees of functionalization (F) of the polymer backbones of polymers **4.4 – 4.6** derived from synthetic yields and UV-visible spectrophotometry.

Compound	% Minimum functionalization (F) derived from synthetic yield	% Minimum functionalization (F) derived from UV-visible absorption
p-SL pol **4.4**	15	25
m-SL pol **4.5**	56	31
p-EL pol **4.6**	64	30

The degrees of functionalization of the backbones of polymers **4.4 – 4.6** were calculated using data from synthetic yields and UV-visible spectrophotometry, as outlined in section 3.4 previously. The F values are given in Table 4.1 above. As was seen for the polymers **3.4 – 3.6**, the analyses yielded low degrees of pendant porphyrin inclusion into the polymer backbone. F values derived from synthetic yields were higher than those derived from UV-visible absorption data for polymers **3.5** and **3.6** however was lower for **3.4**. The low F value for 3.4 using synthetic yield data is likely due to large losses in polymer recovery upon isolation and purification. As mentioned in secton 3.4.3, the above analyses are impacted greatly by factors that are difficult to quantify and therefore only provide minimum thresholds for functionalization.

Attempts to extract useful data on the molecular weight distribution of the polymers **4.4 – 4.6** from GPC experiments were unsuccessful due to similar issues with broad retention peaks as listed in section 3.3.5.3. Comparison of the integrals of the ether linkage methylene protons in the ^{1}H NMR spectrum of *p*-EL pol **4.6** to the integrals of the β-pyrollic protons was suggested as a potential method to approximate the degree of functionalization of the backbone by the pendant units. Upon further inspection of the ^{1}H NMR spectrum, the signal-to-baseline integral ratios were small enough such that the contribution to the integral area by the baseline would cause a significant deviation in the relative integral ratios of the proton environment peaks. This effect was amplified by the very broad profile of the peak due to the ether methylene protons in the ^{1}H NMR spectrum of *p*-EL pol **4.6**, thus making analysis of integral areas a poor method to approximate the degree of functionalization of the backbone in **4.6.**

4.4 Absorption Spectra

The UV-visible absorption spectra for the ether and stilbene linked model compounds and polymers (Figure 4.16) were obtained from solutions of the respective porphyrins in toluene at room temperature. The concentration of all solutions used to obtain the absorption spectra was 3.3 μM, and as such, molar extinction coefficients (ε) were calculated for all compounds, as listed in Table 4.2.

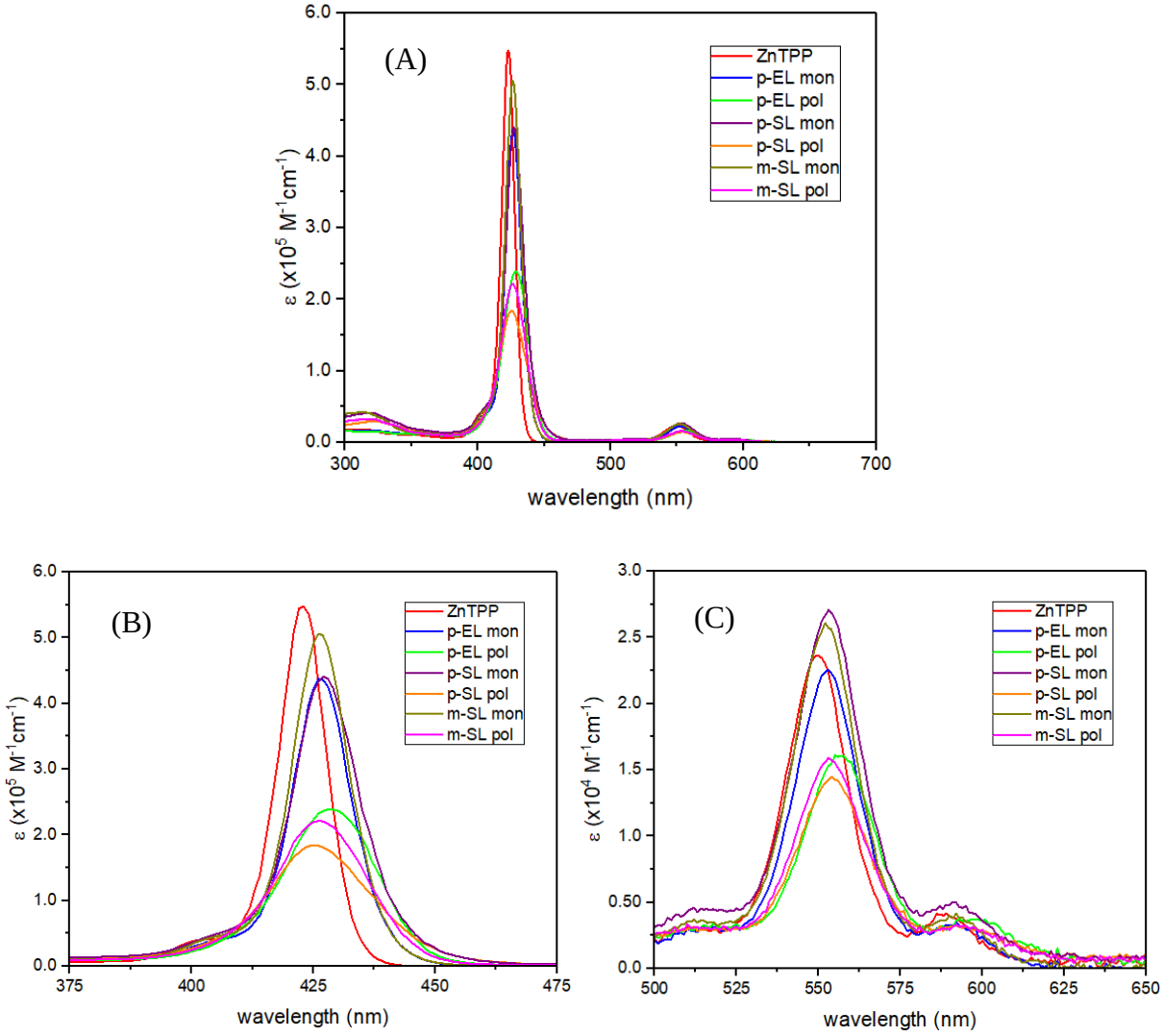

Figure 4.16: (A) UV-visible absorption spectra of ZnTPP **2.4**, the model compounds *p*-SL mon **4.1**, *m*-SL mon **4.2** and *p*-EL mon **4.3**, and the polymers *p*-SL pol **4.4**, *m*-SL pol **4.5** and *p*-EL pol **4.6** in toluene. (B) Spectra in (A) zoomed into Soret absorption region for clarity. (C) Spectra in (A) zoomed into Q-band absorption region for clarity.

Table 4.2: Photophysical data for ZnTPP **2.4**, the model compounds **4.1**, **4.2** and **4.3**, and the polymers **4.4**, **4.5** and **4.6** in toluene at 3.3μM.

Compound	λ_{max} Soret (nm)	ε Soret (10^5 $M^{-1}cm^{-1}$)	λ_{max} Q(1,0) band (nm)	ε Q(1,0) band (10^4 $M^{-1}cm^{-1}$)	ε Q-band at 532 nm (10^3 $M^{-1}cm^{-1}$)
ZnTPP **2.4**	423	5.48	550	2.36	6.05
p-SL mon **4.1**	427	4.41	553	2.71	6.18
m-SL mon **4.2**	426	5.06	552	2.61	5.59
p-EL mon **4.3**	426	4.37	553	2.26	4.77
p-SL pol **4.4**	425	1.84	554	1.45	3.63
m-SL pol **4.5**	426	2.21	553	1.59	3.91
p-EL pol **4.6**	429	2.39	555	1.61	3.47

β-Substitution of the porphyrin macrocycle of ZnTPP **2.4** with π-conjugated substituents that are not directly conjugated into the porphyrin aromatic system introduces only minor changes compared to the conjugation extended compounds seen in Chapter 3. Small increases in the Q-band extinction coefficients of *p*-SL mon **4.1** and *m*-SL mon **4.2** are consistent with a partial degree of conjugation of the stilbene moiety into the porphyrin macrocycle, but no major modifications to the HOMO should occur as there exists nodes for porphyrin HOMOs at the β-pyrrolic carbons. Although steric repulsion between the *ortho*-protons on the phenyl directly linked to the porphyrin plane, and the porphyrin plane itself, will cause the stilbene linker to rotate into a predominantly perpendicular orientation to the plane of the porphyrin as seen in the crystal structures of the monomer compounds (Figures 4.8 and 4.13), some stilbene rotation of the monomers would be still be possible in solution.

The reverse trend compared to that of the Q-bands is seen in the extinction coefficients of the Soret band for all of the compounds, whereby partial β-conjugation decreases the extinction coefficients of the porphyrins. This trend is expected as the porphyrin a_{1u} HOMO-1 orbitals are located at the β-pyrrolic carbons and conjugation extension reduces the net electron density at these positions due to delocalisation. Reduction of the extinction coefficient of the Soret band with increasing conjugation extension has been previously reported by Ventura *et al.* for oligo-phenylene vinylene (oligo-*p*-PV) β-substituted porphyrins[20] and in similar β-substituted porphyrins studied in chapter 3 of this thesis. The Soret band extinction coefficient of *p*-SL pol **4.4** is only three-quarters of the intensity of *p*-EL pol **4.6**, which may indicate that the stilbene moiety adopts a conformation which is more co-planar with respect to the porphyrin when spatially constrained in the pendant porphyrin environment. Spatial constraints due to pendant crowding have been reported to alter the photophysical properties of polymers with oligo-*p*-PV units previously, as twisting of the oligo-*p*-PV pendants due to steric crowding can change the degree of conjugation in the pendant PPV unit.[30]

The Soret absorption maxima of the polymers in Figure 4.16 exhibit broadened peaks and extinction coefficients that are decreased by a factor of approximately 2 with respect to their monomeric analogues. The absorption maxima of the Q-bands and Soret bands of the polymers closely resemble their model compounds as expected, only exhibit minor bathochromic shifting for the Q-bands and almost no shift is observed for the Soret maxima upon inclusion of porphyrins into the pendant polymeric structures. Broadening and bathochromic shifting of absorption maxima has been widely reported for various chromophores upon introduction as pendant units onto a polymeric backbone due to intramolecular electronic interactions between the pendant units.[3,30] Outside of the expected decrease in extinction coefficients of the polymers in comparison to the monomers,[6] the absorption features of the polymers show no distinct features such as excitonic splitting that would detract from their viability as absorber-sensitizers in TTA-UC systems.

4.5 Fluorescence Spectra and Fluorescence Decays

The fluorescence spectra in Figure 4.17 below were obtained from solutions of the respective porphyrins in toluene at room temperature and corrected for the photomultiplier detector wavelength response. Fluorescence quantum yields of all model compounds and polymers were calculated relative to ZnTPP **2.4** (Φ = 0.033 in toluene)[31] and are listed in Table 4.3. All solutions used in the fluorescence spectra measurements had an absorbance of 0.1 ± 0.005 at their respective excitation wavelengths in order to minimize inner filter effects such as reabsorption, and also aggregation quenching. All S_1 fluorescence lifetime measurements and related experimental details were provided by Dr. Amy Stevens (University of Saskatchewan).

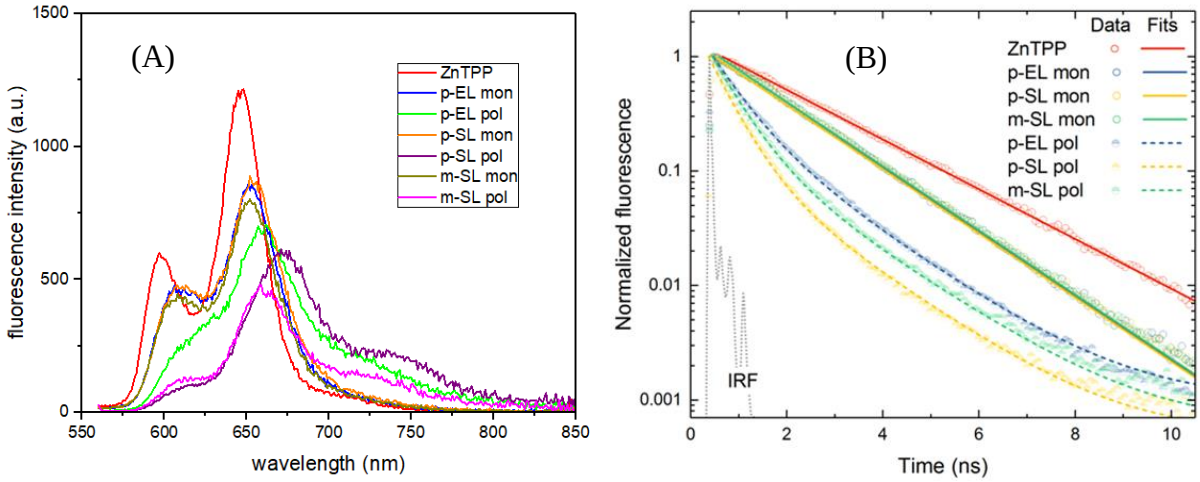

Figure 4.17: (A) Fluorescence spectra of ZnTPP **2.4**, the model compounds *p*-SL mon **4.1**, *m*-SL mon **4.2** and *p*-EL mon **4.3**, and the polymers *p*-SL pol **4.4**, *m*-SL pol **4.5** and *p*-EL pol **4.6** in toluene. All porphyrin samples were excited at their respective absorption maxima, listed in Table 4.1. (B) S_1 fluorescence decay profiles of ZnTPP **2.4**, the model compounds *p*-SL mon **4.1**, *m*-SL mon **4.2** and *p*-EL mon **4.3**, and the polymers *p*-SL pol **4.4**, *m*-SL pol **4.5** and *p*-EL pol **4.6** in toluene. Open circles represent experimental data points, and decay function fitted curves are represented by the bold lines.

Table 4.3: Fluorescence parameters for ZnTPP **2.4**, the model compounds **4.1**, **4.2** and **4.3**, and the polymers **4.4**, **4.5** and **4.6** in toluene. τ_1, α_1, τ_2, α_2, and R^2 values were obtained by Dr. Amy Stevens (University of Saskatchewan).

Compound	λ_{max} Q-band (nm) [(1,0),(0,0)]	Φ_f Q-band	τ_1 (ns)	α_1	τ_2 (ns)	α_2	R^2
ZnTPP **2.4**	589, 644	0.033	2.00 ± 0.06	1.00			0.998
p-SL mon **4.1**	607, 652	0.030	1.55 ± 0.05	1.00			0.999
m-SL mon **4.2**	607, 649	0.028	1.55 ± 0.03	1.00			0.998
p-EL mon **4.3**	606, 651	0.029	1.54 ± 0.04	1.00			1.000
p-SL pol **4.4**	617, 669	0.027	0.47 ± 0.02	0.86	1.49 ± 0.05	0.14	0.998
m-SL pol **4.5**	612, 657	0.019	0.52 ± 0.04	0.81	1.55 ± 0.05	0.19	0.999
p-EL pol **4.6**	657	0.031	0.57 ± 0.02	0.71	1.51 ± 0.07	0.29	0.999

Fluorescence from the Q-bands of the model monomeric compounds (Figure 4.17 (A)) exhibited minor bathochromic shifts of approximately 20 nm (Table 4.3) in comparison to ZnTPP **2.4**, as has been observed in zinc porphyrin derivatives previously with β-aryl substituents,[12] and the S_1 fluorescence profiles of the monomeric compounds and ZnTPP **2.4** are somewhat consistent with vibronic features of their respective absorption spectra. In comparison to their respective monomeric analogues, the S_1 fluorescence profiles of the polymers (Figure 4.17 (A)) appear broadened and extend into the near-infrared, with a lesser degree of vibronic structure and have emission maxima that are bathochromically shifted approximately 10 nm (Table 4.3). The fluorescence quantum yield of the polymers were only slightly reduced in comparison to the monomers, which is consistent with the pendant porphyrin polymers studied by Wang *et al.*[6] that contain flexible linking groups. The nature of the polymer S_1 fluorescence spectra indicate that mixing of the porphyrin electronic states is occurring in the pendant polymer environment, leading to a greater proportion of emission occurring from low energy conformations which become rapidly accessible due to the increased electronic communication between pendant porphyrin excited singlet states and adjacent ground state porphyrins.

The S_1 fluorescence decay profiles in Figure 4.17 (B) for the monomeric compounds were able to be fit to a mono-exponential function, which is consistent with the unperturbed radiative decay of S_1 to the ground singlet state. Previous investigations have demonstrated that electron transfer from the ZnTPP core to rotatable oligo(phenylene vinylene) β-substituents does not contribute to singlet excited state decay of the ZnTPP core, due to a large donor-bridge LUMO-LUMO energy gap and a high degree of rotation of the poly(phenylene vinylene) β-substituent out of the plane due to steric interaction with the adjacent meso-phenyl substitutent.[12] The S_1 fluorescence decay profiles in Figure 4.17 (B) for the polymeric compounds exhibited decay behavior that was able to be fit to bi-exponential functions, indicating that a S_1 decay pathway that is not existent in the monomeric compounds is competing with the radiative relaxation of S_1 to S_0. The bi-exponential behavior of the polymer singlet decays further reinforces the concept that significant electronic communication is present between pendant porphyrin units, as the presence of a fast singlet decay component has been observed for several electronically-coupled multi-porphyrin systems such as supramolecular porphyrin 'boxes'[32], covalently-linked cyclic porphyrin arrays[33] and other pendant zinc porphyrin polymers[3] previously.

Comparison of the decay rates of the mono- and bi-exponential components for the model compounds and polymers show that the slow component is due to monomeric radiative relaxation, and in the pendant polymers, the slow monomeric radiative component contributes to less than 30% of the decay of the total S_1 excited state population. Almost all of the S_1 excited states in the pendant zinc porphyrin polymers studied by Fujitsuka *et al.*[3] decay via the fast decay pathway (87-94% of S_1 fluorescence) and these polymers had fluorescence quantum yields of less than 20% of their monomeric analogues. The fact that the fluorescence quantum yields of the polymers studied in this chapter were similar to their monomeric analogues and relatively consistent across all linker variants may indicate that none of the linker structures force the pendant zinc porphyrin units into orientations which lead to non-radiative quenching of the S_1 excited state to the degree observed for the pendant zinc porphyrin polymers studied by Fujitsuka *et al.,*[3] although a substantial amount of the S_1 population of *p*-SL pol **4.4**, *m*-SL pol **4.5** and *p*-EL pol **4.6** may still be lost via non-radiative exciton decay pathways.

4.6 Probing Non-Coherent Photon Upconversion via Direct S2 Emission

Upconverted fluorescence measurements and calculations for the quantum yields of upconverted fluorescence were performed by Dr. Amy Stevens (University of Saskatchewan). Quantum yields of upconverted fluorescence from S_2 were measured by observing the ratio of upconverted fluorescence intensity of each compound in degassed toluene relative to the upconverted fluorescence intensity of ZnTPP **2.4**, keeping the excitation intensity the same for the compound of interest and ZnTPP **2.4**. The quantum yield of upconverted fluorescence of ZnTPP **2.4** in toluene is 1.5 x 10^{-4} [34] and upconverted fluorescence quantum yields for the monomers and polymers are listed in Table 4.4.

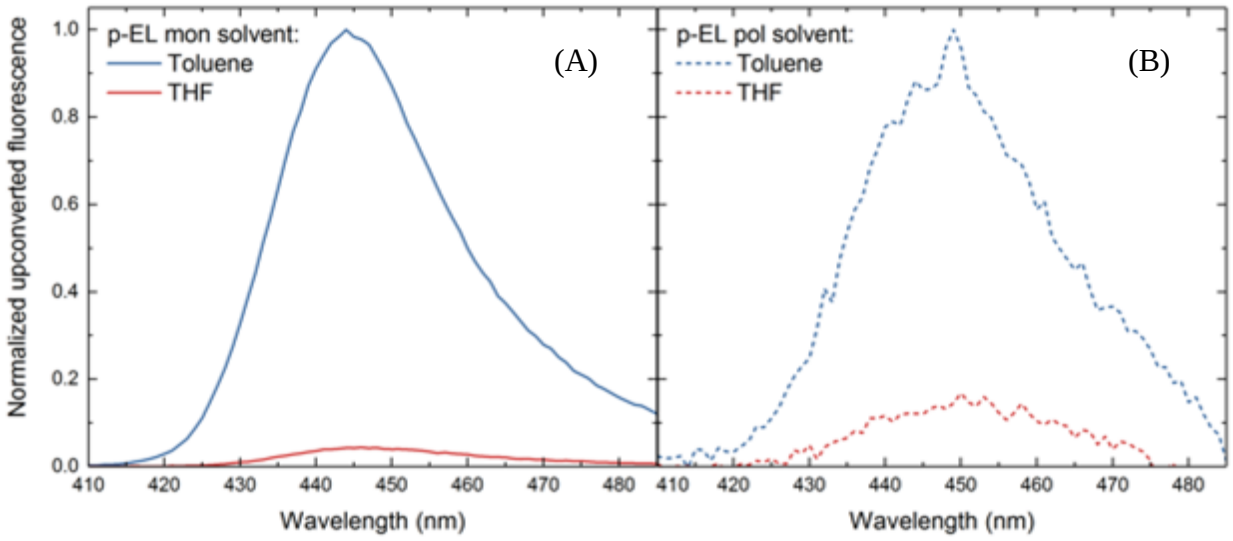

Figure 4.18: NCPU emission intensities in degassed toluene and the degassed coordinating solvent, THF, for the *p*-ether linked monomer *p*-EL mon **4.3** and the *p*-ether-linked polymer *p*-EL pol **4.6** at excitation wavelength of 532 nm.

Fluorescence from the S_2 state of all of the model compounds and polymers **4.1 – 4.6** was observable upon excitation of the compounds at 532 nm in degassed toluene solutions. An example of the UC fluorescence spectra for the best performing monomer/polymer pair, *p*-EL mon **4.3** and polymer *p*-EL pol **4.6**, are shown in Figure 4.18. The greatest UC fluorescence intensity is observed for the non-coordinating solvent toluene (blue line spectra in Figure 4.18). The fluorescence from the S_2 state after excitation at 532 nm was absent upon oxygenation of the solutions, suggesting that the triplet states of the compounds were necessary to produce the

fluorescence observed in the degassed solution samples and thus NCPU-TTA was responsible for the observed emission. The β-substitution pattern of the zinc porphyrin macrocycle in all monomer compounds resulted in a 5-fold or greater reduction of their UC fluorescence quantum yields relative to ZnTPP **2.4** (Table 4.4). The polymers **4.4**, **4.5** and **4.6** exhibited UC quantum yields 2 orders of magnitude lower than for their corresponding monomeric compounds (Table 4.4). Although a reduction in the UC quantum yields of the polymers relative to their monomeric analogues is expected as the S_1 excited state of the polymers is subject to additional fast non-radiative relaxation processes not present in the monomers (Table 4.3), the large magnitude of the decrease in UC quantum yield cannot be predicted solely from the approximate S_1 population available for ISC. The extremely low UC fluorescence quantum yields for the pendant zinc porphyrin polymers **4.4**, **4.5** and **4.6** render them to be poor dual absorber-upconverters for the production of homomolecular NCPU-TTA.

Table 4.4: Quantum yields of upconverted fluorescence from the S_2 state of monomer and polymers compounds **4.1 – 4.6** excited at 532 nm in degassed toluene. The UC quantum yield for ZnTPP **2.4** obtained from reference 33 was used as a standard for calculation of relative UC yields for compounds **4.1 – 4.6**.

Samples (in degassed toluene) λ_{ex} = 532 nm	**S_2-S_0 Intensity (A_{samp}/A_{ref})**	**φ_f (S_2-S_0)**
S_2-S_0 (410 to 485 nm)		
ZnTPP **2.4** at 15 μM	1.00	1.5×10^{-4} (lit.)[34]
p-SL mon **4.1** at 27 μM	0.085	1.3×10^{-5}
m-SL mon **4.2** at 19 μM	0.19	2.8×10^{-5}
p-EL mon **4.3** at 29 μM	0.16	2.3×10^{-5}
p-SL pol **4.4** at 0.9 μM	0.0003	$< 10^{-7}$
m-SL pol **4.5** at 1 μM	0.0017	3×10^{-7}
p-EL pol **4.6** at 1 μM	0.0025	4×10^{-7}

The magnitude of the effect of solvent coordination to the zinc metal centre on the UC fluorescence intensity was studied for *p*-EL mon **4.3** and *p*-EL pol **4.6**, using THF and toluene as coordinating and non-coordinating solvents respectively (Figure 4.18). Sugunan et al. have demonstrated that solvent coordination substantially decreases the observed UC fluorescence intensity in comparison to that observed in non-coordinating solvents for monomeric ZnTPP **2.4**, due to an increase in the average intermolecular separation in the annihilating molecular pair when solvent is coordinated to the zinc porphyrins, thus leading to a lesser degree of mutual orbital overlap between the annihilating porphyrins.[35] The ratio, A_{UC} , of the integrated areas of the UC fluorescence spectra of *p*-EL mon **4.3** in toluene relative to THF (A_{UC} = area *p*-EL mon **4.3** toluene: area *p*-EL mon **4.3** THF) was calculated to be 22, which is consistent with the UC fluorescence integral ratio of ~20 observed for ZnTPP **2.4** in toluene relative to ZnTPP **2.4** in THF previously reported by Sugunan *et al*.[35] The ratio A_{UC} drops to 6 when observing the UC fluorescence intensity of *p*-EL pol **4.6** in both coordinating and non-coordinating degassed solution. The diminished effect of the coordinating solvent on the UC fluorescence intensity for *p*-EL pol **4.6** compared to *p*-EL mon **4.3** suggests that the crowded environment of the pendant units in the polymer inhibits the degree of access of the coordinating solvent to the metal centres of the pendant zinc porphyrin units. The relative A_{UC} ratios determined for *p*-EL mon **4.3** and *p*-EL pol **4.6** provides further evidence for the fact that the pendant porphyrin units in *p*-EL pol **4.6** are likely in relative orientations that on average provide a greater degree of inter-porphyrin orbital overlap than for *p*-EL mon **4.3** in the axially coordinating THF solution.

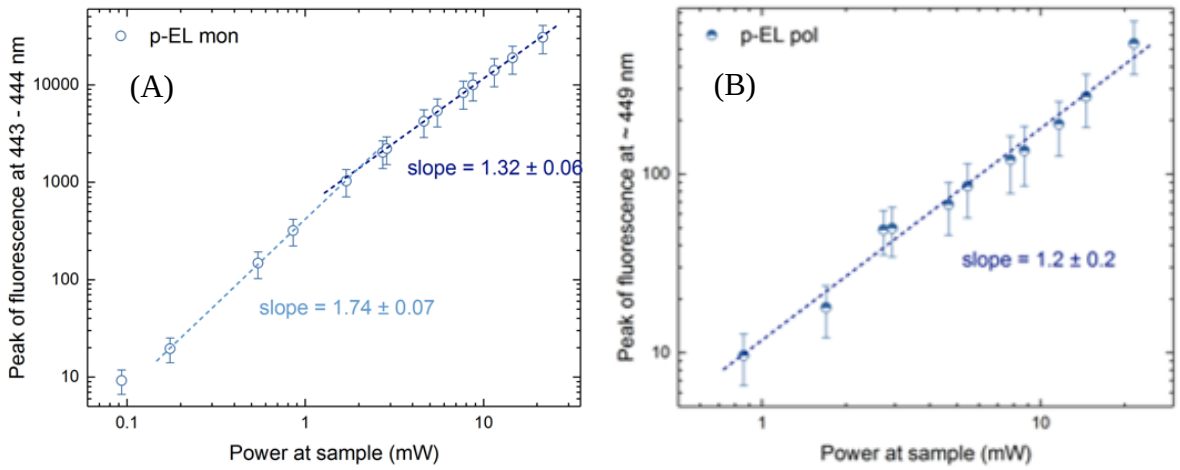

Figure 4.19: (A) Power dependence of the upconverted emission intensity for the *p*-ether-linked model compound *p*-EL mon **4.3** in degassed toluene. (B) Power dependence of the upconverted emission intensity for the *p*-ether-linked polymer *p*-EL pol **4.6** in degassed toluene.

The relationships between the incident excitation power and the intensity of the UC emission maxima of *p*-EL mon **4.3** and *p*-EL pol **4.6** in solution were analysed in log plots shown in Figures 4.19 (A) and (B) respectively. The gradient of the linear slope in Figure 4.19 (A) for UC emission from *p*-EL mon **4.3** solutions subject to low excitation power is 1.74, decreasing to 1.32 at high excitation power. Log plots such as those in Figure 4.19 with slopes having gradient of approximately 2 are consistent with the quadratic relationship between triplet state concentration and TTA, as TTA is a bimolecular excited state reaction that follows second order rate laws. The decrease in slope gradient of the log plots at high excitation power is due to the saturation of triplet excited states which cause the kinetics of the TTA bimolecular reaction to become more pseudo first order in nature. Such a decrease in the log plot slope gradients at high excitation powers have been observed previously for small molecule TTA systems in solution.[36,37] Unlike the monomer in Figure 4.19 (A), the best linear fit to the log plot for *p*-EL pol **4.6** in Figure 4.19 (B) produces a slope with gradient 1.2 over the entire range of excitation powers employed in the study, including the data points obtained at the lowest excitation powers that still produce measurable UC emission. The lack of change in gradient of the linear data fit over all measured excitation powers for *p*-EL pol **4.6** may suggest that the mechanism by which TTA operates between the pendant zinc porphyrin units in *p*-EL pol **4.6** is different in nature to the mechanism of TTA that applies to monomeric metalloporphyrin species.

4.7 Triplet-Triplet Transient Absorption Spectroscopy

All solutions used in the transient absorption analysis were prepared in spectroscopic grade toluene and degassed thoroughly prior to measurements. Solutions of porphyrin were prepared to have the same OD at the desired excitation wavelength (532 nm) so that the concentration of the singlet excited state upon excitation would be similar across all samples. The excitation pulse energy used for all triplet transient absorption spectra in section **4.6** was 8.2 mJ. A gate delay time of 200 ns was set in order to capture the absorption spectrum of the triplet state porphyrins while the population of triplets was still relatively high, and such that the delay comfortably exceeded the time scale in which excitation scatter would be observed in the transient absorption spectrum. The triplet transient absorption spectra for the model and polymer compounds **4.1 – 4.6** are shown in Figure 4.20 and 4.21 below.

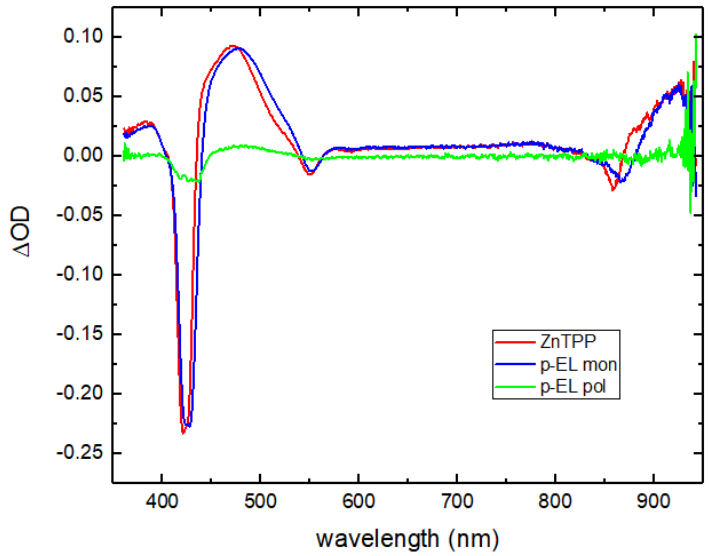

Figure 4.20: Transient absorption spectra of ZnTPP **2.4**, *p*-EL mon **4.3** and *p*-EL pol **4.6**.

The transient absorption spectra in Figures 4.20 and 4.21 all display a large trough between 420 – 430 nm due to the ground state bleaching of the triplets in the Soret band absorption region. Broad transient absorptions appear in the spectra in Figures 4.20 and 4.21 with maxima between 460 – 490 nm. The transient absorption spectra of the model compounds **4.1 – 4.3** exhibit almost

identical properties to ZnTPP **2.4**; similar degrees of ground state bleaching of the Soret band and Q-band, and comparable triplet extinction coefficients at the major transient absorption maxima, which suggests that the substitution at the β-position does not introduce additional decay pathways that would significantly decrease the proportion of singlet excited porphyrins that undergo ISC from the S_1 state to the T_1 state in the model compound, unlike the reduction in triplet absorption exhibited by the oligo PPV linked pendant porphyrins and model compounds discussed in Chapter 3. The dominant T_1-T_s absorption is far weaker for the polymers than for the model compounds (approx. 90% reduction in ΔOD), which is consistent with the non-single exponential fluorescence decays of the polymers and the decreased fluorescence lifetimes seen in section **4.5** that suggest a fast radiationless decay pathway may be competing with ISC, hence lowering the initial population of triplets being formed and thus excited by the probe beam in the TA measurements. The relative magnitudes of the S_1 slow decay components within the polymer series are somewhat proportional to the relative ΔOD values at the triplet absorption maxima within the polymer series, suggesting that the ISC quantum yields may be similar for the pendant polymers.

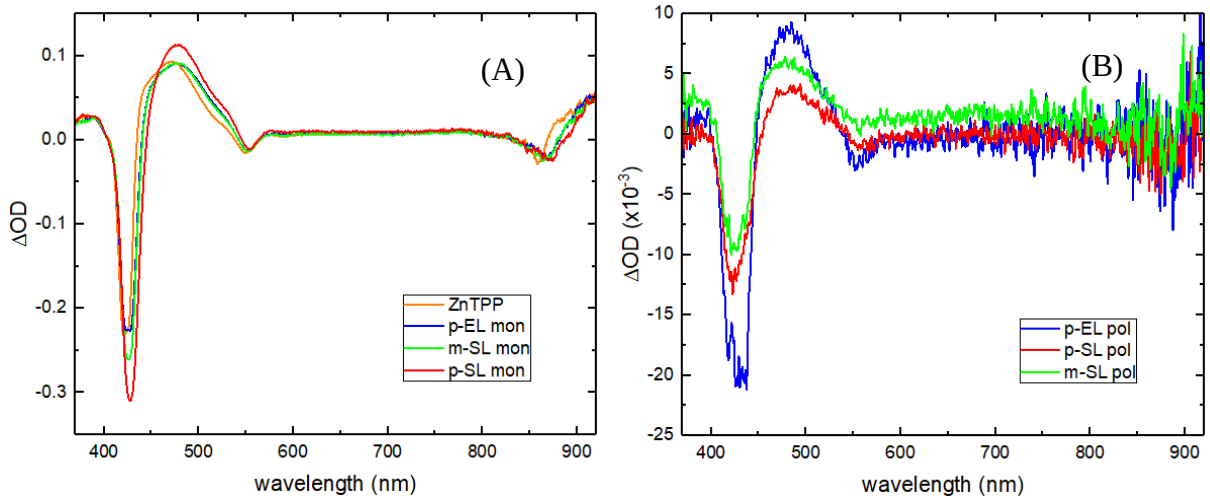

Figure 4.21: (A) Transient absorption spectra of ZnTPP **2.4** and the model compounds **4.1 – 4.3** and (B) polymers **4.4 – 4.6**.

Table 4.5: Triplet absorption maxima for ZnTPP **2.4**, the model compounds **4.1 – 4.3** and polymers **4.4 – 4.6**.

Compound	λ_{max} (nm)
ZnTPP **2.4**	473
p-SL mon **4.1**	480
m-SL mon **4.2**	477
p-EL mon **4.3**	476
p-SL pol **4.4**	494
m-SL pol **4.5**	478
p-EL pol **4.6**	485

β-substitution with the stilbene moiety has close to no effect on the triplet transient absorbance profile for the *meta*-linked model compound, although a small yet observable increase in triplet absorbance is present in the T_1-T_s absorption when the stilbene is linked at the *para*- position (Figure 4.21 (A)). This shows that the β-stilbene moiety does not contribute to the triplet absorption unless there exists a degree of direct conjugation from the stilbene directly into the porphyrin plane in order to significantly modify the triplet energy level manifold in a similar manner to the compounds discussed in chapter 3. The lowest triplet energy of ZnTPP **2.4** (1.59 eV)[20] is significantly lower than that of *trans*-stilbene (2.12 eV),[38] thus ruling out triplet energy transfer from ZnTPP **2.4** to the *trans*-stilbene β-substituent as a viable triplet deactivation pathway for ZnTPP **2.4**. The triplet absorbance decreases in the polymer series with increasing degrees of conjugation into the β-substituent (Figure 4.21 (B)), which may suggest that the close proximity of the polymer pendants causes increased crowding around the stilbene linker that in turn may rotate the stilbene moiety into a more planar orientation in the polymer than would exist in the model compound. The orientation of the stilbene is shown for both *para*- and *meta*-stilbene-linked model compounds, *p*-SL mon **4.1** and *m*-SL mon **4.2**, to be almost perpendicular to the porphyrin plane in the solid state as seen in the crystal structures in Figures 4.8 and 4.13, and in the crystal structures of previously studied β- oligo-*p*-PV substituted ZnTPP derivatives.[12]

4.8 Triplet Decay Kinetics

In order to obtain mechanistic information for the triplet decays in the model and polymer series, their kinetic transient decay traces were obtained by monitoring ΔOD over time. All kinetic traces were obtained by monitoring the T_1-T_s absorption at the respective absorption maxima for each compound in degassed toluene using a 532 nm pump excitation wavelength laser source (Nd:YAG 2^{nd} harmonic). Mechanistic modeling of decay processes was performed in conjunction with Prof. Ronald P. Steer (University of Saskatchewan) and fitting of experimental triplet decay data was assisted by Prof. Trevor A. Smith (University of Melbourne).

4.8.1 Model Compound Triplet Decay Kinetics

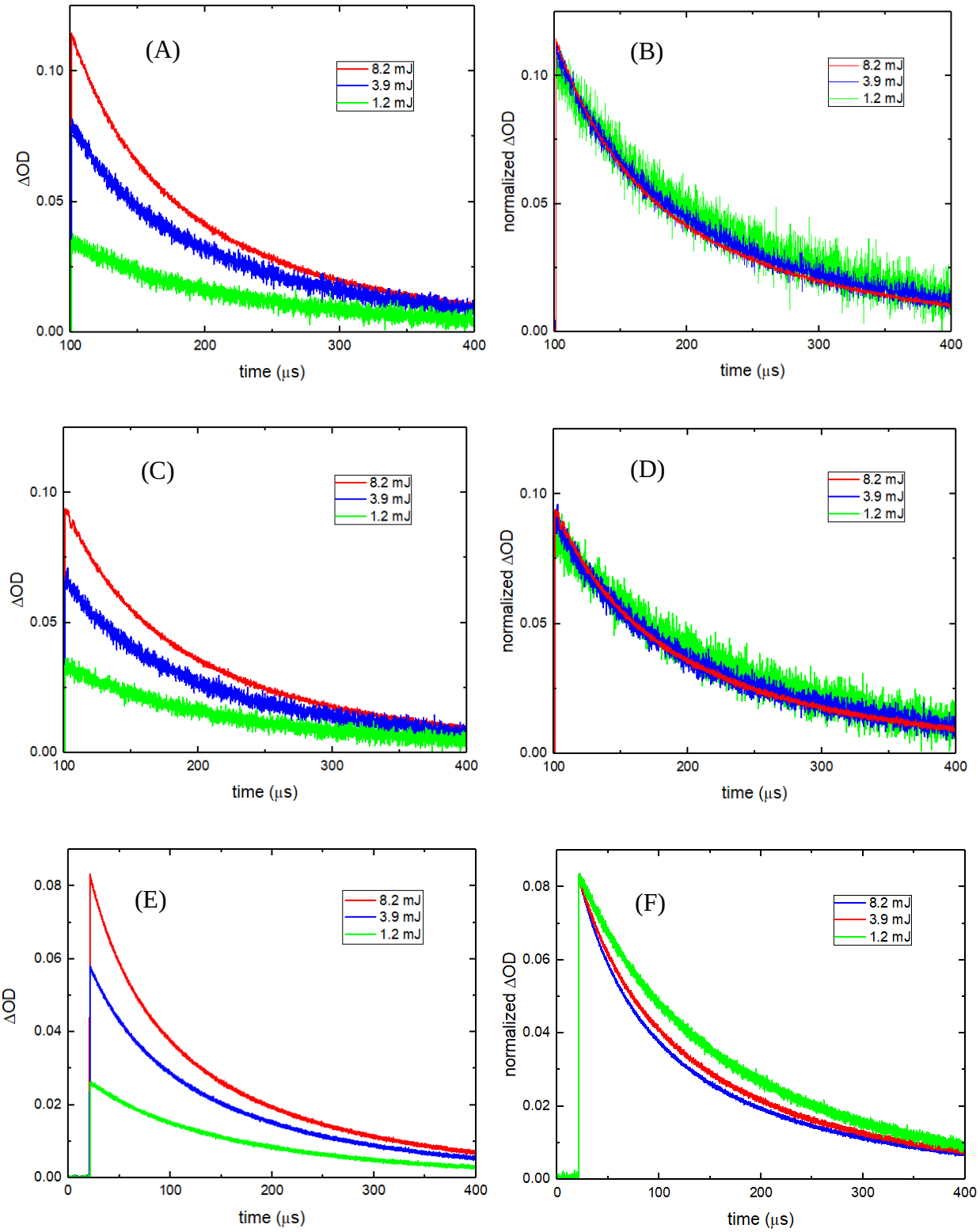

Figure 4.22: (A), (C) and (E) Kinetic traces of ΔOD for *p*-SL mon **4.1**, *m*-SL mon **4.2** and *p*-EL mon **4.3** respectively excited at pump excitation pulse energies of 1.2 mJ (green), 3.9 mJ (blue) and 8.2 mJ (red). (B), (D) and (F) Kinetic traces of ΔOD for *p*-SL mon **4.1**, *m*-SL mon **4.2** and *p*-EL mon **4.3** respectively shown with ΔOD normalized at the onset of decay to the 8.2 mJ pulse data.

From the normalized excitation energy dependent traces in Figure 4.22, the change in the steepness of the curves clearly shows increasing decay rates as the excitation energy from the pump source is increased. The rate equation for a first-order triplet transient absorption decay is represented by Equation 4.1:

$$\Delta OD(t) = \varepsilon_{T1}[C_0]e^{-kt} \qquad 4.1$$

where ΔOD(t) is the difference in absorption before and after the sample is excited by the pump pulse at time t, ε_{T1} is the triplet extinction coefficient at the $T_1 \rightarrow T_s$ absorption maximum, $[C_0]$ is the initial triplet concentration at time t=0, and k is the first-order rate constant for the decay of the triplet state population. ε_{T1} for all monomer compounds was approximated by experimental data obtained by Hurley *et al.* for ZnTPP **2.4** in toluene,[39] as all triplet absorptions measured at the same excitation energy and initial absorption (Figure 4.21) have very similar intensity to ZnTPP **2.4**. From equation 4.1, no change in rate would be expected for a single exponential decay with variation in initial concentration of triplet states, therefore triplet-triplet annihilation in the model compound sample must be occurring, and a combined first-plus-second order rate equation must employed when deriving the lifetimes of the components due to both ISC to the ground state and TTA that contribute to the overall triplet decays. The proposed excited state processes occurring in the model compounds (M) are outlined in Figure 4.23 below. Process I_a represents absorption of pump laser light by the monomer sample, ϕ represents S_1 emission, ϕ_{isc} is intersystem crossing to the triplet state from S_1, k_1 is the first-order intersystem crossing relaxation from T_1 to S_0, k_2 is the second-order TTA process yielding either the second excited singlet state S_2 or a higher excited triplet state T_n where n>1, and ϕ_{T1} represents the triplet recycling of S_2 states formed as a product of TTA in process k_2.

$M(S_0) + h\nu_{532nm} \rightarrow M(S_1)$	I_a
$M(S_1) \rightarrow M(S_0) + h\nu_f$	ϕ
$M(S_1) \rightarrow M(T_1)$	ϕ_{isc}
$M(T_1) \rightarrow M(S_0)$	k_1
$M(T_1) + M(T_1) \rightarrow M(S_2, T_n) + M(S_0)$	k_2
$M(S_2) \rightarrow M(S_1) \rightarrow M(T_1)$	$\phi_{T1} < 10^{-3}$

Figure 4.23: Excited state decay pathways active in the monomeric zinc porphyrins upon exposure to a 532 nm wavelength excitation source in solution.

The kinetic scheme in Figure 4.23 allows for a combined first-plus-second order decay function, outlined by Equation 4.2, to be fit to the triplet-triplet transient absorption decay profiles shown in Figure 4.22:

$$\Delta OD(t) = \varepsilon_{T1}.\frac{[C_0]e^{-k_1 t}}{1 + \frac{k_2}{k_1}[C_0] - \frac{k_2}{k_1}[C_0]e^{-k_1 t}} \qquad 4.2$$

FLASH software from Edinburgh Instruments® was used to globally fit the kinetic traces with varied excitation energy for the model compounds in Figure 4.22 to the first plus second order rate equation (4.2), to yield the rate constants k_1 and k_2 shown in Table 4.6 below. The goodness of fit of the rate equation to the kinetic profiles were determined by the reduced chi-squared (χ^2) parameters calculated by the FLASH software which ranged from 0.937 to 1.055. The calculated triplet concentrations $[C_0]$ are shown in Table 4.6. The fractional contribution of k_1 and k_2 to the overall triplet decays are represented by F_1 and F_2 respectively in Table 4.6. The first-order contribution to the decay profile was estimated by substituting the parameters $[C_0]$ and k_1 obtained from the global fits to the data in Figure 4.22 using the first-plus-second order equation 4.2, and ε_{T1} from Hurley *et al.*,[39] into equation 4.1. The decay curve obtained for the estimated first-order contribution to the overall decay was then normalized to the experimental data at the longest time scale data points where second-order contributions to the overall decay can be assumed to be negligible. F_1 was estimated by calculating the area under curve of the normalised

first-order contribution to the decay profile. The area under experimental decay data was corrected for the contribution at very long decay times, by adding the area under the curve from the estimated first-order decay contribution at timescales beyond the collected data to the experimental data total area under the curve. F_2 was then estimated by subtracting the area from the normalized estimated first-order contribution to the total decay from the corrected area under the experimental decay curve.

Table 4.6: Kinetic parameters obtained from fitting the triplet decay data from the monomer compounds *p*-SL mon **4.1**, *m*-SL mon **4.2** and *p*-EL mon **4.3** to the combined first-plus-second order decay equation 4.2. $[C_0]$ is the initial triplet concentration obtained from the fits, F_n is the fraction of the total decay contributed by decay component n and k_n is the rate constant for decay component n, where n=1 for the first-order decay process and n=2 for the second-order decay process.

Compound	Excitation power (mJ)	$[C_0]$ (M)	F_1	k_1 (s^{-1})	F_2	k_2 ($M^{-1}s^{-1}$)
p-SL mon **4.1**	1.2	4.6×10^{-7}	0.88	5.5×10^{3}	0.12	5.0×10^{9}
	3.9	1.1×10^{-6}	0.83	5.5×10^{3}	0.17	5.0×10^{9}
	8.2	1.6×10^{-6}	0.73	5.5×10^{3}	0.27	5.0×10^{9}
m-SL mon **4.2**	1.2	4.4×10^{-7}	0.84	5.4×10^{3}	0.16	5.3×10^{9}
	3.9	8.8×10^{-7}	0.78	5.4×10^{3}	0.22	5.3×10^{9}
	8.2	1.3×10^{-6}	0.79	5.4×10^{3}	0.21	5.3×10^{9}
p-EL mon **4.3**	1.2	3.7×10^{-7}	0.80	4.1×10^{3}	0.20	7.9×10^{9}
	3.9	7.2×10^{-7}	0.74	4.1×10^{3}	0.26	7.9×10^{9}
	8.2	1.2×10^{-6}	0.71	4.1×10^{3}	0.29	7.9×10^{9}

The model compounds decay over lifetimes similar to those observed for previously studied β-substituted Zn(II) porphyrins.[20] The rate constants for the second-order decay processes (k_2) are on the order of 10^9 $M^{-1}s^{-1}$, suggesting that TTA is diffusion limited in the toluene solution. The fractional contributions of the decay profile due to TTA (F_2) listed in Table 4.6 generally increase with increasing excitation energy. This observation provides further evidence to suggest that the triplet decays of the monomer compounds do indeed follow first-plus-second order kinetics, as the fractional decay would remain similar with varying excitation energy if the monomer decays were able to be fit by a sum of exponential functions representing first-order kinetic processes.

4.8.2 Polymer Compound Triplet Decay Kinetics

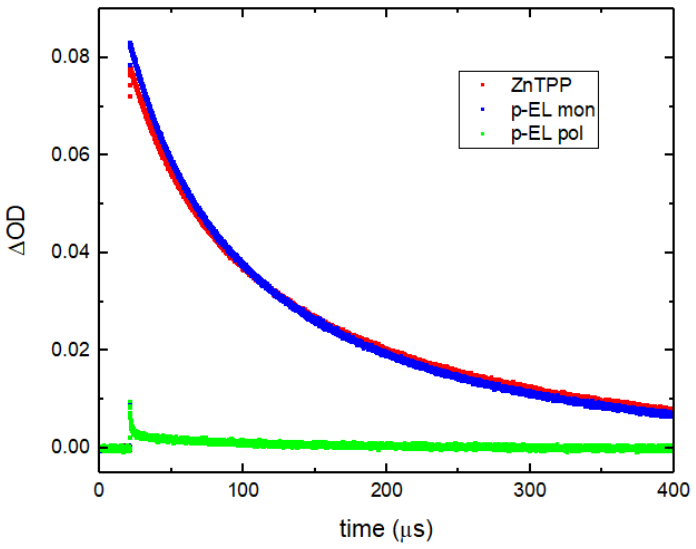

Figure 4.24: Kinetic traces of ΔOD for ZnTPP **2.4**, *p*-EL mon **4.3** and *p*-EL pol **4.6,** measured at their triplet absorption maxima of 473, 476 and 485 nm for ZnTPP **2.4**, *p*-EL mon **4.3** and *p*-EL pol **4.6** respectively. All samples were excited at pump excitation pulse energies of 8.2 mJ.

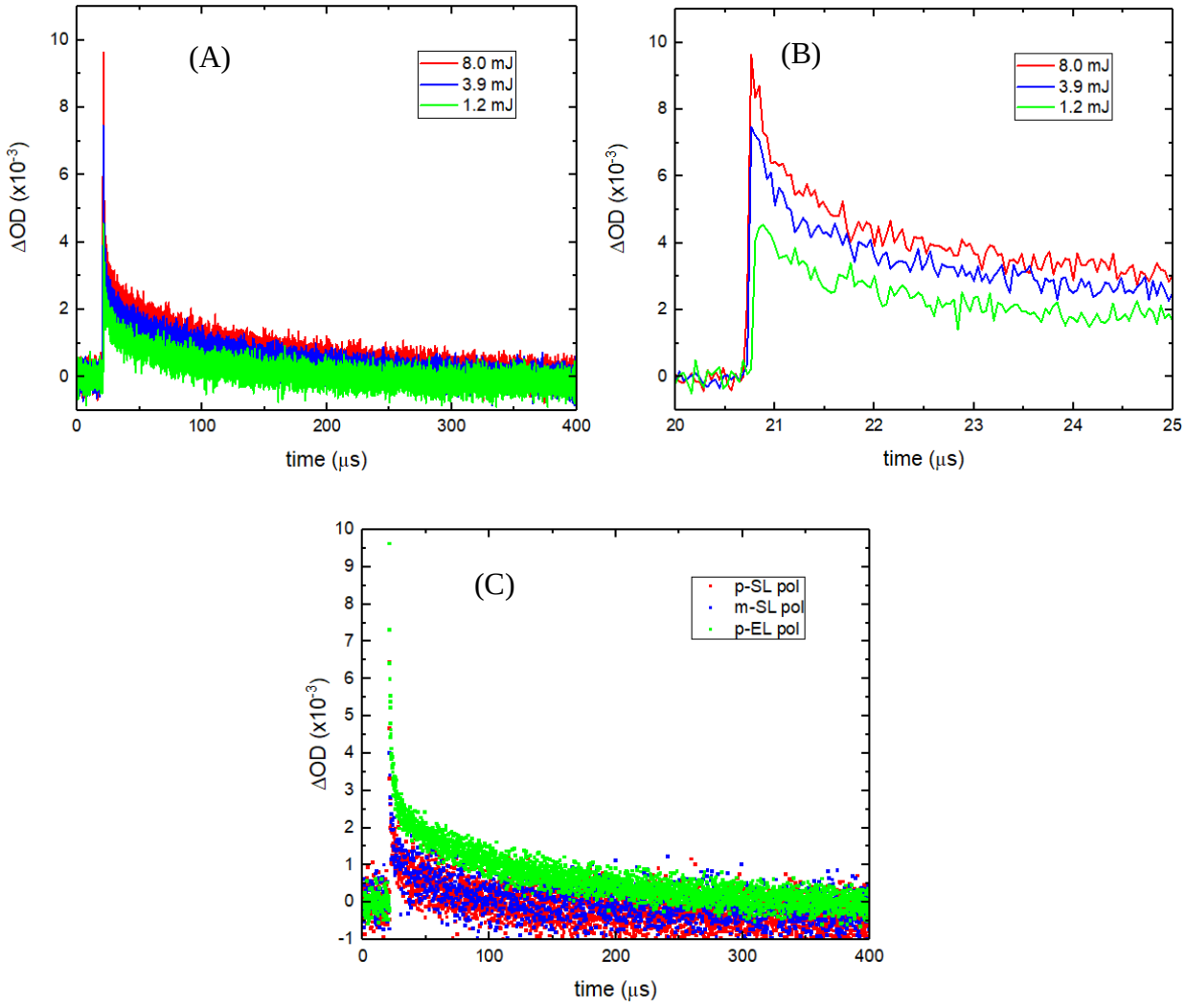

Figure 4.25: (A) Triplet kinetic traces of ΔOD for the *p*-EL pol **4.6** excited at pump excitation pulse energies of 1.2, 3.9 and 8.0 mJ. (B) Polymer triplet kinetic traces in (A) shown in the region of 20 to 25 μs after probe excitation for clarity of fast triplet decay component. (C) Polymer triplet kinetic traces for p-SL pol **4.4**, m-SL pol **4.5** and p-EL pol **4.6** at 8.2 mJ.

The kinetic traces in Figure 4.22 and the fits to the data in Table 4.6 show that ZnTPP **2.4** and the model compound *p*-EL mon **4.3** decay in similar fashion with comparable lifetimes. As seen in the transient absorption spectra in Figures 4.24 and 4.25, the initial ΔOD for the monomers is far larger than that for their respective polymer kinetic trace. The triplet states of the polymers appear to decay faster with increasing conjugation into the porphyrin plane, similar to the trends observed in Chapter 3 with increasing oligo-*p*-PV substituent length. Interestingly, the kinetic triplet decay traces of the polymers **4.4 – 4.6** exhibited fast decay components that exist only over the first few microseconds from the onset of their decay profiles (Figures 4.24 and 4.25). Transient decays obtained by Fujitsuka *et al.* on meso-linked pendant Zn(II) porphyrin polymers show no fast component in the triplet kinetic traces, and can be fit to a single exponential function,[3] suggesting that the β-substitution pattern and/or the relative orientation or spacing of the porphyrins in the polymers **4.4 – 4.6** allow the triplet excited porphyrin pendant units to access additional triplet decay mechanisms not accessible in the meso-linked Zn(II) pendant polymers.

Considering the polymer UC fluorescence quantum yields are approximately 2 orders of magnitude lower than that of their analogous monomers (Table 4.4) and the monomer UC fluorescence quantum yields themselves are very small (on the order of 10^{-4} - 10^{-5}), the contribution of TTA to the overall triplet decay is likely to be negligible and thus cannot account for the rapid decay observed for the polymers **4.4 – 4.6** over the first few μs of their triplet absorption decay profiles. A mechanism to account for the observed excited state decay behavior in Figures 4.24 and 4.25 was proposed, as outlined in Figure 4.26. In this mechanism, the generic polymer P is labeled as $P_n(X)$, numbered n, in excited state X. Upon absorption of light in the Q-band, a single pendant porphyrin unit is excited into the first singlet excited state ie. $X = S_1$. In conditions where the excited pendant porphyrin is isolated from other chromophores or interacts minimally with chromophores in the local environment, the excited polymer can relax to the ground state after ISC into the triplet state first (1A in Figure 4.26 below), in the same manner as the k_1 decay pathway for the monomers in Figure 4.22, or directly to the ground state predominantly via efficient internal conversion (1B) or via fluorescence. Mechanism 1A is the

major pathway for the decay of the triplet states in the polymers as seen by the long-lived tail of the polymer triplet decays in Figure 4.25 above.

Within the lifetime of the S_1 excited state, rotation of the excited pendant units may occur in the polymer chain in solution, bringing the excited pendant chromophores in appropriate proximity and orientation relative to their neighbouring ground state pendant units such that intramolecular transient excimers may form (mechanisms 2A and 2B in Figure 4.26). Excimeric quenching of excited chromophores by neighbouring ground state chromophores in pendant chromophore polymers has been previously described in the studies of Fox *et al.*[2] for singlet excimer formation and Ito *et al.*[4,5] for triplet excimer formation. A rotation-induced transient excimer forming mechanism for the excited state decays of the polymers is consistent with the lack of excitonic splitting observed in the absorption spectra of the polymers (Figure 4.16). An additional transient excimer quenching mechanism may occur due to intermolecular association of excited pendant porphyrins with the ground state pendant porphyrin units on separate polymer chains (mechanisms 3A and 3B in Figure 4.26).

Thus, to account for the portion of excited state porphyrins pendant units decaying on a short timescale in the polymers, kinetically competitive pairs of intramolecular and intermolecular excimer quenching mechanisms, 2A/2B and 3A/3B respectively, were hypothesized to contribute to the singlet decays observed in Figure 4.17 (B) and triplet decays in Figure 4.25. Only a small fraction of the overall triplet decay is assumed to proceed via mechanisms 2A and 3A due to the small area under the curves of the polymer triplet decay profile in the first few microseconds.

$$P_1(S_0) + h\nu_{532} \rightarrow P_1(S_1) \rightarrow P_1(T_1) \rightarrow P_1(S_0) \quad (1A)$$

$$P_1(S_1) \rightarrow P_1(S_0) \quad (1B)$$

$$P_1(S_1)\ldots P_1(S_0) \rightarrow P_1(T_1)\ldots P_1(S_0) \rightarrow P_1(S_0) + P_1(S_0) \quad (2A)$$

$$P_1(S_1)\ldots P_1(S_0) \rightarrow P_1(S_0)\ldots P_1(S_0) \quad (2B)$$

$$P_1(S_1) + P_2(S_0) \rightarrow P_1(T_1)\ldots P_2(S_0) \rightarrow P_1(S_0) + P_2(S_0) \quad (3A)$$

$$P_1(S_1) + P_2(S_0) \rightarrow P_1(S_0) + P_2(S_0) \quad (3B)$$

Figure 4.26: Mechanistic pathways contributing to the decay of the excited states of porphyrins incorporated as pendant units in polymeric structures **4.4 – 4.6**.

Given that the mechanism in 1A Figure 4.26 is a first-order process, and mechanisms 2A and 3A are pseudo-first order processes, the triplet decay profiles in Figure 4.24, 4.25 and 4.27 were able to be fit to a sum of three simultaneous monoexponential functions (Equation 4.3). The rate constant k_{1A} for the triplet decay representing mechanism 1A in Figure 4.26 (Table 4.7) was derived from the best fit of the polymer triplet decays to a single-exponential function at long time scales. The k_{1A} rate constant for *p*-EL pol **4.6** was extracted from global fits to polymer decays at 8.2, 3.9 and 1.2 mJ however the k_{1A} rate constants for *p*-SL pol **4.4** and *m*-SL pol **4.5** were extracted only from fits to the 8.2 mJ run. Although the first order rate constant k_{1A} should not vary with excitation energy, the global fit for the triplet decay of *p*-EL pol **4.6** may be more accurate as the signal-to-noise ratio is high for the polymer decay profiles at long time scales. The kinetic traces for the polymer triplet decays were recorded over the timescale 0-1000 ns in order to maximize resolution of data points in the rapid region of triplet decay in the polymers (Figure 4.27). The 0-1000 ns timescale polymer decay traces at various excitation energies were then globally fitted to triple-exponential functions (Equation 4.3) using FLASH software from Edinburgh Instruments® to obtain the rate constants k_{2A} and k_{3A} for the mechanisms 2A and 3A respectively in Figure 4.26 (Table 4.7). The goodness of fit of the rate equation to the kinetic profiles in Figures **4.25** and **4.27** were determined by the reduced chi-squared (χ^2) parameters calculated by the FLASH software which ranged from 1.048 to 1.123.

$$\Delta OD(t) = \varepsilon_T[C_0]e^{-k_{1A}t} + \varepsilon_T[C_0]e^{-k_{2A}t} + \varepsilon_T[C_0]e^{-k_{3A}t} \qquad 4.3$$

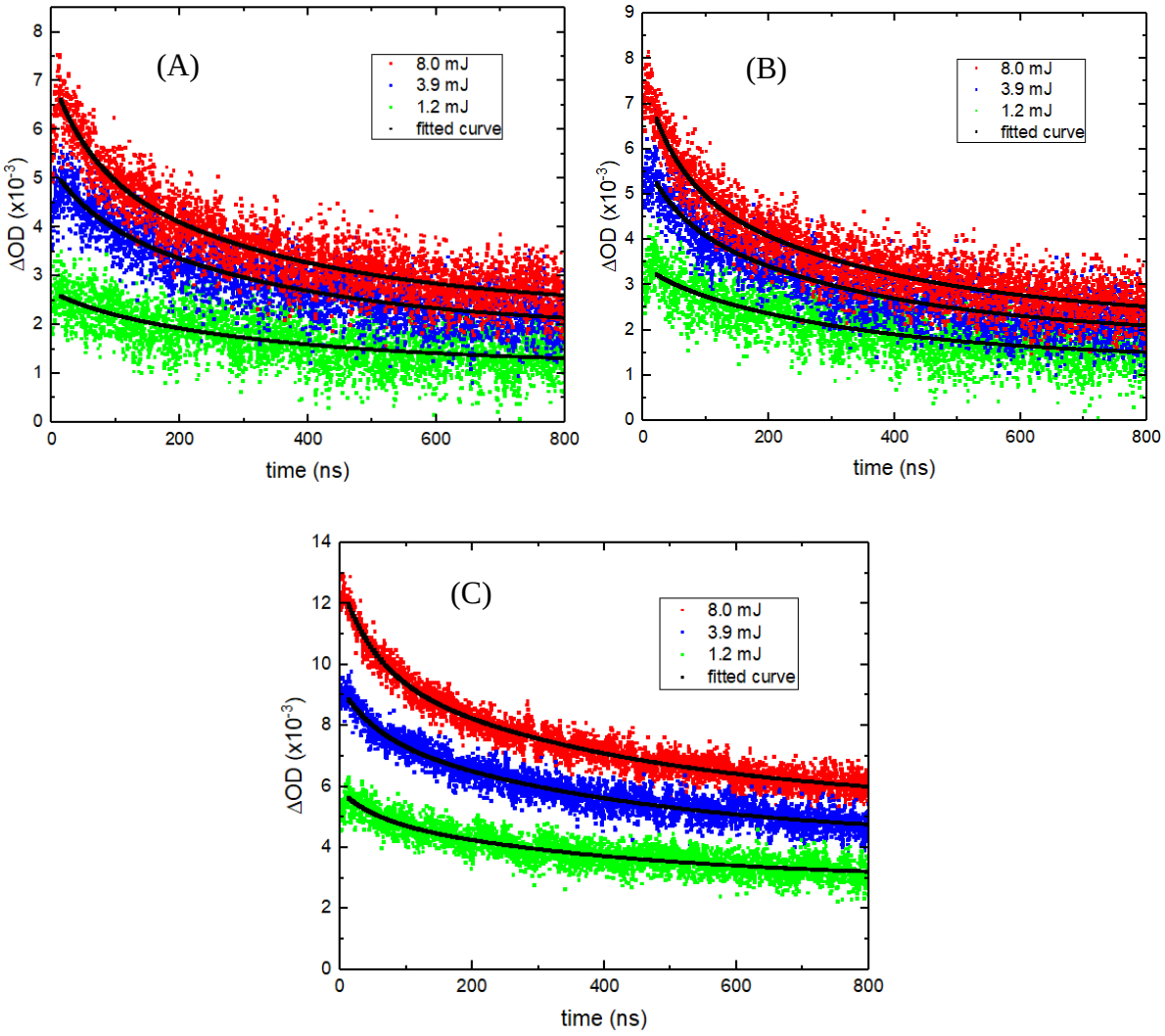

Figure 4.27: Kinetic traces for triplet decays in (A) *p*-SL pol **4.4**, (B) *m*-SL pol **4.5** and (C) *p*-EL pol **4.6** at excitation energies of 8.0 mJ (red dots), 3.9 mJ (blue dots) and 1.2 mJ (green dots). Fits to the triple-exponential mechanism outlined in Figure 4.26 are overlaid on their respective kinetic traces (black lines).

Table 4.7: Kinetic parameters obtained from fitting the triplet decay data from the polymer compounds *p*-SL pol **4.4**, *m*-SL pol **4.5**, and *p*-EL pol **4.6** to the combined triple exponential decay equation 4.3.

Compound	k_{1A} (s^{-1})	k_{2A} (s^{-1})	k_{3A} (s^{-1})
p-SL pol **4.4**	1.14×10^4	2.98×10^6	1.69×10^7
m-SL pol **4.5**	2.41×10^4	2.94×10^6	1.89×10^7
p-EL pol **4.6**	3.82×10^3	2.32×10^6	1.86×10^7

The rate constant $k_{1A} = 3.82 \times 10^3$ s^{-1} for the polymer *p*-EL pol **4.6** lies within the same order of magnitude as the observed rate constant for p-EL mon **4.3** (4.1×10^3 s^{-1} from Table 4.6), consistent with T_1-S_0 ISC occurring in isolated excited pendant porphyrin units. The k_{1A} values for *p*-SL pol **4.4** and *m*-SL pol **4.5** are approximately an order of magnitude greater than their respective monomeric first-order rate constants, which is likely due to greater difficulty fitting their polymer decays created by the large signal-to-noise ratio of those data sets at long timescales. Regardless, the first-order rate constants obtained from these fits were fixed as the parameter k_{1A} in the triple-exponential functions used to fit the short timescale polymer triplet decays in Figure 4.27.

The high qualities of the fits of the triple exponential functions to the polymer triplet decay data (black lines in Figure 4.27) at short timescales corroborate the proposed mechanism outlined in Figure 4.26. The rate constants k_{2A} and k_{3A} were calculated to be on the order of 10^6 and 10^7 s^{-1} respectively for all polymer compounds **4.4 – 4.6**, suggesting that variation of the nature of the linking group within the studied set of polymer compounds does not play an important role in facilitating inter- or intramolecular triplet quenching by ground state metalloporphyrins in close proximity.

4.9 Conclusion

A series of zinc porphyrin appended polymers and their monomeric analogues were designed with varying degrees of backbone-to-pendant flexibility and rotation-induced conjugation for analysis of their intramolecular exciton dynamics in the framework of TTA-UC. The pendant polymers were synthesized by performing post-polymerization functionalization on a polymer backbone previously synthesized using RAFT polymerization. Broadening of ^{1}H NMR signals and UV-visible absorption peaks of the polymers provided evidence for effective inclusion of the zinc porphyrin pendant units into the polymeric structure.

S_1 fluorescence decay profiles of the polymers exhibited additional fast decay components not observed in their monomeric analogues, suggesting enhanced rate of IC due to electronic interactions of neighbouring porphyrins in the pendant polymer structure. The lack of excitonic splitting in the solution-state absorption spectra and the similar fluorescence quantum yield of the polymers compared to their monomeric analogues suggest that the pendant units are not pre-aggregated or otherwise strongly electronically coupled prior to population of the S_1 excited state. The observed S_1 excited state quenching was thus hypothesized to occur between excited state and ground state pendant porphyrin chromophores through singlet excimer-type electronic coupling induced by rotation of the pendant units along the pendant-to-backbone linking moiety.

Upconverted fluorescence yields in solution of all β-substituted monomers decreased considerably with respect to ZnTPP **2.4**, however the degree of conjugation in the rotatable β-phenyl or stilbene substituent did not have a large effect on relative UC yields. UC yields of β-substituted polymers were 2 orders of magnitude lower than their respective analogous monomer compounds. The effect of coordinating solvent on UC fluorescence yields was less pronounced in *p*-EL pol **4.6** compared to *p*-EL mon **4.3**, presumably due to greater obstructed access of solvent molecules to coordination sites in the polymer compared to the monomer. *p*-EL pol **4.6** exhibited a linear relationship in the excitation power-UC fluorescence intensity log-log plots across all excitation energies, suggesting the mechanism of TTA-UC in the polymer is different to that of its monomeric analogue. Further studies are required in order to elucidate the formal difference in the TTA-UC mechanisms between the monomers and polymers.

Transient absorption spectroscopy of the polymers showed a decrease in the transient absorption intensity of the polymers in their triplet state with increasing degrees of rotation-induced conjugation in the linking moiety, which may suggest alignment of the stilbenoid units with the porphyrin planes in the crowded pendant environment. Triplet decay analysis revealed that the polymers did not decay via a first-plus-second order decay mechanism exhibited by all monomers, but via a three-component multi-exponential decay pathway. The hypothetical mechanism for the polymer triplet decays involved contributions from pseudo first-order processes attributed to quenching of the triplet excitons in the pendant porphyrins units by neighbouring ground state pendant units and ground state chromophores on independent polymer chains. Fits to the experimental triplet decay data under the proposed mechanism were excellent and were consistent with the concept that TTA contributed negligibly to the overall triplet decay profiles of the polymers reflected in their very small S_2 UC fluorescence quantum yields. The pendant zinc porphyrin polymers studied in this chapter are thus unlikely to be effective dual absorber-upconverters for use in light harvesting applications.

4.10 References

(1) Solomon, L. A.; Sykes, M. E.; Wu, Y. A.; Schaller, R. D.; Wiederrecht, G. P.; Fry, H. C. *ACS Nano* **2017,** *11*, 9112−9118.

(2) Fox, M. A.; Britt, P. F. *Macromolecules* **1990,** (23), 4533.

(3) Fujitsuka, M.; Okada, A.; Tojo, S.; Takei, F.; Onitsuka, K.; Takahashi, S.; Majima, T. *J. Phys. Chem. B* **2004,** *108*, 11935.

(4) Ito, S.; Katayama, H.; Yamamoto, M. *Macromolecules* **1988,** *21*, 2456.

(5) Ito, S.; Numata, N.; Katayama, H.; Yamamoto, M. *Macromolecules* **1989,** *22*, 2207.

(6) Wang, H.-W.; Liu, Z.-C.; Chen, C.-H.; Lim, T.-S.; Fann, W.; Chao, C.-G.; Yu, J.-Y.; Lee, S.-L.; Chen, C.-H.; Huang, S.-L.et al. *Chem. Eur. J.* **2009,** *15*, 5719

(7) Wuyts, C.; Dermaut, W.; Hoefnagels, R.; Aerts, G.; Goovaerts, E.; Geise, H. J. *Polym. Int.* **2003,** *52*, 1660.

(8) Larsen, J.; Brüggemann, B.; Khoury, T.; Sly, J.; Crossley, M. J.; Sundström, V.; Åkesson, E. *J. Phys. Chem. A* **2007,** *111*, 10589.

(9) Stevens, A. L.; Novakovic, S.; White, J. M.; Wong, W. W. H.; Smith, T. A.; Ghiggino, K. P.; Paige, M. F.; Steer, R. P. *J. Phys. Chem. A* **2018,** *122*, 9605−9614.

(10) Allen, M. T.; Whitten, D. G. *Chem. Rev.* **1989,** *89*, 1691.

(11) Liu, X.; Yeow, E. K. L.; Velate, S.; Steer, R. P. *Phys. Chem. Chem. Phys.* **2006,** *8*, 1298.

(12) Davis, W. B.; Ratner, M. A.; Wasielewski, M. R. *Chem. Phys.* **2002,** *281*, 333.

(13) Yang, S., I.; Prathapan, S.; Miller, M. A.; Seth, J.; Bocian, D., F.; Lindsey, J. S.; Holten, D. *J. Phys. Chem. B* **2001,** *105*, 8249.

(14) Yeow, E. K. L.; Ziolek, M.; Karolczak, J.; Shevyakov, S. V.; Asato, A. E.; Maciejewski, A.; Steer, R. P. *J. Phys. Chem. A* **2004,** *108*, 10980.

(15) Song, H.-e.; Kirmaier, C.; Schwartz, J. K.; Hindin, E.; Yu, L.; Bocian, D. F.; Lindsey, J. S.; Holten, D. *J. Phys. Chem. B* **2006,** *110*, 19121.

(16) Wang, R.; Gao, B.; Jiao, W.; Yu, L.; Pan, W. *J. Appl. Polym. Sci.* **2014,** *131* (15), 40516.

(17) Ragoussi, M.-E.; de la Torre, G.; Torres, T. *Eur. J. Org. Chem.* **2013,** (14), 2832.

(18) Megiatto Junior, J. D.; Spencer, R.; Schuster, D. I. *J. Mater. Chem.* **2011,** *21*, 1544.

(19) Bonfantini, E. E.; Burrell, A. K.; Campbell, W. M.; Crossley, M. J.; Gosper, J. J.; Harding, M. M.; Officer, D. L.; Reid, D. C. W. *J. Porphyrins Phthalocyanines* **2002,** *6*, 708.

(20) Ventura, B.; Flamigni, L.; Marconi, G.; Lodato, F.; Officer, D. L. *New J. Chem.* **2008,** *32*, 166.

(21) Giraudeau, A.; Callot, H. J.; Jordan, J.; Ezhar, I.; Gross, M. *J. Am. Chem. Soc.* **1979,** *101* (14), 3857.

(22) Gao, G.-Y.; Ruppel, J. V.; Allen, D. B.; Chen, Y.; Zhang, X. P. *J. Org. Chem.* **2007,** *72*, 9060.

(23) Di Carlo, G.; Orbelli Biroli, A.; Tessore, F.; Rizzato, S.; Forni, A.; Magnano, G.; Pizzotti, M. *J. Org. Chem.* **2015,** *80*, 4973−4980.

(24) Mo, Y.; Du, L.; Liu, L.; Huang, J.; Pan, Y.; Yang, B.; Xie, Z.; Ma, Y. *J. Phys. Chem. C* **2013,** *117*, 27081−27087.

(25) Sarker, A. N.; Gürel, E. E.; Zheng, M.; Lahti, P. M.; Karasz, F. E. *Macromolecules* **2001,** *34*, 5897.

(26) Sirithip, K.; Morada, S.; Namuangruk, S.; Keawin, T.; Jungsuttiwong, S.; Sudyoadsuk, T.; Promarak, V. *Tetrahedron Lett.* **2013,** *54*, 2435.

(27) Farinha, J. P. S.; Relógio, P.; Charreyre, M.-T.; Prazeres, T. J. V.; Martinho, J. M. G. *Macromolecules* **2007,** *40*, 4680.

(28) Moad, G.; Rizzardo, E.; Thang, S. H. *Polym. Int.* **2011,** *60*, 9.

(29) Willcock, H.; O'Reilly, R. K. *Polym. Chem.* **2010,** *1*, 149.

(30) Tilley, A. J.; Chen, M.; Danczak, S. M.; Ghiggino, K. P.; White, J. M. *Polym. Chem.* **2012,** *3*, 892.

(31) Strachan, J.-P.; Gentemann, S.; Seth, J.; Kalsbeck, W. A.; Lindsey, J. S.; Holten, D.; Bocian, D. F. *J. Am. Chem. Soc.* **1997,** *119*, 11191.

(32) Kim, P.; Lim, J. M.; Yoon, M.-C.; Aimi, J.; Aida, T.; Tsuda, A.; Kim, D. *J. Phys. Chem. B* **2010,** *114*, 9157.

(33) Yoon, M.-C.; Cho, S.; Kim, P.; Hori, T.; Aratani, N.; Osuka, A.; Kim, D. *J. Phys. Chem. B* **2009,** *113*, 15074.

(34) Stel'makh, D. F.; Tsvirko, M. P. *Zh. Prikl. Spektrosk.* **1982,** *36*, 606−619.

(35) Sugunan, S. K.; Tripathy, U.; Brunet, S. M. K.; Paige, M. F.; Steer, R. P. *J. Phys. Chem. A* **2009,** *113*, 8548.

(36) Fukuzaki, A.; Kawai, H.; Sano, T.; Takehara, K.; Nagamura, T. *ACS Biomater. Sci. Eng.* **2017,** *3*, 1809−1814.

(37) Vadrucci, R.; Weder, C.; Simon, Y. C. *Mater. Horiz.* **2015,** *2*, 120.

(38) Herkstroeter, W. G.; Hammond, G. S. *J. Am. Chem. Soc.* **1966,** *88*, 4769.

(39) Hurley, J. K.; Sinai, N.; Linschitz, H. *Photochem. Photobiol.* **1983,** *38* (1), 9.

Chapter 5

Conclusion, Limitations and Future Work

5.1 Summary and Conclusion

The efficiency of solar photovoltaics employing high band gap light-absorbing materials has the potential to be increased by integration of homo-NCPU-TTA systems. The sensitizers currently best suited to homo-NCPU-TTA applications are zinc(II) metalloporphrins however these sensitizers require significant optimization to effectively increase cell efficiencies. As TTA proceeds via a Dexter energy-exchange mechanism, increased proximity and orbital overlap between annihilating species is generally desirable. Electronic interactions between metalloporphyrins in close proximity can result in rapid excited state relaxation processes however that significantly inhibit NCPU-TTA. It was thus necessary to gain a better understanding of the factors that increase energy-exchange between annihilating species and minimize unwanted excited state relaxation processes when designing effective NCPU-TTA systems employing zinc metalloporphyrins. With these considerations in mind, the work presented in this thesis investigated the effects of varying the proximity, relative orientation and degree of orbital overlap between zinc porphyrin chromophores, on the facilitation of homomolecular NCPU-TTA.

Chapter 2 outlined the synthesis and photophysical characterization of a series of *meso*-di-substituted and tetra-substituted zinc(II) tetraphenylporphyrin derivatives in order to investigate the effect of varying the steric bulk of the meso-phenyl substituents on homo-NCPU-TTA yields. Increasing the steric bulk of the meso-positions on the porphyrins from a phenyl group to di-tert-butylphenyl and mesityl groups was found to produce a higher yield of homo-NCPU-TTA fluorescence in the solution state for both di- and tetra-substituted porphyrins. In solid state PVA films however, the di-substituted porphyrins demonstrated no observable UC fluorescence while the tetra-substituted porphyrins produced an increase in UC fluorescence yields compared to the yields in the solution state. Computational studies suggested that the lack of observable UC in solid state PVA films for the di-substituted porphyrins may be due to an increased number of available minimum energy dimeric aggregate orientations in which porphyrins could become trapped in, with respect to the tetra-substituted porphyrin series. In several of such aggregates, porphyrins may not be oriented or spaced appropriately for homo-NCPU-TTA to occur. These results highlighted the necessity to provide adequate conditions for the formation of PVA thin films in zinc(II) metalloporphyrin-sensitized NCPU-TTA applications such that control over the orientation of metalloporphyrin aggregates is exercised. Further work is being pursued in order to optimize conditions for dimeric aggregate formation through the synthesis of porphyrins with asymmetric steric bulk. These porphyrins may allow for control over interplanar porphyrin aggregate orientation through a type of puzzle piece-like dimeric association forcing the formation of potentially optimally oriented dimeric aggregates.

As PVA films are flexible solid state materials, easily fabricated and provide oxygen barrier properties, solid-state PVA based NCPU-TTA systems employing sterically-bulky zinc(II) metalloporphyrins may have promise for future device integration. PVA hydroxyl groups can however bind to the zinc metal centre of the porphyrins, inhibiting formation of minimum energy aggregates optimally oriented for TTA in the film formation process. The most sterically bulky and highly substituted porphyrins are likely to experience reduced PVA binding, thus may be able to form optimum aggregates more readily. Sterically-bulky zinc(II) tetramesitylporphyrin **2.6** was able to improve NCPU-TTA fluorescence yields in solid state PVA by a factor of approximately 20 in comparison to the less-bulky zinc(II) tetraphenylporphyrin **2.4**. Chapter 2

thus demonstrated examples of successful optimization of UC systems through simple covalent design of metalloporphyrin structures. The synthesis of even bulkier porphyrins, such as meso-5,10,15,20-tetrakis(2,4,6-triethyl)phenylporphyrin[1] and meso-5,10,15,20-tetrakis(2,4,6-triphenyl)phenylporphyrin,[2] would be required in the future in order to determine a limit for the maximum steric bulk and thus optimum Zn-Zn separation distances that produce increases in solid-state PVA homo-NCPU-TTA fluorescence yields before a drop-off in yield was observed. Although such syntheses were pursued, including synthesis toward the novel extra bulky meso-5,10,15,20-tetrakis(2,4,6-tri-(3,5-di-tertbutylphenyl)phenylporphyrin, time constraints did not allow for complete synthesis and photophysical analysis of these materials.

The work presented in Chapter 3 was targeted at exploring the effect of extending the π-conjugation of zinc(II) metalloporphyrin polymer pendant units on the potential of the pendant polymers to facilitate intramolecular homo-NCPU-TTA. To this end, a series of polymers and their monomeric analogues with pendant zinc(II) metalloporphyrin substituents, with varying degrees of extended π-conjugation at the β-position of the porphyrin macrocycle were successfully synthesized using Horner-Wadsworth-Emmons reactions and post-polymerization functionalization techniques.

Increasing the π-conjugation of porphyrin pendant units resulted in higher extinction coefficients desirable for TTA, however extinction coefficients were reduced in the polymers compared to the monomers due to inter-pendant electronic interactions. The triplet transient absorption intensity decreased with increasing porphyrin conjugation length as previously reported[3] however triplet absorption was almost absent when extended conjugation porphyrins were included into pendant polymer structures. The very low triplet populations interpreted from the triplet absorption spectra indicate that polymers with β-conjugation-extended pendant porphyrin units are unlikely to yield any significant population of S_2 excited state produced via NCPU-TTA and are thus inappropriate candidates for UC applications.

The weak triplet absorptions coupled with the low S_1 fluorescence quantum yields in the pendant polymers suggested that the majority of the S_1 population that forms upon absorption of light by conjugation-extended pendant porphyrin polymers rapidly relaxes via IC. The high degree of IC in these polymers is likely caused by the proximity of the chromophores in the pendant polymer structure and exacerbated by increased π-π inter-pendant interactions between porphyrins upon porphyrin macrocycle conjugation extension. It is therefore evident that increasing proximity and orbital overlap between porphyrins can play a detrimental role in the facilitation of NCPU-TTA for polymers with pendant units constituted of zinc(II) metalloporphyrins with extended π conjugation.

Chapter 4 investigated in detail the singlet and triplet exciton dynamics in polymers with rotatable pendant zinc(II) metalloporphyrin side groups with varied pendant-to-backbone linking groups. The polymers and monomeric model compounds were successfully synthesized using Horner-Wadsworth-Emmons reactions and post-polymerization functionalization techniques similar to those employed in Chapter 3. A significant outcome of the work in Chapter 4 was the observation of fluorescence from the S_2 state in the polymers **4.4 – 4.6** upon excitation in the Q-band absorption band. To the best our knowledge, no prior report exists in the literature that demonstrates the observation of homo-NCPU-TTA fluorescence from a polymer containing pendant chromophores.

An issue with the observed homo-NCPU-TTA fluorescence yield from the polymer compounds was that they were 2 orders of magnitude less intense than their respective analogous monomeric model compounds. This observation leads to the conclusion that integration of the porphyrin chromophores into the polymer structure is detrimental for the optimization of homo-NCPU-TTA fluorescence yields.

Unlike their monomeric analogues **4.1 – 4.3**, the polymers **4.4 – 4.6** exhibited bi-exponential S_1 relaxation suggesting that orbital interactions with ground state neighbouring porphyrins in close proximity accelerated IC from S_1 to S_0. The lack of excitonic splitting in the polymer absorption spectra further suggested that the accelerated IC observed in these pendant porphyrins is not due to pre-absorption aggregation in pendant units, but may rather be due to rotation of pendants while in their excited states to participate in excimer-like interactions with neighbouring ground state pendant porphyrins. The enhanced S_1 IC likely contributed to the weak triplet absorptions seen in the transient absorption spectra, suggesting low triplet yields in the polymers. The effects of varying the conjugation of the linking groups on the photophysical properties of the polymers was generally minimal across the polymer series, suggesting that the observed exciton quenching in polymers **4.4 – 4.6** was predominately due to the pendant environment of the porphyrins.

The lack of significant second-order triplet decay contribution to the polymer transient absorption decays indicated that only a tiny fraction of the initial triplet population, itself small in comparison to the initial S_1 population, contributed to NCPU-TTA fluorescence. Mechanisms to justify the observed triplet decay data were developed that suggested the monomeric model compounds decayed via first-plus-second order kinetics, while the polymers decayed via a sum of three simultaneous pseudo first-order kinetic processes. These mechanisms describe a transient triplet-excimer quenching process between neighbouring triplet excited and ground state pendant porphyrins that yields considerable ISC relaxation to S_0. The singlet and triplet excimer-like quenching observed for the compounds in Chapter 4 are not desirable for TTA systems and further highlights the sensitivity of proximity, orientation and orbital overlap when using metalloporphyrins as NCPU-TTA sensitizers. In the solid state, these quenching mechanisms would not only affect homo-NCPU-TTA systems but also hetero-NCPU-TTA systems within metalloporphyrin aggregate domains. It is therefore of importance when designing metalloporphyrin-based NCPU-TTA sensitizers to control the way that porphyrins interact in order to achieve optimal UC yields.

Although the rapid quenching of excitons is problematic for the optimizing NCPU-TTA yields in the pendant polymers studied in Chapter 3 and 4, an understanding of the quenching mechanisms as outlined above may aid the design of future NCPU-TTA systems. Future work to control inter-pendant interactions in polymers such as those studied in Chapters 3 and 4 may include the synthesis of polymers with spacing units between pendant groups in order to minimize both singlet and triplet excimer-like quenching while maintaining a degree of proximity control over the porphyrins. Polymer backbone functional group spacing could be achieved through the use of alternating copolymer syntheses such as RAFT polymerization of styrene and maleic anhydride.[4]

Probably the most significant limitations that still remain prominent in the pursuit of effective homo-NCPU-TTA systems based on metalloporphyrins are the short lifetimes of their S_2 excited states and the low fluorescence quantum yields from their S_2 excited states. Manifestation of this limitation was evident in the homo-NCPU-TTA fluorescence yields obtained in chapter 4 that ranged from between 10^{-5} and 10^{-7}. Rather than utilizing S_2 fluorescence directly, this issue may be resolved if effective S_2 excited state energy or electron transfer can be made possible. Such ultrafast S_2 excited state electron transfer from metalloporphyrins has been previously studied using axially-coordinated zinc(II) porphyrin-acceptor complexes[5] and covalently bound zinc(II) porphyrin-acceptor dyads.[6] Although electron transfer from porphyrin S_2 state to acceptor S_1 state was observable, rapid recombination leading to relaxation to S_1 currently hinders efficient S_2 energy extraction, therefore further work is required to optimize electron transfer processes from the S_2 state. Regardless of whether fluorescence or electron transfer from the S_2 state of metalloporphyrins proves the more efficient energy extraction technique, significant research progress is still required to render NCPU-TTA a viable methodology for the enhancement of efficiency of solar cells at the commercial scale.

5.2 References

(1) Moiseev, A. G.; Margulies, E. A.; Schneider, J. A.; Bélanger-Gariépy, F.; Perepichka, D. F. *Dalton. Trans.* **2014,** *43*, 2676.

(2) Suslick, K. S.; Fox, M. M. *J. Am. Chem. Soc.* **1983,** *105*, 3507.

(3) Ventura, B.; Flamigni, L.; Marconi, G.; Lodato, F.; Officer, D. L. *New J. Chem.* **2008,** *32*, 166.

(4) Moriceau, G.; Gody, G.; Hartlieb, M.; Winn, J.; Kim, H.; Mastrangelo, A.; Smith, T.; Perrier, S. *Polym. Chem.* **2017,** *8* (28), 4152.

(5) Harada, K.; Fujitsuka, M.; Sugimoto, A.; Majima, T. *J. Phys. Chem. A* **2007,** *111*, 11430.

(6) Robotham, B.; Lastman, K. A.; Langford, S. J.; Ghiggino, K. P. *J. Photochem. Photobiol. A* **2013,** *251*, 167.

Chapter 6

Experimental

6.1 General Experimental

6.1.1 Materials

Air-free and moisture-free reactions were performed under nitrogen gas atmosphere. All glassware was oven-dried prior to use in synthetic applications. Distilled petroleum spirits was used for washing final compounds. Anhydrous DCM and THF were obtained from a glass contour purification system. Anhydrous DCE was supplied by Sigma Aldrich sealed under nitrogen with a Sure/Seal™ seal. Sodium hydride was provided by Sigma Aldrich as a 60% dispersion in mineral oils and was washed 3 times with THF under nitrogen gas to remove the mineral oils before use. Pyrrole was freshly distilled prior to use. $Pd(PPh_3)_4$ was prepared by the Wong/Jones group and kept under nitrogen and refrigerated between use. α-(Dodecylthiocarbonothioylthio)-ω-(1-carboxyethyl)-poly(4-vinylbenzylchloride) (poly(VBC)-DoPAT) was provided by Dr. John Li from the White group laboratory (M_n = 4273 g/mol, M_n/M_w = 1.07). Reagents were used as provided by their respective suppliers without further purification in all synthetic and spectroscopic applications unless explicitly stated otherwise.

6.1.2 Purities

Thin-layer chromatography (TLC) was performed on aluminium sheets coated with Merck Silica gel 60 using various combinations of 40-60°C boiling point petroleum spirits, DCM, EtOAc, $CHCl_3$, toluene and MeOH. UV light was used as a detection method for TLC analysis. Silica gel column chromatography was performed using Grace Davisil® 40-63 μm (230-400 mesh) amorphous silicon dioxide and various combinations of 40-60°C boiling point petroleum spirits, DCM, EtOAc, $CHCl_3$, toluene and MeOH. Size exclusion chromatography (SEC) was performed using Bio-Beads™ S-X resin, using toluene or THF as eluent. ^{1}H NMR and ^{13}C NMR spectra were obtained on an Agilent 500 MHz spectrometer or Varian 600 MHz spectrometer. All chemical shifts are expressed in parts per million (δ) using residual solvent as reference (^{1}H NMR $CDCl_3$ δ = 7.26,[1] ^{13}C NMR $CDCl_3$ δ = 77.16,[1] ^{1}H NMR CD_2Cl_4 δ = 6.0[2]). ^{1}H NMR data was reported in the format: chemical shift (δ) followed by (integration, multiplicity, coupling constant (Hz), assignment). High-resolution mass spectrometry was performed using a Thermo Scientific MSPF Orbitrap Fusion™ spectrometer. Fourier Transform Infrared (FT-IR) spectra were obtained on a Perkin Elmer Spectrum One spectrometer from neat solid films. CD_2Cl_4 was used as the solvent for the polymer ^{1}H NMR analysis to improve the resolution of the spectrum using high temperature (80°C) conditions.

6.1.3 Porphyrin Nomenclature

The porphyrins with β-substituents of extended length or conjugation were subject to the nomenclature labeling system outlined in Figure 5.1 below. Each ring (excluding the meso-phenyl substituents) was labeled with a prime, with the number of primes increasing moving from the porphyrin ring (zero primes) to the terminal end of the extended β-substituent.

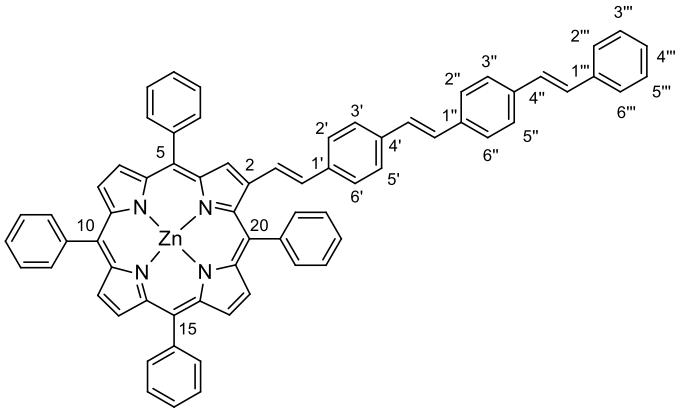

Figure 6.1: Labeling system employed for the assignment of nomenclature for porphyrins with β-substituents of extended length or conjugation.

6.1.4 Steady State Photophysics

Honeywell Burdick & Jackson B&J Brand® spectroscopic grade toluene and THF were used in all photophysical experiments. 6Q quartz cuvettes were used for all steady-state solution photophysical experiments. UV-visible absorption measurements were recorded using a Varian Cary 50 Bio spectrophotometer. Fluorescence spectra were recorded using a Varian Eclipse spectrofluorometer. Fluorescence quantum yields were calculated relative to zinc tetraphenylporphyrin as a standard (0.033 in toluene).[3] Steady-state photophysical measurements were obtained using solutions with optical density no greater than 0.1 in the Q-band of the porphyrins to minimize inner filter effects such as reabsorption or aggregation-induced quenching.

6.1.5 Transient Absorption and Triplet Decay Measurements

Nanosecond laser flash photolysis experiments were performed using a variation of a system previously described,[4] as outlined below. Transient absorption and triplet absorption decay experiments were performed at ambient temperature (301 ± 1 K) on an Edinburgh Instruments LP920 spectrometer using the second harmonic of a Quantel Brilliant B Nd:YAG laser (10 ns pulse, 1.2 – 8.2 mJ, λ = 532 nm) to generate the triplet transient. Triplet absorption was probed with a xenon arc lamp (Xe920, 450 W). Kinetic measurements were carried out by monitoring the ΔOD at the respective triplet absorption maxima of each compound using a Hamamatsu R2856 photomultiplier tube interfaced with a Tektronix TDS 3012 Digital Phosphor oscilloscope for detection. Wavelength resolved absorption spectra were captured using a gated intensified ANDOR DH720 ICCD camera.

Samples were prepared by diluting stock solutions of the porphyrin compounds of interest in toluene or THF to 0.020 ± 0.0005 OD at 532 nm. Oxygen was removed from solutions used in triplet transient absorption spectroscopy and triplet absorption decay measurements prior to use via 4 repetitions of the freeze-pump-thaw technique. Degassing of solutions was performed in custom-made fluorescence cells consisting of 1 x 1 cm 6Q quartz fluorescence cuvettes graded into glass tubing connected to a solvent chamber and a gas adapter, with a Rotaflo® tap sealing the vacuum line from the solvent chamber and cuvette. For the sets of data where the excitation power was varied, each kinetic run within the set was performed on the same day. FLASH software from Edinburgh Instruments® was used to fit the transient decay profile data to the appropriate first-order, first-plus-second order or tri-exponential rate equations 4.1, 4.2 and 4.3 respectively in order to obtain rate constants for triplet decays. In the cases where multiple decay traces were obtained for one compound using varying excitation energies, the rate constants for triplet decays were obtained from global fits to all traces for that sample. For decay profiles with high signal-to-noise ratio (those in Figure 4.25 and 4.27), the data points before the onset of decay were eliminated from the raw data files before fitting in order to avoid the FLASH software fitting the decay profiles to data points before the onset of decay.

6.2 Synthesis

6.2.1 General synthetic procedure for Zinc(II) metalation of porphyrins

All zinc metalations of free-base porphyrins were performed using a variation of a method previously outlined by Wang *et al*.[5] Free-base porphyrin was stirred with $Zn(OAc)_2 \bullet 2H_2O$ (5 molar equivalents) in 3:1 CH_2Cl_2/MeOH (1.0 – 1.5 mg free-base porphyrin/mL) for 16h at RT in the dark. The reaction mixture was then washed with aq. $NaHCO_3$ soln. (5% w/v, 1:1 volume ratio with reaction mixture solvent) and brine (1:1 volume ratio with reaction mixture solvent). The organic layer was subsequently dried over Na_2SO_4, filtered and the solvent removed by rotary evaporation to yield the Zn(II) crude metalated porphyrin. The crude metalloporphyrin was then purified using a combination of 40-60°C boiling point petroleum spirits, DCM, EtOAc, $CHCl_3$, toluene and MeOH in various ratios to yield the pure metalated porphyrin.

6.2.2 Synthesis of Chapter 2 compounds - Sterically bulky di- and tetra- meso-substituted zinc porphyrin derivatives

3,5-Di-tert-butylbenzaldehyde (2.8)

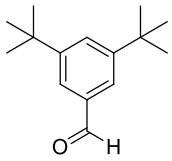

3,5-Di-*tert*-butylbenzaldehyde **2.8** was prepared using a variation of a method previously outlined by Meggiato Jr. *et al*.[6] A solution of 3,5-di-tert-butyltoluene **2.17** (11.9 g, 58.0 mmol), N-bromosuccinimide (15.5 g, 87.0 mmol) and azobisisobutyronitrile (AIBN) (0.50 g, 3.04 mmol) in C_6H_5Cl (400 mL) was heated at reflux and stirred for 4 h. The reaction mixture was cooled, filtered through paper and the solvent was removed by rotary evaporation. The residue was dissolved in 70 mL of a solvent mixture composed by EtOH/H_2O (1:1) and hexamethylenetetramine (25.0 g, 179 mmol) was added and the solution was heated at reflux for 4 h. Concentrated HCl was added (12 mL) and the mixture was refluxed for a further 30 min. The ethanol was removed via rotary evaporation and the remaining aqueous layer was extracted

with ether. The ether layer was dried over Na_2SO_4 and the solvent removed by rotary evaporation. Recrystallization from EtOH afforded 3,5-di-*tert*-butylbenzaldehyde **2.8** as white crystals (6.55 g, 52%). The data reported below was in close agreement with the respective data reported by Meggiato Jr. *et al*.[6]

^{1}H NMR (600MHz, $CDCl_3$) δ 1.38 (18H, s, *tert*-butyl-**H**), 7.71 – 7.73 (1H, m, Ar-**H**, *p-)*, 7.73 – 7.75 (2H, m, Ar-**H**, *o*-), 10.02 (1H, s, C**H**O)

^{13}C NMR (150MHz, $CDCl_3$) δ 31.46, 35.11, 124.28, 129.01, 136.35, 151.97, 193.31

FT-IR (neat, cm^{-1}) 2962, 1690, 1592, 1476, 1389, 1364, 1250, 1191, 884, 818, 707

HRMS (ESI$^+$, *m/z*) 219.1742 ($C_{15}H_{23}O$ $[M+H]^+$ requires 219.1749)

Di-(1H-pyrrol-2-yl)methane (2.19)

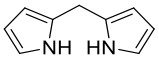

Di-(1H-pyrrol-2-yl)methane **2.19** was prepared using a variation of a method previously outlined by Laha *et al*.[7] Paraformaldehyde (1.94 g, 64.8 mmol) was added to freshly distilled pyrrole **2.9** (450 mL, 6478 mmol) and degassed with N_2 for 10 min while being stirred at RT. The mixture was heated to 55°C and $InCl_3$ (1.43 g, 6.48 mmol) was added in one portion. The mixture was stirred at 55°C for 2h 30 min, after which it was quenched by the addition of powdered NaOH (7.8 g, 195 mmol) and stirred for a further 45 min. The mixture was vacuum filtered and the residual solid washed with a small amount of pyrrole (*ca* 50 mL). The filtrate was concentrated under reduced pressure to produce an off-white solid, which was left overnight to remove remaining pyrrole. The crude solid was purified via column chromatography (silica gel, 14:5:1 petroleum spirit: DCM: EtOAc as eluent) to yield di-(1H-pyrrol-2-yl)methane **2.19** as a white solid (6.17 g, 66%). The data reported below was in close agreement with the respective data reported by Frost *et al.*[8]

^{1}H NMR (600MHz, $CDCl_3$) δ 4.00 (2H, s, -C**H**$_2$), 6.03 - 6.07 (2H, m, C**H**CNH), 6.16 (2H, dd, J = 5.6, 2.8 Hz, C**H**CHNH), 6.67 – 6.70 (2H, m, C**H**NH), 7.92 (2H, s, br., -N**H**)

^{13}C NMR (125MHz, $CDCl_3$) δ 26.36, 106.61, 108.31, 117.50, 129.21

HRMS (ESI^+, *m/z*) 147.0917 ($C_9H_{11}N_2$ $[M+H]^+$ requires 147.0922)

5,15-Diphenylporphyrin (DPP 2.14)

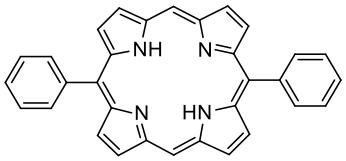

5,15-Diphenylporphyrin (DPP **2.14**) was prepared using a variation of a method previously outlined by DiMagno *et al*.[9] Benzaldehyde **2.7** (0.44 g, 4.11 mmol) and di-(1H-pyrrol-2-yl)methane **2.19** (0.60 g, 4.11 mmol) were dissolved in anhydrous CH_2Cl_2 (700 mL). The solution was purged with N_2 for 15 min, then TFA (0.63 mL, 8.22 mmol) was added and the mixture was stirred for 3h in the dark at RT. DDQ (1.71 g, 7.52 mmol) was then added and the mixture stirred at RT for a further 20 min. Et_3N (4 mL) was added to quench the acid, and the solvent was removed by rotary evaporation. The crude product was purified by column chromatography (silica gel, 1:1 petroleum spirit: DCM as eluent) to yield 5,15-diphenylporphyrin (DPP **2.14**) as a deep purple solid (200 mg, 21%). The data reported below was in close agreement with the respective data reported by Abada *et al.*[10]

^{1}H NMR (600MHz, $CDCl_3$) δ -3.10 (2H, s, -NH inner ring), 7.80 – 7.83 (6H, m, Ar-**H**, meso-phenyl–*m/p*), 8.25 – 8.31 (4H, m, Ar-**H**, meso-phenyl–*o*), 9.09 (4H, d, J = 4.5 Hz, **H**-pyrrole β-), 9.40 (4H, d, J = 4.6 Hz, **H**-pyrrole β-), 10.33 (2H, s, meso-**H**)

^{13}C NMR (150MHz, $CDCl_3$) δ 105.41, 119.25, 127.12, 127.86, 131.20, 131.75, 135.00, 141.54, 145.35, 147.32

HRMS (ESI^+, *m/z*) 463.1915 ($C_{32}H_{23}N_4$ $[M+H]^+$ requires 463.1923)

[5,15-Diphenylporphyrinato]zinc(II) (ZnDPP 2.1)

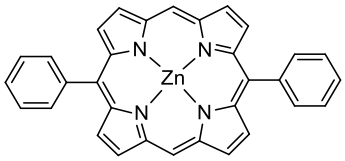

5,15-Diphenylporphyrin (DPP **2.14**) (44mg, 0.095 mmol) was subjected to the general zinc metalation conditions outlined in **5.2.1**. The crude product was purified by column chromatography (silica gel, 1:1 petroleum spirit: DCM as eluent) to yield [5,15-diphenylporphyrinato]zinc(II) (ZnDPP **2.1**) as dark red solid (49 mg, 98%).

^{1}H NMR (600MHz, $C_2D_2Cl_4$) δ 7.80 – 7.87 (6H, m, Ar-**H**, meso-phenyl–*m/p*), 8.28 – 8.31 (4H, m, Ar-**H**, meso-phenyl–*o*), 9.18 (4H, d, J = 4.4 Hz, **H**-pyrrole β-), 9.48 (4H, d, J = 4.4 Hz, **H**-pyrrole β-), 10.36 (2H, s, meso-**H**)

MS (ESI$^+$, *m/z*) 525.1058 ($C_{32}H_{21}N_4Zn$ $[M+H]^+$ requires 525.1058)

5,15-Bis(3,5-di-tert-butylphenyl)porphyrin (DBP 2.15)

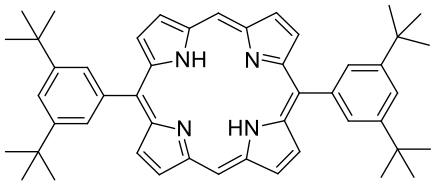

5,15-Bis(3,5-di-tert-butylphenyl)porphyrin (DBP **2.15**) was prepared using a variation of a method previously outlined by Plater *et al.*[11] 3,5-Di-*tert*-butylbenzaldehyde **2.8** (0.90 g, 4.11 mmol) and di-(1H-pyrrol-2-yl)methane **2.19** (0.60 g, 4.11 mmol) were dissolved in anhydrous CH_2Cl_2 (700 mL). The solution was purged with N_2 for 15 min, then TFA (0.63 mL, 8.22 mmol) was added and the mixture was stirred for 3h in the dark at RT. DDQ (1.71 g, 7.52 mmol) was then added and the mixture stirred at RT for a further 20 min. Et_3N (4 mL) was added to quench the acid, and the solvent was removed by rotary evaporation. The crude product was purified by column chromatography (silica gel, 4:1 petroleum spirit: DCM as eluent) to yield 5,15-bis(3,5-

di-tert-butylphenyl)porphyrin (DBP **2.15**) as a deep reddish-purple solid (238 mg, 17%). The data reported below was in close agreement with the respective data reported by Plater *et al*.[11]

^{1}H NMR (600MHz, $CDCl_3$) δ -3.00 (2H, s, -NH inner ring), 1.59 (36H, s, *tert*-butyl-**H**), 7.84 – 7.87 (2H, m, Ar-**H**, meso-(3,5-di-*tert*-butylphenyl) –*p*), 8.15 – 8.18 (4H, m, Ar-**H**, meso-(3,5-di-*tert*-butylphenyl) –*o*), 9.15 (4H, d, J = 4.5 Hz, **H**-pyrrole β-), 9.41 (4H, d, J = 4.5 Hz, **H**-pyrrole β-), 10.32 (2H, s, meso-**H**)

^{13}C NMR (150MHz, $CDCl_3$) δ 31.95, 35.27, 105.22, 120.62, 121.24, 130.35, 131.41, 131.63, 140.55, 145.20, 147.61, 149.28

MS (ESI^+, *m/z*) 687.4488 ($C_{48}H_{54}N_4$ $[M+H]^+$ requires 687.4426)

[5,15-Bis(3,5-di-tert-butylphenyl)porphyrinato]zinc(II) (ZnDBP 2.2)

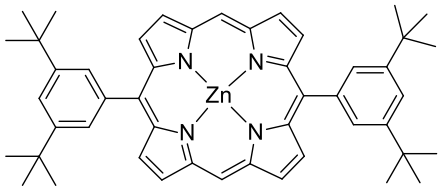

5,15-Bis(3,5-di-tert-butylphenyl)porphyrin (DBP **2.15**) (100mg, 0.146 mmol) was subjected to the general zinc metalation conditions outlined in **5.2.1**. The crude product was purified by column chromatography (silica gel, 1:1 petroleum spirit: DCM as eluent) to yield [5,15-bis(3,5-di-tert-butylphenyl)porphyrinato]zinc(II) (ZnDBP **2.2**) as dark red solid (103 mg, 94%).

^{1}H NMR (500MHz, $CDCl_3$) δ 1.59 (36H, s, *tert*-butyl-**H**), 7.84 – 7.87 (2H, m, Ar-**H**, meso-(3,5-di-*tert*-butylphenyl) –*p*), 8.15 – 8.18 (4H, m, Ar-**H**, meso-(3,5-di-*tert*-butylphenyl) –*o*), 9.22 (4H, d, J = 4.5 Hz, **H**-pyrrole β-), 9.47 (4H, d, J = 4.5 Hz, **H**-pyrrole β-), 10.36 (2H, s, meso-**H**)

^{13}C NMR (150MHz, $CDCl_3$) δ 31.97, 35.26, 106.28, 121.03, 121.67, 130.11, 131.77, 132.99, 141.72, 148.88, 149.59, 150.59

MS (ESI^+, *m/z*) 749.3560 ($C_{48}H_{52}N_4Zn$ $[M+H]^+$ requires 749.3561)

5,15-Dimesitylporphyrin (DMP 2.16)

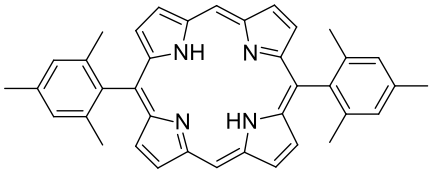

5,15-Dimesitylporphyrin (DMP **2.16**) was prepared using a variation of a method previously outlined by Yu *et al*.[12] Mesitaldehyde **2.12** (0.74 mL, 5.00 mmol) and di-(1H-pyrrol-2-yl)methane **2.19** (0.73 g, 5.00 mmol) were dissolved in anhydrous CH_2Cl_2 (500 mL). EtOH (3.75 mL) was added and the solution was purged with N_2 for 15 min. BF_3•OEt_2 (1.30 mL, 1.25M solution in anhydrous CH_2Cl_2, 1.63 mmol) was added and the mixture was stirred for 1h in the dark at RT. DDQ (0.91 g, 4.00 mmol) was then added and the mixture stirred at RT for a further 20 min. Et_3N (0.3 mL) was added to quench the acid, and the solvent was removed by rotary evaporation. The crude product was purified by column chromatography (silica gel, 1:1 petroleum spirit: DCM as eluent) to yield 5,15-dimesitylporphyrin (DMP **2.16**) as a deep purple solid (366 mg, 27%). The data reported below was in close agreement with the respective data reported by Yu *et al*.[12]

^{1}H NMR (600MHz, $CDCl_3$) δ -3.05 (2H, s, -N**H** inner ring), 1.86 (12H, s, meso-mesityl-C**H**$_3$-*o*), 2.67 (6H, s, meso-mesityl-C**H**$_3$-*p*), 7.34 (4H, s, Ar-**H**, meso-mesityl-*m*), 8.89 (4H, d, J = 4.3 Hz, **H**-pyrrole β-), 9.34 (4H, d, J = 4.3 Hz, **H**-pyrrole β-), 10.23 (2H, s, meso-**H**)

^{13}C NMR (150MHz, $CDCl_3$) δ 21.65, 21.86, 104.72, 117.45, 128.01, 130.15, 131.94, 137.80, 137.99, 139.64

MS (ESI^+, *m/z*) 547.2916 ($C_{38}H_{34}N_4$ $[M+H]^+$ requires 547.2861)

[5,15-Dimesitylporphyrinato]zinc(II)* (*ZnDMP 2.3)

5,15-Dimesitylporphyrin (DMP **2.16**) (100mg, 0.183 mmol) was subjected to the general zinc metalation conditions outlined in **5.2.1**. The crude product was purified by column chromatography (silica gel, 1:1 petroleum spirit: DCM as eluent) to yield [5,15-dimesitylporphyrinato]zinc(II) (ZnDMP **2.3**) as a reddish-pink solid (100 mg, 90%).

^{1}H NMR (500MHz, $CDCl_3$) δ 1.84 (12H, s, meso-mesityl-C**H**$_3$-*o*), 2.68 (6H, s, meso-mesityl-C**H**$_3$-*p*), 7.33 (4H, s, Ar-**H**, meso-mesityl-*m*), 8.97 (4H, d, J = 4.3 Hz, **H**-pyrrole β-), 9.39 (4H, d, J = 4.3 Hz, **H**-pyrrole β-), 10.25 (2H, s, meso-**H**)

^{13}C NMR (150MHz, $CDCl_3$) δ 21.65, 21.82, 105.68, 118.43, 127.86, 131.43, 132.28, 137.68, 138.97, 139.50, 149.62, 150.04

MS (ESI^+, *m/z*) 609.1999 ($C_{38}H_{32}N_4Zn$ $[M+H]^+$ requires 609.1996)

5,10,15,20-Tetraphenylporphyrin (TPP 2.10)

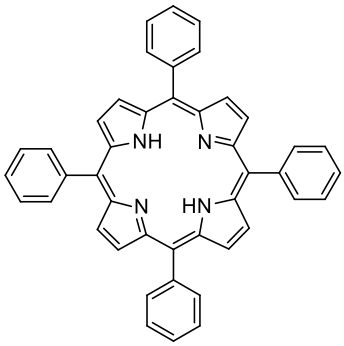

5,10,15,20-Tetraphenylporphyrin (TPP **2.10**) was prepared using a variation of a method previously outlined by Adler *et al.*[13] Freshly distilled pyrrole **2.9** (9.77g, 146 mmol) and benzaldehyde **2.7** (15.5g, 146 mmol) were added to refluxing propionic acid (340 mL) and the mixture allowed to reflux for 30 min while stirring. The reaction mixture was then cooled to

room temperature, filtered, and the filter cake washed with methanol until the filtrate was clear. The filter cake was washed then with hot water (200 mL) and the purple solid dried at the pump before drying *in vacuo* to remove adsorbed acid. The crude product was purified via column chromatography (silica gel, 1:1 $CHCl_3$: petroleum spirit as eluent) to yield 5,10,15,20-tetraphenylporphyrin (TPP **2.10**) as a dark purple solid (3.29g, 15%). The data reported below was in close agreement with the respective data reported by Shi *et al*.[14]

^{1}H NMR (500MHz, $CDCl_3$) δ -2.77 (2H, s, N-**H** inner ring), 7.73-7.81 (12H, m, Ar-**H**, *meso*-phenyl *m-/p-),* 8.21-8.24 (8H, m, Ar-**H**, *meso*-phenyl *o*-), 8.85 (8H, s, **H**-pyrrole β-)

^{13}C NMR (150MHz, $CDCl_3$) δ 120.30, 126.83, 127.86, 134.71, 142.34

HRMS (ESI^+, *m/z*) 615.2544 ($C_{44}H_{30}N_4$ $[M+H]^+$ requires 615.2548)

[5,10,15,20-Tetraphenylporphyrinato] zinc(II) (ZnTPP 2.4)

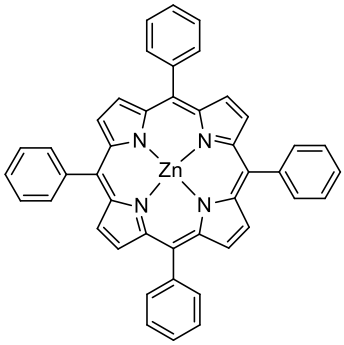

5,10,15,20-Tetraphenylporphyrin (TPP **2.10**) (1.27g, 2.07 mmol) was subjected to the general zinc metalation conditions outlined in **5.2.1**. The crude product was purified by column chromatography (silica gel, 1:1 petroleum spirit: DCM as eluent) to yield [5,10,15,20-tetraphenylporphyrinato] zinc(II) (ZnTPP **2.4**)as fine purple crystals (1.00 g, 71%).

^{1}H NMR (500MHz, $CDCl_3$) δ 7.73-7.80 (12H, m, Ar-**H**, *meso*-phenyl *m-/p-),* 8.21-8.24 (8H, m, Ar-**H**, *meso*-phenyl *o*-), 8.95 (8H, s, **H**-pyrrole β-)

^{13}C NMR (150MHz, $CDCl_3$) δ 121.29, 126.69, 127.64, 132.14, 134.58, 142.98, 150.38

FT-IR (neat, cm^{-1}) 1596, 1486, 1440, 1339, 1220, 1175, 1068, 1003, 995, 798, 772, 719, 701

HRMS (ESI$^+$, *m/z*) 677.1778 ($C_{44}H_{29}N_4Zn$ $[M+H]^+$ requires 677.1684)

5,10,15,20-Tetrakis(3,5-di-tert-butylphenyl)porphyrin (TBP 2.11)

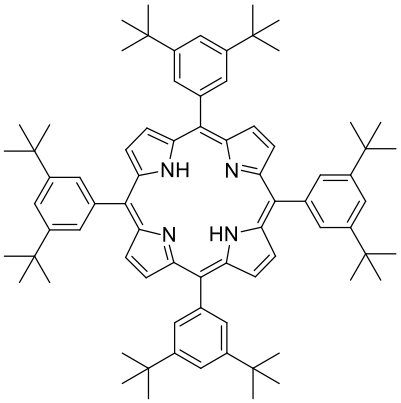

5,10,15,20-Tetrakis(3,5-di-tert-butylphenyl)porphyrin (TBP **2.11**) was prepared using a variation of a method previously outlined by Adler *et al*.[13] Freshly distilled pyrrole **2.9** (2.88g, 43.0 mmol) and 3,5-di-*tert*-butylbenzaldehyde **2.8** (9.38g, 43.0 mmol) were added to refluxing propionic acid (160 mL) and the mixture allowed to reflux for 30 min while stirring. The reaction mixture was then cooled to room temperature, filtered, and the filter cake washed with methanol until the filtrate was clear. The filter cake was washed then with hot water (200 mL) and the purple solid dried at the pump before drying *in vacuo* to remove adsorbed acid. The crude product was purified via column chromatography (silica gel, 1:1 $CHCl_3$: petroleum spirit as eluent) to yield 5,10,15,20-tetrakis(3,5-di-tert-butylphenyl)porphyrin (TBP **2.11**) as a dark purple solid (0.96g, 8%). The data reported below was in close agreement with the respective data reported by Hasegawa *et al*.[15]

^{1}H NMR (600MHz, $CDCl_3$) δ -2.66 (2H, s, -NH inner ring), 1.53 (72H, s, *tert*-butyl-**H**), 7.80 (4H, s, Ar-**H**, *meso*-(3,5-di-*tert*-butylphenyl *p-),* 8.10 (8H, s, Ar-**H**, -(3,5-di-*tert*-butylphenyl *o-),* 8.90 (8H, s, **H**-pyrrole β-)

^{13}C NMR (150MHz, $CDCl_3$) δ 31.91, 35.19, 121.07, 121.36, 129.84, 141.52, 148.80

HRMS (ESI$^+$, *m/z*) 1063.7547 ($C_{76}H_{95}N_4$ $[M+H]^+$ requires 1063.7557)

[5,10,15,20-Tetrakis(3,5-di-tert-butylphenyl)porphyrinato]zinc(II) (ZnTBP 2.5)

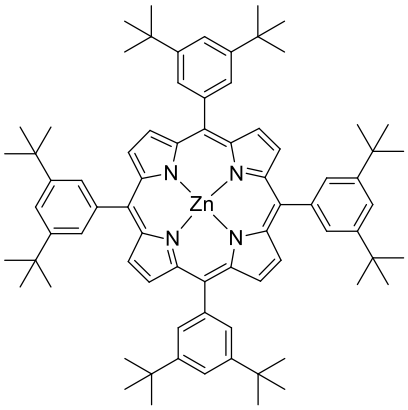

5,10,15,20-Tetrakis(3,5-di-tert-butylphenyl)porphyrin (TBP **2.11**) (200mg, 0.188 mmol) was subjected to the general zinc metalation conditions outlined in **5.2.1**. The crude product was purified by column chromatography (silica gel, 1:1 petroleum spirit: DCM as eluent) to yield [5,10,15,20-tetrakis(3,5-di-tert-butylphenyl)porphyrinato]zinc(II) (ZnTBP **2.5**) as a deep pink solid (199 mg, 94%).

^{1}H NMR (500MHz, $CDCl_3$) δ 1.53 (72H, s, *tert*-butyl-**H**), 7.80 (4H, s, Ar-**H**, *meso*-(3,5-di-*tert*-butylphenyl *p-)*, 8.10 (8H, s, Ar-**H**, -(3,5-di-*tert*-butylphenyl *o-)*, 9.02 (8H, s, **H**-pyrrole β-)

^{13}C NMR (150MHz, $CDCl_3$) δ 31.94, 35.21, 120.91, 122.49, 129.76, 132.27, 142.06, 148.67, 150.53

HRMS (ESI$^+$, *m/z*) 1125.6663 ($C_{76}H_{93}N_4Zn$ $[M+H]^+$ requires 1125.6692)

5,10,15,20-Tetramesitylporphyrin (TMP 2.13)

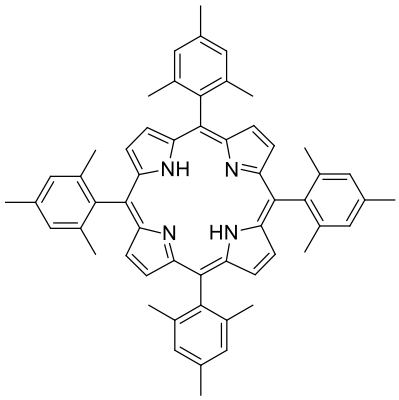

5,10,15,20-Tetramesitylporphyrin (TMP **2.13**) was prepared using a variation of a method previously outlined by Lindsey *et al*.[16] Mesitaldehyde **2.12** (0.75 mL, 5.06 mmol) and pyrrole **2.9** (0.35 mL, 5.06 mmol) were dissolved in anhydrous CH_2Cl_2 (500 mL). EtOH (3.75 mL) was added and the solution was purged with N_2 for 15 min. BF_3•OEt_2 (1.30 mL, 1.25M solution in anhydrous CH_2Cl_2, 1.63 mmol) was added and the mixture was stirred for 1h in the dark at RT. DDQ (0.90 g, 3.96 mmol) was then added and the mixture stirred at RT for a further 20 min. Et_3N (0.3 mL) was added to quench the acid, and the solvent was removed by rotary evaporation. The crude product was purified by column chromatography (silica gel, 1:1 petroleum spirit: DCM as eluent) to yield 5,10,15,20-tetramesitylporphyrin (TMP **2.13**) as a deep purple solid (283 mg, 29%). The data reported below was in close agreement with the respective data reported by Lindsey *et al*.[16]

^{1}H NMR (500MHz, $CDCl_3$) δ -2.49 (2H, s, -N**H** inner ring), 1.86 (24H, s, meso-mesityl-C**H**$_3$-*o*), 2.63 (12H, s, meso-mesityl-C**H**$_3$-*p*), 7.28 (8H, s, Ar-**H**, meso-mesityl-*m*), 8.63 (8H, s, **H**-pyrrole β-)

MS (ESI$^+$, *m/z*) 783.4253 ($C_{56}H_{54}N_4$ $[M+H]^+$ requires 783.4426)

[5,10,15,20-Tetramesitylporphyrinato]zinc(II) (ZnTMP 2.6)

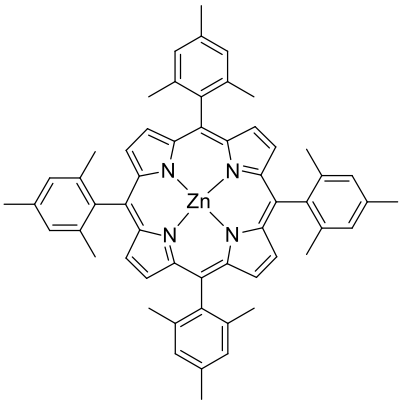

5,10,15,20-Tetramesitylporphyrin (TMP **2.13**) (80mg, 0.102 mmol) was subjected to the general zinc metalation conditions outlined in **5.2.1**. The crude product was purified by column chromatography (silica gel, 1:1 petroleum spirit: DCM as eluent) to yield [5,10,15,20-tetramesitylporphyrinato]zinc(II) (ZnTMP **2.6**) as a deep pink solid (85 mg, 98%).

^{1}H NMR (500MHz, $CDCl_3$) δ 1.85 (24H, s, meso-mesityl-C**H**$_3$-*o*), 2.63 (12H, s, meso-mesityl-C**H**$_3$-*p*), 7.28 (8H, s, Ar-**H**, meso-mesityl-*m*), 8.69 (8H, s, **H**-pyrrole β-)

MS (ESI$^+$, *m/z*) 845.3351 ($C_{56}H_{52}N_4Zn$ $[M+H]^+$ requires 845.3561)

6.2.3 Synthesis of Chapter 3 compounds – Oligo-phenylenevinylene linked pendant porphyin polymers and their monomeric model compound analogues

6.2.3.1 Compounds with linker length of one phenylenevinylene unit (a = 1)

[5,10,15,20-Tetraphenylporphyrinato] copper(II) (3.7)

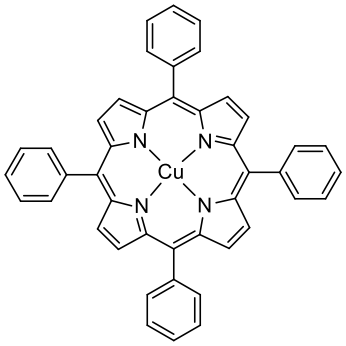

TPP **2.10** (3.30g, 5.37 mmol) and $Cu(CH_3COO)_2.H_2O$ (1.40g, 3.90 mmol) were added to a mixed solvent system comprising of MeOH (150 mL) and toluene (500 mL), and the reaction mixture was then refluxed for 4 h. The reaction mixture was filtered and the filtrate concentrated under reduced pressure. The crude material was purified via column chromatography (silica gel, 1:1 $CHCl_3$: petroleum spirit as eluent) to yield [5,10,15,20-tetraphenylporphyrinato] copper(II) **3.7** as a reddish-brown solid (3.31g, 91%). The data reported below was in close agreement with the respective data reported by Ha-Thi *et al*.[17]

FT-IR (neat, cm^{-1}) 1725, 1598, 1441, 1346, 1262, 1175, 1072, 1004, 996, 802, 752, 702

HRMS (ESI^+, *m/z*) 675.1602 ($C_{44}H_{28}CuN_4$ M^+ requires 675.1610)

2-Formyl-5,10,15,20-tetraphenylporphyrin (3.8)

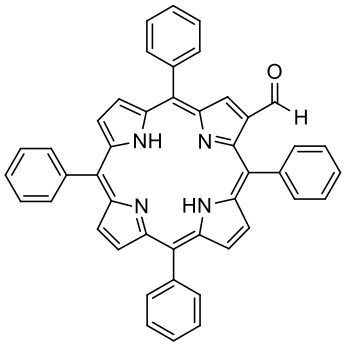

2-Formyl-5,10,15,20-tetraphenylporphyrin **3.8** was prepared using a variation of a method previously outlined by Bonfantini *et al*.[18] DMF (34 mL, 439 mmol) was added to a 1 L, three-necked round bottom flask and the flask cooled to 0°C. While maintaining the temperature at 0°C, phosphorus oxychloride (26 mL, 278 mmol) was added dropwise to the flask while continuously stirring under an N_2 atmosphere to form the Vilsmeier complex. A solution of [5,10,15,20-tetraphenylporphyrinato] copper(II) **3.7** (3.0g, 4.44 mmol) in anhydrous DCE (300 mL) was added dropwise to the Vilsmeier complex over 40 min, and the reaction mixture then refluxed for 5 h. After cooling the reaction mixture to RT, conc. H_2SO_4 (58 mL) was added and the mixture stirred for 5 min. The mixture was poured into an ice-cold solution of NaOH (86 g) in H_2O (3 L). The organic layer was diluted with DCM (500 mL), washed with H_2O (1 L) and the aqueous layer extracted with DCM (500 mL). The organic layers were combined and washed with sat. aq. $NaHCO_3$ (1 L), and then dried over Mg_2SO_4, filtered and concentrated under reduced pressure. The crude product was purified via column chromatography (silica gel, 1:1 DCM: petroleum spirit as eluent) to yield 2-formyl-5,10,15,20-tetraphenylporphyrin **3.8** as a dark purple solid (2.23 g, 78%). The data reported below was in close agreement with the respective data reported by Bonfantini *et al*.[18]

^{1}H NMR (500MHz, $CDCl_3$) δ -2.54 (2H, s, inner ring N-H), 7.73-7.86 (12H, m, Ar-**H**, *meso*-phenyl *m-/p-),* 8.17-8.22 (6H, m, Ar-**H**, *meso*-phenyl *o*-), 8.23-8.26 (2H, m, Ar-**H**, *meso*-phenyl *o*-), 8.77 (1H, d, J = 4.7 Hz, **H**-pyrrole β-), 8.79 (1H, d, J = 4.6 Hz, **H**-pyrrole β-), 8.84-8.87 (2H, m, **H**-pyrrole β-), 8.89 (1H, d, J = 4.7 Hz, **H**-pyrrole β-), 8.92 (1H, d, J = 4.7 Hz, **H**-pyrrole β-), 9.24 (1H, s, **H**-pyrrole-CHO β-), 9.41 (1H, s, ArC**H**O)

^{13}C NMR (150MHz, $CDCl_3$) δ 120.36, 120.62, 120.93, 122.95, 127.17, 127.19, 127.21, 127.72, 128.27, 128.27, 128.49, 129.35, 134.89, 134.93, 134.97, 135.34, 141.92, 142.12, 142.79, 189.63

FT-IR (neat, cm^{-1}) 3326, 3053, 3026, 1670, 1597, 1558, 1501, 1475, 1442, 1350, 1221, 1165, 1073, 1032, 1002, 981, 964, 932, 853, 800, 754, 727, 701

HRMS (ESI$^+$, *m/z*) 643.2494 ($C_{45}H_{31}N_4O$ $[M+H]^+$ requires 643.2498)

[2-Formyl-5,10,15,20-tetraphenylporphyrinato] zinc(II) (3.15)

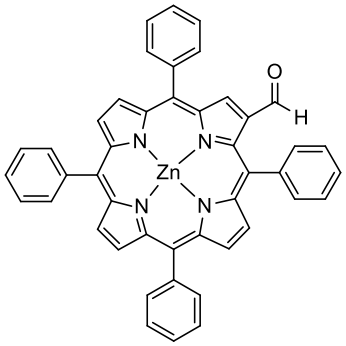

2-Formyl-5,10,15,20-tetraphenylporphyrin **3.8** (550mg, 0.856 mmol) was subjected to the general zinc metalation conditions outlined in **5.2.1**. The crude product was purified by column chromatography (silica gel, 1:1 petroleum spirit: DCM as eluent) to yield [2-formyl-5,10,15,20-tetraphenylporphyrinato] zinc(II) **3.15** as a dark blue-purple solid (602 mg, 99%).

^{1}H NMR (500MHz, $CDCl_3$) δ 7.71-7.85 (12H, m, Ar-**H**, *meso*-phenyl *m-/p-),* 8.16-8.21 (6H, m, Ar-**H**, *meso*-phenyl *o*-), 8.22-8.25 (2H, m, Ar-**H**, *meso*-phenyl *o*-), 8.89-8.92 (4H, m, **H**-pyrrole β-), 8.93 (1H, d, J = 4.6 Hz, **H**-pyrrole β-), 8.95 (1H, d, J = 4.6 Hz, **H**-pyrrole β-), 9.29 (1H, s, **H**-pyrrole-CHO β-), 9.55 (1H, s, ArC**H**O)

^{13}C NMR (150MHz, $CDCl_3$) δ 121.21, 121.58, 121.95, 123.99, 127.05, 127.06, 127.50, 128.05, 128.06, 128.27, 129.12, 132.64, 132.68, 133.04, 133.23, 133.33, 133.68, 134.71, 134.75, 134.78, 134.96, 136.47, 141.95, 142.39, 142.66, 143.54, 146.56, 147.52, 150.44, 150.91, 151.62, 152.01, 152.07, 152.11, 190.27

FT-IR (neat, cm^{-1}) 3052, 3026, 1640, 1597, 1521, 1493, 1441, 1338, 1193, 1154, 1072, 1002, 994, 936, 797, 753, 722, 701

HRMS (ESI^+, *m/z*) 704.1546 ($C_{45}H_{28}N_4OZn$ M^+ requires 704.1555)

Diethyl benzyl phosphonate (3.19)

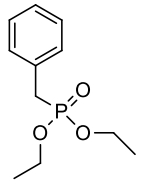

Diethyl benzyl phosphonate **3.19** was prepared using a variation of a method previously outlined by Tilley *et al*. for the synthesis of diisopropyl-4-methylbenzylphosphonate.[19] Benzyl bromide **3.25** (1.00g, 5.85 mmol) in triethylphosphite (15 mL, 87.6 mmol) was stirred at reflux for 24h under N_2. The unreacted triethylphosphite was then removed by Kugel-Rohr distillation (1 mbar, 90°C) to give a clear oil. The oil was then purified by column chromatography (silica gel, 1:1 petroleum spirit: EtOAc as eluent) to yield diethyl benzyl phosphonate **3.19** as a clear oil (1.24 g, 93%). The data reported below was in close agreement with the respective data reported by Vugts *et al*.[20]

^{1}H NMR (500MHz, $CDCl_3$) δ 1.24 (6H, t, J = 7.1 Hz, -$POCH_2C\mathbf{H}_3$), 3.15 (2H, d, J_{HP} = 21.6 Hz, $ArC\mathbf{H}_2P$-), 3.95-4.05 (4H, m, -$POC\mathbf{H}_2CH_3$), 7.22-7.26 (1H, m, Ar-**H**), 7.28-7.34 (4H, m, Ar-**H**)

FT-IR (neat, cm^{-1}) 2983, 1497, 1456, 1393, 1250, 1221, 1162, 1098, 1055, 1027, 963, 772, 699

HRMS (ESI^+, *m/z*) 229.0988 ($C_{11}H_{18}O_3P$ $[M+H]^+$ requires 229.0994)

α-Mercapto-ω-(1-carboxyethyl)-poly(4-vinylbenzyldiethyl phosphonate) (3.20)

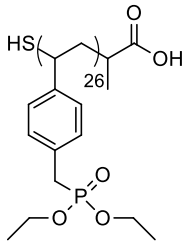

α-(Dodecylthiocarbonothioylthio)-ω-(1-carboxyethyl)-poly(vinylbenzyl diethyl phosphonate) **3.20** was prepared using a variation of a method previously outlined by Tilley *et al.*[21] α-(Dodecylthiocarbonothioylthio)-ω-(1-carboxyethyl)-poly(4-vinylbenzylchloride) **3.26** (790 mg, 0.185 mmol, Mn = 4,273 g/mol) in triethylphosphite (12 mL, 70.0 mmol) was stirred at reflux for 2 days under N_2. The unreacted triethylphosphite was then removed by Kugel-Rohr distillation (10 mbar, 50°C) to give a clear oil. The polymer was precipitated from the residual oil by dissolving in $CHCl_3$ (5 mL) and then adding a large excess of MeOH and concentrating by centrifugation (5 min at 6000 rpm). The concentrated polymer was purified by re-dissolving it in $CHCl_3$ (5 mL), then precipitating the polymer from the solution with MeOH (35 mL) and re-concentrating as a sediment by centrifugation (5 min at 6000 rpm), and the purification process repeated twice more. The polymer was collected by decanting the supernatant after centrifugation and dried under vacuum to yield α-(dodecylthiocarbonothioylthio)-ω-(1-carboxyethyl)-poly(vinylbenzyl diethyl phosphonate) **3.20** as a colourless waxy solid (986 mg, 80%). The data reported below was in close agreement with the respective data reported by Tilley *et al.*[21]

^{1}H NMR (600MHz, $CDCl_3$) δ 0.80-2.32 (br., m ,backbone, -$OCH_2C\mathbf{H}_3$), 3.06 (br., m, $ArC\mathbf{H}_2P$-), 3.95 (br., m, -$POC\mathbf{H}_2$-), 6.18-7.18 (br., m, Ar-**H**)

FT-IR (neat, cm^{-1}) 2987, 2930, 1512, 1393, 1247, 1162, 1098, 1054, 1027, 963, 854, 776

[2-((E)-Styryl)-5,10,15,20-tetraphenylporphyrinato] zinc(II) (3.1)

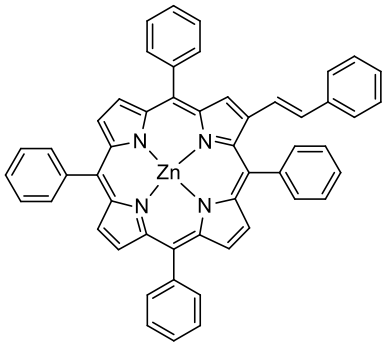

Sodium hydride (20 mg, 0.850 mmol) was added slowly to a solution of diethyl benzyl phosphonate **3.19** (47 mg, 0.204 mmol) and [2-formyl-5,10,15,20-tetraphenylporphyrinato] zinc(II) **3.15** (120 mg, 0.170 mmol) in anhydrous THF (10 mL) and the reaction mixture was stirred for 24h at room temperature. The reaction was diluted with DCM (20 mL) and then added dropwise to H_2O (30 mL). The organic layer was separated and the aqueous layer extracted with DCM (30 mL), and the organic layers were combined and washed with sat. aq. NaCl solution (30 mL), dried over anhydrous Na_2SO_4, filtered and concentrated under reduced pressure to give a reddish-purple solid. The solid was purified by column chromatography (silica gel, 10:10:1 DCM: petroleum spirit: EtOAc as eluent) to yield the product **3.1** as a reddish-purple powder (112 mg, 85%). Compound **3.1** was previously reported by Mitchell *et al.*[22] without corresponding characterization data provided. The data reported below was consistent with expected data upon metalation in comparison to the respective data reported by Bonfantini *et al.*[23] for the analogous free-base porphyrin, from which the compound reported by Mitchell *et al.*[22] was derived.

^{1}H NMR (500MHz, $CDCl_3$) δ 7.03 (1H, d, J = 16.0 Hz, β-pyrrole-C**H**$_2$Ar styryl), 7.23-7.29 (4H, m, β-pyrrole-C**H**$_2$Ar styryl and Ar-**H** styryl *–o/-p*), 7.32-7.36 (2H, m, Ar-**H** styryl -*m*), 7.72-7.85 (12H, m, Ar-**H**, *meso*-phenyl *m-/p*-), 8.17-8.23 (6H, m, Ar-**H**, *meso*-phenyl *o*-), 8.24-8.27 (2H, m, Ar-**H**, *meso*-phenyl *o*-), 8.82 (1H, d, J = 4.6 Hz, **H**-pyrrole β-), 8.88-8.92 (4H, m, **H**-pyrrole β-), 8.94 (1H, d, J = 4.7 Hz, **H**-pyrrole β-), 9.10 (1H, s, **H**-pyrrole β- styryl)

FT-IR (neat, cm^{-1}) 3056, 3023, 1597, 1485, 1440, 1338, 1217, 1195, 1177, 1135, 1070, 1004, 995, 960, 937, 832, 796, 752, 700, 666

HRMS (ESI$^+$, *m/z*) 778.2062 ($C_{52}H_{34}N_4Zn$ M^+ requires 778.2075)

α-Mercapto-ω-(1-carboxyethyl)-poly([2-((E)-4'-vinylstyryl)-5,10,15,20-tetraphenylporphyrinato] zinc(II)) (3.4)

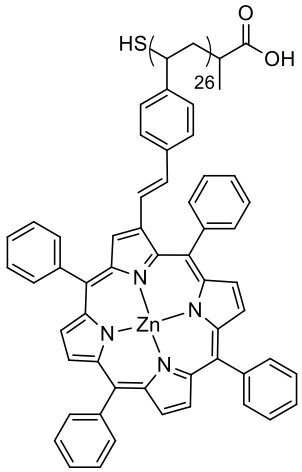

Sodium hydride (38 mg, 1.60 mmol) was added to a solution of poly(vinylbenzyldiethyl phosphonate) **3.20** (82 mg, 0.319 mmol VBC units) and [2-formyl-5,10,15,20-tetraphenylporphyrinato] zinc(II) **3.15** (450 mg, 0.637 mmol) dissolved in anhydrous THF (10 mL) and the reaction mixture stirred for 5 days at room temperature. The reaction was diluted in DCM (20 mL) and then added dropwise to H_2O (100 mL) and the mixture extracted with $CHCl_3$ (100 mL). The organic layer was washed with sat. aq. NaCl solution (50 mL), dried over Na_2SO_4, filtered and concentrated under reduced pressure. The residue was purified by size exclusion column chromatography (Bio S-X beads, THF as eluent) to yield the porphyin-appended polymer **3.4** as a brownish-purple powder (134 mg, 52%). Compound **3.4** has not been previously reported in the literature and thus all data below for **3.4** constitutes novel characterization.

^{1}H NMR (500MHz, $CDCl_3$) δ 0.80-2.56 (br., m, backbone, alkyl-**H**), 6.45-8.34 (br., m, Ar-**H**-mesophenyl, Ar-**H**-stilbene linker), 8.37-9.06 (br., m, **H**-pyrrole β-)

FT-IR (neat, cm^{-1}) 3054, 3020, 2926, 1597, 1509, 1484, 1441, 1338, 1217, 1194, 1177, 1135, 1071, 1004, 993, 963, 866, 833, 795, 752, 722, 701, 664

6.2.3.2 Compounds with linker length of two phenylenevinylene units (a = 2)

2-Hydroxymethyl-5,10,15,20-tetraphenylporphyrin (3.9)

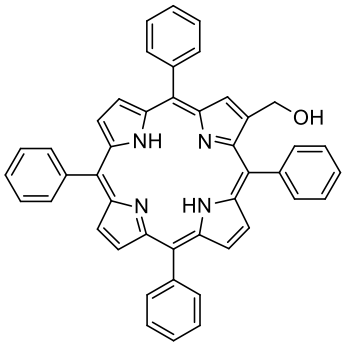

2-Hydroxymethyl-5,10,15,20-tetraphenylporphyrin **3.9** was prepared using a variation of a method previously outlined by Bonfantini *et al*.[18] $NaBH_4$ (50 mg, 1.31 mmol) was added to a solution of 2-formyl-5,10,15,20-tetraphenylporphyrin **3.8** (700 mg, 1.09 mmol) dissolved in a mixture of $CHCl_3$ (300 mL) and EtOH (150 mL), and the reaction mixture was then stirred at RT for 16 h. The solvent was removed under reduced pressure and the residue was taken up in H_2O (400 mL). The aqueous residue mixture was extracted with DCM (400 mL) and the organic layer washed with sat. aq. NaCl solution (400 mL). The organic layer was dried over $MgSO_4$, filtered and the solvent was removed under reduced pressure. The crude product was purified via column chromatography (silica gel, 5:5:1 DCM: petroleum spirit: EtOAc as eluent) to yield 2-hydroxymethyl-5,10,15,20-tetraphenylporphyrin **3.9** as a purple solid (681 mg, 97%). The data reported below was in close agreement with the respective data reported by Bonfantini *et al*.[18]

^{1}H NMR (500MHz, $CDCl_3$) δ -2.78 (2H, s, inner ring N-**H**), 1.95 (1H, bt, J = 6.3 Hz, -CH_2O**H**), 4.91 (2H, bd, J = 6.1 Hz, -C**H**$_2$OH), 7.71-7.84 (12H, m, Ar-**H**, *meso*-phenyl *m-/p-)*, 8.09-8.12 (2H, m, Ar-**H**, *meso*-phenyl *o*-), 8.18-8.23 (6H, m, Ar-**H**, *meso*-phenyl *o*-), 8.60 (1H, d, J = 4.7 Hz, **H**-pyrrole β-), 8.77-8.81 (2H, m, **H**-pyrrole β-), 8.82-8.86 (3H, m, **H**-pyrrole β-), 8.95 (1H, s, **H**-pyrrole β- CH_2OH)

^{13}C NMR (150MHz, $CDCl_3$) δ 61.58, 119.51, 119.77, 120.64, 120.99, 126.99, 127.00, 127.09, 127.62, 128.08, 129.02, 133.41, 134.81, 134.83, 134.92, 142.27, 142.49, 142.57, 142.81

FT-IR (neat, cm^{-1}) 3311, 3056, 3027, 1597, 1474, 1441, 1352, 1219, 1178, 1073, 1031, 1002, 994, 966, 846, 800, 753, 731, 701

HRMS (ESI^+, *m/z*) 645.2649 ($C_{45}H_{33}N_4O$ $[M+H]^+$ requires 645.2645)

2-Chloromethyl-5,10,15,20-tetraphenylporphyrin (3.10)

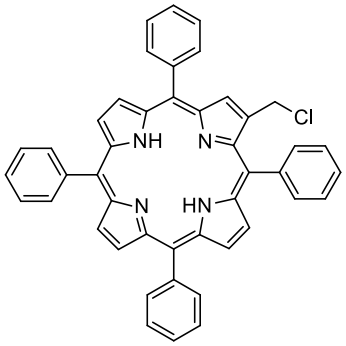

2-Chloromethyl-5,10,15,20-tetraphenylporphyrin **3.10** was prepared using a variation of a method previously outlined by Bonfantini *et al.*[18] 2-Hydroxymethyl-5,10,15,20-tetraphenylporphyrin **3.9** (650 mg, 1.01 mmol) was dissolved in dry DCM (120 mL) under an N_2 atmosphere and cooled in an ice bath. Dry pyridine (0.80 mL, 10.0 mmol) was added via syringe to the reaction mixture, followed by dropwise addition of thionyl chloride (0.30 mL, 4.12 mmol) via syringe. The reaction was stirred for 15 min at 0°C then warmed to RT and stirred for 30 additional min. The reaction mixture was diluted with DCM (200 mL) and washed with H_2O (2 x 200 mL) followed by sat. aq. $NaHCO_3$ (200 mL). The organic layer was dried over $MgSO_4$, filtered and concentrated under reduced pressure to yield 2-chloromethyl-5,10,15,20-tetraphenylporphyrin **3.10** as a purple powder (617 mg, 92%). The data reported below was in close agreement with the respective data reported by Bonfantini *et al.*[18]

^{1}H NMR (500MHz, $CDCl_3$) δ -2.76 (2H, s, inner ring N-**H**), 4.79 (2H, s, -C**H**$_2$Cl), 7.72-7.85 (12H, m, Ar-**H**, *meso*-phenyl *m-/p-),* 8.13-8.16 (2H, m, Ar-**H**, *meso*-phenyl *o*-), 8.18-8.23 (6H, m, Ar-**H**, *meso*-phenyl *o*-), 8.66 (1H, d, J = 4.7 Hz, **H**-pyrrole β-), 8.78-8.86 (5H, m, **H**-pyrrole β-), 8.96 (1H, s, **H**-pyrrole β- CH_2Cl)

^{13}C NMR (150MHz, $CDCl_3$) δ 42.17, 119.60, 120.30, 120.70, 120.92, 127.02, 127.03, 127.12, 127.58, 128.12, 128.19, 129.10, 133.81, 134.86, 134.91, 134.93, 141.93, 142.17, 142.47, 142.61

FT-IR (neat, cm^{-1}) 3326, 3027, 1596, 1473, 1441, 1350, 1263, 1219, 1071, 1001, 965, 802, 750, 659

HRMS (ESI$^+$, *m/z*) 663.2310 ($C_{45}H_{32}ClN_4$ $[M+H]^+$ requires 663.2315)

[(5,10,15,20-Tetraphenylporphyrin-2-yl)methyl]diethyl phosphonate (3.21)

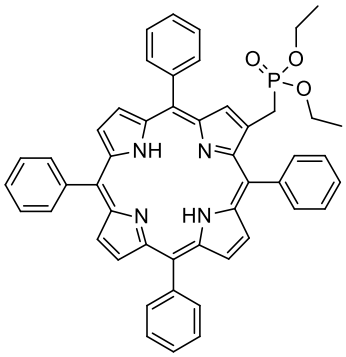

2-Chloromethyl-5,10,15,20-tetraphenylporphyrin **3.10** (400 mg, 0.603 mmol) in triethylphosphite (15 mL, 93.2 mmol) was stirred at reflux for 2 days under N_2. The bulk of the unreacted triethylphosphite was then removed by Kugel-Rohr distillation (10 mbar, 50°C) to give an oily purple residue. The purple residue was purified via column chromatography (silica gel, 10:10:1 DCM: petroleum spirit: EtOAc as eluent) to yield [(5,10,15,20-tetraphenylporphyrin-2-yl)methyl]diethyl phosphonate **3.21** as a metallic purple solid (225 mg, 49%). Compound **3.21** has not been previously reported in the literature and thus all data below for **3.21** constitutes novel characterization.

^{1}H NMR (600MHz, $CDCl_3$) δ -2.74 (2H, s, inner ring N-**H**), 1.06 (6H, t, J = 7.0 Hz, -$POCH_2C\mathbf{H}_3$), 3.39 (2H, d, J_{HP} = 21.7 Hz, $ArC\mathbf{H}_2P$-), 3.81-3.93 (4H, m, -$POC\mathbf{H}_2CH_3$), 7.72-7.82 (12H, m, Ar-**H**, *meso*-phenyl *m-/p-)*, 8.14-8.17 (2H, m, Ar-**H**, *meso*-phenyl *o*-), 8.20-8.23 (6H, m, Ar-**H**, *meso*-phenyl *o*-), 8.68 (1H, d, J = 4.8 Hz, **H**-pyrrole β-), 8.77 (1H, d, J = 4.8 Hz, **H**-pyrrole β-), 8.80 (1H, d, J = 4.7 Hz, **H**-pyrrole β-), 8.82 (1H, d, J = 4.7 Hz, **H**-pyrrole β-), 8.84

(1H, d, J = 4.8 Hz, **H**-pyrrole β-), 8.85 (1H, d, J = 4.8 Hz, **H**-pyrrole β-), 9.01 (1H, s, **H**-pyrrole β- CH_2P)

^{13}C NMR (150MHz, $CDCl_3$) δ 16.42, 16.46, 27.12, 28.04, 62.02, 62.07, 119.73, 120.24, 120.59, 126.73, 126.78, 126.90, 127.22, 127.86, 127.89, 128.51, 133.97, 134.61, 134.66, 134.74, 141.84, 142.01, 142.41, 142.68

FT-IR (neat, cm^{-1}) 3304, 3054, 2984, 1597, 1560, 1474, 1442, 1351, 1252, 1164, 1053, 1029, 1002, 972, 799, 732, 702

HRMS (ESI$^+$, *m/z*) 765.3002 ($C_{49}H_{42}N_4O_3P$ $[M+H]^+$ requires 765.2995)

Triphenyl[(5,10,15,20-tetraphenylporphyrin-2-yl)methyl]phosphonium chloride (3.11)

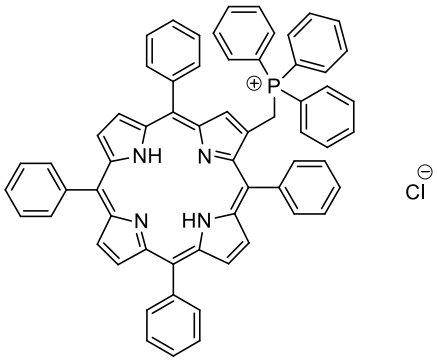

Triphenyl[(5,10,15,20-tetraphenylporphyrin-2-yl)methyl]phosphonium chloride **3.11** was prepared using a variation of a method previously outlined by Bonfantini *et al.*[18] 2-Chloromethyl-5,10,15,20-tetraphenylporphyrin **3.10** (900 mg, 1.36 mmol) was refluxed with PPh_3 (3.67 g, 14.0 mmol) in $CHCl_3$ (120 mL) for 16 h. The reaction mixture was cooled to RT and run directly onto a short silica gel column. DCM was used as eluent first to remove excess PPh_3 and any other low polarity materials. Once the eluent was free of PPh_3 by TLC, the desired material was eluted using a gradient of 2.5% to 10% MeOH in DCM. The solvent was removed under reduced pressure to yield triphenyl[(5,10,15,20-tetraphenylporphyrin-2-yl)methyl]phosphonium chloride **3.11** as a purple powder (1.21 g, 98%). The data reported below was in close agreement with the respective data reported by Bonfantini *et al.*[18]

^{1}H NMR (500MHz, $CDCl_3$) δ -2.76 (2H, s, inner ring N-**H**), 5.34 (2H, d, $^{2}J_{HP}$ = 15.0 Hz, -C**H**$_2$P), 7.17 (6H, dd, $^{3}J_{HP}$ = 12.6 Hz, ^{3}J = 8.1 Hz, Ar-**H** *o*-PPh_3), 7.29 (6H, td, J = 7.9 Hz, $^{4}J_{HP}$ = 3.4 Hz, Ar-**H** *m*-PPh_3), 7.41 (2H, d, ^{3}J = 8.0 Hz, Ar-**H**, *meso*-phenyl *o*-), 7.56-7.69 (7H, m, Ar-**H**, *meso*-phenyl *m-/p-* and *p*-PPh_3*)*, 7.71-7.83 (9H, m, Ar-**H**, *meso*-phenyl *o-/m-/p-),* 7.88 (1H, t, ^{3}J = 7.6 Hz, Ar-**H**, *meso*-phenyl *p-),* 8.16-8.20 (4H, m, Ar-**H**, *meso*-phenyl *o*-), 8.35 (1H, d, $^{4}J_{HP}$ = 3.5 Hz, **H**-pyrrole β- CH_2P), 8.45 (1H, d, J = 5.0 Hz, **H**-pyrrole β-), 8.74-8.77 (2H, m, **H**-pyrrole β-), 8.80 (1H, d, J = 4.7 Hz, **H**-pyrrole β-), 8.82 (1H, d, J = 4.7 Hz, **H**-pyrrole β-), 8.85 (1H, d, J = 4.8 Hz, **H**-pyrrole β-)

^{13}C NMR (150MHz, $CDCl_3$) δ 25.75, 26.07, 117.49, 118.06, 119.35, 120.68, 121.02, 121.10, 127.06, 127.09, 127.21, 128.05, 128.17, 128.28, 129.12, 130.31, 130.39, 134.25, 134.31, 134.41, 134.81, 134.84, 135.60, 135.61, 141.29, 141.71, 141.87, 142.11

FT-IR (neat, cm^{-1}) 3337, 3054, 1596, 1473, 1439, 1349, 1113, 1001, 965, 801, 748, 727, 704

HRMS (ESI^{+}, *m/z*) 889.3457 ($C_{63}H_{46}N_4P$ $[M-Cl]^{+}$ requires 889.3460)

2-((E)-4'-Formylstyryl)-5,10,15,20-tetraphenylporphyrin (3.13)

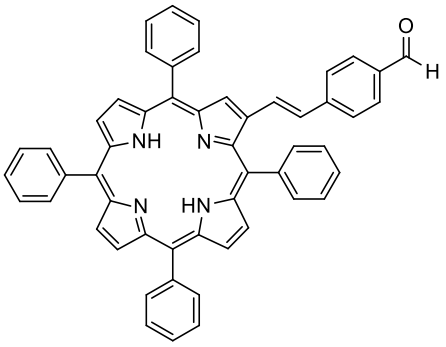

2-((E)-4'-Formylstyryl)-5,10,15,20-tetraphenylporphyrin **3.13** was prepared using a variation of a method previously outlined by Ventura *et al.*[24] Triphenyl[(5,10,15,20-tetraphenylporphyrin-2-yl)methyl]phosphonium chloride **3.11** (1.17 g, 1.28 mmol) and terephthaldehyde **3.12** (200 mg, 1.49 mmol) were stirred in DCM (250 mL) at RT and DBU (1.1 mL, 7.36 mmol) was added dropwise to the solution. After stirring at RT for 1 min, the reaction mixture was subject to flash column chromatography (silica gel, 1:1 DCM/petroleum spirits as eluent) and the solvent

evaporated under reduced pressure to give a purple solid. The material was dissolved in DCM (400 mL) and I_2 (230 mg, 0.906 mmol) was added before stirring at RT for 16 h. The reaction was diluted with DCM (200 mL) and washed with 1M aq. $Na_2S_2O_3$ (2 x 200 mL) and H_2O (2 x 200 mL), dried over $MgSO_4$ and the solvent was removed under reduced pressure. The crude product was purified via column chromatography (silica gel, 10:10:1 DCM: petroleum spirit: EtOAc as eluent) to yield 2-((E)-4'-formylstyryl)-5,10,15,20-tetraphenylporphyrin **3.13** as a dark purple powder (818 mg, 86%). The data reported below was in close agreement with the respective data reported by Ventura *et al*.[24]

^{1}H NMR (500MHz, $CDCl_3$) δ -2.58 (2H, s, inner ring N-**H**), 7.15 (1H, d, J = 15.9 Hz, β-pyrrole-C**H**$_2$Ar styryl), 7.31 (1H, d, J = 15.9 Hz, β-pyrrole-C**H**$_2$Ar styryl), 7.38 (2H, d, J = 8.0 Hz, Ar-**H** AB quartet), 7.73-7.86 (14H, m, Ar-**H**, *meso*-phenyl *m-/p*- and Ar-**H** AB quartet), 8.19-8.23 (6H, m, Ar-**H**, *meso*-phenyl *o*-), 8.24-8.27 (2H, m, Ar-**H**, *meso*-phenyl *o*-), 8.73 (1H, d, J = 4.7 Hz, **H**-pyrrole β-), 8.78-8.80 (2H, m, **H**-pyrrole β-), 8.81-8.84 (3H, m, **H**-pyrrole β-), 9.02 (1H, s, **H**-pyrrole β- styryl), 10.02 (1H, s, ArC**H**O)

^{13}C NMR (150MHz, $CDCl_3$) δ 120.23, 120.28, 120.52, 120.91, 127.04,127.07, 127.14,127.38, 127.59, 128.12, 128.13, 128.20, 128.77, 130.34, 134.71, 134.85, 134.91, 135.42, 142.14, 142.45, 142.55, 142.83, 144.29, 191.98

FT-IR (neat, cm^{-1}) 3306, 3056, 3025, 1698, 1598, 1565, 1473, 1441, 1350, 1218, 1166, 1073, 1002, 965, 841, 799, 770, 728, 701

HRMS (ESI$^+$, *m/z*) 745.2960 ($C_{53}H_{37}N_4O$ $[M+H]^+$ requires 745.2967)

[2-((E)-4'-Formylstyryl)-5,10,15,20-tetraphenylporphyrinato] zinc(II) (3.14)

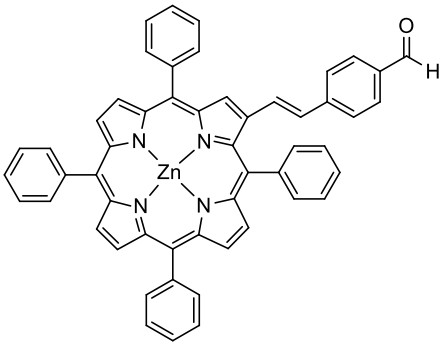

[2-((E)-4'-Formylstyryl)-5,10,15,20-tetraphenylporphyrinato] zinc(II) **3.14** was prepared using a variation of a method previously outlined by Ventura *et al*.[24] 2-((E)-4-Formylstyryl)-5,10,15,20-tetraphenylporphyrin **3.13** (760mg, 1.02 mmol) was subjected to the general zinc metalation conditions outlined in **5.2.1**. The crude product was purified by column chromatography (silica gel, 10:10:1 petroleum spirit: DCM: EtOAc as eluent) to yield [2-((E)-4'-formylstyryl)-5,10,15,20-tetraphenylporphyrinato] zinc(II) **3.14** as a dark purple powder (808 mg, 98%). The data reported below was in close agreement with the respective data reported by Ventura *et al*.[24]

^{1}H NMR (500MHz, $C_2D_2Cl_4$) δ 7.28 (1H, d, J = 16.0 Hz, β-pyrrole-C**H**$_2$Ar styryl), 7.33 (1H, d, J = 16.0 Hz, β-pyrrole-C**H**$_2$Ar styryl), 7.44 (2H, d, J = 8.0 Hz, Ar-**H** AB quartet), 7.76-7.89 (14H, m, Ar-**H**, *meso*-phenyl *m-/p*- and Ar-**H** AB quartet), 8.23-8.28 (6H, m, Ar-**H**, *meso*-phenyl *o*-), 8.29-8.32 (2H, m, Ar-**H**, *meso*-phenyl *o*-), 8.86 (1H, d, J = 4.6 Hz, **H**-pyrrole β-), 8.93-8.96 (4H, m, **H**-pyrrole β-), 8.98 (1H, d, J = 4.7 Hz, **H**-pyrrole β-), 9.19 (1H, s, **H**-pyrrole β-styryl), 10.05 (1H, s, ArC**H**O)

FT-IR (neat, cm^{-1}) 3052, 3026, 1695, 1596, 1485, 1441, 1339, 1219, 1166, 1072, 1004, 995, 833, 796, 700, 701

HRMS (ESI$^+$, *m/z*) 806.2014 ($C_{53}H_{34}N_4OZn$ M^+ requires 806.2024)

[2-((E)-4'-((E)-Styryl)styryl)-5,10,15,20-tetraphenylporphyrinato] zinc(II) (3.2)

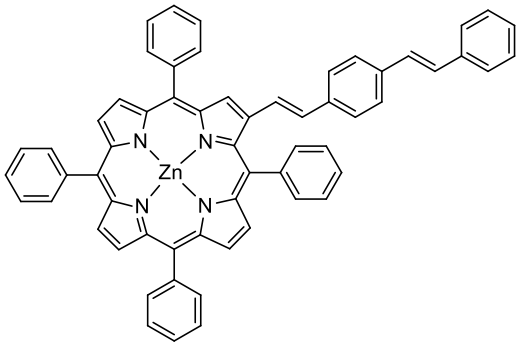

Sodium hydride (22 mg, 0.930 mmol) was added slowly to a solution of diethyl benzyl phosphonate **3.19** (51 mg, 0.223 mmol) and [2-((E)-4'-formylstyryl)-5,10,15,20-tetraphenylporphyrinato] zinc(II) **3.14** (150 mg, 0.186 mmol) in anhydrous THF (10 mL) and the reaction mixture was stirred for 24h at room temperature. The reaction was diluted with DCM (20 mL) and then added dropwise to H_2O (30 mL). The organic layer was separated and the aqueous layer extracted with DCM (30 mL), and the organic layers were combined and washed with sat. aq. NaCl solution (30 mL), dried over anhydrous Na_2SO_4, filtered and concentrated under reduced pressure to give a brownish-purple solid. The solid was purified by column chromatography (silica gel, 10:10:1 petroleum spirit: DCM: EtOAc as eluent) to yield the product **3.2** as a brownish-purple solid (136 mg, 83%). Compound **3.2** has not been previously reported in the literature and thus all data below for **3.2** constitutes novel characterization.

^{1}H NMR (500MHz, $C_2D_2Cl_4$) δ 7.12 (1H, d, J = 16.0 Hz, PPV vinylene -C**H**$_2$), 7.17 (1H, d, J = 16.1 Hz, PPV vinylene -C**H**$_2$), 7.22 (1H, d, J = 16.2 Hz, PPV vinylene -C**H**$_2$), 7.27-7.35 (4H, m, PPV phenylene terminal Ar-**H** *–o/-p*, PPV vinylene -C**H**$_2$), 7.43 (2H, t, J = 7.6 Hz, PPV phenylene terminal Ar-**H** *–m*), 7.54 (2H, d, J = 8.1 Hz, PPV phenylene Ar-**H**), 7.60 (2H, d, J = 7.9 Hz, PPV phenylene Ar-**H**), 7.76-7.92 (12H, m, Ar-**H**, *meso*-phenyl *m-/p-*), 8.23-8.29 (6H, m, Ar-**H**, *meso*-phenyl *o-*), 8.30-8.33 (2H, m, Ar-**H**, *meso*-phenyl *o-*), 8.86 (1H, d, J = 4.7 Hz, **H**-pyrrole β-), 8.93-8.97 (4H, m, **H**-pyrrole β-), 8.98 (1H, d, J = 4.7 Hz, **H**-pyrrole β-), 9.16 (1H, s, **H**-pyrrole β- PPV)

FT-IR (neat, cm^{-1}) 3053, 3022, 1597, 1509, 1485, 1441, 1339, 1195, 1176, 1134, 1072, 1004, 996, 959, 833, 794, 772, 750, 731, 722, 699, 688, 662

HRMS (ESI$^+$, *m/z*) 881.2603 ($C_{60}H_{41}N_4Zn$ $[M+H]^+$ requires 881.2623)

α-Mercapto-ω-(1-carboxyethyl)-poly[2-((E)-4'-((E)-4''-vinylstyryl)styryl)-5,10,15,20-tetraphenylporphyrinato] zinc(II) (3.5)

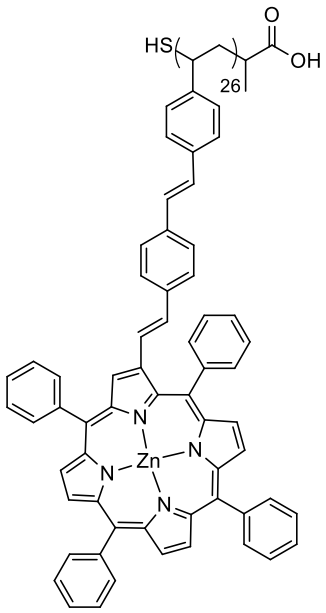

Sodium hydride (41 mg, 1.70 mmol) was added to a solution of poly(vinylbenzyldiethyl phosphonate) **3.20** (88 mg, 0.340 mmol VBC units) and [2-((E)-4'-formylstyryl)-5,10,15,20-tetraphenylporphyrinato] zinc(II) **3.14** (550 mg, 0.680 mmol) dissolved in anhydrous THF (10 mL) and the reaction mixture stirred for 5 days at room temperature. The reaction was diluted in DCM (20 mL) and then added dropwise to H_2O (100 mL) and the mixture extracted with $CHCl_3$ (100 mL). The organic layer was washed with sat. aq. NaCl solution (50 mL), dried over Na_2SO_4, filtered and concentrated under reduced pressure. The residue was purified by size exclusion column chromatography (Bio S-X beads, THF as eluent) to yield the porphyin-appended polymer **3.5** as a brownish-purple powder (276 mg, 90%). Compound **3.5** has not been previously reported in the literature and thus all data below for **3.5** constitutes novel characterization.

^{1}H NMR (500MHz, $C_2D_2Cl_4$) δ -0.09-2.84 (br., m, backbone, alkyl-**H**), 6.18-7.84 (br., m, Ar-**H** *meso*-phenyl *m-/p-*, Ar-**H** phenylene vinylene and -C**H**$_2$ phenylene vinylene), 7.86-8.34 (br., m, Ar-**H** *meso*-phenyl *o-),* 8.40-9.20 (br., m, **H**-pyrrole β-)

FT-IR (neat, cm^{-1}) 3055, 3023, 2926, 1597, 1513, 1485, 1441, 1339, 1218, 1195, 1177, 1137, 1071, 1004, 995, 959, 834, 796, 754, 723, 701, 665

6.2.3.3 Compounds with linker length of three phenylenevinylene units (a = 3)

1,4-Xylenebis(diethylphosphonate) (3.16)

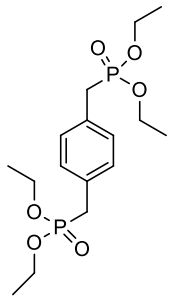

1,4-Xylenebis(diethylphosphonate) **3.16** was prepared using a variation of a method previously outlined by Ventura *et al*.[24] α,α-Dichloro-*p*-xylene **3.22** (1.75g, 10.0 mmol) in triethylphosphite (15 mL, 87.6 mmol) was stirred at reflux for 24h under N_2 . The unreacted triethylphosphite was then removed by Kugel-Rohr distillation (10 mbar, 50°C) to give a colourless waxy solid. The solid was then purified by column chromatography (silica gel, 9:1 EtOAc: MeOH as eluent) to yield 1,4-xylenebis(diethylphosphonate) **3.16** as a colouress oily crystalline solid (3.76 g, 99%). The data reported below was in close agreement with the respective data reported by Ventura *et al*.[24]

^{1}H NMR (500MHz, $CDCl_3$) δ 1.23 (12H, t, J = 7.1 Hz, -OCH$_2$C**H**$_3$), 3.12 (4H, d, J_{HP} = 20.2 Hz, -Ar-C**H**$_2$P), 3.95-4.05 (8H, m, -OC**H**$_2$CH$_3$), 7.24 (4H, s, Ar-**H**)

^{13}C NMR (125MHz, $CDCl_3$) δ 16.22, 16.27, 16.30, 16.32, 16.37, 33.72, 32.73, 33.82, 33.84, 62.00, 62.05, 62.07, 62.10, 62.15, 129.80, 129.86, 129.88, 129.89, 129.95, 130.05, 130.12, 130.14, 130.16, 130.22

FT-IR (neat, cm^{-1}) 2984, 1514, 1393, 1222, 1164, 1062, 1023, 965, 863, 773

HRMS (ESI$^+$, *m/z*) 379.1436 ($C_{16}H_{29}O_6P_2$ $[M+H]^+$ requires 379.1439)

[2-((E)-4'-((Diethylphosphonato)methyl)styryl)-5,10,15,20-tetraphenylporphyrinato] zinc(II) (3.17)

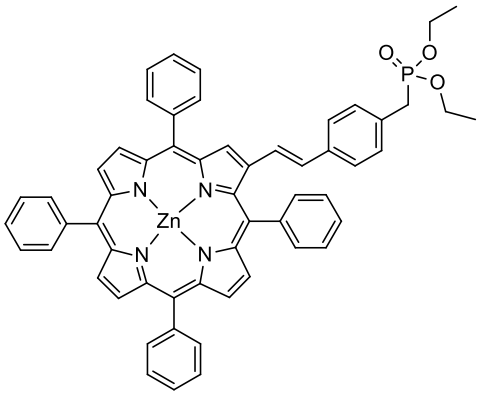

[2-((E)-4'-((Diethylphosphonato)methyl)styryl)-5,10,15,20-tetraphenylporphyrinato] zinc(II) **3.17** was prepared using a variation of a method previously outlined by Ventura *et al.*[24] [2-Formyl-5,10,15,20-tetraphenylporphyrinato] zinc(II) **3.15** (1.23 g, 1.74 mmol) and 1,4-xylenebis(diethylphosphonate) **3.16** (2.63 g, 6.96 mmol) were dissolved in anhydrous THF (250 mL) under an N_2 atmosphere. The solution was set to stir and t-BuOK (976 mg, 8.70 mmol) was added in 15 min intervals over 1h. The solvent was then evaporated from the reaction mixture under reduced pressure and the residue was purified by column chromatography (silica gel, DCM followed by 19:1 DCM: MeOH as eluent) to yield [2-((E)-4'-((diethylphosphonato)methyl)styryl)-5,10,15,20-tetraphenylporphyrinato] zinc(II) **3.17** as purple powder (748 mg, 46%). The data reported below was in close agreement with the respective data reported by Ventura *et al.*[24]

FT-IR (neat, cm^{-1}) 1597, 1483, 1440, 1338, 1231, 1025, 1002, 992, 962, 845, 793, 750, 721, 700

HRMS (ESI$^+$, *m/z*) 929.2589 ($C_{57}H_{46}N_4O_3PZn$ $[M+H]^+$ requires 929.2599)

[2-((E)-4'-((E)-4''-Formylstyryl)styryl)-5,10,15,20-tetraphenylporphyrinato] zinc(II) (3.18)

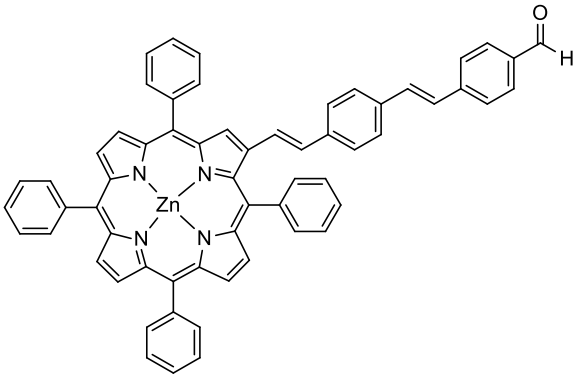

[2-((E)-4'-((E)-4''-Formylstyryl)styryl)-5,10,15,20-tetraphenylporphyrinato] zinc(II) **3.18** was prepared using a variation of a method previously outlined by Ventura *et al*.[24] Diethyl 4-(trans-2'-(2''-(5'',10'', 15'', 20''-tetraphenylporphyrinato zinc(II)yl)ethen-1'-yl)benzylphosphonate **3.17** (650 mg, 0.699 mmol) and terephthaldicarbaldehyde **3.12** (376 mg, 2.80 mmol) were dissolved in anhydrous THF (150 mL) under an N_2 atmosphere. The solution was set to stir and t-BuOK (393 mg, 3.50 mmol) was added in 15 min intervals over 2h. The solvent was then evaporated from the reaction mixture under reduced pressure and the residue was purified by column chromatography (silica gel, 10:10:1 petroleum spirit: DCM: EtOAc as eluent) to yield [2-((E)-4'-((E)-4''-formylstyryl)styryl)-5,10,15,20-tetraphenylporphyrinato] zinc(II) **3.18** as a dark green-brown powder (291 mg, 46%). The data reported below was in close agreement with the respective data reported by Ventura *et al*.[24]

^{1}H NMR (500MHz, $C_2D_2Cl_4$) δ 7.15 (1H, d, J = 15.9 Hz, vinylene -C**H**$_2$), 7.23 (1H, d, J = 16.1 Hz, vinylene -C**H**$_2$), 7.27-7.35 (4H, m, vinylene -C**H**$_2$ and Ar-**H** AB quartet phenylene), 7.56 (2H, d, J = 8.2 Hz, Ar-**H** AB quartet phenylene), 7.71 (2H, d, J = 8.1 Hz, Ar-**H** AB quartet phenylene), 7.76-7.89 (12H, m, Ar-**H**, *meso*-phenyl *m-/p*-), 7.91 (2H, d, J = 8.2 Hz, Ar-**H** AB quartet phenylene), 8.23-8.30 (6H, m, Ar-**H**, *meso*-phenyl *o*-), 8.30-8.35 (2H, m, Ar-**H**, *meso*-phenyl *o*-), 8.87 (1H, d, J = 4.7 Hz, **H**-pyrrole β-), 8.93-8.97 (4H, m, **H**-pyrrole β-), 8.99 (1H, d, J = 4.6 Hz, **H**-pyrrole β-), 9.17 (1H, s, **H**-pyrrole β- phenylene vinylene), 10.03 (1H, s, ArC**H**O)

FT-IR (neat, cm^{-1}) 2956, 1692, 1598, 1441, 1339, 1166, 1069, 1004, 994, 958, 835, 793, 758, 722, 700

HRMS (ESI$^+$, *m/z*) 909.2559 ($C_{61}H_{41}N_4OZn$ $[M+H]^+$ requires 909.2572)

[2-((E)-4'-((E)-4''-((E)-Styryl)styryl)styryl)-5,10,15,20-tetraphenylporphyrinato] zinc(II) (3.3)

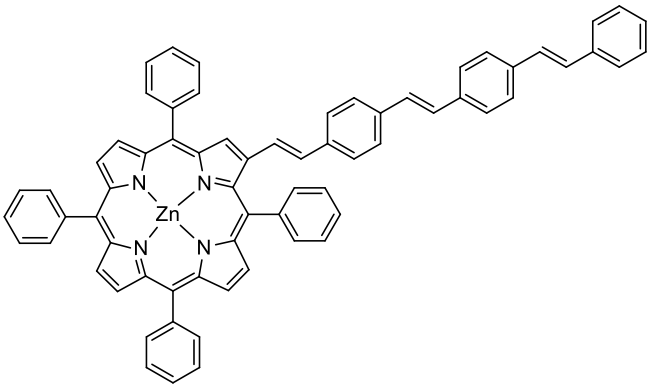

Sodium hydride (8 mg, 0.330 mmol) was added slowly to a solution of diethyl benzyl phosphonate **3.19** (23 mg, 0.099 mmol) and 2-((E)-4'-((E)-4''-formylstyryl)styryl)-5,10,15,20-tetraphenylporphyrinato] zinc(II) **3.18** (60 mg, 0.066 mmol) in anhydrous THF (5 mL) and the reaction mixture was stirred for 24h at room temperature. The reaction was diluted with DCM (20 mL) and then added dropwise to H_2O (30 mL). The organic layer was separated and the aqueous layer extracted with DCM (30 mL), and the organic layers were combined and washed with sat. aq. NaCl solution (30 mL), dried over anhydrous Na_2SO_4, filtered and concentrated under reduced pressure to give a brownish-purple solid. The solid was purified by column chromatography (silica gel, DCM: EtOAc 4:1 as eluent) to yield the product **3.3** as a brownish-purple solid (55 mg, 85%). Compound **3.3** has not been previously reported in the literature and thus all data below for **3.3** constitutes novel characterization.

^{1}H NMR (500MHz, $C_2D_2Cl_4$) δ 7.13 (1H, d, J = 15.7 Hz, PPV vinylene -C**H**$_2$), 7.17-7.19 (2H, m, PPV vinylene -C**H**$_2$), 7.19-7.22 (2H, m, PPV vinylene -C**H**$_2$), 7.28-7.34 (4H, m, PPV phenylene terminal Ar-**H** *–o/-p*, PPV vinylene -C**H**$_2$), 7.42 (2H, t, J = 7.7 Hz, PPV phenylene terminal Ar-**H** *–m*), 7.53-7.61 (8H, m, PPV phenylene Ar-**H**), 7.76-7.92 (12H, m, Ar-**H**, *meso*-phenyl *m-/p*-), 8.24-8.29 (6H, m, Ar-**H**, *meso*-phenyl *o*-), 8.30-8.33 (2H, m, Ar-**H**, *meso*-phenyl *o*-), 8.86 (1H, d, J = 4.7 Hz, **H**-pyrrole β-), 8.93-8.96 (4H, m, **H**-pyrrole β-), 8.98 (1H, d, J = 4.6 Hz, **H**-pyrrole β-), 9.16 (1H, s, **H**-pyrrole β- PPV)

FT-IR (neat, cm^{-1}) 3053, 3021, 1596, 1514, 1486, 1441, 1420, 1339, 1197, 1177, 1158, 1135, 1072, 1004, 994, 965, 937, 833, 817, 796, 771, 757, 733, 719, 701, 689, 661

HRMS (ESI$^+$, *m/z*) 983.3075 ($C_{68}H_{47}N_4Zn$ $[M+H]^+$ requires 983.3092)

α-Mercapto-ω-(1-carboxyethyl)-poly[2-((E)-4'-((E)-4''-((E)-4'''-vinylstyryl)styryl)styryl)-5,10,15,20-tetraphenylporphyrinato] zinc(II) (3.6)

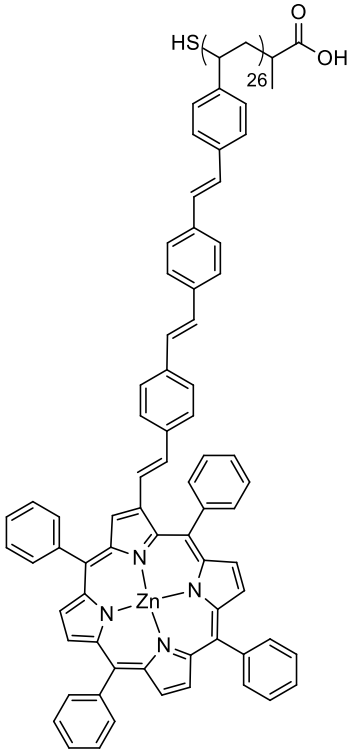

Sodium hydride (13 mg, 0.550 mmol) was added to a solution of poly(vinylbenzyldiethyl phosphonate) **3.20** (28 mg, 0.110 mmol VBC units) and 2-((E)-4'-((E)-4''-formylstyryl)styryl)-5,10,15,20-tetraphenylporphyrinato] zinc(II) **3.18** (200 mg, 0.220 mmol) dissolved in anhydrous THF (10 mL) and the reaction mixture stirred for 5 days at room temperature. The reaction was diluted in DCM (20 mL) and then added dropwise to H_2O (100 mL) and the mixture extracted with $CHCl_3$ (100 mL). The organic layer was washed with sat. aq. NaCl solution (50 mL), dried over Na_2SO_4, filtered and concentrated under reduced pressure. The residue was purified by size exclusion column chromatography (Bio S-X beads, THF as eluent) to yield the porphyin-appended polymer **3.6** as a brownish-purple powder (82 mg, 73%). Compound **3.6** has not been

previously reported in the literature and thus all data below for **3.6** constitutes novel characterization.

^{1}H NMR (500MHz, $C_2D_2Cl_4$) δ 0.74-2.56 (br., m, backbone, alkyl-**H**), 6.15-7.86 (br., m, Ar-**H** *meso*-phenyl *m-/p-*, Ar-**H** phenylene vinylene and -C**H**$_2$ phenylene vinylene), 7.88-8.38 (br., m, Ar-**H** *meso*-phenyl *o-),* 8.41-9.16 (br., m, **H**-pyrrole β-)

FT-IR (neat, cm^{-1}) 3054, 3024, 2922, 1597, 1514, 1486, 1440, 1420, 1339, 1219, 1195, 1177, 1136, 1071, 1004, 995, 958, 833, 796, 770, 755, 723, 701, 662

6.2.4 Synthesis of Chapter 4 compounds – Stilbene and ether linked pendant porphyin polymers and their monomeric model compound analogues

2-Bromo-5,10,15,20-tetraphenylporphyrin (4.11)

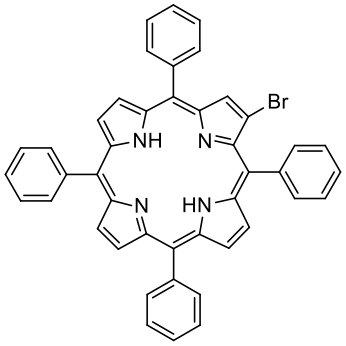

2-Bromo-5,10,15,20-tetraphenylporphyrin **4.11** was prepared using a variation of a method previously outlined by Gao *et al.*[25] TPP **2.10** (1.86 g, 3.03 mmol) and pyridine (30 mL) were dissolved in $CHCl_3$ (750 mL) and refluxed for 5 min. A solution of N-bromosuccinimide (1.08 g, 6.06 mmol, dissolved in 750 mL $CHCl_3$) was added slowly to the refluxing solution over 4h. The solution was refluxed for an additional 30 min then quenched with acetone (400 mL) after which the solvent was removed by rotary evaporation. The residue was then purified via gravity-assisted column chromatography (silica gel, 1:2 toluene: petroleum spirit as eluent) to yield 2-bromo-5,10,15,20-tetraphenylporphyrin **4.11** as a purple powder (890 mg, 42%). The data reported below was in close agreement with the respective data reported by Gao *et al.*[25]

^{1}H NMR (600MHz, $CDCl_3$) δ -2.85 (2H, s, inner ring N-**H**), 7.70-7.81 (12H, m, Ar-**H**, *meso*-phenyl *m-/p-),* 8.07-8.11 (2H, m, Ar-**H**, *meso*-phenyl *o*-), 8.17-8.22 (6H, m, Ar-**H**, *meso*-phenyl *o*-), 8.76 (1H, d, J = 4.7 Hz, **H**-pyrrole β-), 8.77 (1H, d, J = 4.7 Hz, **H**-pyrrole β-), 8.82 (1H, d, J = 5.0 Hz, **H**-pyrrole β-), 8.85 (1H, d, J = 4.9 Hz, **H**-pyrrole β-), 8.87 (1H, s, **H**-pyrrole β-bromo), 8.88 (1H, d, J = 5.0 Hz, **H**-pyrrole β-), 8.91 (1H, d, J = 4.8 Hz, **H**-pyrrole β-)

^{13}C NMR (150MHz, $CDCl_3$) δ 119.72, 120.17, 120.44, 120.87, 126.85, 126.88, 126.96, 127.10, 127.97, 128.09, 128.37, 134.45, 134.66, 134.69, 134.73, 140.95, 141.86, 142.18

FT-IR (neat, cm^{-1}) 3325, 3056, 1597, 1473, 1442, 1349, 1178, 1025, 1002, 977, 965, 829, 799, 750, 722

HRMS (ESI^{+}, *m/z*) 693.1653 ($C_{44}H_{30}BrN_4$ $[M+H]^+$ requires 693.1654)

[2-(4'-Formylphenyl)-5,10,15,20-tetraphenylporphyrinato] zinc(II) (4.8)

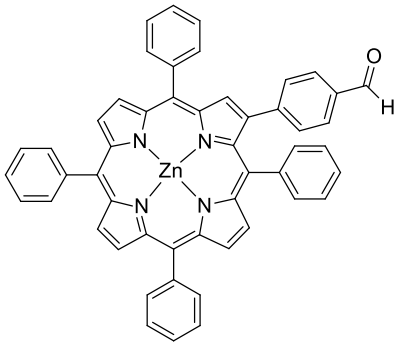

A crude mixture of brominated TPP derivatives with various degrees of bromination was prepared using a variation of a method previously outlined by Gao *et al*.[25] TPP **2.10** (1.40g, 2.28 mmol) and pyridine (20 mL) were dissolved in $CHCl_3$ (350 mL) and refluxed for 5 min. A solution of N-bromosuccinimide (810 mg, 4.56 mmol, dissolved in 350 mL $CHCl_3$) was added slowly to the refluxing solution over 4h. The solution was refluxed for an additional 30 min then quenched with acetone (200 mL) after which the solvent was removed by rotary evaporation. The resultant mixture of brominated TPP derivatives with various degrees of bromination was carried through to the next step without purification.

$Zn(CH_3COO)_2.2H_2O$ (2.19 g, 10.0 mmol) was added to a solution of the brominated TPP derivatives (1.39 g, 2.00 mmol) dissolved in a mixture of CH_2Cl_2 (600 mL) and MeOH (200 mL) and the reaction stirred at RT for 16h in the dark. The reaction mixture was then washed with 5% (w/v) aq. $NaHCO_3$ (400 mL) and brine (400 mL) and subsequently dried over Na_2SO_4, filtered and the solvent removed by rotary evaporation. The resultant product was carried through to the next step without further purification.

The synthesis of [2-(4'-formylphenyl)-5,10,15,20-tetraphenylporphyrinato] zinc(II) **4.8** was prepared using a variation of a method previously outlined by Sirithip *et al*. for the analogous meso-tetra-(3,5-di-*tert*-butylphenyl) substituted porphyrin.[26] A flask charged with a mixture of brominated ZnTPP derivatives (1.37 g, 1.81 mmol Zn mono-bromo weighted equivalent), 4-formylphenylboronic acid pinacol ester (504 mg, 2.17 mmol) and $Pd(PPh_3)_4$ (209 mg, 0.181 mmol) was evacuated and backfilled with nitrogen gas. THF (20 mL) and a 2M aq. solution of Na_2CO_3 (10 mL), both of which had been degassed by bubbling with nitrogen gas for 20 min, were added to the flask and the mixture stirred at 65°C for 16h. The mixture was then cooled, diluted with CH_2Cl_2 (400 mL) and washed with brine (200 mL). The solution was then dried over Na_2SO_4, filtered and the solvent removed by rotary evaporation. The residue was then purified via column chromatography (silica gel, 1:1 toluene: petroleum spirit then 2:1 toluene: EtOAc as eluent) to yield [2-(4'-formylphenyl)-5,10,15,20-tetraphenylporphyrinato] zinc(II) **4.8** as a reddish-purple solid (807 mg, 45% over 3 steps). Compound **4.8** has not been previously reported in the literature and thus all data below for **4.8** constitutes novel characterization.

^{1}H NMR (500MHz, $CDCl_3$) δ 7.51 (2H, d, J = 8.0 Hz, Ar-H formylphenyl), 7.65 (2H, d, J = 8.0 Hz, Ar-H formylphenyl), 7.70-7.80 (12H, m, Ar-**H**, *meso*-phenyl *m-/p-)*, 7.87-7.89 (2H, m, Ar-**H**, *meso*-phenyl *o*-), 8.19-8.24 (6H, m, Ar-**H**, *meso*-phenyl *o*-), 8.81 (1H, d, J = 4.6 Hz, **H**-pyrrole β-), 8.87 (1H, d, J = 4.6 Hz, **H**-pyrrole β-), 8.88 (1H, s, **H**-pyrrole-Ar-formylphenyl β-), 8.92 (1H, d, J = 4.6 Hz, **H**-pyrrole β-), 8.93 (2H, m, **H**-pyrrole β-), 8.95 (1H, d, J = 4.5 Hz, **H**-pyrrole β-), 10.00 (1H, s, Ar-C**H**O formylphenyl)

^{13}C NMR (150MHz, $CDCl_3$) δ 120.99, 121.36, 121.78, 122.27, 126.22, 126.73, 126.75, 126.77, 127.43, 127.74, 127.76, 128.73, 131.02, 131.82, 132.31, 132.41, 132.45, 132.94, 133.65, 134.51, 134.57, 134.58, 135.40, 135.97, 141.47, 142.75, 142.77, 142.97, 145.81, 144.26, 146.65, 147.66, 150.49, 150.57, 150.64, 150.68, 150.84, 151.27, 192.41

FT-IR (neat, cm^{-1}) 3053, 1699, 1603, 1485, 1441, 1339, 1210, 1194, 1072, 1004, 994, 831, 797, 752, 723, 701, 661

HRMS (ESI$^+$, *m/z*) 781.1917 ($C_{51}H_{32}N_4OZn$ $[M+H]^+$ requires 781.1946)

[2-((E)-4'-Styrylphenyl)-5,10,15,20-tetraphenylporphyrinato] zinc(II) (4.1)

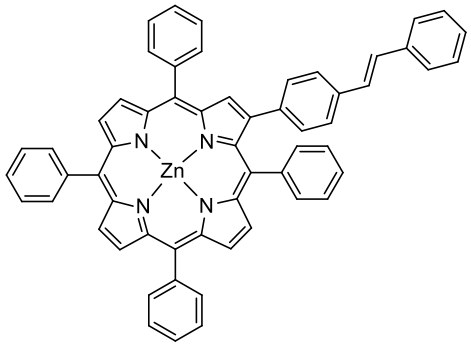

A suspension of sodium hydride (9 mg, 0.375 mmol) in THF (5 mL) was added slowly to a solution of diethyl benzyl phosphonate **3.19** (20 mg, 0.088 mmol) and [2-(4-formylphenyl)-5,10,15,20-tetraphenylporphyrinato] zinc(II) **4.8** (56 mg, 0.072 mmol) in anhydrous THF (5 mL) and the reaction mixture was stirred for 24h at room temperature. The reaction was quenched by addition of MeOH (5 mL) and the mixture was diluted in DCM (30 mL) and washed with H_2O (30 mL). The organic layer was separated and the aqueous layer extracted with DCM (30 mL), and the organic layers were combined and washed with sat. aq. NaCl solution (30 mL), dried over anhydrous Na_2SO_4, filtered and concentrated under reduced pressure to give a reddish-pink solid. The solid was purified by column chromatography (silica gel, 19:1 toluene: EtOAc as eluent) to yield the product **4.1** as a reddish-pink solid (54 mg, 88%). Compound **4.1** has not been previously reported in the literature and thus all data below for **4.1** constitutes novel characterization.

^{1}H NMR (500MHz, $CDCl_3$) δ 7.11 (1H, d, J = 16.4 Hz, ArC**H**$_2$Ar stilbene), 7.16 (1H, d, J = 16.3 Hz, ArC**H**$_2$Ar stilbene), 7.21-7.25 (2H, m, -CH_2-*m*-Ar-**H** stilbene), 7.27-7.35 (5H, m, -CH_2-*p*-Ar-**H** stilbene and pyrrole-Ar-**H** AB quartet), 7.39-7.43 (2H, m, -CH_2-*o*-Ar-**H** stilbene), 7.58-7.62 (2H, m, Ar-**H**, *meso*-phenyl *m-/p-)*, 7.70-7.80 (10H, m, Ar-**H**, *meso*-phenyl *m-/p-),*

7.88-7.91 (2H, m, Ar-**H**, *meso*-phenyl *o*-), 8.21-8.25 (6H, m, Ar-**H**, *meso*-phenyl *o*-), 8.82 (1H, d, J = 4.6 Hz, **H**-pyrrole β-), 8.87 (1H, d, J = 4.6 Hz, **H**-pyrrole β-), 8.89 (1H, s, **H**-pyrrole-stilbene β-), 8.93-8.95 (3H, m, **H**-pyrrole β-), 8.96 (1H, d, J = 4.6 Hz, **H**-pyrrole β-)

^{13}C NMR (125MHz, $CDCl_3$) δ 120.72, 121.15, 121.67, 122.62, 125.52, 126.09, 126.62, 126.68, 126.71, 126.74, 127.18, 127.64, 127.67, 128.09, 128.87, 128.99, 130.65, 131.59, 132.09, 132.16, 132.22, 132.32, 132.87, 134.52, 134.58, 134.61, 135.34, 135.8 4, 137.71, 139.21, 141.53, 142.87, 142.90, 143.03, 146.86, 147.22, 148.08, 150.31, 150.38, 150.45, 150.49, 150.65, 151.43

FT-IR (neat, cm^{-1}) 3050, 3024, 1598, 1488, 1441, 1339, 1218, 1194, 1178, 1159, 1072, 1004, 995, 964, 817, 798, 752, 724, 701, 661

HRMS (ESI$^+$, *m/z*) 854.2376 ($C_{58}H_{38}N_4Zn$ M^+ requires 854.2388)

α-Mercapto-ω-(1-carboxyethyl)-poly{[2-(4'-((E)-4''-vinylstyryl)phenyl)-5,10,15,20-tetraphenylporphyrinato] zinc(II)} (4.4)

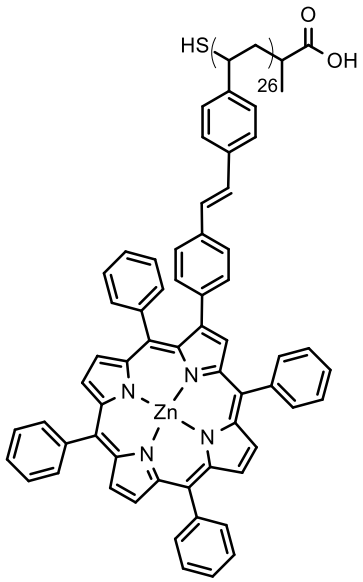

A suspension of sodium hydride (23 mg, 0.960 mmol) in THF (10 mL) was added to a solution of α-(dodecylthiocarbonothioylthio)-ω-(1-carboxyethyl)-poly(4-vinylbenzyldiethyl phosphonate) **3.20** (49 mg, 0.192 mmol) and [2-(4-formylphenyl)-5,10,15,20-tetraphenylporphyrinato] zinc(II) **4.8** (300 mg, 0.384 mmol) dissolved in anhydrous THF (10 mL) and the reaction mixture stirred

for 5 days at room temperature. The reaction was quenched by addition of MeOH (5 mL) and the mixture was diluted in $CHCl_3$ (100 mL) and washed with H_2O (100 mL). The organic layer was washed with sat. aq. NaCl solution (50 mL), dried over Na_2SO_4, filtered and concentrated under reduced pressure. The residue was purified by size exclusion column chromatography (Bio S-X beads, toluene as eluent) to yield the porphyin-appended polymer as a brownish-purple powder (68 mg, 40%). Compound **4.4** has not been previously reported in the literature and thus all data below for **4.4** constitutes novel characterization.

^{1}H NMR (125MHz, $C_2D_2Cl_4$) δ 0.80-2.56 (br., m, backbone, alkyl-**H**), 6.45-8.34 (br., m, Ar-**H**-mesophenyl, Ar-**H**-stilbene linker), 8.37-9.06 (br., m, **H**-pyrrole β-)

FT-IR (neat, cm^{-1}) 3054, 3021, 2922, 1598, 1509, 1487, 1441, 1338, 1215, 1194, 1178, 1158, 1071, 1048, 1004, 994, 962, 844, 832, 796, 752, 723, 700, 661

[2-(3'-Formylphenyl)-5,10,15,20-tetraphenylporphyrinato] zinc(II) (4.9)

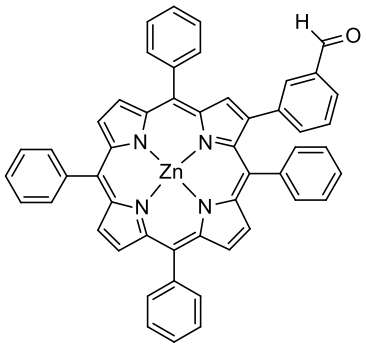

A crude mixture of brominated TPP derivatives with various degrees of bromination was prepared using a variation of a method previously outlined by Gao *et al*.[25] TPP **2.10** (1.40g, 2.28 mmol) and pyridine (20 mL) were dissolved in $CHCl_3$ (350 mL) and refluxed for 5 min. A solution of N-bromosuccinimide (810 mg, 4.56 mmol, dissolved in 350 mL $CHCl_3$) was added slowly to the refluxing solution over 4h. The solution was refluxed for an additional 30 min then quenched with acetone (200 mL) after which the solvent was removed by rotary evaporation. The resultant mixture of brominated TPP derivatives with various degrees of bromination was carried through to the next step without purification.

$Zn(CH_3COO)_2.2H_2O$ (2.29 g, 10.5 mmol) was added to a solution of the brominated TPP derivatives (1.45 g, 2.09 mmol mono-bromo weighted equivalent) dissolved in a mixture of DCM (600 mL) and MeOH (200 mL) and the reaction mixture stirred at RT for 15h in the dark. The reaction mixture was then washed with 5% (w/v) aq. $NaHCO_3$ (400 mL) and brine (400 mL) and subsequently dried over Na_2SO_4, filtered and the solvent removed by rotary evaporation. The resultant product was carried through to the next step without further purification.

The synthesis of [2-(3'-formylphenyl)-5,10,15,20-tetraphenylporphyrinato] zinc(II) **4.9** was prepared using a variation of the method for the analogous porphyrin **4.8**, based on similar syntheses performed by Sirithip et al.[26] A flask charged with a mixture of brominated ZnTPP derivatives (1.36 g, 1.80 mmol Zn mono-bromo TPP weighted equivalent), 3-formylphenylboronic acid (324 mg, 2.16 mmol) and $Pd(PPh_3)_4$ (208 mg, 0.180 mmol) was evacuated and backfilled with nitrogen gas. THF (20 mL) and a 2M aq. solution of Na_2CO_3 (10 mL), both of which had been degassed by bubbling with nitrogen gas for 20 min, were added to the flask and the mixture stirred at 65°C for 16h. The mixture was then cooled, diluted with DCM (400 mL) and the organic layer washed with H_2O (200 mL) and brine (200 mL). The solution was then dried over Na_2SO_4, filtered and the solvent removed by rotary evaporation. The residue was then purified via column chromatography (silica gel, 19:1 toluene: EtOAc as eluent) to yield [2-(3'-formylphenyl)-5,10,15,20-tetraphenylporphyrinato] zinc(II) **4.9** as a reddish-purple solid (926 mg, 52% over 3 steps). Compound **4.9** has not been previously reported in the literature and thus all data below for **4.9** constitutes novel characterization.

^{1}H NMR (500MHz, $CDCl_3$) δ 7.15-7.24 (3H, m, Ar-H formylphenyl), 7.35 (1H, t, J = 7.6 Hz, Ar-H formylphenyl), 7.65-7.81 (12H, m, Ar-**H**, *meso*-phenyl *m-/p-),* 7.88 (2H, bd, J = 6.5 Hz, Ar-**H**, *meso*-phenyl *o*-), 8.20-8.25 (6H, m, Ar-**H**, *meso*-phenyl *o*-), 8.79 (1H, d, J = 4.7 Hz, **H**-pyrrole β-), 8.87 (1H, d, J = 4.7 Hz, **H**-pyrrole β-), 8.89 (1H, s, **H**-pyrrole-Ar-formylphenyl β-), 8.93-8.95 (3H, m, **H**-pyrrole β-), 8.96 (1H, d, J = 4.6 Hz, **H**-pyrrole β-), 9.91 (1H, s, Ar-C**H**O formylphenyl)

^{13}C NMR (125MHz, $CDCl_3$) δ 120.90, 121.33, 121.77, 122.14, 126.12, 126.72, 126.73, 126.75, 126.85, 127.55, 127.72, 127.73, 128.10, 128.36, 129.17, 131.77, 132.11, 132.28, 132.36, 132.42, 132.83, 134.51, 134.58, 135.24, 135.56, 135.78, 136.05, 140.81, 141.39, 142.79, 142.81, 142.94, 145.55, 146.25, 147.71, 150.50, 150.52, 150.59, 150.62, 150.79, 151.30

FT-IR (neat, cm^{-1}) 3053, 3023, 1697, 1671, 1597, 1485, 1440, 1339, 1194, 1156, 1072, 1004, 994, 833, 796, 753, 723, 701, 661

HRMS (ESI$^+$, *m/z*) 781.1937 ($C_{51}H_{32}N_4OZn$ $[M+H]^+$ requires 781.1946)

[2-((E)-3'-Styrylphenyl)-5,10,15,20-tetraphenylporphyrinato] zinc(II) (4.2)

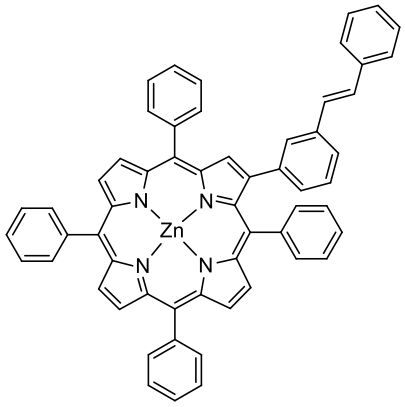

A suspension of sodium hydride (29 mg, 1.21 mmol) in THF (5 mL) was added slowly to a solution of diethyl benzyl phosphonate **3.19** (53 mg, 0.232 mmol) and [2-(3-formylphenyl)-5,10,15,20-tetraphenylporphyrinato] zinc(II) **4.9** (150 mg, 0.192 mmol) in anhydrous THF (5 mL) and the reaction mixture was stirred for 24h at room temperature. The reaction was quenched by addition of MeOH (5 mL) and the mixture was diluted in DCM (30 mL) and washed with H_2O (30 mL). The organic layer was separated and the aqueous layer extracted with DCM (30 mL), and the organic layers were combined and washed with sat. aq. NaCl solution (30 mL), dried over anhydrous Na_2SO_4, filtered and concentrated under reduced pressure to give a reddish-pink solid. The solid was purified by column chromatography (silica gel, 19:1 toluene: EtOAc as eluent) to yield the product **4.2** as a reddish-pink solid (127 mg, 77%). Compound **4.2** has not been previously reported in the literature and thus all data below for **4.2** constitutes novel characterization.

^{1}H NMR (500MHz, $CDCl_3$) δ 7.02 (1H, d, J = 16.6 Hz, ArC**H**$_2$Ar stilbene), 7.06 (1H, d, J = 16.6 Hz, ArC**H**$_2$Ar stilbene), 7.17-7.30 (6H, m, β-phenyl-Ar-**H** *–o/-m/-p* and Ar-**H**, *meso*-phenyl *m-/p-*), 7.33-7.38 (3H, m, terminal stilbene phenyl Ar-**H** *–m/-p)*, 7.43 (1H, s, β-phenyl-Ar-**H** –

o), 7.52 (2H, d, J = 8.0 Hz, terminal stilbene phenyl Ar-**H** –*o*), 7.69-7.80 (9H, m, Ar-**H**, *meso*-phenyl *m-/p-),* 7.88-7.96 (2H, m, *meso*-phenyl *o*-), 8.21-8.26 (6H, m, Ar-**H**, *meso*-phenyl *o*-), 8.82 (1H, d, J = 4.6 Hz, **H**-pyrrole β-), 8.88 (1H, d, J = 4.7 Hz, **H**-pyrrole β-), 8.91 (1H, s, **H**-pyrrole-stilbene β-), 8.93-8.95 (3H, m, **H**-pyrrole β-), 8.97 (1H, d, J = 4.7 Hz, **H**-pyrrole β-)

^{13}C NMR (125MHz, $CDCl_3$) δ 120.77, 121.17, 121.68, 122.59, 124.37, 126.57, 126.70, 126.71, 126.75, 127.49, 127.62, 127.66, 127.67, 127.75, 128.51, 128.82, 128.84, 128.97, 129.61, 131.62, 132.12, 132.17, 132.23, 132.32, 132.85, 134.51, 134.58, 135.43, 136.03, 137.69, 140.04, 141.32, 142.87, 142.90, 143.03, 146.76, 147.24, 148.02, 150.34, 150.40, 150.45, 150.51, 150.65, 151.41

FT-IR (neat, cm^{-1}) 3055, 3023, 2921, 1598, 1488, 1441, 1339, 1195, 1177, 1158, 1072, 1004, 996, 958, 845, 797, 747, 723, 698, 661

HRMS (ESI^+, *m/z*) 854.2378 ($C_{58}H_{38}N_4Zn$ M^+ requires 854.2388)

α-Mercapto-ω-(1-carboxyethyl)-poly{[2-(-3'-((E)-4''-vinylstyryl)phenyl)-5,10,15,20-tetraphenylporphyrinato] zinc(II)} (4.5)

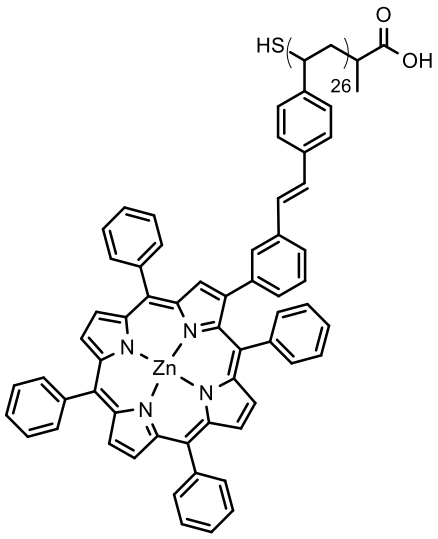

A suspension of sodium hydride (23 mg, 0.958 mmol) in THF (10 mL) was added to a solution of α-mercapto-ω-(1-carboxyethyl)-poly(4-vinylbenzyldiethyl phosphonate) **3.20** (49 mg, 0.192 mmol phosphonate units) and [2-(3-formylphenyl)-5,10,15,20-tetraphenylporphyrinato] zinc(II)

4.9 (300 mg, 0.384 mmol) dissolved in anhydrous THF (10 mL) and the reaction mixture stirred for 5 days at room temperature. The reaction was quenched by addition of MeOH (5 mL) and the mixture was diluted in $CHCl_3$ (100 mL) and washed with H_2O (100 mL). The organic layer was washed with sat. aq. NaCl solution (50 mL), dried over Na_2SO_4, filtered and concentrated under reduced pressure. The residue was purified by size exclusion column chromatography (Bio S-X beads, toluene as eluent) to yield the porphyin-appended polymer **4.5** as a brownish-purple powder (116 mg, 69%). Compound **4.5** has not been previously reported in the literature and thus all data below for **4.5** constitutes novel characterization.

^{1}H NMR (500MHz, $C_2D_2Cl_4$) δ -0.43-0.24 (br., m, backbone, alkyl-**H**), 0.26-2.53 (br., m, backbone, alkyl-**H**), 6.05-7.82 (br., m, Ar-**H**-mesophenyl o-/m-/p-, Ar-H- stilbene linker, ArC**H**$_2$Ar stilbene), 7.83-8.30 (br., m, Ar-**H**-mesophenyl o-), 8.37-9.06 (br., m, **H**-pyrrole β-)

FT-IR (neat, cm^{-1}) 3053, 3023, 2921, 1598, 1508, 1485, 1441, 1339, 1219, 1178, 1072, 1004, 995, 960, 796, 753, 723, 700, 661

[2-((4'-Hydroxymethyl)phenyl)-5,10,15,20-tetraphenylporphyrinato] zinc(II) (4.10)

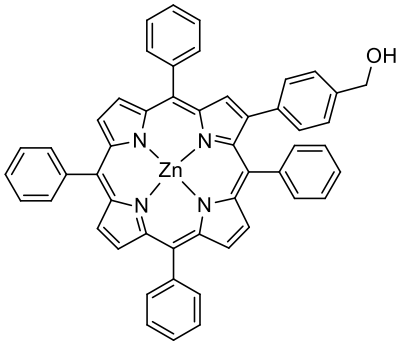

$NaBH_4$ (23 mg, 0.613 mmol) was added to a solution of [2-(4-formylphenyl)-5,10,15,20-tetraphenylporphyrinato] zinc(II) **4.8** (400 mg, 0.511 mmol) in 2:1 $CHCl_3$/EtOH (360 mL) and stirred for 20h at RT. The solvent was removed under reduced pressure and the residue taken up in H_2O (200 mL). DCM (200 mL) was added to the mixture and the organic layer separated and washed with sat. aq. NaCl solution (100 mL). The organic layer was then dried over $MgSO_4$, filtered and concentrated under reduced pressure. The crude product was then purified by column

chromatography (silica gel, 5:4:1 petroleum spirit: DCM: EtOAc as eluent) to yield [2-((4-hydroxymethyl)phenyl)-5,10,15,20-tetraphenylporphyrinato] zinc(II) **4.10** as a pinkish-purple solid (386 mg, 96%). Compound **4.10** has not been previously reported in the literature and thus all data below for **4.10** constitutes novel characterization.

^{1}H NMR (500MHz, $CDCl_3$) δ 4.47 (2H, d, J = 5.9 Hz, Ar-C**H**$_2$OH hydroxymethylphenyl), 7.02 (2H, d, J = 8.1 Hz, Ar-**H** hydroxymethylphenyl), 7.15-7.22 (3H, m, Ar-**H**, *meso*-phenyl *m-/p-),* 7.33 (2H, d, J = 8.1 Hz, Ar-**H** hydroxymethylphenyl), 7.69-7.79 (9H, m, Ar-**H**, *meso*-phenyl *m-/p-),* 7.84-7.87 (2H, m, Ar-**H**, *meso*-phenyl *o*-), 8.20-8.25 (6H, m, Ar-**H**, *meso*-phenyl *o*-), 8.78 (1H, d, J = 4.7 Hz, **H**-pyrrole β-), 8.86 (1H, s, **H**-pyrrole β- hydroxymethylphenyl), 8.87 (1H, d, J = 4.7 Hz, **H**-pyrrole β-), 8.93-8.95 (3H, m, **H**-pyrrole β-), 8.96 (1H, d, J = 4.7 Hz, **H**-pyrrole β-)

^{13}C NMR (125MHz, $CDCl_3$) δ 65.21, 120.67, 121.14, 121.64, 122.39, 125.05, 126.06, 126.64, 126.69, 126.72, 126.93, 127.60, 127.65, 130.61, 131.58, 132.10, 132.14, 132.22, 132.31, 132.77, 134.51, 134.58, 134.59, 135.36, 135.73, 137.40, 139.36, 141.57, 142.01, 142.04, 143.07, 146.67, 146.99, 147.95, 150.30, 150.39, 150.44, 150.48, 150.64, 151.39

FT-IR (neat, cm^{-1}) 3052, 1598, 1484, 1441, 1338, 1217, 1177, 1194, 1072, 1004, 993, 843, 796, 752, 723, 701, 661

HRMS (ESI$^+$, *m/z*) 782.2014 ($C_{51}H_{34}N_4OZn$ M^+ requires 782.2024)

[2-((4'-Benzyloxymethyl)phenyl)-5,10,15,20-tetraphenylporphyrinato] zinc(II) (4.3)

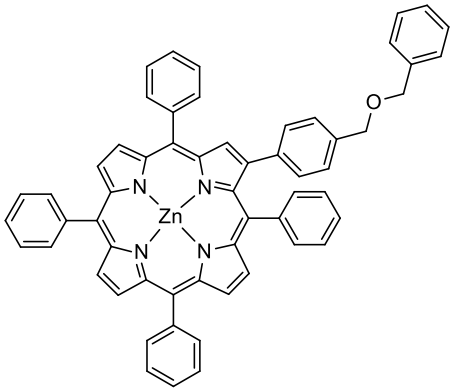

A suspension of sodium hydride (13 mg, 0.542 mmol) in THF (5 mL) was added slowly to a solution of benzyl bromide **3.25** (55 mg, 0.322 mmol) and [2-((4-hydroxymethyl)phenyl)-5,10,15,20-tetraphenylporphyrinato] zinc(II) **4.10** (85 mg, 0.108 mmol) in anhydrous THF (5 mL). The reaction mixture was then allowed to stir for 24h at room temperature. The reaction was quenched by addition of MeOH (5 mL) and the mixture was diluted in DCM (30 mL) and washed with H_2O (30 mL). The organic layer was separated and the aqueous layer extracted with DCM (30 mL), and the organic layers were combined and washed with sat. aq. NaCl solution (30 mL), dried over anhydrous Na_2SO_4, filtered and concentrated under reduced pressure to give a reddish-pink solid. The solid was purified by column chromatography (silica gel, 5:4:1 petroleum spirit: DCM: EtOAc as eluent) to yield the product **4.3** as a reddish-pink solid (81 mg, 86%). Compound **4.3** has not been previously reported in the literature and thus all data below for **4.3** constitutes novel characterization.

^{1}H NMR (500MHz, $CDCl_3$) δ 4.46 (2H, s, Ar-CH_2-O), 4.48 (2H, s, Ar-CH_2-O), 7.08 (2H, d, J = 8.0 Hz, β-phenyl-H AB quartet), 7.18-7.21 (3H, m, Ar-**H**, *meso*-phenyl *m-/p-),* 7.34 (2H, d, J = 8.0 Hz, β-phenyl-H AB quartet), 7.32-7.36 (1H, m, Ar-**H**, benzyloxy *p-*), 7.38-7.44 (4H, m, Ar-**H**, benzyloxy *o-/m-*), 7.69-7.80 (9H, m, Ar-**H**, *meso*-phenyl *m-/p-),* 7.86-7.89 (2H, m, Ar-**H**, *meso*-phenyl *o-*), 8.20-8.25 (6H, m, Ar-**H**, *meso*-phenyl *o-*), 8.78 (1H, d, J = 4.6 Hz, **H**-pyrrole β-), 8.87 (1H, d, J = 4.5 Hz, **H**-pyrrole β-), 8.87 (1H, s, **H**-pyrrole- β-phenyl substituted), 8.93-8.95 (3H, m, **H**-pyrrole β-), 8.96 (1H, d, J = 4.6 Hz, **H**-pyrrole β-)

^{13}C NMR (125MHz, $CDCl_3$) δ 71.00, 71.49, 120.70, 121.15, 121.66, 122.51, 125.95, 126.66, 126.70, 126.73, 126.83, 127.05, 127.61, 127.65, 127.73, 127.81, 128.54, 130.41, 131.59, 132.09, 132.15, 132.22, 132.32, 132.80, 134.52, 134.59, 135.21, 135.57, 135.79, 138.44, 139.17, 141.63, 142.90, 142.93, 143.06, 146.77, 147.25, 148.04, 150.29, 150.37, 150.44, 150.50, 150.65, 151.43

FT-IR (neat, cm^{-1}) 3054, 1597, 1484, 1441, 1338, 1194, 1177, 1157, 1072, 1004, 994, 845, 797, 749, 699, 661

HRMS (ESI$^+$, *m/z*) 873.2546 ($C_{58}H_{41}N_4OZn$ M^+ requires 873.2572)

α-Mercapto-ω-(1-carboxyethyl)-poly{[2-(4'-((4''-vinylbenzyloxy)methyl)phenyl)-5,10,15,20-tetraphenylporphyrinato] zinc(II)} (4.6)

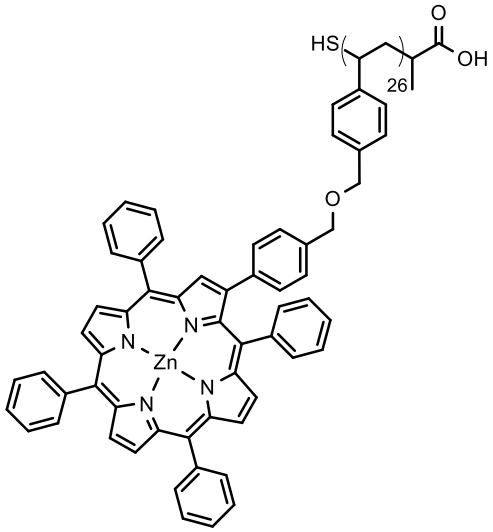

A suspension of sodium hydride (27 mg, 1.13 mmol) in THF (10 mL) was added to a solution of α-(dodecylthiocarbonothioylthio)-ω-(1-carboxyethyl)-poly(4-vinylbenzylchloride) **3.20** (34 mg, 0.221 mmol VBC units) and [2-((4-benzyloxymethyl)phenyl)-5,10,15,20-tetraphenylporphyrinato] zinc(II) **4.10** (260 mg, 0.332 mmol) dissolved in anhydrous THF (10 mL). The reaction mixture was then allowed to stir for 5 days at room temperature under N_2 atmosphere. The reaction was quenched by addition of MeOH (5 mL) and the mixture was diluted in $CHCl_3$ (100 mL) and washed with H_2O (100 mL). The organic layer was washed with sat. aq. NaCl solution (50 mL), dried over Na_2SO_4, filtered and concentrated under reduced pressure. The residue was purified by size exclusion column chromatography (Bio S-X beads, toluene as eluent) to yield the porphyrin-appended polymer **4.6** as a brownish-purple powder (138 mg, 70%). Compound **4.6** has not been previously reported in the literature and thus all data below for **4.6** constitutes novel characterization.

^{1}H NMR (500MHz, $C_2D_2Cl_4$) δ 0.50-2.49 (m, backbone, alkyl-**H**), 3.34-4.57 (m, $ArCH_2O$-), 6.17-7.85 (br., m, Ar-**H**-mesophenyl, Ar-**H**- β-benzyloxy and backbone- Ar-**H**), 7.91-8.27 (m, Ar-**H**-mesophenyl *o*-), 8.51-9.01 (m, **H**-pyrrole β-)

FT-IR (neat, cm^{-1}) 3053, 2929, 1598, 1484, 1441, 1338, 1217, 1194, 1177, 1072, 1004, 994, 844, 797, 753, 723, 701, 661

6.3 References

(1) Gottlieb, H. S.; Kotlyar, V.; Nudelman, A. *J. Org. Chem.* **1997,** *62*, 7512.

(2) https://www.isotope.com/userfiles/files/assetLibrary/NMR_solvents_data_chart_&_storage.pdf.

(3) Strachan, J.-P.; Gentemann, S.; Seth, J.; Kalsbeck, W. A.; Lindsey, J. S.; Holten, D.; Bocian, D. F. *J. Am. Chem. Soc.* **1997,** *119*, 11191.

(4) Nathanael, J. G.; Hancock, A. N.; Wille, U. *Chem. Asian J.* **2016,** *11*, 3188.

(5) Wang, H.-W.; Liu, Z.-C.; Chen, C.-H.; Lim, T.-S.; Fann, W.; Chao, C.-G.; Yu, J.-Y.; Lee, S.-L.; Chen, C.-H.; Huang, S.-L.et al. *Chem. Eur. J.* **2009,** *15*, 5719

(6) Megiatto Junior, J. D.; Spencer, R.; Schuster, D. I. *J. Mater. Chem.* **2011,** *21*, 1544.

(7) Laha, J. K.; Dhanalekshmi, S.; Taniguchi, M.; Ambroise, A.; Lindsey, J. S. *Org. Process Res. Dev.* **2003,** *7*, 799−812.

(8) Frost, J. R.; Huber, S. M.; Breitenlechner, S.; Bannwarth, C.; Bach, T. *Angew. Chem. Int. Ed.* **2015,** *54*, 691

(9) DiMagno, S. G.; Lin, V. S.-Y.; Therien, M. J. *J. Org. Chem.* **1993,** *58*, 5983.

(10) Abada, Z.; Ferrié, L.; Akagah, B.; Lormier, A. T.; Figadère, B. *Tetrahedron Lett.* **2011,** *52*, 3175.

(11) Plater, M. J.; Aiken, S.; Bourhill, G. *Tetrahedron* **2002,** *58*, 2405.

(12) Yu, L.; Muthukumaran, K.; Sazanovich, I. V.; Kirmaier, C.; Hindin, E.; Diers, J. R.; Boyle, P. D.; Bocian, D. F.; Holten, D.; Lindsey, J. S. *Inorg. Chem.* **2003,** *42* (21), 6629.

(13) Adler, A. D.; Longo, F. R.; Finarelli, J. D.; Goldmacher, J.; Assour, J.; Korsakoff, L. *J. Org. Chem.* **1967,** *32*, 476.

(14) Shi, B.; Boyle, R. W. *J. Chem. Soc., Perkin Trans. 1* **2002**, 1397.

(15) Hasegawa, T.; Miyamoto, T. K.; Sasaki, Y. *J. Coord. Chem.* **1996,** *37*, 299.

(16) Lindsey, J. S.; Wagner, R. W. *J. Org. Chem.* **1989,** *54* (4), 828.

(17) Ha-Thi, M.-H.; Shafizadeh, N.; Poisson, L.; Soep, B. *J. Phys. Chem. A* **2013,** *117*, 8111−8118.

(18) Bonfantini, E. E.; Burrell, A. K.; Gosper, J. J.; Campbell, W. M.; Harding, M. M.; Officer, D. L.; Crossley, M. J.; Reid, D. C. W. *J. Porphyrins Phthalocyanines* **2002,** *6*, 708.

(19) Tilley, A. J.; Danczak, S. M.; Browne, C.; Young, T.; Tan, T.; Ghiggino, K. P.; Smith, T. A.; White, J. *J. Org. Chem.* **2011,** *76*, 3372.

(20) Vugts, D. J.; Koningstein, M. M.; Schmitz, R. F.; de Kanter, F. J. J.; Groen, M. B.; Orru, R. V. A. *Chem. Eur. J.* **2006,** *12*, 7178

(21) Tilley, A. J.; Chen, M.; Danczak, S. M.; Ghiggino, K. P.; White, J. M. *Polym. Chem.* **2012,** *3*, 892.

(22) Mitchell, R.; Wagner, K.; Barnsley, J. E.; van der Salm, H.; Gordon, K. C.; Officer, D. L.; Wagner, P. *Eur. J. Org. Chem.* **2017**, 5750.

(23) Bonfantini, E. E.; Burrell, A. K.; Officer, D. L.; Reid, D. C. W.; McDonald, M. R.; Cocks, P. A.; Gordon, K. C. *Inorg. Chem.* **1997,** *36*, 6270.

(24) Ventura, B.; Flamigni, L.; Marconi, G.; Lodato, F.; Officer, D. L. *New J. Chem.* **2008,** *32*, 166.

(25) Gao, G.-Y.; Ruppel, J. V.; Allen, D. B.; Chen, Y.; Zhang, X. P. *J. Org. Chem.* **2007,** *72*, 9060.

(26) Sirithip, K.; Morada, S.; Namuangruk, S.; Keawin, T.; Jungsuttiwong, S.; Sudyoadsuk, T.; Promarak, V. *Tetrahedron Lett.* **2013,** *54*, 2435.

Appendix

A1. Calibration Data for ICP-OES Analysis of Polymer 3.5

Calibration

Zn concentration (mg/L)	Mean corrected intensity
0	-1.9
0.01	36.5
0.05	213.6
0.2	821.9
0.4	1769.3
0.6	2496.2
Slope	4229.5
Intercept	1.1

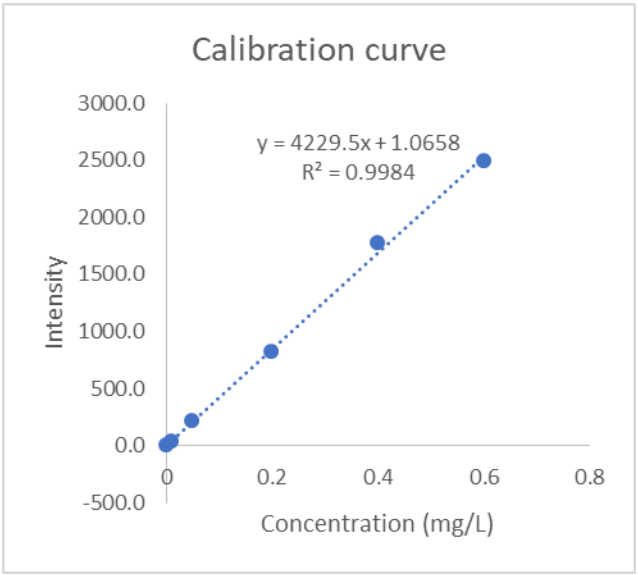

A2. ICP-OES Analysis of Polymer 3.5

Sample (duplicate measurements)

ID	Intensity	Concentration in analysed solution (mg/L)	Dilution factor	Conc before diluition (mg/L)	m(Zn) in 50 mL soliution (mg)	mass of sample used (mg)	Zn content in sample (ppm)
Sample 5A	139.3987136	0.033	10	0.327068	0.016	2.22	7366
Sample 5B	178.3970622	0.042	10	0.419274	0.021	2.27	9235

A3. Crystal data and structure refinement for *p*-SL mon 4.1

Identification code	shelx	
Empirical formula	$C_{58}H_{38}N_4Zn.(C_2H_6O)$	
Formula weight	902.36	
Temperature	100.0(2) K	
Wavelength	0.82653 Å	
Crystal system	Triclinic	
Space group	P -1	
Unit cell dimensions	a = 10.545(2) Å	α= 99.80(3)°.
	b = 13.183(3) Å	β= 90.49(3)°.
	c = 18.978(4) Å	γ = 112.79(3)°.
Volume	2388.6(10) $Å^3$	
Z	2	
Density (calculated)	1.255 Mg/m^3	
Absorption coefficient	0.832 mm^{-1}	
F(000)	940	
Crystal size	0.10 x 0.05 x 0.005 mm^3	
Theta range for data collection	2.145 to 30.284°.	
Index ranges	-12<=h<=12, -16<=k<=16, -23<=l<=23	
Reflections collected	30760	
Independent reflections	8149 [R(int) = 0.0420]	
Completeness to theta = 29.730°	90.5 %	
Absorption correction	None	
Refinement method	Full-matrix least-squares on F^2	
Data / restraints / parameters	8149 / 52 / 664	
Goodness-of-fit on F^2	1.061	
Final R indices [I>2sigma(I)]	R1 = 0.0584, wR2 = 0.1578	
R indices (all data)	R1 = 0.0658, wR2 = 0.1640	
Extinction coefficient	n/a	
Largest diff. peak and hole	0.728 and -1.041 $e.Å^{-3}$	

A4. Crystal data and structure refinement for *m*-SL mon 4.1

Identification code	shelx	
Empirical formula	$C_{58}H_{38}N_4Zn$	
Formula weight	856.29	
Temperature	130.00(10) K	
Wavelength	1.54184 Å	
Crystal system	Monoclinic	
Space group	I 2	
Unit cell dimensions	a = 12.2429(8) Å	α= 90°.
	b = 7.4802(7) Å	β= 94.374(7)°.
	c = 48.640(3) Å	γ = 90°.
Volume	4441.5(6) $Å^3$	
Z	4	
Density (calculated)	1.281 Mg/m^3	
Absorption coefficient	1.101 mm^{-1}	
F(000)	1776	
Crystal size	0.15 x 0.12 x 0.01 mm^3	
Theta range for data collection	3.801 to 74.660°.	
Index ranges	-14<=h<=12, -8<=k<=9, -59<=l<=57	
Reflections collected	10673	
Independent reflections	6390 [R(int) = 0.0641]	
Completeness to theta = 67.684°	88.9 %	
Absorption correction	Semi-empirical from equivalents	
Max. and min. transmission	1.00000 and 0.31389	
Refinement method	Full-matrix least-squares on F^2	
Data / restraints / parameters	6390 / 769 / 569	
Goodness-of-fit on F^2	1.375	
Final R indices [I>2sigma(I)]	R1 = 0.1110, wR2 = 0.3141	
R indices (all data)	R1 = 0.1296, wR2 = 0.3448	
Absolute structure parameter	-0.02(3)	
Extinction coefficient	0.0007(4)	
Largest diff. peak and hole	1.171 and -0.906 $e.Å^{-3}$	

A5. Crystal data and structure refinement for *p*-EL mon 4.3

Identification code	shelx	
Empirical formula	$C_{58}H_{40}N_4OZn.(CHCl_3)$	
Formula weight	993.68	
Temperature	100.0(2) K	
Wavelength	0.71079 Å	
Crystal system	Monoclinic	
Space group	P 21/n	
Unit cell dimensions	a = 18.217(4) Å	α= 90°.
	b = 13.176(3) Å	β= 114.44(3)°.
	c = 21.321(4) Å	γ = 90°.
Volume	4659.0(19) $Å^3$	
Z	4	
Density (calculated)	1.417 Mg/m^3	
Absorption coefficient	0.748 mm^{-1}	
F(000)	2048	
Crystal size	0.1 x 0.1 x 0.01 mm^3	
Theta range for data collection	1.242 to 32.193°.	
Index ranges	-27<=h<=27, -18<=k<=18, -31<=l<=31	
Reflections collected	80954	
Independent reflections	13752 [R(int) = 0.0527]	
Completeness to theta = 25.244°	99.4 %	
Absorption correction	None	
Refinement method	Full-matrix least-squares on F^2	
Data / restraints / parameters	13752 / 0 / 614	
Goodness-of-fit on F^2	1.039	
Final R indices [I>2sigma(I)]	R1 = 0.0711, wR2 = 0.2123	
R indices (all data)	R1 = 0.0803, wR2 = 0.2233	
Extinction coefficient	0.0046(7)	
Largest diff. peak and hole	1.248 and -2.122 $e.Å^{-3}$	